ABSTRACT OF THE DISSERTATION

Petrochemistry and Geochronology of Ngorongoro Volcanic Highland Complex (NVHC) and its relationship to Laetoli and Olduvai Gorge, Tanzania

by GODWIN FANUEL MOLLEL

Dissertation Director:

Professor Carl C. Swisher III

The Ngorongoro Volcanic Highland Complex (NVHC) of northern Tanzania is situated at the southern divergence of the Gregory Rift, part of the East African Rift System. The NVHC consists of at least nine major volcanic centers that erupted lavas, ash flows, and other pyroclastic materials from Pliocene to Present. These volcanoes are considered the source of lavas and other volcaniclastic material found interbedded in the adjacent anthropological sites of Olduvai Gorge and Laetoli.

This dissertation focuses on the petrochemistry and geochronology of six major NVHC centers: Satiman, Lemagurut, Oldeani, Ngorongoro caldera, Olmoti, and Embagai, as well as Laetoli Ogol lava flows, Olduvai Gorge Bed I lava and the isolated cone of Engelosin. The overall intent is to provide a geochemical and geochronological framework for the NVHC and refine correlations of the NVHC volcanoes with Olduvai and Laetoli.

Interpretation of petrographic and x-ray fluorescence data (major element) indicate that the studied volcanoes produced magmas that vary in composition from foidite to phonolite and basalt to rhyolite. Laser ablation data (trace element) from all lavas support an origination from a K-rich peridotite. The Sr-Nd-Pb isotopes (TIMs data) show wide variation in all centers that is considered to indicate crust-magma interaction, an interpretation supported by Ce/Pb ratios (< 25 ± 5) lower than expected for mantle derived melts. Lava samples with mantle values (Ce/Pb) have Sr-Nd-Pb isotope ratios that can be explained by mixing between high-μ and enriched mantle reservoirs.

$^{40}Ar/^{39}Ar$ dating of matrix and anorthoclase from the sampled NVHC volcanoes indicates a range in activity from 4.65 Ma to ~ 0.60 Ma. Satiman is the oldest, followed by Engelosin 2.97 Ma, Lemagurut 2.40 Ma, Ngorongoro 2.28 Ma, Olmoti 2.01 Ma, Oldeani 1.61 Ma and Embagai ~1.20 Ma. Overlapping activity is recorded between Lemagurut, Ogol and Ngorongoro as well as between Ngorongoro and Olmoti. Correlation of ages and mineral assemblages from these volcanoes and that of the tephra from Olduvai and Laetoli, confirm a Satiman and Ngorongoro source for the Laetolil and Naibadad Beds in the Laetoli area respectively, whereas, that of Olmoti upper section correlates with Olduvai Bed I lava, confirming an Olmoti source.

PREFACE

This dissertation is a culmination of over five years of field and laboratory work on the lavas from the Ngorongoro Volcanic Highland Complex (NVHC), Tanzania. I was first introduced to Olduvai Landscape Paleoanthropology Project (OLAPP) in 1995 by Professor F.T. Masao immediately after graduating from the University of Dar Es Salaam. I matriculated to Rutgers in the Spring of 2000 and completed my M.S. degree under the supervision of Professor G.M. Ashley in October, 2002. My M.S. dealt with the geochemistry and petrology of the southeastern portion of the NVHC. Following the availability of $^{40}Ar/^{39}Ar$ facility with the arrival of Professor C.C. Swisher III to Rutgers, and the acquisition of a new Thermal Ionization Mass Spectrometer (TIMS) by Professor M.D. Feigenson and Professor M.J. Carr, it became feasible to conduct a systematic geochronology and isotope geochemistry of the NVHC. The focal point of this dissertation is centered on providing systematic geochronological and geochemical evolutionary history of the NVHC which was surprisingly unequally explored compared to the adjacent archaeological sites of Olduvai and Laetoli.

The first field season of this study was conducted in the summer of 2000 when 25 lava samples were collected from Olmoti, Ngorongoro, Satiman and Lemagurut, primarily for petrography and bulk chemistry studies. These were studied in the following year and constitute part of my M.S. thesis. In the summers of 2003 and 2004 more samples were collected from Embagai, Oldeani and Ogol flows. During this field season Olmoti, Ngorongoro and Lemagurut were revisited and more samples were collected with much attention given in collecting samples for $^{40}Ar/^{39}Ar$ geochronology. Two samples from Engelosin cone were collected in 1999 when C. Swisher and I briefly visited Engelosin while working with the OLAPP team. I consider the samples collected and studied in that this dissertation represents most of the major volcanic centers, cones and lava flows of the NVHC.

$^{40}Ar/^{39}Ar$ geochronology was done at the Rutgers University (RU) Ar-Laboratory under supervision of Professor Swisher. Sr and Nd isotope by thermal ionization mass spectrometry were colleceted by Professor Feigenson at RU. Pb isotopes were analyzed at the University of Rochester, NY, by Professor A. Basu. Mineral phase data by electron microprobe was conducted by me at RU and partly at the American Museum of Natural History, NY. A few samples were also analyzed at the University of Wisconsin-Madison by Dr. L. McHenry. Bulk chemistry by X-ray fluorescence and Laser ablation was done at the Department of Geological Sciences, Michigan State University. Field studies, sample preparations, data interpretation and conclusions are my own, and were made in consultation with my advisor and dissertation committee.

Introduction to chapters

This dissertation is divided into seven chapters. The different chapters are designed to address problems pertaining to individual volcanic centers or set of related volcanic centers. In chapter one, I provide an overview on rift development and volcanism related to the Ngorongoro Volcanic Highland Complex (NVH). I also provide a summary of previous work in the NVHC and outlines existing problems that need to be addressed.

Chapter two deals with the methodology used in this study. Here I provide detailed descriptions of each method used and includes both field and laboratory methods. This chapter also provides description of data reduction and presentation.

Chapters three through five are written in manuscript format ready for submission to peer review journals. In chapter three, I discuss the volcanic centers of Oldeani, Satiman and Lemagurut and include Ogol lava flows. I outline the petrochemistry and chronology of these lavas and compare them with those from other known volcanic centers in the region and finally, correlate the ages and compositions of these lavas with the volcanic deposits of Laetoli and pinpoints sources for the Laetolil and Ndolanya Beds.

In chapter four, I discuss the geochemical evolution of the Ngorongoro Caldera (NC). I provide a detailed documentation of lava chemistry recorded on the Caldera wall and look into the influence the crust might have had during NC magma ascent. Isotopic data from these lavas are compared with those from other volcanic centers in the region to identify the NC sources. I also provide new dates and revise the age of the paleomagnetic record on the NC wall. Finally, I compare the new ages and compositions of NC with those from the Naabi Ignimbrite at Olduvai Gorge in an attempt to pinpoint the Naabi Ignimbrite source.

Chapter five documents the petrogenesis of the Olmoti lavas and Olduvai Bed I lava. In this chapter, I provide detailed descriptions on the cause for the observed Zr/Nb fractionation, the petrogenesis of trachybasalt lower in the section and that of the trachytic upper section. I also provide a detailed geochronology of these lavas and compare the new ages and compositions to the Olduvai Bed I stratigraphy as well as that of the Olpiro tuff in Laetoli area.

Chapter six documents the petrochemistry and chronology of lavas from Embagai and Engelosin. Here I provide a detail petrography of Embagai and a comparison of the bulk chemistry of Embagai to that of Engelosin. I also documented a detailed geochronology of Embagai and Engelosin lavas and a compilation of the Sr, Nd and Pb isotope data of all the NVHC centers from pervious chapters.

Chapter seven brings together chapters three through six by providing an overview on the temporal and spatial evolution of the NVHC lavas. This chapter also documents the NVHC source rock lithology and provides a model for NVHC volcanism which constrains the depth at which melting of the NVHC source occurs.

ACKNOWLEDGEMENTS

Sincere thanks to the Tanzania Commission on Science and Technology, the Tanzania Department of Antiquities, and the Ngorongoro Conservation Area Authority for granting permits and allowing this research to be conducted. This study was partly supported by a two year fellowship from L.S.B. Leakey Foundation, a teaching and a graduate assistantship from the Department of Geological Sciences and a grant from Sigma Xi. Major support for field research was provided by Olduvai Landscape Paleoanthropology Project and Laetoli Project through grants from National Science Foundation (grants to Swisher: BCS-0109027; Harrison: BCS-0309513; Ashley: EAR 9903258; Feibel: BCS-0218511 and Blumenschine).

Many thanks to Carl Swisher for careful guidance, support and advice during data acquisition, reduction, and in report writing. Thanks to Mark Feigenson for running my Sr and Nd analyses. Michael Carr is thanked for his constructive comments during report writing. I am grateful to Asish Basu of the University of Rochester, NY for running my Pb analyses. Professor Tanya Furman of the Department of Geological Sciences, Pennsylvania State University is greatly thanked for answering my eleventh hour call to be in my dissertation committee after the loss of Professor R. L. Hay. T. Furman is also thanked for sharing her database on East African volcanics.

Professor Gail Ashley is thanked for introducing me to Rutgers and for support during field work. Dr. R. Blumenschine of Rutgers University, F. Masao of Dar Es Salaam Open University, and T. Harrison of the New York University are thanked for providing field support. Dr. C. Feibel is thanked for support during data acquisition and J. S. Delaney for introducing me into the world of electron microprobe. Thanks to Dr. Brent

Turrin who was always there when the Argon system needed trouble shooting. Brent was also helpful during data reduction.

Dr. L. McHenry is thanked for probing Olmoti samples and R. Quinn for teaching me column chemistry. Professor C. Herzberg commented on source rock petrology. Sincere thanks go to my fellow graduate students Ian Saginor for commenting on my writing, Esteban Gazel for sharing his wealth in Adobe Illustrator and comments on geochemistry and Fara Lindsay for help during column chemistry.

Many great thanks to my family, my wife Violet and our sons Solomon and Simon for their love, patience and trust during the study.

TABLE OF CONTENTS

LIST OF TABLES

LIST OF FIGURES

CHAPTER 1: INTRODUCTION AND BACKGROUND

INTRODUCTION

Ngorongoro Volcanic Highland Complex (NVHC) is located in northern Tanzania, at the southern bifurcation of the Gregory rift (part of the East African Rift System EARS; Figure 1.1). The area is perhaps best known for its association with the nearby archaeological sites of Olduvai and Laetoli, famous for hominin and other vertebrate and invertebrate fossil remains as well as numerous stone artifacts. Beginning with archaeological work at Olduvai and Laetoli by the Leakey's in the early 1930s, and currently being continued by the Olduvai Landscape Paleoanthropology Project –OLAPP (headed by R. Blumenschine and F. Masao) and at Laetoli (T. Harrison and others) it became apparent that a detailed geochemical and geochronological framework of the NVHC was needed for better understanding of hominin land use as well as determining source areas for volcaniclastic material now covering and preserving fossil materials. As this work progressed, it became equally apparent how little was known of the genesis and relationship of the NVHC in general to the EARS. This dissertation reports new $^{40}Ar/^{39}Ar$ ages and the petrochemistry of lavas from most of the NVHC centers. It provides a model for NVHC volcanism, which constrains the depth at which melting of the source rock occurs.

The EARS has been a focus of numerous studies to investigate processes controlling continental rifting and associated volcanism (e.g., Wilson, 1989; Girdler and McConnell, 1994; Foster *et al*., 1997; Ebinger *et al*., 1989, 1997, 1999, 2000). Most studies prefer an active model over a passive one whereby, an upwelling mantle splits the continent along pre-weakened zones (e.g. Ebinger and Sleep, 1998; Lithgow-Bertelloni and Silver, 1998; Nyblade and Langston, 2002), views supported by geochronological, geochemical and seismic data. A single large mantle plume has been identified as the source for extensive volcanism in the Ethiopia region (Montelli *et al*., 2004). However, the number of plumes influencing magmatism along the entire EARS is unclear. So far up to three mantle plumes located at different areas along the EARS have been proposed (Burke, 1996; Ebinger and Sleep, 1998; George *et al*., 1998; Rogers *et al*., 2000). The $^{3}He/^{4}He$ data are contradictory, instead suggesting a single mantle plume in the Ethiopia region alone (Marty *et al*., 1996, Scarsi and Craig, 1996). The helium data shows plume signature in the Lake Turkana in Kenya area (Furman *et al.,* 2006), but none has been observed in the areas to the south of Lake Turkana and northern Tanzania.

The NVHC (measuring about 45 X 60 km of volcanic massif) centered at the southern splay of the Gregory Rift also known as the Tanzanian divergence (Dawson, 1992), is less studied despite its favorable geographic location (at the bifurcation of the Gregory Rift). Sr, Nd and Pb isotope and petrological data collected in this study permit better comparison with the well-studied areas of the EARS such as Ethiopia, Kenya and Uganda and provide insights into the magmatic evolutionary history of the NVHC as well as a better understanding of rift-related magmatism in East Africa.

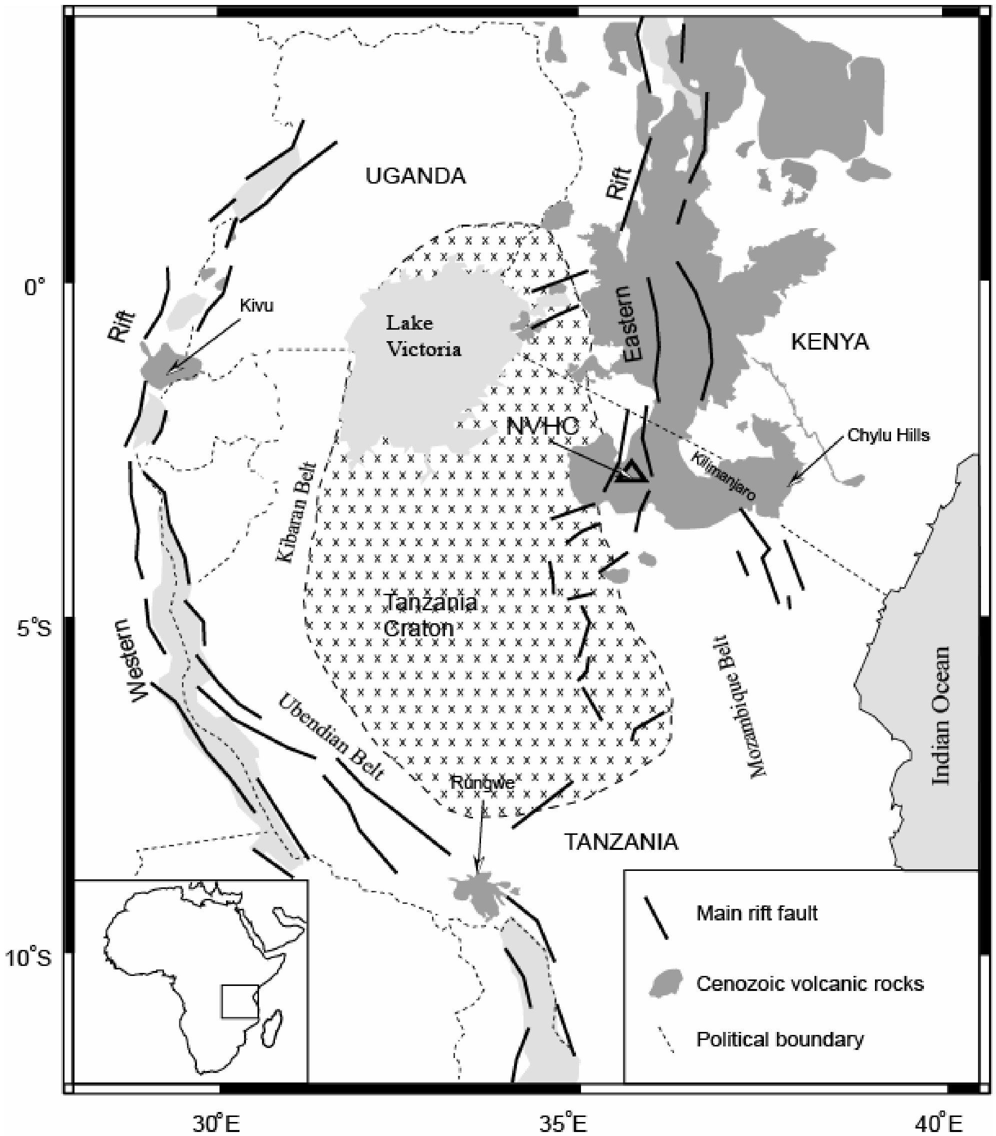

Figure 1.1: Simplified geological map of the East Africa showing political boundaries and the location of Ngorongoro Volcanic Highland Complex (NVHC), the study area in relation to the East African Rift System (EARS). Also shown are exposures of Cenozoic volcanic rocks, major rift boundary faults, Precambrian terranes, and large rift lakes (Modified from Nyblade *et al*., 2000 and Späth *et al*., 2001).

OBJECTIVES AND SIGNIFICANCE

The NVHC consists of nine major volcanic eruptive centers: Lemagurut, Satiman, Oldeani, Ngorongoro, Olmoti, Loolmalasin, Embagai, Kerimasi and Oldoinyo Lengai, along with numerous smaller, lesser-known vents (Figure 1.2). Much of our understanding of the development, age and eruptive sequence of the NVH comes from a few K-Ar dates made in the 1970s and 80s, and from interpretations of possibly correlative dated lava and ignimbritic flows and air fall deposits of Olduvai and Laetoli (Grommé *et al*., 1970; Curtis and Hay, 1972; Hay, 1976, 1987; Drake and Curtis, 1987; Walter *et al*., 1991, 1992; Manega, 1993).

Problems with existing K-Ar dates for the NVHC are of mixed quality and the accuracy of the dates is difficult to ascertain. This is, in part, due to incorporation of detrital materials resulting in ages that are too old (Grommé *et al*., 1970; Curtis and Hay, 1972) and possibly excess Ar in some dated mineral phases such as nepheline and biotite which unaccounted for, also would result in erroneously older age (Bagdasaryan *et al*., 1973). In some cases, poor sample site documentation has resulted in difficulty to interpret or correlate good data with any particular volcanic center (Manega, 1993).

The Sr, Nd and Pb isotope studies provide means to evaluate mixing processes during magma emplacement. Igneous rocks erupted through thick continental crust, such as the NVHC, are commonly enriched in chemical and isotopic signatures. These signatures can be inherited from mantle or crust (Depaolo, 1981). The NVHC is bordered by Archean Tanzanian Craton to the west and by Precambrian Mozambican belt in the east (Figure 1.2). A possibility exists that processes such as assimilation and/or magma mixing associated with reworked craton margins or the Mozambican belt (Smith and

Morsely, 1993) have occurred during magma emplacement (e.g. Hawkesworth *et al*., 1984; Thrilwall and Jones, 1983). In younger lavas (a few million years old), higher $^{87}Sr/^{86}Sr$ ratios (> 0.7050) most likely are due to crustal contribution during magma emplacement (e.g. Briqueu and Lancelot, 1979; Carlson *et al*., 1981; Huppert and Sparks, 1985; Davies and Macdonald, 1987; Halliday *et al*., 1988).The $^{87}Sr/^{86}Sr$ ratios of 0.716654 and 0.727279 were measured from metapelite and gneiss collected from the Mozambican belt in northeastern Tanzania and the Tanzanian Craton respectively (Möller *et al*., 1998) making both potential contaminants. High $^{87}Sr/^{86}Sr$ ratios were also measured on some mantle xenoliths collected from Lashaine (e.g. from clinopyroxene 0.8360; garnet 0.8345; and phlogopite 0.8196) separated from a garnet lherzolite (BD-738; Cohen *et al.,* 1984). These values suggest that lower crust could as well be potential contaminants.

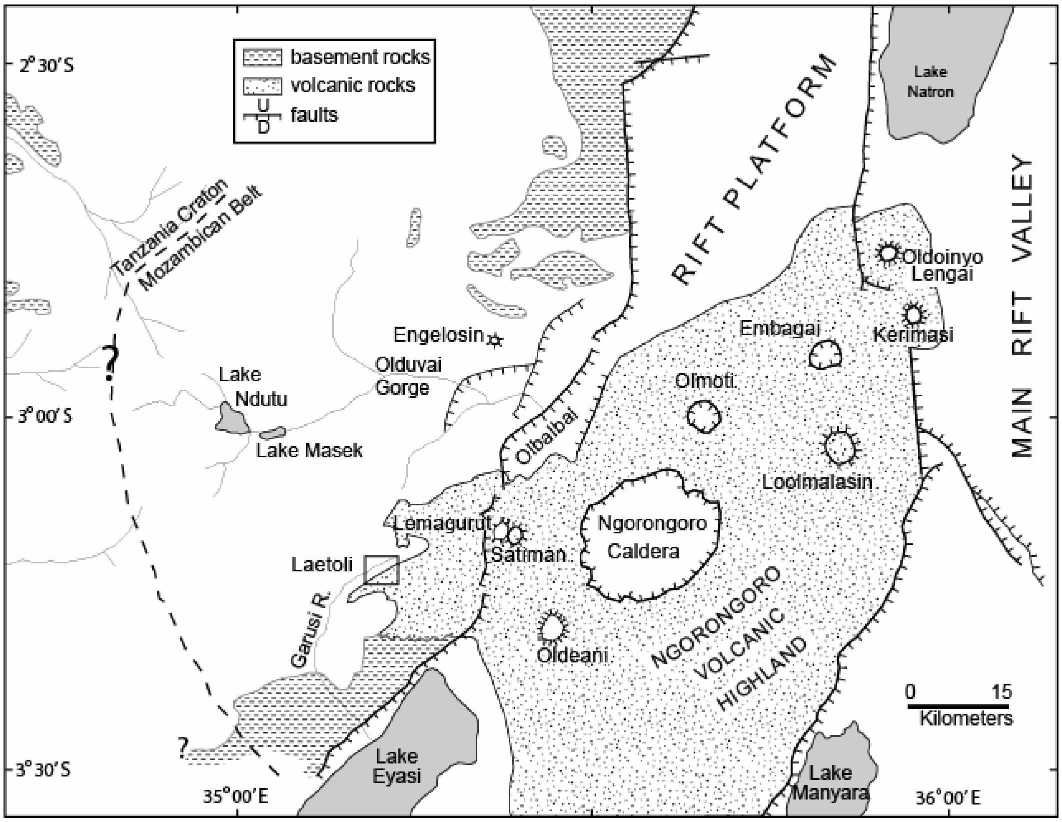

Figure 1.2: Detailed map shows location of the major volcanic centers of the NVHC and Laetoli and Olduvai Gorge archaeological sites. (Modified from Hay, 1976).

The objectives of this study are to:

1. Provide a chronological framework for the eight major NVHC centers (Embagai, Olmoti, Ngorongoro, Oldeani, Satiman, Lemagurut, Ogol flows and Engelosin cone) as well Olduvai Bed I using the $^{40}Ar/^{39}Ar$ dating method.
2. Characterize the petrology and geochemistry of the NVHC based on data obtained from optical microscopy, electron microprobe, X-ray fluorescence (XRF), and Laser Ablation Inductive Coupled Plasma Mass Spectrometry (LA ICPMS).
3. Characterize the magmatic evolution and sources for the NVHC lavas through isotopic studies of Sr, Nd and Pb data obtained using Thermal Ionization Mass Spectrometer (TIMS).
4. Ultimately relate volcanic activity of individual NVHC centers with Olduvai and Laetoli sequences following the established ages and chemistry.

BACKGROUND

Geological setting

East African Rift System (EARS)

The East African Rift System (EARS) represents one of the largest known igneous provinces. It is part of a much larger rift, the Afro-Arabian Rift System extending about 4000 km from the Red Sea and Gulf of Aden to Zambezi River in Mozambique (Baker and Wohlenberg, 1971; McConnell, 1972). The rift system is entirely intercontinental and formed within an ancient African Precambrian Platform. The Afro-Arabian Rift System consists of the eastern and western branches of the East African Rift, the Ethiopian Rift, the Gulf of Aden, the Red Sea and the Levantine Rift. The eastern branch of the EARS (Gregory Rift) that is relevant to this study includes part of southern Ethiopia, north, central and south Kenya and northern Tanzania where the NVHC is located. The general trend of the Gregory Rift approximately follows the lineaments within the mobile belts (N-S to NNE-SSW) along the margins of a stable craton although it is known to disturb the craton margin in northern Tanzania (Baker and Wohlenberg, 1971; McConnell, 1972; Baker *et al.*, 1971; Williams, 1978; King, 1978; Owens *et al.*, 2000).

The southern part of the Gregory Rift (i.e. in northern Tanzania) is superimposed on two major geologic provinces, the Tanzanian Archean Craton basement rocks (Cahen *et al.*, 1984) on the western and the Late-Proterozoic Mozambican Belt basement rocks on the eastern (Figure 1.1; Key *et al.*, 1989). The craton consists primarily of migmatites, granulites and metamorphosed ultra-basic rocks and is dated to about 3.1 to 2.5 Ga (Cahen *et al.*, 1984). Rocks of the Mozambican Belt are primarily granulites, amphibolites, gneisses, schists and marble dated between 1100 and 400 Ma (Cahen *et al.,* 1984; Maboko *et al.*, 1985, Stern, 1994; Möller *et al*., 1998; Maboko, 2000; Sommer *et al.*, 2003). In the vicinity of the NVHC, the rift orientation diverges from a single ~ 50 km wide zone in southern Kenya to ~ 200 km wide in northern Tanzania consisting of three distinctively oriented branches: the Natron-Manyara-Balangida, the Eyasi-Wembere and the Pangani rifts. The change in the rift morphology may be a result of the transition from the rifting of Proterozoic Mozambican belt lithosphere to the rifting of cratonic Archean lithosphere (Foster *et al*., 1997). Heat flow, and mantle xenolith data indicate that the lithosphere beneath the Tanzania Archean craton was and is colder and stronger than the post-Archean lithosphere (Cohen *et al*., 1984; Nyblade and Pollack, 1992; Rudnick *et al.,* 1993; Nyblade *et al*., 1996; Dawson *et al.,* 1997; Dawson, 2002). Geophysical and geochemical data suggest that topography at the base of the lithosphere guided the location of rifting in northern Tanzania, producing a broader rift zone (Fairhead, 1980; Ebinger *et al*., 1989, 1997; Foster *et al*., 1997).

Rift Evolution

Hypotheses on mechanisms responsible for creating continental rifts are still debatable. The debate is whether upwelling of the lithospheric mantle (active rifting) or rising of mantle as the continents are pulled apart (passive rifting) is they key process (Illies, 1981; Mohr, 1982; Keen, 1985; Ebinger, 1989). Geophysical data testifies that asthenospheric upwelling is the fundamental feature of the present active continental rift zones (Sandiford and Powell, 1986; Masters *et al.,* 1996; Grand *et al.,* 1997; van der Hilst *et al*., 1997; Ritsema *et al*., 1999; Owens *et al.*, 2000; Ni and Helmberger, 2003). The origin of the EARS is thought to be associated with vertical shear zones that vertically traverse the crust and upper mantle. These lineaments whose origin is unclear are avenues for localized heat flow induced by underling hot fluids (Beloussov, 1966; McConnell, 1972). The entire length of the EARS is located on a topographic high with elevation rising from an average of about 500 m above sea level to 1000 - 2000 m along the rift (Ebinger, 1989; Nyblade and Robinson, 1994). This anomalous elevation is referred to as the “East African Superswell". The rift is also associated with negative gravity anomaly as well as elevated heat flow (Ebinger, 1989; Owens *et al*., 2000). The main episode of regional rifting along the EARS is <13 Ma (Davidson and Rex, 1980; Courtillot *et al*., 1984).

Volcanism in the EARS

Two main phases of volcanic activities are outlined using K-Ar and $^{40}Ar/^{39}Ar$ geochronology in southern Ethiopia area: An early eruption interval between 45-34 Ma and a later interval at ~19-12 Ma (Berhe, *et al.*, 1987; Coulié *et al.*, 2003). In Kenya, lavas of Miocene to Recent occur along the Gregory Rift (Baker *et al*., 1971) while in northern Tanzania the age range is ~ 8 Ma to Present. An extensive description of volcanic activity and lava types along the Gregory Rift in Kenya is given by Baker *et al*. (1971) and Baker (1987). In general, the Kenya rift volcanics were erupted nearly continuously from early Miocene to Holocene times. Miocene volcanism was mostly of nephelinites, alkali basalts and phonolites. Pliocene activity was trachytic, phonolitic and nephelinitic in central and southern parts of the rift valley, while contemporaneous basaltic volcanism took place in its whole length. Late Pleistocene and Quaternary volcanism was strongly bimodal with trachytic activity dominating the rift floor, whereas, extensive basaltic activity occurred east of the rift valley (Baker *et al*., 1971; Baker 1987).

The earliest volcanic activity along the Gregory rift in northeastern Tanzania occurred during Late Miocene with the eruption of phonolitic lava at the Essimingor volcano (Bagdasaryan *et al*., 1973). Alkali basalt-trachyte-phonolite association lavas followed at the beginning of Pleistocene. These eruptions were mainly in the NVHC area. Volcanic centers included in this eruption are Satiman, Lemagurut, Ngorongoro, Olmoti, Oldonyo Sambu, Loolmalasin, Oldeani, Terosero, Kitumbeine, Gelai, Embagai, Meru and Kilimanjaro (Baker *et al*., 1971; Wilkinson *et al*., 1986; Dawson, 1992; Foster *et al*., 1997).

A second phase of volcanic activity occurred after the 1.2 Ma faulting (Macintyre *et al*., 1974). Unlike the first phase of eruptions, this was smaller in volume and highly explosive. Pyroclastic volcanic cones of Meru, Monduli, Oldonyo Lengai and Kerimasi are thought to be part of this eruption. The magma is ultra-basic to ultra-alkaline in composition and the rocks are mainly phonolites and feldspathoidal syenites (Wilkinson *et al*., 1986; Dawson, 1992; Manega, 1993; Foster *et al*., 1997). Carbonatite lavas, pyroclasts, nephelinites and phonolites occur at Oldonyo Lengai and Kerimasi (Dawson, 1962; Hay, 1983, 1989; Dawson *et al*., 1992; Bell and Simonetti, 1996).

PREVIOUS WORK IN NVHC

Geochronological study of the NVHC, Olduvai Gorge and Laetoli began over four decades ago with K-Ar dating of lavas and tuffs interbedded with Zinjanthropus fossils discovered by Louis and Mary Leakey at Olduvai Gorge (Koenigswald *et al*., 1961; Leakey *et al*., 1962; Evernden and Curtis, 1965). Recently, there have been attempts to refine the dating at Olduvai and Laetoli using K-Ar techniques (Curtis and Hay, 1972; Bagdasaryan *et al*., 1973; Leakey *et al*., 1976; Drake and Curtis, 1987; Manega, 1993) and by $^{40}Ar/^{39}Ar$ techniques in the 1990's (Manega, 1993; Walter *et al*., 1991, 1992; Deino et al., in progress). Paleomagnetics (Grommé *et al*., 1970; Grommé and Hay, 1963, 1967, 1971; Tamrat *et al*., 1995), amino acid racemization (Manega, 1993) and Electron Spin Resonance [ESR] (Skinner *et al*., 2003) have also been applied. Although there is a growing consensus as to the chronology of the Laetoli and Olduvai sequences, the age and evolutionary history of the NVHC remains poorly understood. Much of the more recent data occur in a Ph.D. dissertation by Manega (1993). Table 1.1 summarizes age information obtained by different researchers for the NVHC using different methods as indicated. The following is a description of dated material and methods used starting from the east to west.

Embagai is a small caldera (8-10 km in diameter) to the northeast of Olmoti (Figure 1.2). Rocks from Embagai range from phonolite to nephelinite in composition (Guest, *et al*., 1961) and have been proposed to be the likely source for upper beds at Olduvai (Hay, 1976). Manega (1993) reported both K-Ar and $^{40}Ar/^{39}Ar$ dates for Embagai. According to Manega (1993), nephelinite, nepheline and biotite from samples collected along the caldera rim and from slopes of the caldera indicate that Embagai was active between 1.2 to 0.5 Ma (Table 1.1).

Table1.1: Published K-Ar and $^{40}Ar/^{39}Ar$ dates for the NVHC

Volcano	Age (Ma)	Material dated	Source	Analyses
Lemagurut	2.39 4.3	vogesite (w/rock) phonolite (w/rock)	Hay 1976 Bagdasaryan *et al*., 1973	1 1
Satiman	3.7 3.3 4.5	nepheline nepheline nepheline	Curtis, in Hay, 1972 Manega, 1993 Bagdasaryan *et al*., 1973	1 1 1
Oldeani	Not dated			
Ngorongoro	2.81 - 2.23 2.95 - 2.15 2.02 *	w/rock and Feldspar w/rock and Feldspar anorthoclase	Grommé *et al*. 1970; Curtis and Hay, 1972. Manega, 1993	4 8 2
Olmoti	1.85 - 1.1+	w/rock and Feldspar	Manega, 1993	5
Embagai	1.2 - 0.5+	nepheline and biotite	Manega, 1993	6
Ogol vent	2.41	vogesite (w/rock)	Drake and Curtis, 1987	2
Engelosin	2.68	Phonolite (w/rock)	Manega, 1993	1

All ages are K-Ar except * are $^{40}Ar/^{39}Ar$, + are both K-Ar and $^{40}Ar/^{39}Ar$

Olmoti is composed of basalt and trachyandesite (Hay, 1976; Mollel, 2002) and is thought to be the source for Olduvai Bed I lava as well as the majority of Bed I and Bed II tuffs in Olduvai Gorge (Hay, 1976). Olmoti dates are reported in Manega, (1993). Manega collected samples from slopes of Olmoti and from lava flows aligned with Olmoti. These samples include trachytic basalt, an ignimbrite and phonolitic tephrite. K-Ar ages from the trachytic lava and ignimbrite range from 1.85 to 1.1 Ma. Single crystal laser fusion (SCLF) of feldspar concentrates from the ignimbrite yield $^{40}Ar/^{39}Ar$ ages ranging from 1.85 to 1.81 Ma. Manega concluded that Olmoti was active between 1.85 and 1.1 Ma. This would imply that Olmoti and Embagai eruption histories overlap in time.

Ngorongoro Caldera (Ngorongoro) is basaltic to rhyolitic in composition (Hay, 1976; Manega, 1993; Mollel, 2002). Ages for Ngorongoro consist of K-Ar and $^{40}Ar/^{39}Ar$ dates on lavas and tuffs. Grommé *et al.* (1970) and Curtis and Hay (1972) report ages ranging from 2.95 – 2.15 Ma from the middle and the bottom of the main Ngorongoro section exposed on the Lerai Ascending Road (LAR). These dates gave a mean age of 2.45 Ma for the Ngorongoro activity. $^{40}Ar/^{39}Ar$ SCLF data on feldspar from an ignimbrite collected from upper half of the crater-wall section on the Western Descending Road (WDR), produced younger ages of 2.02 Ma (Manega, 1993). K-Ar ages on feldspar from the WDR section by Manega produced even younger ages of 1.98 to 1.83 Ma.

Paleomagnetic data obtained by Grommé *et al*. (1970) from the LAR revealed a polarity change from Normal to Reversed geomagnetic polarity in the lower part of the section. Based on the 2.45 Ma K-Ar date, Grommé *et al*. (1970) correlated the N-R transition to the upper Gauss Normal to lower Matuyama reverse boundary considered at that time to be about 2.43 Ma (Cox, 1969).

Oldeani is a large volcano to the southwest of Ngorongoro Caldera. According to Pickering 1964, it is composed primarily of basalt. Age and duration of its volcanic activity has never been determined but based on the degree of weathering of its valleys, it is thought to range within the activity of Ngorongoro and Lemagurut. Oldeani has been considered to be a possible source for basaltic cobbles found in Laetoli basin (Adelsberger *et al*., 2002) that were used by hominins to make stone tools. Hay (1987) suggested a distant source for upper Ndolanya Beds based on the small size of pumice fractions and the difference in age between lower (~3.5 Ma) and Upper Ndolanya Beds

(>2.4 Ma; Figure 1.3). He mentioned a volcano to the east of Satiman as a likely source but dismissed Lemagurut and Ngorongoro on the basis of their rock composition.

Satiman is foidite and phonolitic tephrite in composition (Hay, 1976; Mollel, 2002) and is thought to be the source for Lower Laetoli beds (Figure 1.3) based on similarity in mineral composition (Hay, 1987). Dates for Satiman consist of a single K-Ar date of 3.7 Ma on nepheline from a nephelinite (G. Curtis, in Hay, 1976). A similar age of 3.3 Ma was obtained by Manega (1993) by dating similar material. A significantly older age for Satiman was reported by Bagdasaryan *et al*., (1973). These authors reported an age of 4.5 Ma on phonolite. K-Ar dates ranging between 4.3 and 3.8 Ma obtained from biotite were reported for Lower Laetoli beds (Drake and Curtis, 1987). The 4.3 Ma date is similar to the 4.5 Ma and the two dates together with mineralogical similarity further support the interpretation that Satiman is the possible source for Lower Laetoli beds. Biotite can however contain excess Ar which if not accounted for would make these ages too old (McDougall and Harrison, 1999).

Lemagurut is basaltic to trachyandesite in composition (Mollel, 2002). Attempt to date Lemagurut by different researchers has met with mixed results. A K-Ar date of 2.39 Ma (Hay, 1976) was obtained from a vogesite flow collected in Laetoli area (Figure 1.2) and interpreted to have originated from Lemagurut. If this interpretation is correct, the age would mean that Lemagurut and Ngorongoro overlapped during their evolutionary history. However, field observations shows that Lemagurut is much older than Ngorongoro on the basis of the degree of weathering on valleys exposed on both volcanoes. Hay, (1987) pointed that the vogesite must have originated from Ogol vents that occur as a series of rounded top cones in Laetoli area. This date may therefore not represent Lemagurut activity. Bagdasaryan *et al*. (1973) reported a K- Ar date of 4.3 Ma on a phonolite.

Phonolite contains nepheline that has been known to yield anomalously old ages as a result of excess or trapped argon (McDougall and Harrison, 1999). In addition, lavas of phonolitic compositions are unknown in Lemagurut (Mollel, 2002). Manega (1993) also attempted to date Lemagurut, but unfortunately his samples are now considered distal eruptions from Ngorongoro.

Engelosin is a volcanic cone situated about 8 km to the north of Olduvai Gorge. It is about 500 m in diameter and 145 m high. It is composed primarily of fine-grained to slightly porphyritic greenish phonolite (Hay, 1976; Manega, 1993). A $^{40}Ar/^{39}Ar$ date on phonolite indicated that Engelosin was active 2.68 Ma (Manega, 1993).

Ogol lavas are a series of flows located southwest of Lemagurut considered to have erupted from a series of small isolated vents or cones. The vents or cones appear to lie in an east-west orientation extending about 25 km in length and range from 0.5 to 1.5 km in diameter and 50 to 150 m high (Hay, 1987). The name Ogol comes from Massai word *ogol* meaning hard. Ogol lavas overlie the Ndolanya beds (~3.5-2.4 Ma, Figure 1.3) and occasionally cutting though into Laetoli beds (>2.5 Ma). The Ogol lavas are porphyritic with phenocrysts of olivine, augite, alkali feldspar, and biotite and may include plagioclase, nepheline and opaque minerals (Hay, 1987). Hay (1987) reported reverse magnetic polarity on the Ogol lavas based on field measurements obtained by Alan Cox of Stanford University. Whole rock K-Ar dates of vogesite produced ages ranging from 2.52 – 2.21 Ma with a mean age of 2.41 Ma (Drake and Curtis, 1987). The mean age of 2.41 and reversed magnetic polarity, would seem to correlate well with Ngorongoro activity and thus the Matuyama chron.

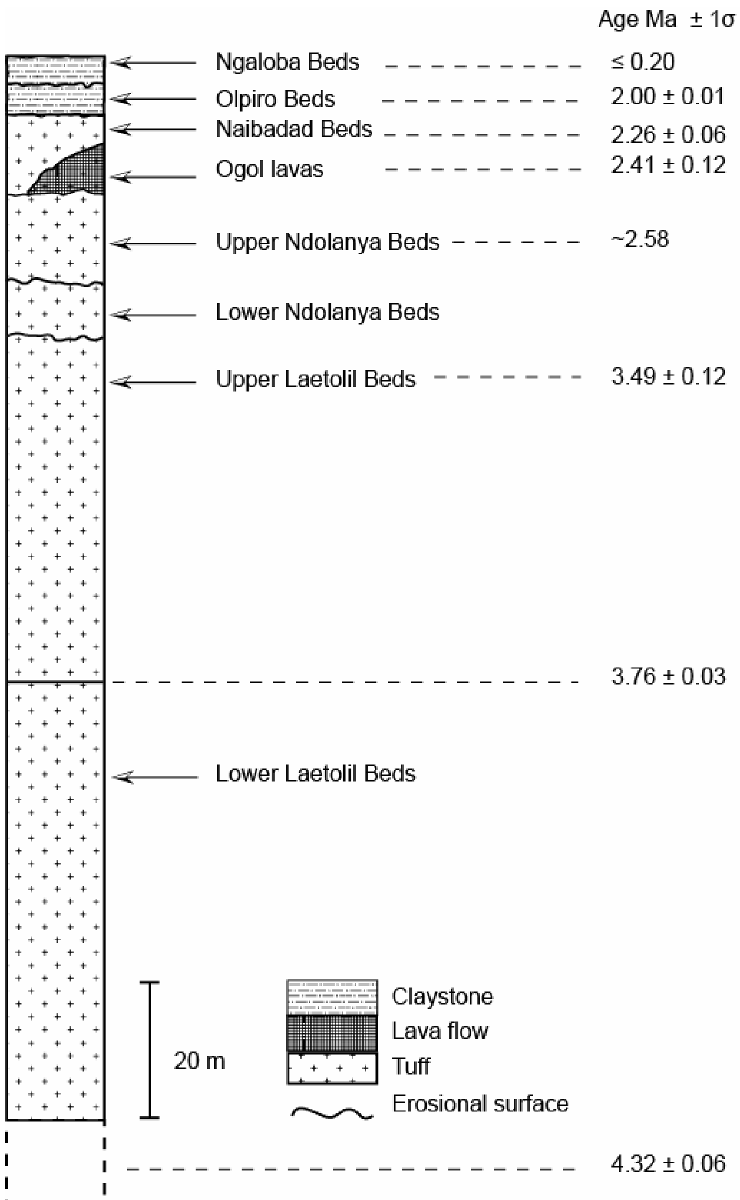

Figure 1.3: Generalized stratigraphic units in Laetoli area (after Hay, 1987). K-Ar and $^{40}Ar/^{39}Ar$ ages from Drake and Curtis, (1987); Dessokia, (1990); Manega, (1993).

Limited Sr and Nd isotopic data for the NVHC are based on three samples from (Ngorongoro, Satiman, and Lemagurut).The $^{87}Sr/^{86}Sr$ ratios of about 0.7048 are reported on a trachyte from Ngorongoro Caldera, 0.7054 on a foidite from Satiman and 0.7051 on a trachyte from Lemagurut (Paslick *et al.,* 1995). Additional analyses for the NVHC appear in Manega's Ph.D. dissertation adding data for Olmoti, Ngorongoro and Embagai (Manega, 1993) and appear to be consistent with the published values of Paslick *et al*. (1995). Manega (1993) reported similar ratios for a trachyte from Ngorongoro and slightly lower ratios of 0.7049 for Satiman nephelinite. He also reported similar ratios of 0.7040 from Olmoti and Embagai phonolite. $^{143}Nd/^{144}Nd$ from Lemagurut trachyte and Satiman foidite are similar ~0.5124 whereas ratios from Ngorongoro Crater trachyte are slightly higher ~0.5127 (Paslick *et al*., 1995). Manega reported $^{143}Nd/^{144}Nd$ ratios of ~0.5126 from Olmoti and Embagai phonolite. Unfortunately, in some cases it appears that correlation of sampled sites to individual source centers is uncertain and in some cases may have been mistakenly sampling adjacent volcanoes. No isotopic studies have been done on Oldeani, Ogol and Engelosin lava.

Olduvai and Laetoli archaeological sites

Adjacent to the NVHC, along the western slopes, are the well known Olduvai Gorge and Laetoli archaeological and paleoanthropological sites (Figure 1.2). More than 90 hominin fossils and thousands of stone artifacts have been recovered from these sites (Leakey, L. S. B., 1958; Leakey, M. D., 1971; Hay, 1976; White, 1977; Johnson and White, 1979; Day *et al*., 1980; White, 1980, 1981; Blumenschine and Masao, 1991; Blumenschine *et al*., 2003). The fossils and artifacts occur in volcaniclastic and lake-margin sediments interbedded with widespread air-fall and ash-flow tuffs. The geology of Olduvai has been studied by numerous workers (Curtis and Hay, 1972; Hay, 1976; Walter *et al*., 1991, 1992; Hay, 1992; Manega, 1993; Ashley, 2000; Ashley and Driese, 2000; Ashley and Hay, 2002; Deocampo *et al.*, 2002; Liutkus and Ashley, 2003; Skinner *et al.*, 2003) and that of Laetoli by Hay, (1987) and Drake and Curtis, (1987). Currently the paleoanthropology and paleontology is being conducted at Olduvai by members of OLAPP headed by R. Blumenschine and F. Masao, and at Laetoli by T. Harrison and others. Detailed tephrostratigraphy of the Olduvai Bed I tuffs was done by McHenry (2001, 2003, 2004, 2005).

Olduvai stratigraphy, which consists of lava, ash flow, air fall and water-lain tuff as well as lake sediments, has been subdivided in to six units: Bed I, II, III, IV, Masek Beds and Ndutu and Naisiusiu beds (Hay, 1976). The entire sequence overlays a rhyolitic ignimbrite from Ngorongoro Caldera (Hay, 1976; Figure 2.1), the Naabi Ignimbrite. Bed I consists of lava and trachytic and rhyolitic tuff (Figure 1.4). Olduvai Bed I lava is mainly trachybasalt and trachyte (Hay, 1976) in composition and is exposed in many parts of the Gorge (Hay, 1976). It is fully exposed on the up faulted block at the third fault were a thickness of about 20 m is attained. The K-Ar dating of whole rocks produced ages ranging from 2.04 to 1.83 Ma (Curtis and Hay, 1972). The $^{40}Ar/^{39}Ar$ whole rock date on trachytic lava produced an age of 1.87 ± 0.01 Ma (Walter *et al.*, 1991, 1992). These ages are not significantly different from the whole rock age of 1.83 ± 0.03 Ma for Ngorongoro as well as the SCLF age of 1.85 ± 0.02 Ma on anorthoclase from Olmoti (Manega, 1993). The source for Olduvai bed I lava that is important for landscape evolution model of Peters and Blumenschine (1995) previously implied to be the Olmoti on the bases of chronology and paleomagnetics (Hay, 1976) may be incorrect. Moreover lava of trachytic composition was found in Olmoti during my preliminary work in July 2003. Previously, lava of trachytic composition was thought to occur in Ngorongoro crater only (Hay, 1976).

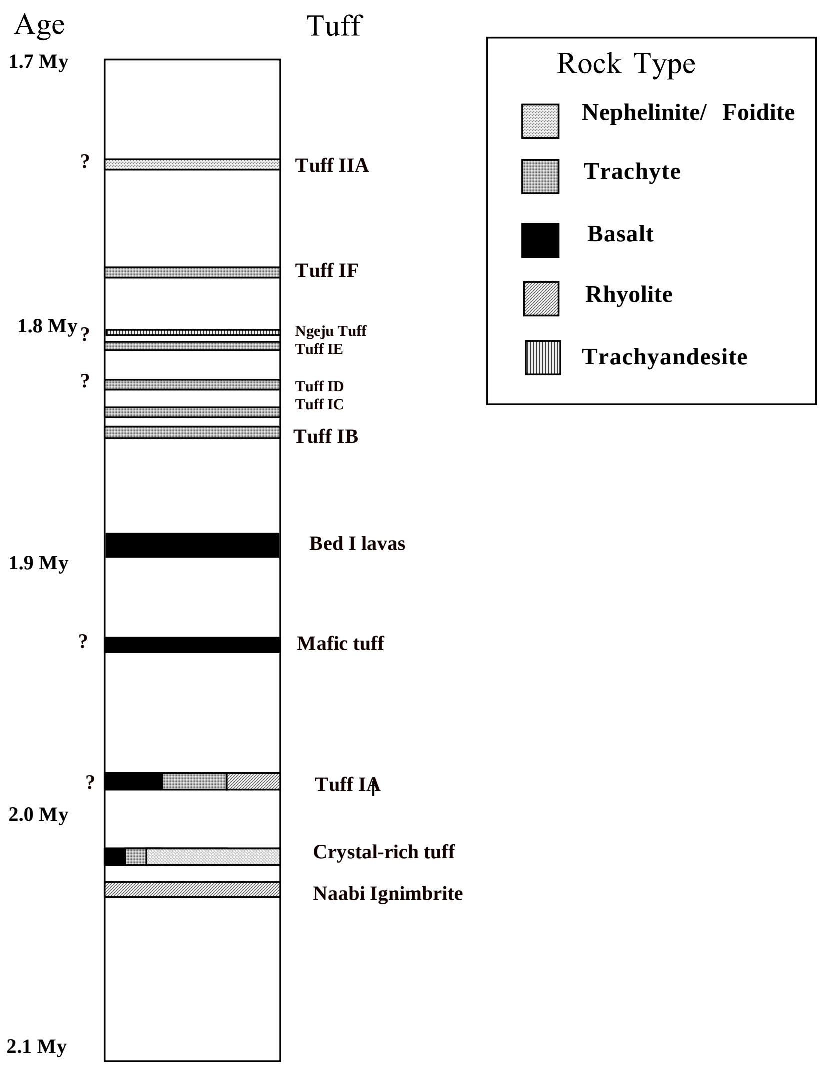

Figure1.4: Olduvai Gorge Bed I rock types (After McHenry, 2004).

The Laetoli Beds have been subdivided into two units, a Lower and an Upper unit (Figure 1.3). Hay (1987) described the Upper unit to be composed of aeolian, air-fall and water worked tuff, xenoliths and limestone. Carbonatite ash is present in most of the beds except in the yellow maker tuff that is nephelinitic to phonolitic in composition. Xenoliths in the upper unit are nephelinitic but olivine basalt and trachyte are common in other units. Hay suggested that Satiman is the source for the nephelinite lavas and associated tuffs but the source for basalts and trachytes is still unclear, possible sources include Lemagurut and Oldeani volcanoes that are in the vicinity of Laetoli.The K-Ar dates on biotite range from 3.8 - 3.5 Ma for the upper unit and 4.3 - 3.8 Ma for the lower unit (Drake and Curtis 1987). Biotite commonly contains excess Ar that might make these ages too old (McDougall and Harrison, 1999). SCLF $^{40}Ar/^{39}Ar$ analyses of five K-feldspar crystals from a tuff collected from the upper unit by Manega (1993) produced inconsistent ages. Two grains gave an age of 3.76 Ma that are similar to K-Ar dates. One of the crystals produced a younger age of about 1.70 Ma while another produced an older age of 44.34 Ma. The fifth crystal gave an age of 4.1 Ma. These ages show that the tuff is reworked and contaminated. More work to refine the proper age for Laetoli section is underway by A. Deino. Ages for Lemagurut and Oldeani may help to determine the source for Laetoli lavas and xenoliths.

CHAPTER 2: METHODS AND DATA PRESENTATION

METHODS

Field methods

A total of 67 lava samples have been collected from NVHC during field seasons of July 2000 through July 2004. Sample selection is based on availability of outcrops and sample freshness (none of the samples show significant weathering) as well as the presence of datable mineral phases. In order to assure correct assignment of lavas to their respective volcanic centers, samples were collected from inside volcano craters or from volcano tops. Topographic maps, Garmin Global Positioning System (GPS) and compass were used during field orientation. UTM coordinates of all samples sites are provided in Chapter 3 through 6.

Ngorongoro lavas were colleted from the well-exposed Lerai Ascending Road (LAR) section (Figure 2.1). One welded tuff NGDS was collected from the Ngorongoro Western Descending road (WDR) and another one, NGAS from the base of the LAR below NG1.

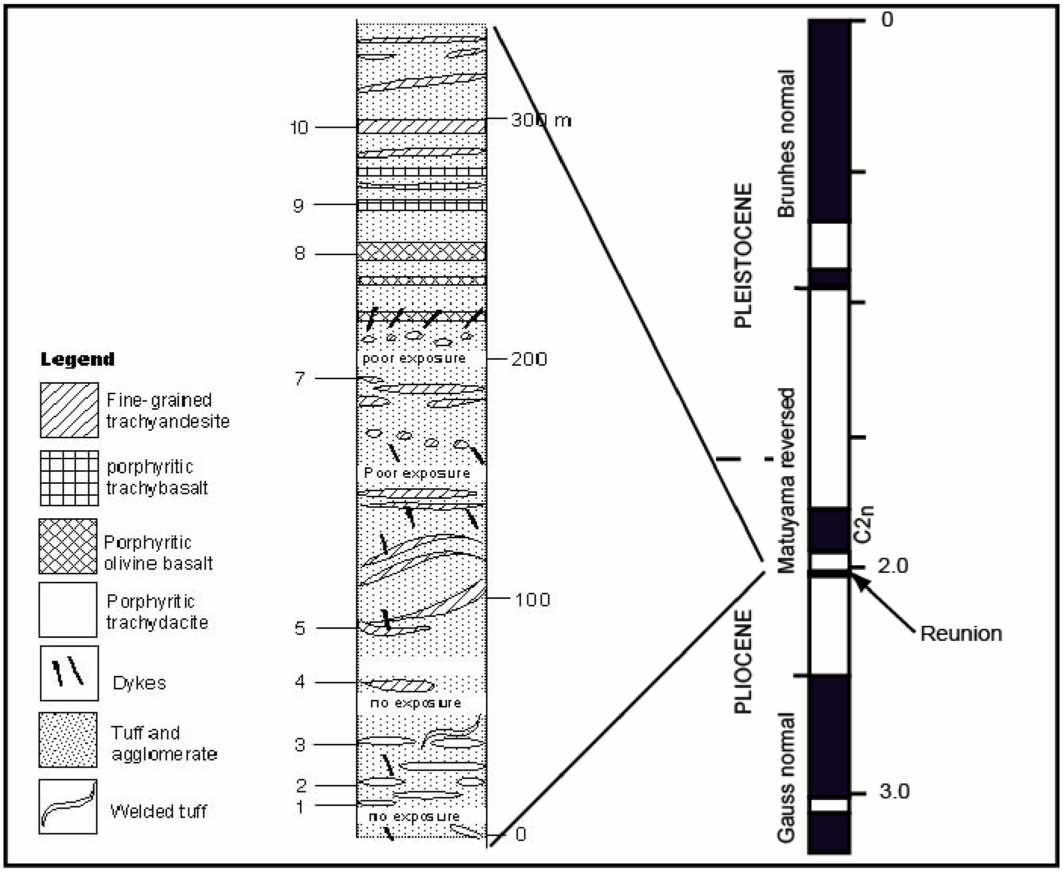

Figure 2.1: Stratigraphy of the Ngorongoro Caldera at the LAR section. Numbers indicates positions where samples were collected (Modified from Grommé *et al.*, 1970). The geomagnetic polarity time scale on the right indicates the position of Reunion event a magnetic transition recorded on the LAR section.

Laboratory methods

In the laboratory, samples were made in to three splits. One split was made into thin sections at the Spectrum Petrographics, Inc. for microscopic and electron microprobe studies. The second split was powdered in a ball-mill-grinder before being sent to the Department of Geological Sciences at Michigan State University (MSU) where major and trace element analyses were made. Following careful study of the thin sections, non weathered samples with K-rich minerals were picked for $^{40}Ar/^{39}Ar$ age analyses.

Optical microscopy

Standard optical microscopy was used to study mineral compositions and textural relations for all the samples. Samples for age determination were picked under a binocular scope to insure sample quality (none weathered).

Electron-microprobe

Selected set of representative samples were studied in detail using an electron microprobe to determine mineral compositions as well as mineral phase relations. Standard 30μm thick thin sections prepared at Spectrum Petrographics, Inc were polished and carbon coated before being analyzed using a Cameca SX100 electron microprobe at the American Museum of Natural History, NY following procedures and standards similar to those of Mandeville *at al*. (2002). Running conditions were 10 nA beam current, 15 KV accelerating voltage and 20 μm beam diameter. A few samples were analyzed by a Cameca XS50 electron microprobe at the University of Wisconsin-Madison, following the procedures and standards outlined in McHenry *et al.* (2007).

X-ray Fluorescence Spectrometry (XRF)

Major elements were determined using an SMAX Rigaku X-ray spectrograph following fundamental parameter method initially introduced by Shiraiwa and Fujino, (1966). This technique does not require putting the samples into solution, thus eliminates problems with insoluble residues. At MSU, rock powders were made into glass disks using high dilution fusion (HDF) technique by mixing the powder with lithium tetraborate as a flux and ammonium nitrate as an oxidizer (Hannah *et al*., 2002). The proportions are 1 gm rock, 9 gm lithium tetraborate and 0.25 gm ammonium nitrate.

These materials are mixed, fused at 1000 °C in a platinum crucible in an oxidizing flame for 30 minutes and then poured into platinum molds. Major element analyses were reduced by the fundamental parameter data reduction method (Criss, 1980) using XRFWIN software. Compared to USGS (AGV-1) standard (Gladney *et al.*, 1988) % error is < ± 3 for all major oxides except for TiO_2 and P_2O_5 where % error is < ± 5.

Laser Ablation Inductive Coupled Plasma (LA-ICP-MS)

Trace and rare earth element concentrations were determined on the same glass disks by Laser Ablation using a Platform Inductively Coupled Plasma Mass Spectrometer (ICP-MS). The procedures followed are similar to those outlined by Hannah *et al.,* (2002). Precision and accuracy of the technique has been checked by comparing the analyses of REE by laser ablation ICP-MS with a well-established analytical method, Instrumental Neutron Activation Analysis (INAA) see Hannah *et al*., (2002). Compared to USGS (AGV-1) standard (Eggins *et al*., 1996), % error for all NVHC lavas is < ± 6 for all trace and REE elements except for Pt, Eu, Gd and Rb where % error is < ± 8.

Thermal Ionization Mass Spectrometry (TIMS)

Selected samples from each volcanic center were analyzed for Sr, Nd and Pb isotopes. The Sr and Nd isotopes analyses were conducted at Rutgers University using a multi-collector GVI Isoprobe Thermal Ionization Mass Spectrometer (TIMS). Sample preparation procedures followed those of Bolge *et al.,* (2006). Measured values for SRM-987 Sr and La Jolla Nd standards were $^{87}Sr/^{86}Sr$ = 0.710237 ± 5 and $^{144}Nd/^{143}Nd$ = 0.511846 ± 2 respectively. Pb isotopes were measured at the University of Rochester, NY following methods similar to those outlined in Basu *et al*. (1991) and Tatsumoto *et al*. (1992).

$^{40}Ar/^{39}Ar$ dating method

The $^{40}Ar/^{39}Ar$ is a standard technique for dating geological processes in both terrestrial and extraterrestrial environments; details on how the method works are given in McDougall and Harrison, (1999). The method requires minerals rich in potassium. The NVHC centers contain anorthoclase, sanidine, nepheline, amphibole and biotite (Hay, 1976; Manega, 1993; Mollel, 2002) as well as lava that contain potassium that is needed for $^{40}Ar/^{39}Ar$ age determinations. A total of 35 samples have been crushed, sieved, between –20 to –40 and –40 to -60 mesh, washed in ultra sonic baths of distilled water and dilute acids where necessary. Minerals rich in K were handpicked under a binocular microscope. Matrix and whole rock lava were purified by removing any altered or secondary materials. The purified samples were loaded into Al sample disks along with aliquots of Alder Creek Sanidine (ACs = 1.194 Ma, Renne *et al*., 2005) or Fish Canyon sanidine (FCs = 28.02 Ma, Renne *et al*., 1998), wrapped in Al foil, sealed in glass quartz tube, and then irradiated in Cadmium-Lined, In-Core Irradiation Tube (CLICIT) facility of the Oregon State University Triga Research Reactor [OSTR] for 15 to 240 minutes. Interference corrections used are $^{36}Ar/^{37}ArCa = 2.72 \pm 0.01(x10^{-4})$, $^{39}Ar/^{37}ArCa = 7.11 \pm 0.024\ (10^{-4})$, and $^{40}Ar/^{39}Ar_K = 7 \pm 3\ (10^{-4})$ (Deino and McBrearty, 2002). Mass discrimination was monitored during the analyses from replicate aliquots delivered from an online air pipette system and J was calculated from replicate analyses of the co-irradiated mineral standards. At Rutgers University Ar-lab, samples were heated in step-wise increments for 60 seconds each using a 40-Watt CO_2 laser focused though a 6mm integrator lens. A few single grain total fusion analyses were done by focusing the laser through a 2 mm integrator lens for 9 second. The released argon isotopes were measured on a MAP215-50 mass spectrometer, and $^{40}Ar/^{39}Ar$ ages calculated using automated software by A. Deino following procedures similar to those outlined in Renne *et al*., (1998) developed based on the following formula:

$t = 1/\lambda \ln(1+J\,^{40}Ar^{*}/^{39}Ar_K)$, modified by (McDougall and Harrison, 1999) from (Mitchell, 1968).

Where:

t = Age of the sample
λ = Decay constant for ^{40}K
$^{40}Ar^{*}$ = Radiogenic ^{40}Ar produced by natural decay ^{40}K
$^{39}Ar_K$ = Radiogenic ^{39}Ar produced by bombarding ^{39}K with fast neutrons
J = Irradiation parameter

Unlike the K-Ar technique, $^{40}Ar/^{39}Ar$ with its laser capability, allows age information to be evaluated at discrete temperature increments. This method is suitable for NVHC lavas that may have experienced low temperature alteration due to the wet and warm East African climate. Age information obtained during low temperature fusion allows the assessment of sample freshness when compared to high temperature ages. This procedure improves both precision and accuracy of the dates.

Plotting the incremental heating data on isochron plot helps address excess Ar issues (McDougall and Harrison, 1999) that are a common problem in NVHC (Evernden and Curtis, 1965; Grommé and Hay, 1971; and Curtis and Hay, 1972).

DATA PRESENTATION

All the major oxides in weight percent (wt %) and trace and rare earth elements in parts per million (ppm) are reported in Chapter 3 through 6. Electron microprobe analyses (point counts) of individual mineral phases are also reported in wt %. Only analyses with totals between 97 and 101 percent are considered correct, low totals may be due to the fact that light elements were not analyzed. The total for oxides is low (as low as 94 wt %) because all the Fe is reported as Fe^{2+}. Other mineral phases with low totals are those containing significant amounts of H_2O (e.g. apatite, biotite, melilite and amphibole). This is because H_2O was not analyzed.

The $^{40}Ar/^{39}Ar$ data are reported as plateaus, inverse isochron (simply isochron) and integrated or total fusion ages. Apparent ages from individual steps were plotted against cumulative percent $^{39}Ar^*$ obtained from all incremental-heating steps. All plateaus ages were calculated following typical procedures constituting at least three contiguous steps that are indistinguishable at 95% confidence level, and totaling at least 50 % of the total $^{39}Ar^*$ released. Detailed evaluation of analytical data used here can be found in Carr *et al*. (2007).

Isochron ages were obtained from a slope resulted by plotting and fitting the atmospheric related $^{36}Ar/^{40}Ar$ component against the radiogenic component $^{39}Ar/^{40}Ar$. Isochron ages were considered reliable if they were analytically indistinguishable from the plateau age and the total fusion age (weighted sum of individual increment ages). The Y-intercept ($^{36}Ar/^{40}Ar$) should be analytically indistinguishable from the atmospheric ratio of 295 ± 1. The quality of the fit obtained by the mixing line between $^{36}Ar/^{40}Ar$ and $^{39}Ar/^{40}Ar$ determines the slope and thus the age. The goodness of the fit is defined as the mean sum of the weighted deviates (MSWD) of individual temperature-increment ages. MSWD is a reduced χ^2 variable that determines the scatter of data about a best-fit linear regression (Bevington, 1969). Results with MSWD >> 1 indicate poor fitting hence large uncertainty. Data with MSWD > 2.5 were considered unreliable (see Turrin *et al.*, 2007; Carr *et al.*, 2007).

CHAPTER 3

RESULTS

Petrology, geochemistry, and age of Satiman, Lemagurut, and Oldeani: sources of the volcanic deposits of the Laetoli area.

Abstract

The petrochemistry and geochronology of lavas from Satiman, Lemagurut and Oldeani volcanoes of the Ngorongoro Volcanic Highland Complex (NVHC) in northern Tanzania are presented. These lavas are proximal and likely sources of volcaniclastic deposit of Pliocene Laetolil Beds. Lava compositions vary between centers, with Satiman composed primarily of foidite and phonolite. Lemagurut ranges from basalt through benmorite and includes hawaiite and mugearite, whereas Oldeani is composed of basalt and trachyandesite. Ogol, derived from small cones in Laetoli area is basaltic. The silica undersaturated Satiman is relatively high in alkali oxides as well as trace elements suggesting it was derived by lesser degree partial melting of the parent compared to the others. Satiman and Oldeani are characterized by unique Zr/Nb values of 2.16 and 5.54 respectively whereas Lemagurut and Ogol share similar ratios of ~3.75 and OIB-normalized trace elements suggest an OIB source.

The Sr-Nd isotopes of these lavas are characterized by relative unradiogenic Nd but with radiogenic Sr ($^{87}Sr/^{86}Sr > 0.7037$), suggesting a source that can be explained by mixing high-μ and enriched mantle reservoir. The $^{87}Sr/^{86}Sr$ ratios are however restricted within centers and when compared to Ngorongoro caldera which has yielded ratios ranging from 0.70405 – 0.70801, these lavas appear to have undergone less crustal contamination. This is also supported by Ce/Pb and Nb/U ratios that are within the range of mantle values (> 25 ± 5 and > 43 ± 10 respectively) for Oldeani and Ogol lavas whereas those of Lemagurut and Satiman are lower.

The $^{40}Ar/^{39}Ar$ dating of these centers indicate an age range for Satiman of 4.63 ± 0.05 Ma to 4.02 ± 0.02 Ma, Lemagurut and Ogol from 2.40 ± 0.01 Ma to 2.22 ± 0.10 Ma

and Oldeani, 1.61 ± 0.01 Ma to 1.52 ± 0.02 Ma. The Satiman age and its silica undersaturated composition make it the likely source of the > 4.3 to 2.5 Ma Laetolil Beds. The similarity in age and composition of Lemagurut and Ogol lavas suggest a common genesis. Age and composition of Naibadad Beds that overly the Laetoli Beds is consistent with the composition and revised ages of 2.29 ± 0.02 Ma to 2.02 ± 0.01 Ma for Ngorongoro. The Olpiro Beds are of phonolitic composition and the fine-grained nature of these ashes may correlate well with the more distal Olmoti Crater (2.01 ± 0.03 Ma to 1.80 ± 0.01 Ma).

BACKGROUND

The Pliocene Laetolil Beds of northern Tanzania, as described by Hay (1987), consists primarily of coarse to fine grained volcaniclastic and sedimentary deposits, rich in vertebrate and invertebrate fossil remains, including hominins. Interbedded air-fall, lahar, water-worked tuff, conglomerates and breccia are considered to be derived from eruptions from the adjacent uplands of the Ngorongoro Volcanic Highland Complex (NVHC). The interbedded volcanics and volcaniclastic deposits of the Laetolil Beds, as well as the younger overlying Naibadad and Olpiro Beds, are correlated to source volcanoes based on their general structure, lithology, and composition. This chapter provides detailed petrography and geochemistry, as well as new $^{40}Ar/^{39}Ar$ ages for the NVHC volcanoes: Satiman, Lemagurut and Oldeani and correlate these with the deposits of the Laetolil sequence. These volcanoes are situated to the south and southwest of the Ngorongoro Caldera (Ngorongoro, Figure 1.2), the source of much of the volcanic materials in the lower part of the nearby Olduvai Beds. Local flows of the Ogol lava that overly the Laetolil Beds are also discussed in relation to NVHC centers.

The closest of the NVHC volcanoes to the Laetoli deposits is Lemagurut, a highly eroded and dissected volcano, today reaching a maximum elevation of 3090 m (Figure 1.2). Descriptions of volcanic clasts from streams draining the Lemagurut (Hay, 1976), indicate that the volcano is composed primarily of trachybasalt and nephelinite. Hay (1976) reported a K-Ar date of 2.39 Ma on a vogesite flow collected in the Laetoli area, interpreted to have originated from Lemagurut. Later, Hay (1987) reinterpreted the vogesite to have instead originated from the Ogol lavas that occur as a series of volcanic remnants that overly the Laetoli Beds (Figure 1.3). Thus, the 2.39 Ma date may not represent Lemagurut activity.

Bagdasaryan *et al*. (1973) reported a K- Ar date of 4.3 Ma on a phonolite from Lemagurut, however, based on its composition, it is more likely that the phonolite is derived from nearby Satiman, as phonolites are unknown from Lemagurut (Mollel, 2002). Manega (1993) reported a $^{40}Ar/^{39}Ar$ age of 1.92 ± 0.04 Ma on an ignimbrite from the western flanks of Lemagurut. However, it is now considered that this ignimbrite is a distal flow originating from Ngorongoro, not Lemagurut.

Satiman is situated to the east, on the far side of Lemagurut from Laetolil, and reaches a maximum elevation of 2880 m. The volcano is highly eroded, lacks any caldera and for the most part is heavily covered by vegetation. Outcrops of Satiman are rare and of limited extent. Satiman consists primarily of nephelinitic and phonolitic lavas (Pickering, 1964; Hay, 1976; Mollel, 2002).The K-Ar dates on nepheline suggest that Satiman was active between 4.5 - 3.7 Ma (Curtis and Hay, 1972; Bagdasaryan *et al*., 1973).

The largest volcano adjacent to the Laetolil Beds is the 3000 m high Oldeani volcano, located southeast of Satiman and southwest of Ngorongoro. Pickering (1964), described Oldeani as consisting primarily of basalt. No dates have been reported previously for Oldeani. However, based on the degree of weathering of its slopes and adjacent valleys, it was thought to fall within the range of activity of Ngorongoro and Lemagurut. Based on similarity in lava composition, Oldeani has been inferred to be the source for stone tools recovered from the hominin bearing Upper Ngaloba Beds that overly the Laetolil Beds (Adelsberger *et al*., 2002).

Hay (1987) described scoriaceous lavas that overly the Laetolil Beds southwest of Lemagurut, associated with a series of cones or vents. The outcrops are of limited extent and were collectively grouped as the Ogol lavas. The Ogol lavas lie in an east-west orientation extending about 25 km in length, about 15 km from the lower limits of Lemagurut. Individual flows range from 0.5 to 1.5 km in length and 50 to 150 m above the Laetoli beds. Most of these flows have rounded erosional tops, although Hay (1987) reported one to the southeast edge of the Laetoli area to have a well-preserved crater. According to Hay (1987), the Ogol lavas are porphyritic with phenocrysts of olivine, augite, alkali feldspar, and biotite and may include plagioclase, nepheline and opaque minerals. Hay (1987) reported reverse magnetic polarity on the Ogol lavas, based on field measurements obtained by Alan Cox of Stanford University. Drake and Curtis (1987) gave whole rock K-Ar dates on vogesite ranging from 2.52 to 2.21 Ma, with a mean age of 2.41 Ma, placing the Ogol lavas within the lower Matuyama Chron (Cox, 1969). The age and reverse polarity of the Ogol lavas suggests correlation with activity of Ngorongoro.

METHODS

Field methods

A total of 33 lava samples were collected from Lemagurut, Satiman, and Oldeani volcanoes and Ogol flows between 2000 through July 2004. Samples were taken from the tops and flanks of Satiman, Lemagurut and Oldeani to ensure unambiguously assignment to those particular volcanoes. Samples collected from lower elevations, as part of previous studies, are thus now known to be distal flows from various volcanic centers.

Sample selection was based on availability of outcrops, sample freshness and the presence of datable mineral phases. Locations of sampled sites are provided in UTM coordinates (Table 3.1).

Laboratory methods

Samples were examined in the laboratory using binocular and petrographic microscopes. Thin sections were made and analyzed prior to all dating and chemistry sample preparations. Representative samples were prepared for $^{40}Ar/^{39}Ar$ dating, major and minor elemental analyses by X-ray fluorescence, trace elemental analyses by LA-ICPMS (Laser Ablation Inductively Coupled Plasma Mass Spectrometry), Sr and Nd by TIMS (Thermal Ionization Mass Spectrometry), and elemental phase determinations by electron microprobe.

Major and trace element analyses

Splits of all samples were pulverized and powdered. At Michigan State University, the powders were fused into glass discs using high dilution fusion (HDF) technique by mixing the powder with lithium tetraborate as a flux and ammonium nitrate as an oxidizer. Major and minor elements were determined by X-ray fluorescence using a SMAX Rigaku X-ray spectrograph. Trace elements were determined using LA-ICPMS following procedures similar to those of Hannah *et al.* (2002). Analytical data were monitored using co-analyzed USGS rock standards. Major element oxides in weight percent (wt %) and trace elements in parts per million (ppm) are given in Table 3.1.

Sr and Nd isotope analyses

Sr and Nd isotopic analyses were made on selected samples from Satiman, Lemagurut, Oldeani and Ogol, at Rutgers University (RU) using a multicollector GVI Isoprobe TIMS. Sample preparation followed the method of Bolge *et al*. (2006). Measured values for SRM-987 Sr and La Jolla-Nd standards were $^{87}Sr/^{86}Sr = 0.710237 \pm 5$ and $^{144}Nd/^{143}Nd = 0.511846 \pm 2$ respectively. Analyses are reported in Table 3.1.

Table 3.1: UTM coordinate of locations, major and trace elements, and Sr, and Nd isotope analyses of lavas from volcanics associated with Laetolil area

Sample	03-OLDI-1	03-OLDI-2	03-OLDI-3	03-OLDI-4	03-OLDI-5	03-OLDI-6	04-OLDI-1A	04-OLDI-1B	04-OLDI-2	04-OLDI-3	04-OLDI-4	01-SM-1	01-SM-2	01-Sm-3	01-Sm-4	01-Sm-5	00-SM-5	04-NT-3
UTM E	761335	762177	762318	762724	763286	763460	768361	768361	770104	769777	768331	766339	766403	767024	768029	768059	763994	747715
UTM S	9632496	9633434	9633420	9633574	9633408	9633394	9640028	9640028	9639102	9640084	9641768	9646910	9646618	9646684	9647014	9646774	9645907	9634578
XRF	data																	
SiO2	50.1	49.5	46.4	52.0	50.1	52.2	52.4	51.6	52.2	54.1	52.8	45.3	45.7	41.9	51.0	44.4	53.0	53.6
TiO2	3.3	3.4	3.3	3.1	3.0	3.0	3.0	2.8	2.8	2.1	2.7	1.9	1.8	2.0	0.6	1.9	0.7	1.1
Al2O3	14.6	14.6	14.2	15.4	14.7	15.1	16.1	15.0	15.0	16.8	15.5	17.7	17.6	13.5	18.4	15.7	19.6	19.7
FeO	12.7	13.5	13.2	11.9	12.7	11.6	12.5	11.8	11.9	9.7	11.7	9.1	8.8	13.1	8.3	10.9	6.4	6.6
MnO	0.2	0.2	0.2	0.1	0.2	0.2	0.2	0.2	0.2	0.1	0.2	0.2	0.2	0.4	0.2	0.3	0.2	0.2
MgO	3.7	3.8	3.5	3.2	4.2	3.1	1.8	3.4	3.1	2.2	2.9	1.8	1.6	2.2	0.2	1.8	0.4	0.7
CaO	7.8	8.2	10.3	7.2	7.6	6.8	5.7	6.8	6.6	6.1	6.7	7.7	7.1	9.5	2.9	8.2	2.9	2.9
Na2O	3.8	3.5	3.3	4.1	3.7	4.4	3.8	3.9	4.0	4.6	3.6	6.9	7.0	6.9	9.8	8.8	9.7	8.9
K2O	1.3	1.3	1.2	1.6	1.3	1.8	1.6	1.6	1.7	1.8	1.6	4.2	2.5	3.8	6.3	3.2	4.7	4.9
P2O5	0.5	0.4	0.4	0.6	0.5	0.6	0.6	0.6	0.6	0.5	0.5	0.3	0.3	0.5	0.1	0.3	0.1	0.2
Total	97.9	98.6	96.1	99.1	98.0	98.7	97.6	97.7	98.0	98.1	98.1	95.2	92.5	93.9	97.8	95.5	97.6	98.6
LA ICP MS	data																	
Rb	27.7	32.5	28.5	32.5	25.7	39.7	41.0	40.0	41.0	39.0	40.0	93.0	70.0	124.0	164.0	83.0	113.5	132.0
Sr	582.2	626.7	609.3	607.2	591.9	655.9	901.0	676.0	634.0	702.0	661.0	1892.0	1022.0	1700.0	1873.0	1131.0	1401.1	1412.0
Zr/Nb	5.61	5.3	5.42	5.4	4.8	6.08	5.09	5.02	5.02	5.51	5.46	1.79	1.86	2.48	2.72	2.11	2.03	1.24
Zr	308.9	247.7	243.6	302.4	286.1	339.1	347.0	324.0	336.0	331.0	309.0	352.8	350.8	525.7	444.7	501.2	422.0	210.0
Ba	477.5	566.3	495.5	539.7	551.9	569.5	963.6	543.8	569.9	623.1	592.0	1434.9	1362.0	1545.8	2397.2	1278.0	1602.3	1695.7
La	51.2	47.0	43.0	53.8	55.7	55.2	78.1	59.4	67.9	59.8	58.1	138.7	115.8	91.9	115.2	130.6	155.0	118.8
Ce	93.5	83.3	80.7	94.3	100.9	100.4	101.9	101.1	108.2	100.7	98.5	213.6	167.3	103.7	149.7	194.4	241.1	179.6
Pr	12.0	11.0	10.4	12.6	13.3	13.2	16.1	13.3	15.9	13.4	13.1	22.9	17.8	10.8	14.4	21.9	21.8	18.5
Nd	47.4	43.7	41.6	50.9	53.2	53.2	65.0	53.5	65.0	53.7	53.0	79.5	60.7	36.3	44.5	78.8	66.7	61.2
Sm	9.6	8.8	8.4	10.1	10.6	10.7	12.1	10.0	12.9	9.8	9.9	12.7	10.2	7.6	7.5	13.7	10.0	8.9
Eu	2.9	2.7	2.6	3.1	3.3	3.2	3.8	2.9	3.9	3.0	2.9	3.5	3.0	2.5	2.2	3.8	2.9	2.5
Gd	9.2	8.4	7.9	9.6	10.1	9.7	13.1	10.7	13.7	10.3	10.3	12.9	11.1	8.9	8.8	13.7	9.3	11.5
Tb	1.3	1.2	1.1	1.3	1.4	1.4	1.7	1.4	1.9	1.3	1.3	1.6	1.5	1.4	1.2	1.8	1.2	1.1
Y	36.6	30.5	29.4	37.2	39.7	37.7	47.7	38.9	51.7	36.8	38.9	33.6	33.4	47.7	36.2	43.7	36.4	31.4
Dy	6.8	6.1	5.7	7.0	7.3	7.0	8.8	7.1	9.8	6.4	6.9	6.8	6.4	7.6	5.7	8.2	6.0	5.2
Ho	1.3	1.2	1.1	1.4	1.4	1.4	1.7	1.3	1.9	1.2	1.3	1.3	1.2	1.6	1.2	1.6	1.3	1.0
Er	3.4	2.8	2.7	3.3	3.5	3.3	3.9	3.1	4.5	2.9	3.0	3.1	2.9	4.1	3.2	4.1	3.4	2.6
Yb	3.4	2.7	2.6	3.2	3.3	3.1	3.9	3.0	4.5	2.7	2.9	6.2	5.5	5.6	5.7	6.7	3.2	2.9
Lu	0.4	0.3	0.3	0.4	0.4	0.4	0.6	0.4	0.7	0.4	0.4	0.4	0.4	0.5	0.4	0.5	0.5	0.4
V	241.0	258.4	179.5	194.7	129.5	250.5	137.3	141.7	131.8	109.1	423.4	133.0	99.0	238.4	54.6	138.2	32.0	40.8
Cr	14.9	3.9	3.8	6.2	2.0	47.1	4.5	3.9	3.3	4.7	16.5	2.9	1.5	1.9	1.8	4.2	17.5	3.6
Nb	55.1	46.7	44.9	56.0	59.6	55.8	68.2	64.6	67.0	60.1	56.6	197.4	189.1	212.4	163.4	237.5	208.1	169.2
Hf	8.2	6.5	6.3	8.4	8.1	8.2	9.0	8.4	8.7	8.2	7.6	8.0	7.6	10.7	8.8	11.1	7.8	5.9
Ta	3.6	3.1	3.0	3.7	3.8	3.6	4.1	3.8	4.0	3.4	3.2	9.8	8.6	4.5	3.1	10.5	5.9	7.8
Pb	3.9	3.5	1.8	4.0	3.7	3.9	5.1	3.8	4.1	6.6	4.7	9.2	8.4	14.0	22.1	10.8	41.1	14.4
Th	6.3	5.6	5.5	6.5	6.9	6.3	8.1	7.4	8.1	8.5	7.4	22.8	16.4	5.7	26.9	16.5	39.0	24.5
U	1.1	0.9	0.6	1.0	1.3	0.9	1.5	1.2	1.3	1.3	1.2	3.0	2.7	4.4	4.4	2.7	6.8	0.6
TIMS	data																	
87Sr/86Sr	0.70406	0.70432	0.70476		0.70427									0.70412	0.70527	0.70609		0.70630
.43Nd/144N	0.51250	0.51248	0.51239		0.51239										0.51240	0.51206		

Table 3.1 continued

Sample	00-LM-3	00-LM-4	00-LM-5	00-LM-6	00-LM-7	00-LM-8	02-LM-1	02-LM-2	02-LM-3	02-LM-4	04-OS-1	04-OS-2	04-OS-3	04-OS-4	04-OS-5	04-OG-1	04-OG-2	04-OG-3	04-OG-4
UTM E	763806	764002	764010	765702	765714	764257	756819	759091	759091	759091	754434	754534	754996	755157	756058	741129	748119	747489	739719
UTM S	9658840	9646167	9646244	9648519	9648623	9647742	9656243	9657156	9657156	9657156	9643730	9643654	9643374	9643570	9643206	9642378	9644426	9644950	9644638
XRF	data																		
SiO2	44.9	45.7	53.7	55.5	54.8	52.2	51.4	50.7	50.6	50.0	57.1	57.5	57.3	57.2	48.0	43.8	45.5	45.6	46.2
TiO2	2.5	3.6	2.0	1.9	1.4	2.0	1.9	2.6	2.7	2.8	1.4	1.5	1.5	1.5	3.1	3.1	3.0	3.0	3.2
Al2O3	10.3	13.2	17.3	17.4	17.5	17.4	16.8	15.9	16.0	15.5	18.0	17.9	17.7	17.8	9.5	7.4	9.4	9.2	10.8
FeO	14.6	15.9	9.2	9.1	8.2	9.6	8.8	10.9	11.3	11.7	7.3	7.5	7.6	7.5	15.6	14.8	14.5	14.4	14.4
MnO	0.2	0.2	0.2	0.2	0.2	0.2	0.2	0.2	0.2	0.2	0.2	0.2	0.2	0.2	0.2	0.2	0.2	0.2	0.2
MgO	10.0	5.2	2.1	2.1	1.5	2.2	2.5	3.1	3.0	3.2	1.6	1.6	1.7	1.8	9.8	11.2	11.4	11.7	7.8
CaO	11.4	8.2	5.4	4.9	3.9	5.1	5.1	5.9	6.1	6.3	4.0	3.9	4.0	4.1	10.2	14.2	10.8	11.3	11.1
Na2O	2.2	4.1	5.2	5.6	6.2	5.3	4.8	4.2	4.0	3.8	5.9	5.9	5.9	6.0	2.2	1.6	2.7	2.2	2.8
K2O	0.9	1.8	2.4	2.5	3.1	2.6	2.6	2.6	2.6	2.6	3.3	3.2	3.3	3.3	1.1	0.9	1.1	1.1	1.3
P2O5	0.3	0.6	0.8	0.7	0.5	0.8	0.6	0.8	0.8	0.8	0.5	0.5	0.5	0.5	0.3	0.5	0.4	0.4	0.5
Total	97.2	98.6	98.4	99.8	97.3	97.2	94.6	96.7	97.2	96.8	99.1	99.7	99.6	99.7	99.8	97.6	99.1	99.0	98.2
LA ICP MS	data																		
Rb	21.6	42.3	53.4	66.8	81.3	61.9	62.0	70.0	67.0	62.0	92.0	80.0	85.0	84.0	34.0	23.0	24.0	24.0	30.0
Sr	535.3	1040.5	1210.3	1294.1	1103.2	1169.4	1293.0	1198.0	1419.0	1348.0	1688.0	1087.0	1289.0	1059.0	424.0	522.0	626.0	616.0	762.0
Zr/Nb	3.44	3.6	3.92	3.52	3.76	4.05	3.32	3.68	3.53	3.58	3.54	3.55	3.62	3.63	4.82	4.04	3.58	3.53	3.79
Zr	190.5	368.5	438.8	430.2	499.7	475.3	423.0	395.0	399.0	382.0	438.0	436.0	455.0	449.0	176.0	191.0	213.0	207.0	246.0
Ba	403.6	853.6	1151.2	1104.9	1386.2	1172.2	1079.5	1051.7	986.6	931.3	1558.1	2064.0	1111.6	1301.3	358.9	593.1	475.8	468.5	567.3
La	48.0	88.6	111.3	104.9	110.8	135.1	105.8	95.0	98.4	92.7	103.2	121.2	103.1	106.1	48.1	40.1	54.9	49.7	57.6
Ce	87.6	158.9	208.8	196.8	206.1	194.7	180.5	165.0	168.0	160.7	176.4	181.9	176.0	180.2	63.0	73.6	92.2	85.6	98.9
Pr	10.0	20.2	23.3	22.6	22.5	27.5	22.3	21.3	21.4	20.4	20.9	22.0	20.9	21.3	11.0	10.0	12.0	11.4	13.0
Nd	38.9	79.1	86.7	83.4	81.0	102.4	83.0	83.5	82.7	79.2	74.0	79.8	76.9	77.5	44.1	41.0	47.8	46.6	52.1
Sm	7.7	14.0	14.8	14.8	13.5	17.3	13.6	14.3	14.2	13.6	11.9	12.4	12.6	12.2	8.1	8.5	8.8	8.4	9.2
Eu	2.2	3.9	4.4	4.2	3.9	4.7	3.9	4.0	4.0	3.8	3.4	3.5	3.5	3.4	2.3	2.6	2.6	2.4	2.7
Gd	7.1	11.8	12.7	12.8	11.4	14.8	15.0	15.4	15.0	15.3	13.6	14.2	14.3	13.8	8.1	8.9	9.2	8.8	9.7
Tb	1.0	1.5	1.7	1.7	1.5	1.9	1.7	1.7	1.7	1.7	1.5	1.6	1.5	1.5	1.1	1.1	1.1	1.0	1.1
Y	25.6	39.2	39.5	42.4	39.8	53.6	41.0	40.9	41.5	41.0	37.7	46.3	37.8	37.1	27.3	21.6	26.5	25.4	28.8
Dy	5.0	7.8	7.7	8.0	7.2	9.7	7.6	8.0	8.0	7.7	6.9	7.3	6.8	7.0	5.4	5.0	5.3	4.9	5.5
Ho	0.9	1.4	1.4	1.3	1.3	1.8	1.4	1.5	1.5	1.4	1.3	1.4	1.3	1.3	1.0	1.0	0.9	0.9	1.0
Er	2.2	3.3	3.4	3.6	3.1	4.4	3.2	3.3	3.4	3.1	3.0	3.4	3.1	3.0	2.4	2.5	2.2	1.9	2.2
Yb	2.0	2.8	3.1	3.1	3.3	3.9	3.2	3.3	3.3	3.2	3.2	3.6	3.3	3.2	2.4	2.6	2.0	1.8	2.1
Lu	0.3	0.4	0.5	0.4	0.4	0.5	0.4	0.4	0.4	0.4	0.4	0.5	0.4	0.4	0.3	0.4	0.3	0.3	0.3
V	333.4	299.0	89.0	44.9	17.9	69.0	46.7	100.5	101.1	114.6	22.2	23.5	21.3	24.8	335.5	271.6	260.5	258.5	217.7
Cr	494.9	43.0	20.7	14.7	15.2	13.1	3.4	4.8	4.9	6.1	4.3	4.5	3.9	3.6	537.5	863.2	538.3	574.5	513.9
Nb	55.4	102.4	112.0	122.2	133.0	117.4	127.5	107.4	112.9	106.8	123.9	122.7	125.8	123.7	36.5	47.3	59.5	58.6	64.9
Hf	4.5	8.7	9.3	9.6	10.7	11.1	10.3	10.0	10.3	8.9	10.3	10.6	10.9	10.3	4.6	5.6	5.4	5.3	6.1
Ta	3.0	6.0	5.9	6.7	7.3	6.4	7.1	6.2	6.4	5.6	6.7	6.5	6.8	6.6	2.2	2.9	3.5	3.2	3.6
Pb	4.4	15.1	13.7	14.3	17.2	12.7	9.9	9.3	9.5	8.8	12.8	11.5	12.8	11.6	4.2	3.0	4.0	3.7	1.7
Th	6.2	10.5	12.1	13.8	16.2	14.1	15.9	13.7	13.7	11.8	16.7	15.8	16.7	16.0	6.5	4.7	6.3	6.0	6.8
U	1.3	2.3	2.5	1.4	3.0	1.7	2.7	2.4	2.6	1.5	3.5	1.7	3.3	2.7	0.6	0.7	1.1	0.9	1.1
TIMS	data																		
87Sr/86Sr		0.70472		0.70503				0.70472			0.70519		0.70517	0.70522		0.70375	0.70371	0.70379	0.70381
143Nd/144Nd		0.51246		0.51241				0.51247			0.51219		0.51238	0.51238		0.51261	0.51257		0.51255

Mineral Phase analyses

Mineral phases were determined using a Cameca SX100 electron microprobe at the American Museum of Natural History, following procedures and standards similar to those of Mandeville e*t al*. (2002). Running conditions were 10 nA beam current, 15 KV accelerating voltage and 20 μm beam diameter. Samples were also analyzed at Rutgers University using a JEOL-8600 electron microprobe (see Mollel, 2002). At RU, the same beam current was used; accelerating voltage was set at 20 KV with a beam diameter of one micrometer. Microprobe analyses (point counts) are reported in Table 3.2 as oxides in wt %.

$^{40}Ar/^{39}Ar$ dating

Representative samples from all volcanic centers were crushed and sieved to a size of 0.425 to 0.25 mm and washed in ultrasonic baths of distilled water. Minerals rich in K were handpicked under a binocular microscope. Matrix (crushed whole rock) was purified by removing any altered or secondary materials. The purified samples were loaded in Al sample disks along with aliquots of the Fish Canyon sanidine or Alder Creek sanidine standards, wrapped in Al foil, sealed in quartz glass tubes, and then irradiated in the Cadmium-Lined, In-Core Irradiation Tube [CLICIT] facility of the Oregon State University Triga Research Reactor [OSTR]. Interference corrections used are $^{36}Ar/^{37}Ar_{Ca}$ = 2.72 ± 0.01(x10^{-4}), $^{39}Ar/^{37}Ar_{Ca}$ = 7.11 ± 0.024 (10^{-4}), and $^{40}Ar/^{39}Ar_{K}$ = 7 ± 3 (10^{-4}) (Deino and McBrearty, 2002). At the Rutgers University Ar-lab, about 100 milligrams of the matrix were heated in step-wise increments for 60 seconds each using a 40 Watt CO_2 laser defocused though a 6mm integrator lens. The released argon isotopes were measured on a MAP215-50 mass spectrometer, and $^{40}Ar/^{39}Ar$ ages calculated using automated software by A. Deino following procedures similar to those outlined in Renne *et al*. (1998). Plateau, isochron and total fusion ages are reported in Table 3.3. All plateaus ages were calculated following typical procedures constituting at least three contiguous steps, and totally at least 50 % of the total ^{39}Ar released. Detailed evaluation of analytical data can be found in Carr *et al.* (2007) and Turrin *et al.* (2007).

RESULTS

Petrography

Lavas from the NVHC volcanoes associated with the Laetolil deposits are alkaline, silica undersaturated to silica saturated compositions. The silica undersaturated lavas (see results in Table 3.1) are restricted Satiman and include foidite and phonolite (Figure 3.1). The silica saturated lavas are from Lemagurut, Oldeani, and Ogol. Lemagurut ranges in composition from basalt through benmorite, and includes hawaiite and mugearite. Oldeani lavas range from basalt to trachyandesite, while Ogol flows are primarily basaltic in composition.

The silica undersaturated (Satiman) and saturated (Lemagurut, Oldeani, and Ogol) lavas display distinct textural features and mineral assemblages. Foidite and phonolite from Satiman are primarily porphyritic. The phenocrysts are nepheline and augite and occasionally andradite in a groundmass of augite and nepheline (Figure 3.2a; Table 3.2). The main oxide mineral is titanomagnetite, other minerals are apatite, olivine, titanite, and sanidine. The augite is commonly zoned and embayed, and its composition ranges from $En_{32}Fs_{18}Wo_{50}$ to $En_{10}Fs_{48}Wo_{42}$, concentrations of TiO_2 and Na_2O range up to 1.5 and 4.6 wt % respectively. Nepheline compositions from different crystals range from $Na_{5.41}K_{0.82}Al_{5.4}Si_{6.3}O_{24}$ to $Na_{2.94}K_{0.84}Al_{5.5}Si_{6.8}O_{24}$. Andradite is cubic shaped, pink to dark brown, and its average composition is $Ca_{6.1}(Fe_{1.8}Ti_{2.4})(Fe_{1.1}Si_{4.9})O_{24}$. The Satiman andradite is schorlomitic (TiO_2 >15 wt %; Mollel, 2002), and is different from pyrope garnet found in Lashaine and Labait in northern Tanzania that are characterized by relatively low TiO_2 contents < 8.5 wt % (Jones et al., 1983, Lee and Rudnick, 1999). One sample contains sanidine laths ranging in composition from $Ab_{51}Or_{49}$ to $Ab_{47}Or_{53}$ (Mollel, 2002). Titanomagnetite is ophitic with augite and nepheline, low in Ti (14.33 wt %) and rich in Mn (1.57 wt %).

Lavas from Lemagurut are phaneritic, mostly fine to medium grained and occasionally porphyritic, ranging in composition from basalt through hawaiite, mugearite and benmorite. The Lemagurut mineral assemblage includes augite, plagioclase, anorthoclase, and titanomagnetite, sodic and titanian amphibole ± olivine and fluoroapatite (Figure 3.2b; Table 3.3). The phenocrysts are of plagioclase, augite, olivine and occasionally amphibole in a groundmass of plagioclase, anorthoclase and augite. Feldspar composition ranges from $An_{14}Ab_{64}Or_{22}$ to $An_{27}Ab_{64}Or_{9}$. Augite is occasionally zoned, its composition ranging between $En_{41}Fs_{15}Wo_{44}$ and $En_{32}Fs_{22}Wo_{46}$ and containing up to 3 wt % TiO_2. Olivine phenocrysts range in composition between forsteritic ($Fo_{65}Fa_{35}$) in the most basaltic to fayalitic ($Fo_{30}Fa_{70}$) in the most evolved lava. Titanomagnetite is ophitic with augite and olivine and its TiO_2 content ranges from ~23 - 25 wt %. The titanomagnetite is Al_2O_3 and MnO rich, with concentrations ranging between 1.4-0.7 and 1.3-0.4 wt % respectively. One sample contains rare phenocrysts of kaersutite and fluororichterite.

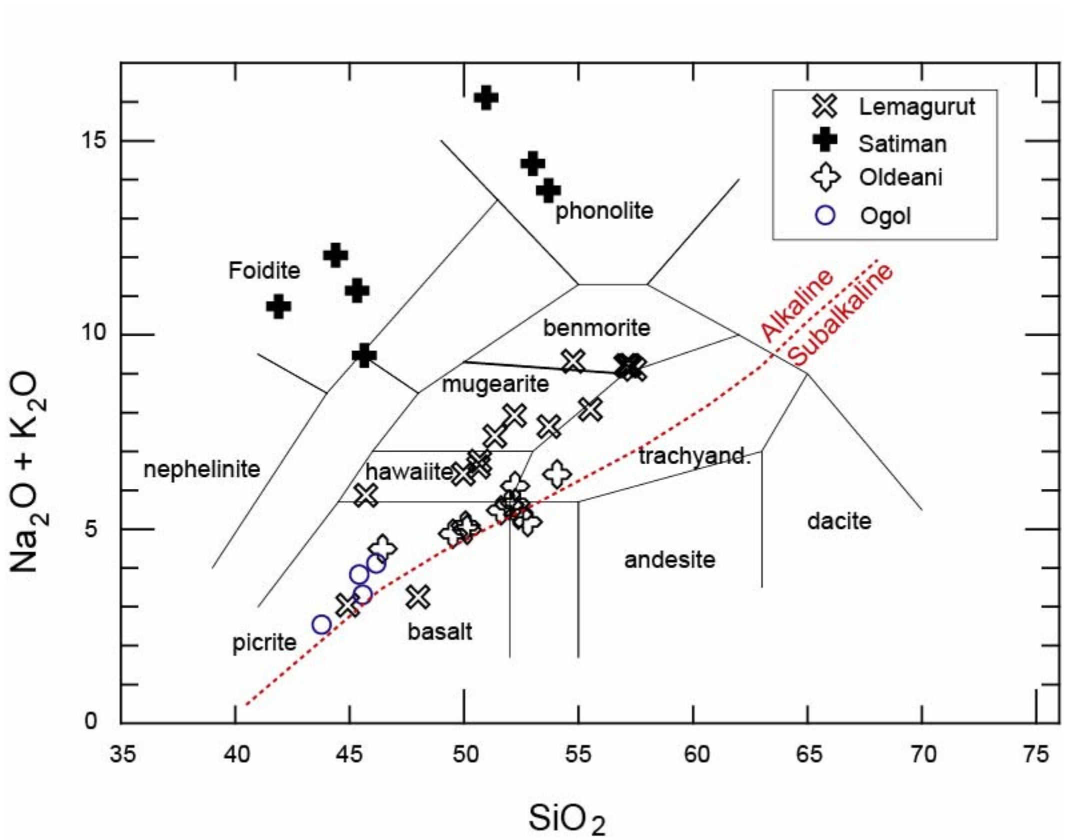

Figure 3.1. Total Alkali versus Silica classification of Cox *et al.* (1979) for NVHC rock types associated with the Laetolil Beds.

Table 3.2: Satiman mineral compositions (electron microprobe analyses)

Pyroxene	SiO2	TiO2	Al2O3	MgO	MnO	FeO	CaO	Na2O	K2O	P2O5	BaO	Total
1	49.66	1.01	1.32	6.46	0.64	18.14	20.39	3.15	0.01	0.00	0.15	100.92
2	50.13	1.05	1.11	5.73	0.56	19.61	18.47	3.82	0.03	0.01	0.00	100.51
3	50.31	0.96	1.11	5.93	0.65	19.58	18.64	3.86	0.01	0.00	0.07	101.11
4	51.21	1.29	0.88	5.60	0.62	19.67	17.04	4.57	0.00	0.02	0.00	100.90
5	49.00	1.54	3.20	11.00	0.31	11.00	23.00	1.00	0.00	0.00	0.07	100.12
Andradite												
1	28.00	15.00	0.45	0.56	0.36	20.00	32.00	0.28	0.00	0.00	0.25	97.50
2	29.00	15.00	0.23	0.73	0.32	21.00	31.00	0.39	0.00	0.00	0.21	97.89
3	27.00	18.00	0.45	0.70	0.33	19.00	32.00	0.37	0.00	0.00	0.20	98.21
Nepheline												
1	46.86	0.10	28.71	0.32	0.09	3.58	1.25	17.00	3.21	0.02	0.00	101.13
2	46.57	0.00	31.42	0.06	0.01	1.94	0.00	17.39	3.77	0.00	0.15	101.30
3	42.00	0.00	32.00	0.08	0.00	1.35	0.03	17.00	6.70	0.00	0.01	99.91
4	42.00	0.04	34.00	0.00	0.00	1.51	0.32	16.00	6.10	0.00	0.04	100.12
5	41.00	0.06	31.00	0.00	0.02	3.60	0.06	16.00	8.30	0.00	0.00	100.63
Apatite												
1	0.83	0.00	0.00	0.01	0.02	0.12	57.75	0.06	0.04	39.21	0.09	98.12
Tmagnetite												
1	0.03	14.62	0.00	0.06	1.56	78.90	0.00	0.01	0.01	0.00	0.00	95.19
2	0.50	14.38	0.06	0.03	1.41	76.07	1.24	0.11	0.02	0.79	0.00	94.58
3	0.07	14.49	0.05	0.03	1.52	78.39	0.02	0.03	0.01	0.01	0.04	94.65
4	0.02	14.03	0.05	0.04	1.90	78.51	0.00	0.02	0.01	0.03	0.05	94.64
5	0.47	14.18	0.16	0.04	1.29	77.79	0.06	0.04	0.04	0.02	0.00	94.10
Feldspar												
1	65.32	0.18	20.26	0.01	0.00	0.26	0.23	7.47	5.88	0.01	0.47	100.07
2	65.61	0.07	19.72	0.00	0.02	0.51	0.26	6.83	6.32	0.00	0.98	100.31
3	64.86	0.11	18.94	0.00	0.00	0.42	0.14	5.72	8.58	0.00	0.17	98.94
Titanite												
1	29.95	37.55	1.54	0.02	0.02	1.28	30.14	0.03	0.00	0.06	0.11	100.69
2	32.55	34.09	3.52	0.01	0.05	1.68	26.52	1.78	0.50	0.02	0.00	100.74
3	30.00	37.00	0.53	0.00	0.04	1.95	27.00	0.22	0.10	0.00	1.82	98.25

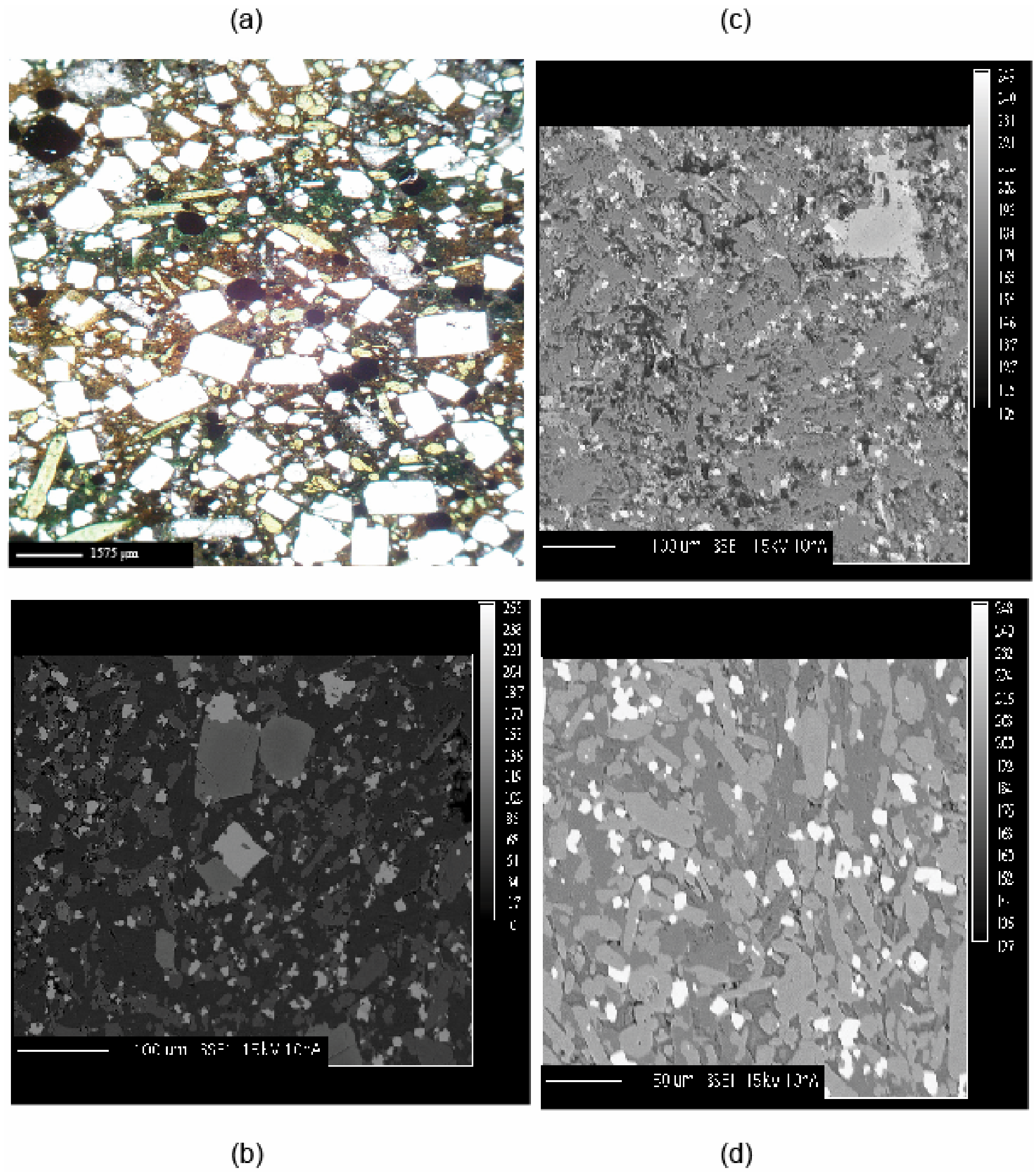

Figure 3.2. (a) Microphotograph of porphyritic foidite from Satiman volcano showing abundant titanian andradite (red and black “cubes”) sitting on nepheline (white tabular grains) and augite (green lath-shaped grains). (b) Back-Scatter Electron microprobe (BSE) image of Lemagurut basalt showing abundant feldspar (dark gray), augite (light gray), large olivine (at the middle of the image) and titanomagnetite (white specks). (c) Back-Scatter Electron (BSE) image of fine-grained Oldeani basalt showing abundant feldspar and a large olivine grain on top right. The white specks are of titanomagnetite. (d) Back-Scatter Electron (BSE) image of Ogol basalt showing near equigranular texture. Abundant pyroxene and olivine (200-220 on the gray scale) sitting on plagioclase dark colored. The white specks are of titanomagnetite.

Table 3.3: Lemagurut mineral compositions (electron microprobe analyses)

Olivine	SiO2	TiO2	Al2O3	MgO	MnO	FeO	CaO	Na2O	K2O	P2O5	F	Total
1	37.42	0.12	0.00	35.03	0.30	27.90	0.25	0.00	0.00	0.05	0.05	101.11
2	37.73	0.05	0.01	35.49	0.36	27.10	0.24	0.04	0.01	0.00	0.00	101.04
3	34.82	0.12	0.00	23.66	0.64	41.61	0.34	0.01	0.02	0.02	0.06	101.28
4	35.26	0.08	0.00	25.52	0.52	39.12	0.35	0.00	0.00	0.00	0.10	100.95
Pyroxene												
1	51.09	1.03	1.49	11.57	0.63	13.35	20.81	0.74	0.05	0.00	0.07	100.83
2	51.74	0.88	1.03	11.80	0.68	12.91	21.04	0.68	0.02	0.00	0.08	100.87
3	49.00	2.52	3.63	14.00	0.24	10.00	21.00	0.62	0.01	0.00	0.00	100.50
4	50.92	0.91	1.32	11.20	0.53	12.89	21.07	0.86	0.03	0.01	0.09	99.84
5	48.00	3.01	4.66	14.00	0.28	10.00	21.00	0.63	0.02	0.00	0.00	100.94
6	54.26	0.54	1.41	17.63	0.09	5.29	20.75	0.36	0.00	0.01	0.00	100.33
Feldspar												
1	65.34	0.04	21.96	0.00	0.00	0.55	1.93	8.65	2.38	0.05	0.00	100.89
2	66.12	0.10	19.98	0.04	0.00	0.58	0.24	5.38	8.26	0.01	0.04	100.74
3	66.20	0.12	21.18	0.00	0.00	0.37	1.12	7.81	4.24	0.00	0.01	101.04
4	66.09	0.14	20.73	0.00	0.00	0.38	0.89	7.27	5.37	0.00	0.00	100.86
5	64.46	0.10	22.63	0.04	0.00	0.48	2.61	8.36	2.29	0.00	0.00	100.96
6	65.92	0.06	22.80	0.04	0.00	0.53	2.68	4.95	2.28	0.05	0.00	99.31
7	66.59	0.12	20.91	0.00	0.02	0.36	0.87	7.73	4.73	0.00	0.01	101.34
8	66.00	0.06	20.87	0.01	0.00	0.30	0.85	6.80	6.05	0.04	0.00	100.99
9	65.94	0.10	20.44	0.02	0.01	0.54	0.63	5.93	7.11	0.00	0.00	100.73
10	66.25	0.14	20.87	0.00	0.00	0.36	0.78	7.38	5.46	0.02	0.00	101.26
Tmagnetite												
1	0.11	24.12	1.21	0.65	1.26	68.83	0.01	0.08	0.01	0.00	0.12	96.38
2	0.04	23.68	1.18	0.71	1.19	72.22	0.00	0.03	0.01	0.00	0.13	99.19
3	0.10	24.76	1.25	0.75	1.31	67.60	0.01	0.10	0.00	0.00	0.15	96.02
4	0.19	25.03	1.24	0.67	1.27	68.34	0.00	0.01	0.00	0.00	0.18	96.93
5	0.10	23.73	0.66	0.53	1.29	69.06	0.24	0.00	0.03	0.07	0.14	95.85
6	0.10	25.19	1.07	1.84	0.52	66.62	0.26	0.10	0.03	0.00	0.13	95.86
7	0.04	23.67	1.44	1.50	0.52	69.01	0.21	0.00	0.03	0.00	0.13	96.55
8	0.14	25.23	1.06	1.76	0.52	67.83	0.05	0.22	0.04	0.00	0.14	96.99
9	0.07	24.93	1.10	1.77	0.51	67.72	0.28	0.08	0.03	0.00	0.17	96.65
10	0.17	23.98	1.24	1.77	0.40	67.46	0.40	0.01	0.03	0.00	0.14	95.61
Amphibole												
1	41.81	5.07	11.30	12.03	0.36	14.03	11.45	3.16	0.78	0.05	0.82	100.86
2	41.10	5.17	11.38	12.09	0.32	14.64	11.26	3.24	0.74	0.03	1.28	101.25
3	40.66	5.75	12.43	12.33	0.18	12.95	11.51	2.76	0.74	0.03	0.72	100.06
4	41.42	5.03	11.44	12.10	0.26	13.67	11.43	2.99	0.79	0.04	0.70	99.88
5	45.42	1.87	7.18	13.52	0.37	13.87	10.50	3.43	1.23	0.01	3.84	101.24
6	53.03	0.87	7.79	8.04	0.14	7.81	16.10	2.49	1.76	1.62	0.20	99.84
7	57.63	0.85	14.34	5.28	0.09	5.52	10.11	4.91	1.79	0.02	0.04	100.57
Apatite												
1	0.16	0.00	0.00	0.20	0.00	0.42	54.75	0.07	0.01	41.04	5.86	102.50
2	0.24	0.03	0.00	0.20	0.11	0.64	55.23	0.08	0.01	40.97	4.94	102.46

Basalt and trachyandesite from Oldeani are mostly fine-grained, phaneritic to aphanitic and occasionally porphyritic and scoriaceous. Oldeani mineral assemblages include plagioclase, augite, olivine and titanomagnetite (Figure 3.2c; Table 3.4). Amphibole is common and biotite is rare. The phenocrysts are of augite, plagioclase and olivine commonly within a plagioclase and augite groundmass. Average augite composition is $En_{37}Fs_{24}Wo_{39}$ and its TiO_2 content range from 1.79-1.11 wt %. Feldspar composition varies from alkalic ($An_{32}Ab_{57}Or_{11}$) to plagioclase ($An_{53}Ab_{45}Or_2$). The olivine is fayalite ranging from Fa_{72} to Fa_{65}. Titanomagnetite is ophitic with augite and olivine. The TiO_2 content in the titanomagnetite ranges from 18.5-19 wt % and its Al_2O_3 and MgO content ranges from 4.2-3.8 and 4.1-3.5 wt % respectively.

Table 3.4: Oldeani mineral compositions (electron microprobe analyses)

Olivine	SiO2	TiO2	Al2O3	MgO	MnO	FeO	CaO	Na2O	K2O	P2O5	BaO	Total
1	33.90	0.16	0.00	17.73	0.71	46.47	0.29	0.03	0.01	0.21	0.07	99.58
2	36.32	1.88	1.88	19.19	0.56	38.88	0.30	0.53	0.91	0.03	0.00	100.46
3	31.43	0.14	0.04	23.29	0.76	43.52	0.35	0.04	0.02	0.15	0.03	99.76
4	33.70	0.10	0.00	19.81	0.81	45.63	0.26	0.02	0.01	0.10	0.00	100.45
5	34.88	0.09	0.00	20.43	0.60	44.13	0.28	0.03	0.01	0.09	0.05	100.59
Pyroxene												
1	51.02	1.39	2.83	14.57	0.14	8.42	22.36	0.44	0.02	0.07	0.06	101.32
2	50.55	1.70	2.70	14.32	0.24	11.22	20.35	0.33	0.00	0.05	0.00	101.46
3	49.93	1.79	2.54	13.21	0.36	12.48	20.17	0.53	0.06	0.08	0.14	101.28
4	50.34	1.50	1.80	14.07	0.32	13.25	19.32	0.38	0.03	0.21	0.06	101.28
5	52.07	1.11	3.15	12.40	0.39	12.74	17.60	0.80	0.58	0.02	0.03	100.86
Feldspar												
	54.55	0.16	28.10	0.09	0.00	0.80	11.41	5.30	0.37	0.00	0.01	100.77
	58.20	0.26	25.87	0.11	0.01	1.33	9.11	6.44	0.63	0.05	0.14	102.15
	60.97	0.21	24.23	0.04	0.00	0.78	7.06	6.82	1.87	0.05	0.09	102.12
Tmagnetite												
1	0.04	19.15	3.79	3.53	0.34	69.11	0.00	0.03	0.00	0.01	0.05	96.04
2	0.38	18.55	4.16	3.84	0.25	67.05	0.00	0.07	0.02	0.01	0.07	94.41
3	0.07	18.50	3.78	4.11	0.29	68.23	0.02	0.01	0.01	0.00	0.12	95.15
4	0.08	19.03	3.81	3.75	0.32	70.09	0.00	0.04	0.00	0.00	0.00	97.12

The Ogol lavas are phaneritic coarse-grained to porphyritic basalt. The phenocrysts are mostly olivine and augite within a feldspar and augite groundmass (Figure 3.2d and Table 3.5). The olivines range in composition from Fo_{78} to Fo_{73}. Augite is mostly lath-shaped and its composition ranges from $En_{48}Fs_{8}Wo_{44}$ to $En_{35}Fs_{16}Wo_{49}$ with TiO_2 and Na_2O contents up to 2.8 and 0.9 wt % respectively. The plagioclase is andesine (An_{23}). Titanomagnetite is ophitic with olivine, augite, and plagioclase and its TiO_2 content ranges from 24.5-23.9 wt %

Table 3.5: Ogol mineral compositions (electron microprobe analyses)

Olivine	SiO2	TiO2	Al2O3	MgO	MnO	FeO	CaO	Na2O	K2O	P2O5	BaO	Total
1	37.93	0.04	0.00	37.35	0.37	24.01	0.28	0.03	0.00	0.00	0.00	100.01
2	39.23	0.01	0.00	39.11	0.31	21.05	0.31	0.00	0.00	0.00	0.09	100.10
3	39.03	0.00	0.00	40.50	0.25	20.58	0.19	0.01	0.00	0.05	0.01	100.60
4	39.50	0.03	0.00	40.91	0.25	19.74	0.21	0.00	0.00	0.03	0.00	100.67
5	39.22	0.05	0.00	41.23	0.30	19.94	0.18	0.00	0.00	0.00	0.02	100.95
6	37.88	0.00	0.00	37.63	0.36	24.50	0.35	0.00	0.01	0.00	0.01	100.73
Pyroxene												
1	53.10	0.54	1.60	17.50	0.13	4.72	22.27	0.73	0.01	0.01	0.03	100.63
2	52.48	0.72	2.73	16.34	0.13	6.82	21.72	0.79	0.00	0.02	0.02	101.76
3	49.38	2.29	3.88	13.82	0.18	7.48	24.00	0.50	0.00	0.02	0.00	101.53
4	53.48	0.59	2.45	16.63	0.18	6.17	19.71	0.74	0.04	0.01	0.00	100.00
5	47.88	2.77	4.22	13.33	0.19	9.12	23.12	0.56	0.06	0.11	0.00	101.36
6	47.27	2.61	4.64	12.69	0.20	9.07	23.53	0.89	0.03	0.07	0.00	101.00
Feldspar												
1	60.63	0.13	23.23	0.24	0.00	1.02	5.28	7.85	1.42	0.02	0.42	100.25
Tmagnetite												
1	0.40	23.89	0.66	1.63	0.69	67.58	0.55	0.06	0.02	0.10	0.11	95.69
2	0.02	24.31	0.27	1.46	0.68	68.33	0.24	0.06	0.02	0.00	0.05	95.44
3	0.07	24.05	0.35	1.43	0.69	68.15	0.36	0.06	0.04	0.01	0.05	95.27
4	0.17	24.51	0.41	1.42	0.71	67.11	0.37	0.04	0.04	0.00	0.15	94.93
5	0.53	23.86	0.42	1.72	0.73	68.10	0.47	0.04	0.01	0.00	0.11	95.98

Geochemistry

Harker diagrams (Figure 3.3) show a continuous decrease in TiO_2, FeO_t, MgO, CaO, and P_2O_5, and an increase in Al_2O_3, Na_2O and K_2O with increasing silica content. Mg numbers defined as (Mg#)[100*(Mg/Mg+Fe)] are lowest in Satiman lavas (5-27) and highest in Ogol flows (56-59). For Lemagurut and Oldeani lavas, the Mg# varies from 18-39. Two Lemagurut lavas (00-LM-3 and 04-OS-5) have higher values of 56 and 54 respectively. MnO is generally low for all samples 0.15-0.2 wt % (Table 3.1), although some Satiman lavas display values as high as 0.37 wt %

Compatible trace element concentrations (e.g., Cr) are generally low in Satiman, Lemagurut, and Oldeani ranging from 1.5 - 47 ppm (Table 3.1), but significantly high in Ogol lavas ranging from 514-863 ppm. Two Lemagurut lavas (00-LM-3 and 04-OS-5) show higher values of 495 ppm and 537 ppm respectively. Compared to ordinary chondrites, all the lavas associated with Laetoli deposits are enriched in rare earth elements (REEs, Figure 3.4). Compared to primitive mantle, the Satiman lavas show negative Ti and P anomalies (Figure 3.5). Satiman lavas are also more enriched in Large Ion Lithophile Elements (LILE) compared to the other volcanoes. In all lavas REEs increase with decreasing MgO (not illustrated).

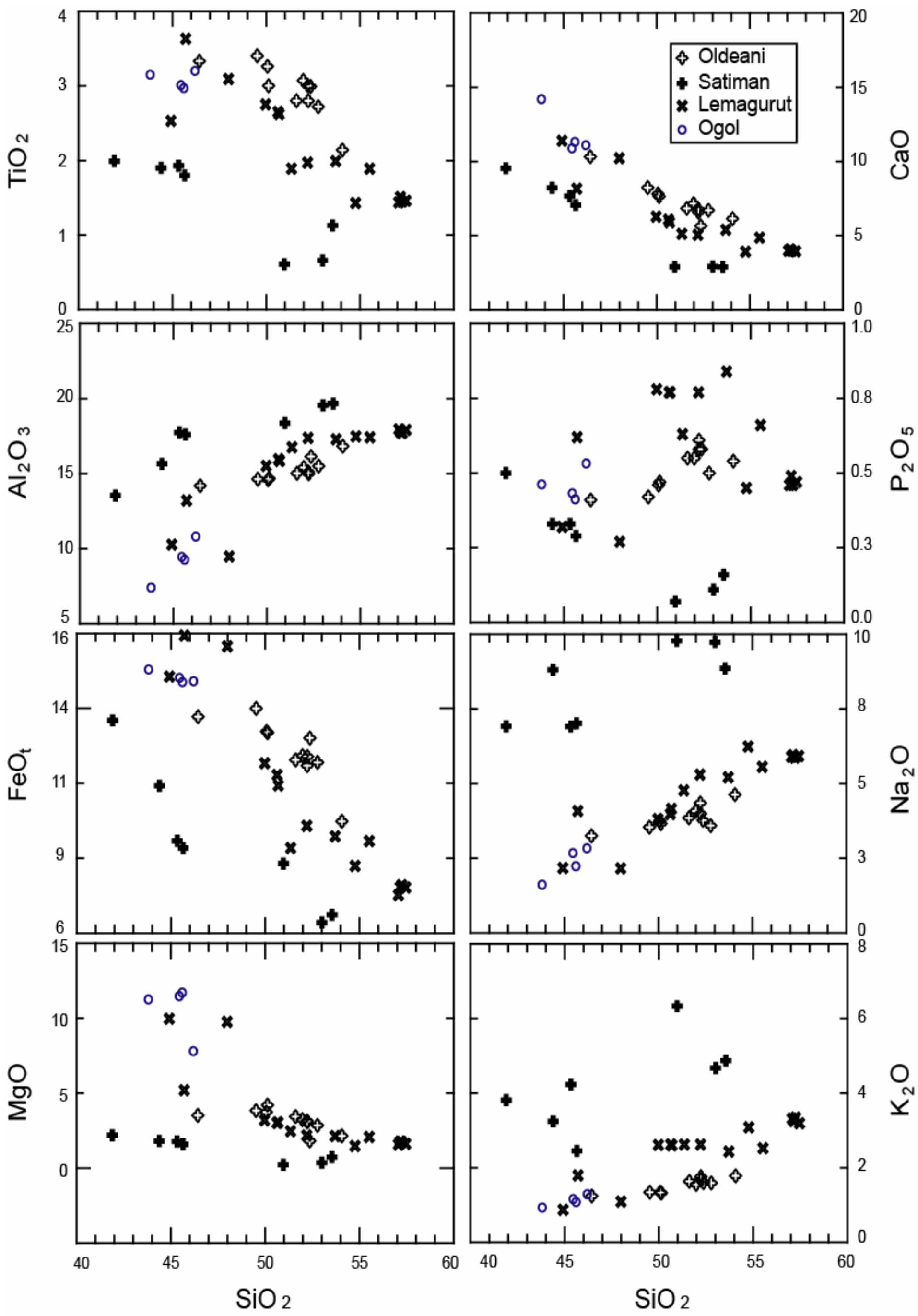

Figure 3.3. Major elements versus silica Harker diagrams. Decrease in MgO, FeOt, CaO and TiO_2 with increasing silica content is consistent with fractional crystallization. The fractionating phases are of olivine, augite, and titanomagnetite for the silicic lavas. The decrease of TiO_2 and P_2O_5 also indicates the crystallization of titanite and apatite in the silica undersaturated lavas.

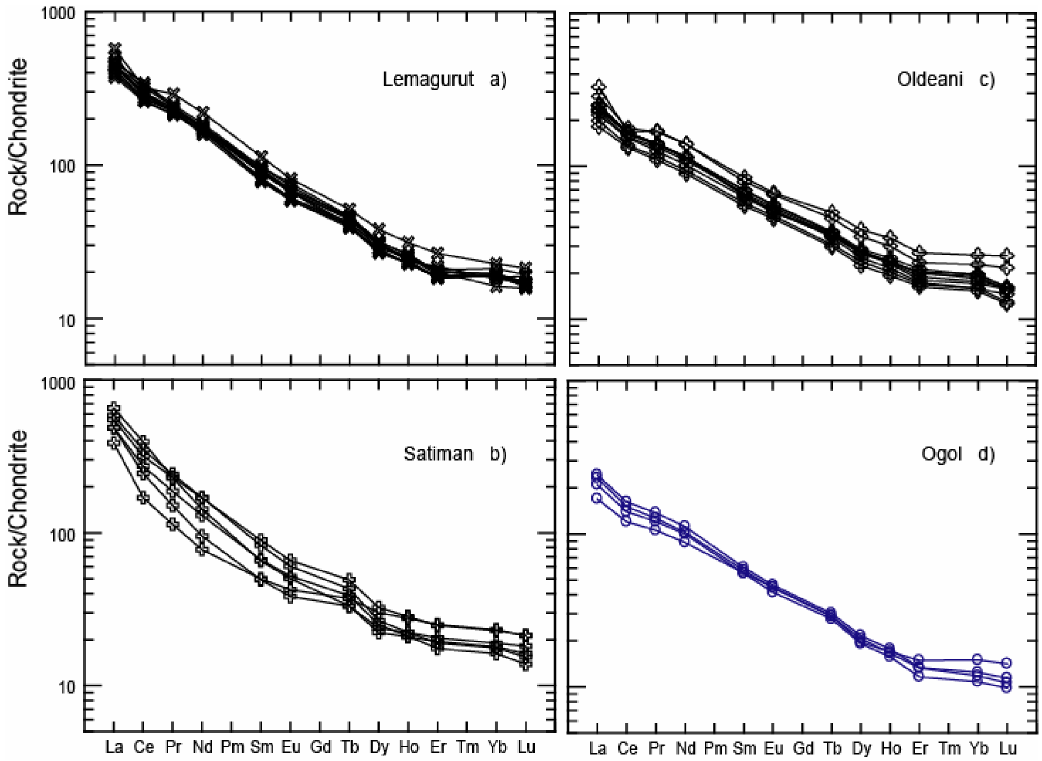

Figure 3.4: Chondritic normalized Rare Earth Elements (REEs) diagram indicate that volcanics associated with the deposition of Laetolil Beds are enriched in REEs abundances. Normalizing values of Sun and McDonough (1989).

Abundances of most of the trace elements and REEs are positively correlated with La in all silica-saturated lavas, but show almost no change in foidite and phonolite (e.g., the Ba, Pb, Zr, and Nb data for Satiman in Figure 3.6). Zr/Nb and La/Nb are not affected by fractionation (MgO value in Figure 3.7) and clearly separate into three groups, Satiman, Lemagurut & Ogol, and Oldeani. There is an apparent temporal progression from low Zr/Nb and La/Nb at Satiman to high values of these ratios at Oldeani (Figure 3.7). Ratios of other incompatible elements (e.g. Ba/La, La/Yb, U/Th, Zr/Hf) are heterogeneous among all the volcanoes (not illustrated).

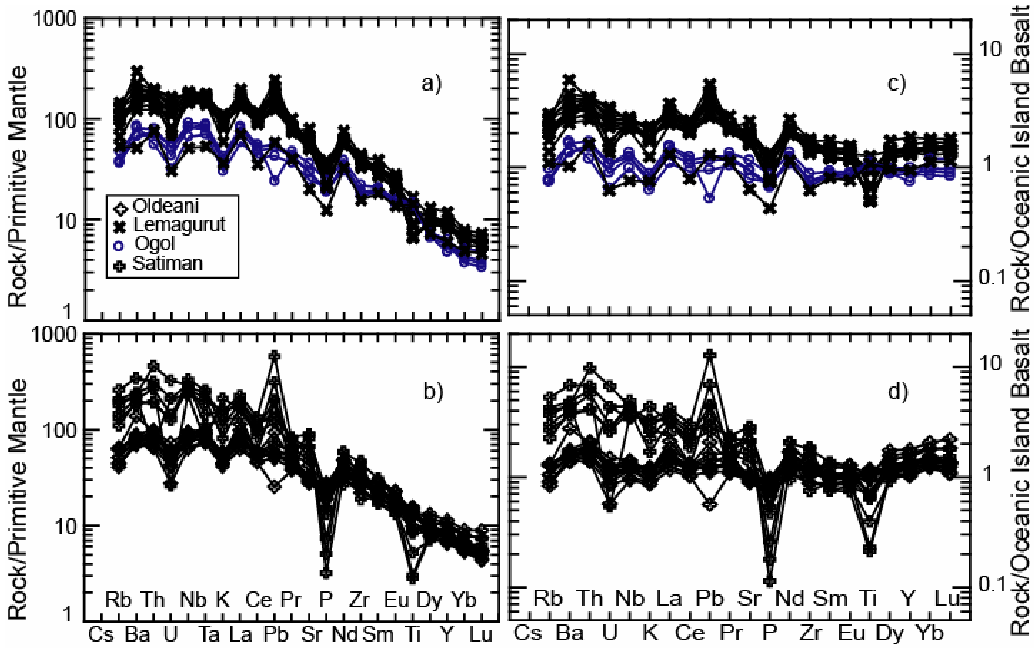

Figure 3.5. (a; b) Primitive mantle normalized incompatible elements diagram indicate that the lavas associated with the Laetolil Beds are enriched in incompatible elements. Troughs of P and Ti indicate fractionation of apatite and titanite while the positive Pb anomaly indicates more crustal contamination of Satiman lavas compared to others (c; d) Oceanic Island Basalt (OIB) normalized trace element ratios for lavas associated with Laetolil Beds are close to one suggesting an IOB source. (Normalizing values of Sun and McDonough, 1989).

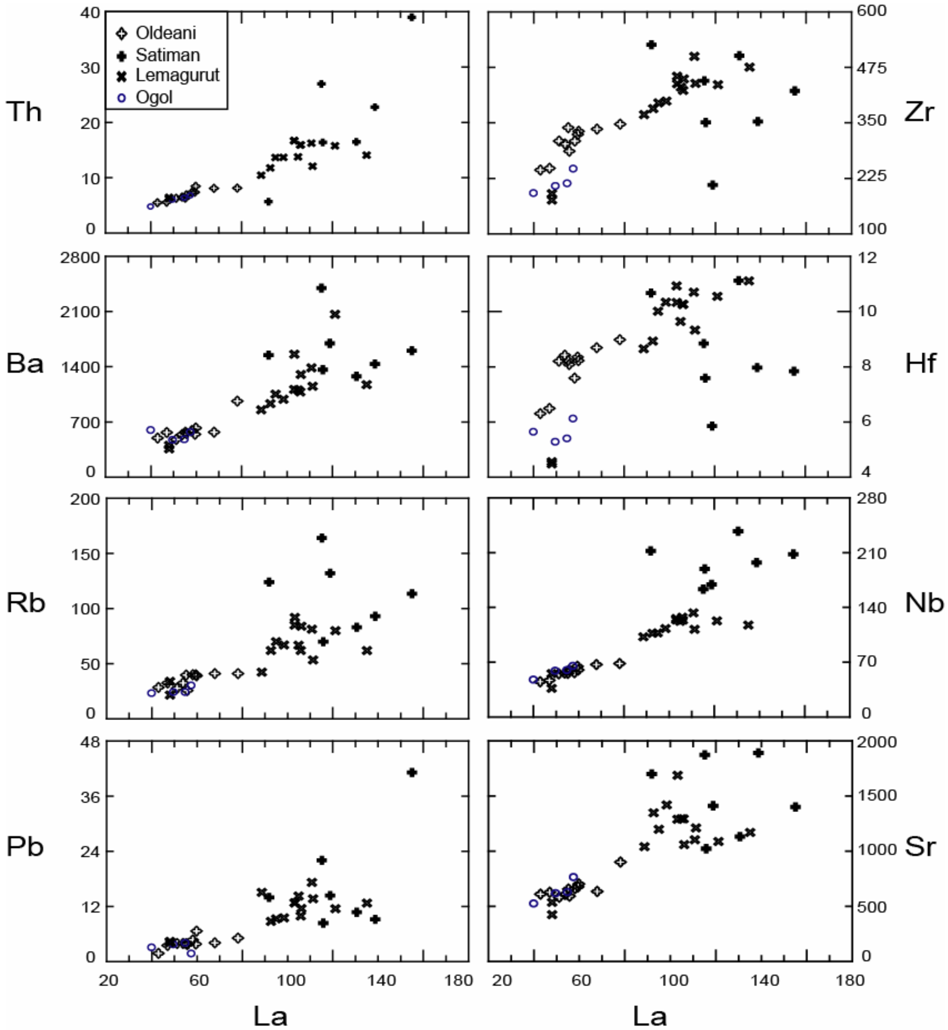

Figure 3.6. Large Ion Lithophile Elements (LILE) as well as Rare Earth Elements correlates positively with La consistent with fractional crystallization for all of the lavas associated with Laetolil Beds. Satiman appear to be higher in most of these elements suggesting an origin from a more enriched liquid or from lesser degree partial melting of the source compared to the others.

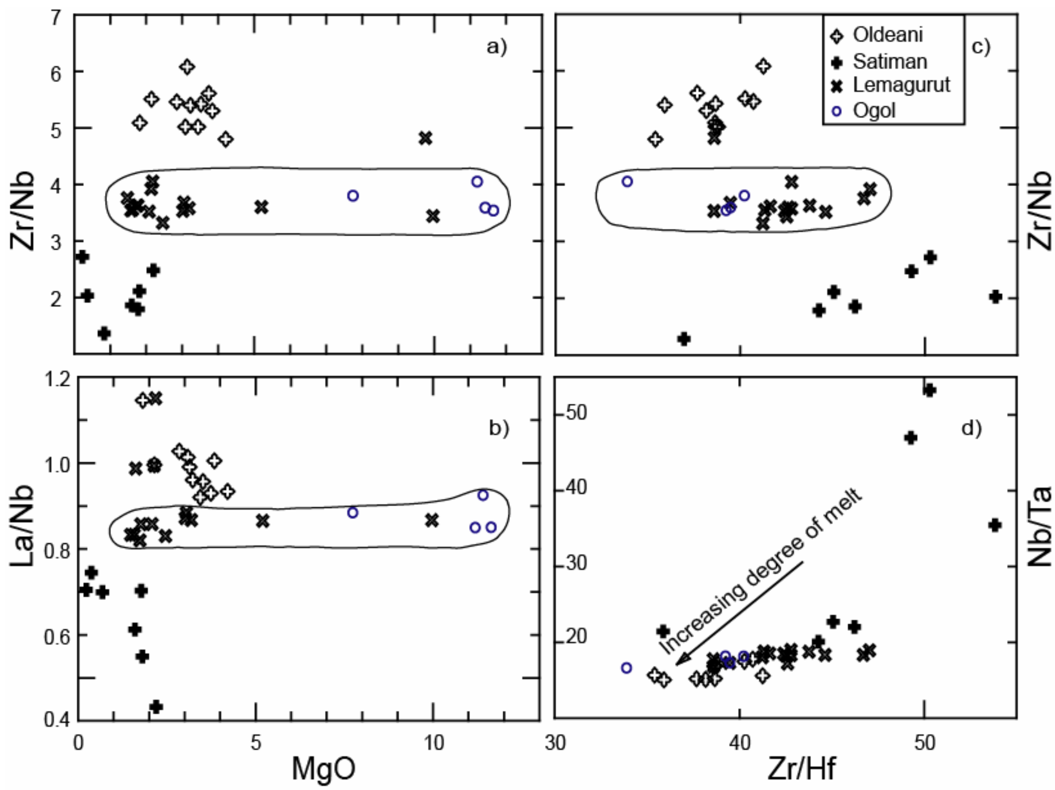

Figure 3.7: High field strength elements (HFSE) ratios are similar for Lemagurut and Ogol flows and unique from that of Oldeani and Satiman. Zr/Hf and Nb/Ta show that Satiman was derived by small degree partial melt compared to the other silicic lavas.

Isotopic ratios of Sr and Nd (Table 3.1) display an overall negative correlation, typical of most volcanic areas. Ogol has the lowest Sr isotope ratios (0.70371-0.70381), highest Nd isotope ratios (0.512554-0.512610), next is Oldeani ($^{87}Sr/^{86}Sr$ = 0.70406-0.70476, $^{143}Nd/^{144}Nd$ = 0.512390-512482), then Lemagurut ($^{87}Sr/^{86}Sr$ = 0.70472-0.70522, $^{143}Nd/^{144}Nd$ = 0.512190-0.512470), and finally Satiman, which has the highest Sr isotope ($^{87}Sr/^{86}Sr$ = 0.70412-0.70609, and the lowest Nd isotope ($^{143}Nd/^{144}Nd$ = 0.512056-0.512402). Satiman has a wide dispersion in Sr isotope ratios, suggestive of variable contamination, supported by positive correlation between Sr isotope ratio and SiO_2 content. There is no simple correlation between Sr isotope ratios and SiO_2 content in Ogol and Oldeani lavas (not illustrated). Sr isotope ratios are negatively correlated to Mg# in all lavas (Figure 3.8).

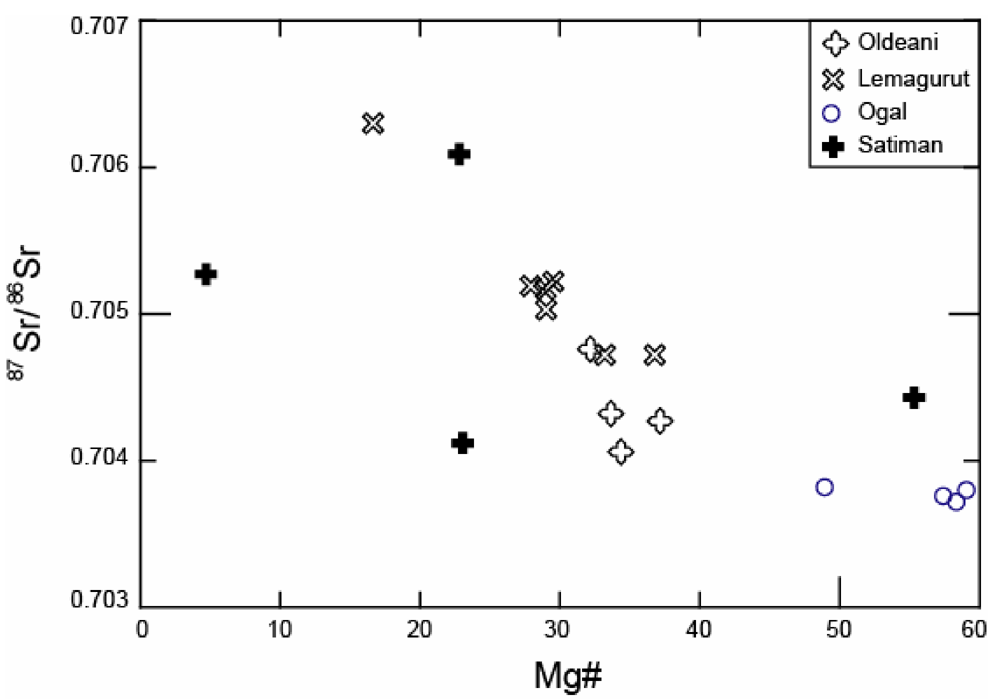

Figure 3.8. $^{87}Sr/^{86}Sr$ versus Mg# for lavas associated with Laetolil Beds. Increasing $^{87}Sr/^{86}Sr$ with decreasing Mg# suggest increasing crust-magma interaction concomitant with fractionation.

DISCUSSION

Evaluation of major elements for the basalt, hawaiite, mugearite, and benmorite from Lemagurut, and Ogol and for basalt and trachyandasite from Oldeani (Figure 3.3), shows that fractional crystallization was a key process in creating the observed variation. Although the same can be said for the foidite and phonolite from Satiman, the process appears slightly different. The foidite and phonolite, as well as the silica-saturated lavas, indicate similar fractionation trends of major elements where there is a decrease in TiO_2, FeO_t, MgO, MnO and CaO with increasing silica content. Incompatible element Na_2O and K_2O increase with increasing silica content consistent with fractionation. P_2O_5 is incompatible in the silicic lavas and decreases with increasing silica content in the foidite and phonolite, indicating crystallization of apatite from the melt. The decrease in FeO_t, MgO and CaO accounts for fractional crystallization of olivine and augite. Decrease in TiO_2 indicates the crystallization of titanomagnetite in the saturated lavas and sphene in the foidite and phonolite. The foidite and phonolite are consistently lower in TiO_2, FeO_t, MgO, CaO, and P_2O_5 (Figure 3.3) compared to the silica saturated lavas, but are higher in incompatible elements (i.e., Na_2O, and K_2O), perhaps indicating that they are derived from a more enriched melt. P_2O_5 is however low, probably suggesting that the source is not enriched in P. The silica-undersaturated lavas are also higher in LILE (e.g., Rb, Sr, Ba and Th in Figures 3.4, 3.5 and 3.6) compared to the saturated ones. While the variations of trace elements with La supports fractional crystallization process (positively correlated) for the silica-saturated lavas (Figure 3.6), High Field Strength Elements (HFSE) such as Nb, Zr, Y and Hf, are almost constant for the silica undersaturated lavas, perhaps indicating that fractional crystallization was not as important in generating the

Satiman lavas. The higher concentrations of LILE in Satiman lavas suggest origin from a more enriched source or by a smaller degree of partial melt (e.g., Mertz *et al*., 2001; Johnson *et al*., 2005). HFSE ratios (e.g., Zr/Nb, Hf/Nb and La/Nb) are distinct for the different volcanic centers, perhaps indicating that they are derived as a result of different degrees of partial melting. The degree of partial melting is estimated from the ratios of Zr/Hf and Nb/Ta (Figure 3.7d). These elements are used because only a very small degree of partial melt can fractionate Zr from Hf and Nb from Ta (e.g., Vukadinovic, 1994; Bolge *et al*., 2006). Because Zr and Nb are slightly more incompatible than Hf and Ta (Sun and McDonough, 1989), lower Zr/Hf and Nb/Ta indicate a higher degree of melting. Three Satiman lavas have unusually high Nb/Ta ratios, but even discounting these, Figure 3.7d suggests that Satiman lavas were derived from lower degrees of partial melting than the lavas of Lemagurut, Ogol and Oldeani.

Source and crustal influence

There is a general consensus that an OIB source is responsible for lavas in northern Tanzania and in other parts of the East African Rift (Paslick *et al*., 1995; Späth *et al.*, 2001; Furman *et al.*, 2004, 2006). OIB-normalized trace element ratios close to one for Oldeani and Ogol lavas and higher for Lemagurut and Satiman (Figure 3.5b) possibly indicating that Lemagurut and Satiman are more fractionated or derived by lower degrees of partial melt. Although there is a clear evidence for crustal-magma interaction (Figure 3.8), the $^{144}Nd/^{143}Nd$ versus $^{87}Sr/^{86}Sr$ plot for most of the lavas under study, fall within or near the field defined by lavas from northern Tanzania that include lavas from Oldoinyo Lengai (Figure 3.9a; Paslick *et al*., 1995; Bell and Tilton, 2001). Sources for lavas from

Oldoinyo Lengai and from other volcanic centers in northern Tanzania have been described to be a result of mixing between high-μ (HIMU) and enriched mantle (EMI) reservoirs (Paslick *et al*., 1995; Bell and Tilton, 2001; Bizimis *et al*., 2003), suggesting a similar source for the lavas associated with the Laetolil Beds. Moderate, chondritic normalized $(Tb/Yb)_n$ ~2.6-1.0 for these lavas [normalizing values of Sun and McDonough, 1989], are within the range of values found in Turkana lavas that have been implied to indicate melting depth in the lithospheric mantle (greater than the garnet-stability field; Furman *et al*., 2006).

Compared to the lower section of the Ngorongoro that yielded a wide range of $^{87}Sr/^{86}Sr$ (0.70405 – 0.70801), the Oldeani and Ogol lavas are less radiogenic, perhaps indicating that they are less contaminated by crustal rocks. Ce/Pb and Nb/U are $> 25 \pm 5$ and $> 43 \pm 7$ respectively for mantle derived melts (Hofmann *et al*., 1986; Sun and McDonough, 1989). Compared to Naivasha in southern Kenya Rift where crust-magma interaction has been documented (Davies and MacDonald, 1987), most of the Oldeani and Ogol samples plot within the range of mantle values whereas most of Lemagurut and Satiman are below the mantle range (Figure 3.9b). Augite from Satiman are zoned and embayed, a feature that was also identified by Paslick *et al*. (1996) in a study of the chemistry of minerals from alkali basalts and nephelinites from northern Tanzania. The latter study concluded that there is a chemical and isotopic disequilibrium between the minerals and their host rocks. They argued that the disequilibrium resulted from up to 10% assimilation of upper crust. The NVHC is erupting through Precambrian basement rocks, the Tanzanian Craton (Cahen *et al*., 1984), on the west of the NVHC, and the Mozambican mobile belt (Key *et al*., 1989, Möller *et al*., 1998) to the east. Assimilation-fractional crystallization (AFC) modeling on Pb isotopic ratios (Paslick *et al.,* 1995) is in agreement with a lower crust contaminant. High $^{87}Sr/^{86}Sr$ ratios measured on some mantle xenoliths collected from Lashaine (e.g., from clinopyroxene 0.8360, garnet 0.8345, and phlogopite 0.8196) separated from a garnet lherzolite (BD-738, Cohen *et al*., 1984), are high enough to cause the lower crust a contaminant.

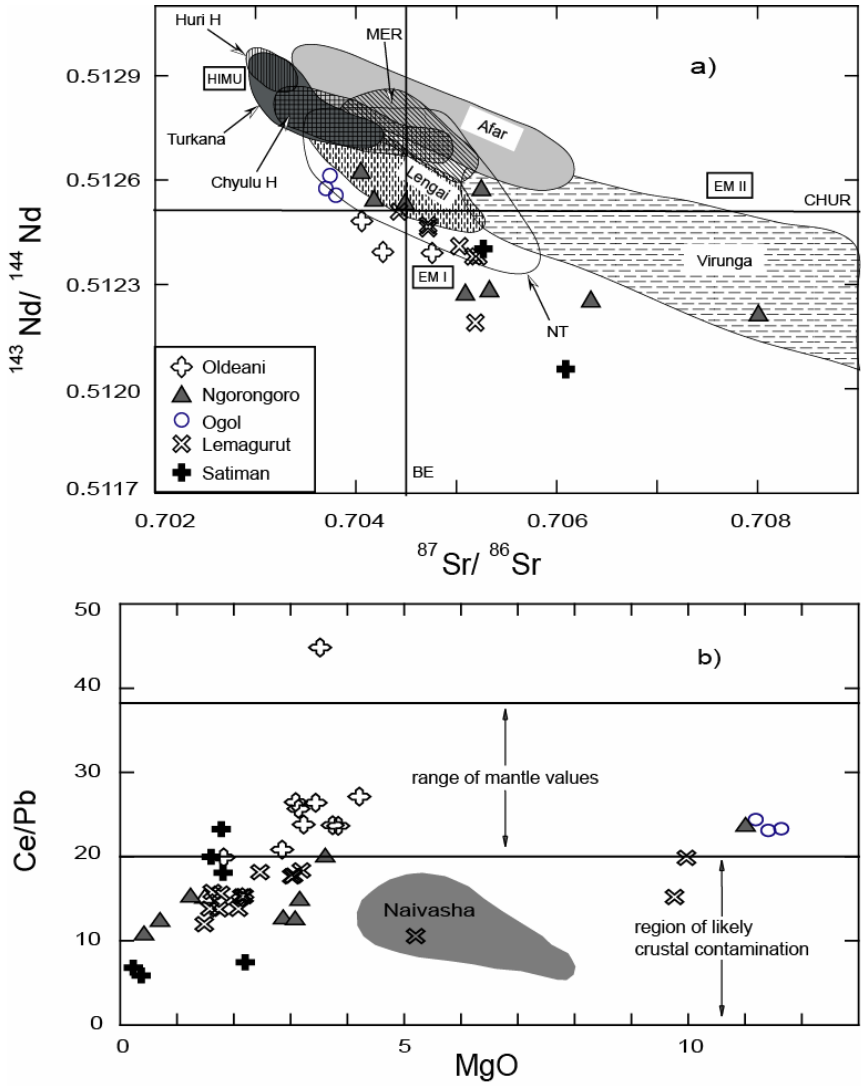

Figure 3.9. (a) $^{143}Nd/^{144}Nd$ versus $^{87}Sr/^{86}Sr$ variation for lavas from volcanics associated with Laetolil Beds compared to other lavas from the East African Rift System as well as hypothetic mantle endmember compositions. BE, Bulk Earth; CHUR, Chondritic Uniform Reservoir; Huri H., Huri Hills; Chyulu H., Chyulu Hills; MER, Main Ethiopian Rift; NT, Northern Tanzania; Lengai, Oldoinyo Lengai. Source of data: Class *et al*., 1994; Deniel *et al.*, 1994; Paslick *et al*., 1995; Bell and Simonetti, 1996; Kalt *et al*., 1997; Rogers *et al*., 1998; Trua *et al*., 1999; Bell and Tilton, 2001; Späths *et al*., 2001; Furman *et al*., 2004, 2006; Keller *et al*., 2006; Ngorongoro data from chapter 4. HIMU, EMI and EM II fields from Hart *et al*., 1992). Most of the representative lavas from Lemagurut, Oldeani and Ogol flow plot within or close to a field defined lavas from northern Tanzania and Oldoinyo Lengai suggesting a source defined by mixing EMI and HIMU mantle endmembers. (b) Variation of Ce/Pb sensitive to crustal contamination as inferred from Naivasha (shaded) area (Davies and MacDonald, 1987; Furman, 2007). The majority of Satiman and Lemagurut lavas plot with the region of crustal contamination similar to lavas from lower Ngorongoro section (Chapter 4). Most of Oldeani and Ogol lavas are less contaminated and fall within the range of mantle values (Hofmann *et al.,* 1986; Sun and McDonough, 1989).

GEOCHRONOLOGY

Oldeani

Matrix from four lava samples collected from the eastern (03-OLDI-1 and 03-OLDI-2) and western (04-OLDI-4 and 04-OLDI-5) flanks of Oldeani were dated using $^{40}Ar/^{39}Ar$ laser incremental-heating techniques. The analyses resulted in well-behaved Ar release patterns forming plateau ages ranging from 1.61 ± 0.01 Ma to 1.52 ± 0.02 Ma (Figure 3.10a; Table 3.6). Integrated ages are comparable to the plateau ages except for 03-OLDI-1, which produced a much younger age, likely due to low temperature alteration of the sample. A combined isochron age for the four analyses yielded an age of 1.57 ± 0.02 Ma that is indistinguishable from the mean plateau age. Two other samples (04-OLDI-3 and 04-OLDI-4) from the western flanks did not yield plateau ages, but gave comparable integrated ages of 1.73 ± 0.01 Ma and 1.61 ± 0.01 Ma respectively. These two samples also yielded indistinguishable isochron ages of 1.57 ± 0.03 Ma and 1.61 ± 0.03 Ma respectively (Table 3.6). These ages suggest that Oldeani activity was of very short duration, lasting for about 90 ka between 1.61 ± 0.01 Ma and 1.52 ± 0.02 Ma.

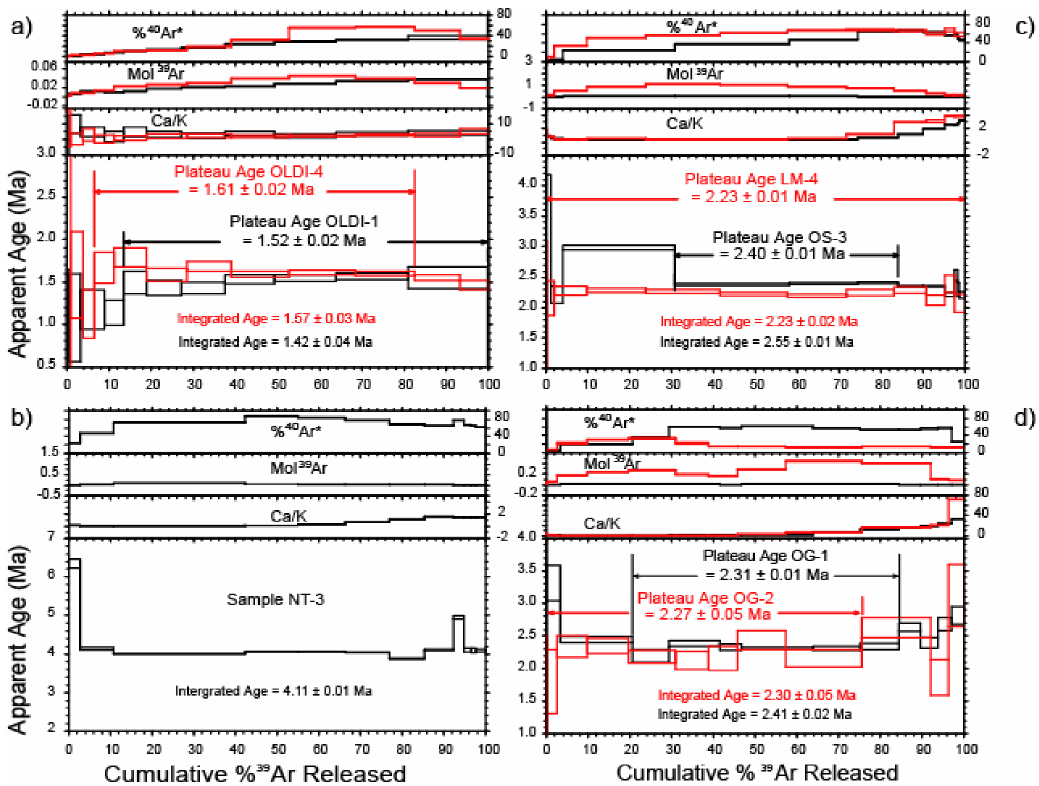

Figure 3.10: $^{40}Ar/^{39}Ar$ Incremental-heating spectra for lavas associated with Laetolil Beds. (a) Seven-step plateau ages for matrix from Oldeani basalts. The integrated age is indistinguishable from its plateau age for the lower boundary, whereas that of the upper boundary is younger than its plateau age likely due to K loss during low temperature alteration of the lava. Cumulative % $^{39}Ar^*$ released on the plateau steps are 86 and 75 for the upper and lower boundary respectively. Plateau temperatures are about 850 ºC and 1100 ºC. (b) Total fusion age spectrum for Satiman phonolite collected from Noiti 3 area. (c) Three and twelve-step plateau ages for matrix from Lemagurut lavas. The integrated age is indistinguishable from its plateau age for the upper boundary but that of the lower boundary is much older (2.55 ± 0.01 Ma) likely due to excess argon resulted from low-temperature alteration of the lava (lower temperature ages are much older). Cumulative %^{39A}r* released on the plateaus are 100 and 53 for the upper and lower boundaries respectively. Plateau temperatures are between 500 ºC and 1200 ºC for the upper boundary and 850 ºC and 950 ºC for the lower boundary. (d) Plateau age for matrix from Ogol basalt is indistinguishable from its integrated age for the upper boundary while that of the lower boundary is much younger than its integrated age likely due to excess argon resulted from low-temperature alteration of the basalt. Cumulative %$^{39}Ar^*$ for the plateau steps are 75 and 55 for the upper and lower boundary, obtained from a nine and six step's plateau produced at temperatures between 550 – 1000 ºC and 570 – 900 ºC respectively.

Table 3.6: $^{40}Ar/^{39}Ar$ ages for volcanics associated with Laetolil area (bold are preferred Ages)

Sample Id	Material	Total Fusion Age (Ma)	Plateau Age (Ma)	Isochron Age (Ma)	$^{40}Ar/^{36}Ar$ Intercept	MSWD	% $^{39}Ar^*$ on Plateau
03-OLDI-1	matrix	1.42 +/- 0.04	**1.52 ± 0.02**	1.53 ± 0.05	294.7 ± 1.6	2.9	86.10
03-OLDI-2	matrix	1.63 +/- 0.05	**1.58 ± 0.02**	1.55 ± 0.03	296.8 ± 1.2	2.6	63.7
03-OLDI-4	matrix	1.57 ± 0.03	**1.61 ± 0.01**	1.59 ± 0.03	295.1 ±1.1	2.0	75.8
03-OLDI-5	matrix	1.50 ± 0.04	**155 ± 0.02**	1.56 ± 0.03	294.4 ± 1.5	2.1	98.5
04-OLDI-3	matrix	1.73 ± 0.01		**1.57 ± 0.03**	296 ± 2	4.3	
04-OLDI-4	matrix	1.61 ± 0.01		**1.61 ± 0.03**	292 ± 3	3.4	
00-LM-6	matrix	2.25 ± 0.01	**2.25 ± 0.01**	2.25 ± 0.01	295 ± 8	0.92	100
00-LM-7	matrix	2.27 ± 0.004	**2.26± 0.005**	2.24 ± 0.02	303 ± 9	4.3	75.1
02-LM-4	matrix	2.23 ± 0.01	**2.23 ± 0.01**	2.22 ± 0.02	297 ± 3	1.0	100
04-OS-1	anorthoclase	2.20 ± 0.10	**2.22 ± 0.10**	2.23 ± 0.1	293 ± 3	0.72	100
04-OS-3	matrix	2.55 ± 0.01	**2.40 ± 0.01**	2.38 ± 0.02	294.7 ± 1.4	2.9	53.3
04-OS-4	matrix	2.34 ± 0.004	**2.29 ± 0.004**	2.30 ± 0.02	297 ± 6	14	56
04-OG-1	matrix	2.41 ± 0.02	**2.31 ± 0.01**	2.29 ±0.01	299.8 ± 1	1.0	55
04-OG-2	matrix	2.3 ± 0.05	**2.27 ± 0.05**	2.30 ± 0.12	296 ± 3	1.5	75.6
04-OG-4	matrix	2.52 ± 0.01		2.51 ± 0.05	316 ± 6	9.9	
01-SM-3	matrix	6.0 ± 3.00	**4.63 ± 0.05**	5.7 ± 0.3	271 ± 4	12	53.2
01-SM-3	nepheline	6.29 ± 0.04		5.7 ± 0.3	290 ± 20	6.4	
01-SM-5	nepheline	4.99 ± 0.03		4.51 ± 0.02	291± 6	7.1	
01-SM-5	matrix	4.35 ± 0.01		**4.19 ± 0.02**	297.3 ± 1.1	2.9	
04-NT-3	matrix	4.11 ± 0.01		**4.02 ± 0.02**	301 ± 4	5.1	

Standard used, irradiation time and irradiation parameter (J):

Sample Id	Standard used	Time	J value
03-OLDI-1	AC	40 min	$1.791 \times 10^{-4} \pm 7.7782 \times 10^{-7}$
03-OLDI-2, 4, 5	AC	40 min	$1.785 \times 10^{-4} \pm 2.1524 \times 10^{-6}$
04-OLDI-3, 4	AC	40 min	$1.8039 \times 10^{-4} \pm 3.287 \times 10^{-6}$
00-LM-6	FC2	60 min	$2.5849 \times 10^{-4} \pm 2.8788 \times 10^{-7}$
00-LM-7	AC	40 min	$1.734 \times 10^{-4} \pm 2.9112 \times 10^{-7}$
02-LM-4	FC2	60 min	$2.5891 \times 10^{-4} \pm 3.3285 \times 10^{-7}$
04-OS-1	FC2	6 hours	$1.58 \times 10^{-3} \pm 1.0 \times 10^{-5}$
04-OS-3, 4	AC	40 min	$1.8139 \times 10^{-4} \pm 2.653 \times 10^{-7}$
04-OG-1, 2, 4	AC	40 min	$1.8009 \times 10^{-4} \pm 2.7542 \times 10^{-7}$
01-SM-3, 5	AC	15 min	$7.16 \times 10^{-5} \pm 1.3781 \times 10^{-7}$
04-NT-3	AC	40 min	$1.8009 \times 10^{-4} \pm 2.7542 \times 10^{-7}$

Satiman

Matrix and nepheline from three lavas (01-SM-3, 01-SM-5 and 04-NT-3) were analyzed by the incremental-heating $^{40}Ar/^{39}Ar$ technique. 01-SM-3 and 01-SM-5 was collected from the present-day summit of Satiman volcano, whereas 04-NT-3 is from the Noiti area, a lowland south of Satiman from which Satiman lahar has been deposited. Analysis of nepheline from lava 01-SM-3 produced an integrated age of 6.29 ± 0.04 Ma (Table 3.3) that is older than its isochron age of 5.7 ± 0.3 Ma (Table 3.6). Although the $^{40}Ar/^{36}Ar$ intercept of the isochron is within atmospheric ratio (295.5 ± 2), the Mean Square of Weighted Deviates (MSWD) is large (6.4).

Analysis of matrix from the same sample produced an integrated age of 6 ± 3 Ma that is indistinguishable from the nepheline isochron age as well as its plateau age of 4.63 ± 0.05 Ma (Table 3.6). Its isochron age of all increments is 5.7 ± 0.3 Ma, analytically indistinguishable from that obtained from the nepheline separate. The $^{40}Ar/^{36}Ar$ intercept is, however, not atmospheric (271 ± 4 and MSWD is large 12). The isochron of only the plateau age yielded an age of 4.8 ± 0.4 Ma (MSWD = 2.1, and $^{40}Ar/^{36}Ar$ intercept of 292 ± 7) suggesting that the plateau age is a better age estimate for this sample. The higher temperature increments may contain excess ^{40}Ar. Analysis of nepheline from 01-SM-5 gave an integrated age of 4.99 ± 0.03 Ma that is older than its isochron age of 4.51 ± 0.02 Ma (Table 3.6), again suggesting slight excess ^{40}Ar in the higher temperature increments. Analysis of matrix from the same sample gave an integrated age of 4.35 ± 0.01 Ma and an isochron age of 4.19 ± 0.02 Ma (Table 3.3). The $^{40}Ar/^{36}Ar$ intercept for 01-SM-5 is within atmospheric ratio and the MSWD is 2.9 suggesting that the isochron age is a better age estimate for this sample.

Analysis of matrix from a phonolite 04-NT-3, gave an integrated age of 4.11 ± 0.01 Ma (Figure 3.10b; Table 3.6) and a slightly younger (by 2.2%) isochron age of 4.02 ± 0.02 Ma. The $^{40}Ar/^{36}Ar$ intercept is within atmospheric ratio but the MSWD of the isochron is large (5.1).

Taken together, the $^{40}Ar/^{39}Ar$ dates for Satiman volcano range between 4.63 ± 0.05 Ma and 4.02 ± 0.02 Ma, and can be as old as 4.8 ± 0.4 Ma. Intergrated ages are consistently older than plateau and isochron ages suggesting that excess ^{40}Ar in nepheline may explain some of the erroneously old K-Ar ages for Satiman.

Lemagurut

Matrix from three representative lava samples 00-LM-6, and 00-LM-7, from the south and 02-LM-4 from the northwestern flanks of Lemagurut were analyzed. Matrix from 02-LM-4 yielded an integrated and plateau age of 2.23 ± 0.01 Ma and an isochron age of 2.22 ± 0.02 Ma (Figure 3.10c; Table 3.3). Matrix from 00-LM-6 gave the same integrated, plateau and isochron age of 2.25 ± 0.01 (Table 3.6).

Matrix from 00-LM-7 gave a plateau age of 2.26 ± 0.005 Ma that is slightly younger than its integrated age of 2.27 ± 0.004 Ma (Table 3.6). Its isochron age of 2.24 ± 0.2 Ma is indistinguishable from the plateau age, but has a large MSWD (4.3). Three samples (04-OS-1, 04-OS-3 and 04-OS-4) collected from the southeast flanks of Lemagurut in Osilale village were also dated. Anorthoclase from 04-OS-1 gave a plateau age of 2.22 ± 0.10 Ma that is indistinguishable from its integrated and isochron age of 2.20 ± 0.10 Ma and 2.23 ± 0.10 respectively (Table 3.6). Matrix from 04-OS-4 yielded a plateau age of 2.29 ± 0.004 Ma that is slightly younger than its integrated age of 2.34 ±

0.004. This plateau age is indistinguishable from that obtained from 04-OS-1 anorthoclase. A combined isochron plot of the two analyses gave an age of 2.30 ± 0.02 Ma that is indistinguishable from both plateau ages. Matrix from the third sample (04-OS-3) yielded a plateau age of 2.40 ± 0.01 Ma that is much younger than its integrated age of 2.55 ± 0.01 Ma (Figure 3.10c; Table 3.6). The isochron age of 2.38 ± 0.02 Ma is analytically indistinguishable from the plateau age. These age data suggest that Lemagurut activity was short in duration lasting only about 180 ka between 2.40 ± 0.01 Ma and 2.22 ± 0.10 Ma.

Ogol

Three lavas (04-OG-1, 04-OG-2 and 04-OG-4) were analyzed. 04-OG-1 was collected from a ridge near fossil Locality 10E, 04-OG-2 from Oldoinyo Mati (= Ndonyamati) and 04-OG-4 from a ridge near Ndolanya Hill. Whole rock analysis of 04-OG-1 and 04-OG-2 yielded indistinguishable plateau ages of 2.31 ± 0.01 Ma and 2.27± 0.05 Ma respectively. Integrated ages for both samples are comparable to their plateau ages (Figure 3.10d; Table 3.6). Combined isochron ages of the two analyses yielded an age of 2.29 ± 0.02 Ma indistinguishable from the plateau ages.

The third sample (04-OG-4) did not produce a plateau age, but yielded an integrated age of 2.52 ± 0.01 Ma that is indistinguishable from an isochron age of 2.51 ± 0.05 Ma (Table 3.6). The $^{40}Ar/^{36}Ar$ intercept for the isochron is 316 ± 6 indicating that the lava contains excess argon and its age may therefore be unreliable. These data suggest that Ogol flows erupted between 2.31 ± 0.01 Ma and 2.27 ± 0.05 Ma.

Implications for Laetolil deposits and NVHC

The new $^{40}Ar/^{39}Ar$ ages for Satiman lavas indicate that Satiman volcano was active between 4.63 ± 0.05 Ma and 4.02 ± 0.02 Ma. These ages are comparable to those previously reported by Bagdasaryan *et al*. (1973). These samples range from the flanks of Satiman to core samples near its summit. The dates do not cover the entire range of ages reported for the duration of the Laetolil Beds from > 4.3 Ma to 3.49 ± 0.12 Ma (Hay, 1987; Drake and Curtis, 1987). Moreover, no coarse-grained xenocrystic flows comparable to those interbedded within the Laetoli Beds were recovered on Satiman. There are three likely explanations for this discrepancy: (1) The eruptions associated with the deposition of Laetolil Beds were primarily tuffaceous with no lava flows. Although Plinian and Vulcanian eruptions are typical in silicic lavas (e.g., the Vesuvius 79 AD eruption, they can also occur in silica undersaturated volcanism e.g. Oldoinyo Lengai Dawson *et al*., 1968, Nielsen and Veksler, 2002). (2). Those younger flows may now be entirely eroded and missing from Satiman itself, and (3) a slightly younger vent of similar composition was the source of the Upper Laetolil ashes, perhaps now buried by the thick flows of the younger Lemagurut volcano. For these reasons the source for the Ndolanya Beds (3.5 to 2.6 Ma; Hay, 1987; Ndessokia, 1990) could also not be located.

The composition and age of analyzed samples from Lemagurut and the Ogol lavas are similar, ranging in age from 2.40 ± 0.01 to 2.22 ± 0.10 Ma. Previously older and younger ages for Lemagurut by Manega (1993) and others are attributed to analyses made of distal flows of adjacent volcanoes, not Lemagurut itself. Ages for Ogol lavas from Locality 10E and that from Oldoinyo Mati are indistinguishable, suggesting that the lavas were likely from the same event. It is possible that they are different lava flows, given the distance (~6 km) between them but that cannot be resolved with the current data. The new plateau age of 2.31 ± 0.01 Ma is younger than the 2.52 ± 0.07 Ma obtained by K-Ar technique from lava collected from Locality 10E (Drake and Curtis, 1987). Age data of lava from the Ndolanya Hill contains excess argon, indicating the age may be less reliable. The presence of excess argon was likely the cause for older K-Ar ages.

Overall, these dates indicate that Ogol lava erupted between 2.31 ± 0.01 Ma and 2.27 ± 0.05 Ma. These ages fall within the range of Lemagurut activity (from 2.40 ± 0.01 Ma to 2.22 ± 0.10 Ma) suggesting overlapping activity between Lemagurut and Ogol. Although Hay (1987) suggested that Ogol lavas erupted from a series of individual vents, three lines of evidence from this study suggest that Ogol flows likely erupted from Lemagurut: (1). Absence of volcanic vents: Three lava ridges were sampled during this study and no intrusive or obvious vent was seen in the vicinity of these ridges. Most of the lavas are massive and only a few outcrops of scoria were seen on one of the ridges. (2). Petrography: Although Ogol lavas are mostly porphyritic compared to most of those from Lemagurut, which are generally medium-grained, this work has shown that their chemistry and mineral assemblages are similar. (3). Geochronology: Age and duration of volcanic activity for Ogol and Lemagurut from this study are indistinguishable within experimental error suggesting overlapping activity. These results suggest that the Ogol lavas may be genetically related to nearby Lemagurut volcanism and may be distal flows that followed paleodrainages. The limited expanse of the Ogol flows are now the result of inverted topography and differential erosion of the adjacent sediments compared with the more resistant lavas. Additional fieldwork is required to verify this hypothesis.

The age of Lemagurut is consistent with volcanic deposits of the Naibadad Beds overlying the Laetolil Beds. However, the Naibadad mineral assemblage includes quartz (Hay, 1987), a composition not compatible with Lemagurut. Revised $^{40}Ar/^{39}Ar$ age for Ngorongoro (2.28 ± 0.02 to 2.02 ± 0.01 Ma; Chapter 4) suggest overlapping activity with Lemagurut, and indicate that Ngorongoro is a better source for Naibadad deposits in terms of age and composition, as previously inferred by Hay (1987).

The Olpiro Beds (2.00 ± 0.01 Ma; Ndessokia, 1990; Manega, 1993) that overlie the Naibadad Beds is phonolitic in composition and its age is consistent with an Olmoti Crater source (Olmoti: 2.01 ± 0.03 Ma to 1.80 ± 0.01 Ma; Chapter 5). Correlation of the Olpiro deposit with Olduvai Beds has been suggested by Hay (1987), and supported by age data from Ndessokia (1990) and Manega (1993). The Olduvai Coarse Feldspar Crystal Tuff (CFCT), which has been correlated with Olpiro by Ndessokia (1990) and Manega (1993), has been show to consist of three different compositions: basaltic, trachytic and rhyolitic (McHenry, 2004). Olmoti, which has been inferred as the source for most of the Olduvai Bed I (Hay, 1976; McHenry *et al*., 2007) is basaltic to trachytic in composition (Mollel *et al*., 2005). The trachyte from Olmoti contains silica undersaturated minerals, (e.g., sodalite), and may in fact be a better source for the Olpiro Beds. The fine-grained nature of the Olpiro Beds (Hay, 1987) may also support a distal source.

Oldeani is the youngest basaltic center in the NVHC. Oldeani activity was very short in duration lasting for 90 ka between 1.61 ± 0.01 Ma and 1.52 ± 0.02 Ma. The age data and the geographic location of Oldeani are inconsistent with the northward younging direction previously proposed by Manega (1993). New Oldeani ages are inconsistent with this general trend and may relate to satellite vents of similar age that followed the collapse of the 2.29 to 2.02 Ma Ngorongoro (Chapter 4).

CONCLUSIONS

Major and trace elements from volcanoes associated with the formation of the Laetolil Beds show that fractional crystallization was a key process in producing Oldeani, Lemagurut and Ogol lavas. Fractionating phases include olivine, augite, plagioclase and titanomagnetite. Apatite, amphibole and biotite are rare. Satiman appears to have been derived by small degrees of partial melting of the source that led to the enrichment of HFSE, and LILE. The Satiman mineral assemblage includes nepheline, augite ± titanomagnetite, andradite, analcite, apatite, olivine, sphene and sanidine.

Similarity in HFSE ratios for Lemagurut and Ogol (Zr/Nb = 3.75) and La/Nb suggests a common parent lineage. Satiman and Oldeani have unique HFSE ratios, e.g., Zr/Nb = 2.16 and 5.54 respectively. Sr and Nd isotope data from this work are in agreement with previous workers, who suggested an OIB source for the volcanics in northern Tanzania. In a plot of $^{87}Sr/^{86}Sr$ versus $^{144}Nd/^{143}Nd$, most of the samples fall within the EMI and HIMU mantle fields. Moreover Sr and Nd isotope data suggest limited crustal contamination of Oldeani lavas compared to Satiman and Lemagurut.

The study has so far failed to recover lavas dating between 4.0 – 2.5 Ma, an age bracketing a large part of the Laetolil section (Upper Laetolil and Ndolanya Beds). Satiman is still the only plausible source for Upper Laetolil and Ndolanya Beds based on its composition and geographical location. This suggests that tuffs and volcaniclastic material forming the Laetolil and Ndolanya Beds were deposited by Plinian eruptions from Satiman or a satellite vent from Satiman now covered by younger eruptions from Lemagurut.

Lavas from the ancestral Satiman volcano are dated between 4.63 ± 0.05 Ma to 4.02 ± 0.02 Ma. Lemagurut and Ogol flows are coeval and erupted between 2.40 ± 0.01 Ma and 2.22 ± 0.10 M. The Naibadad composition and age is compatible with Ngorongoro source while Olpiro Beds may have originated from a more distal Olmoti Crater.

Oldeani is the youngest (1.61 ± 0.01 Ma and 1.52 ± 0.02 Ma) basaltic center in the NVHC. Its age and geographic location are inconsistent with the northward younging direction previously proposed by Manega (1993). This may relate to satellite vent eruptions following the collapse of the adjacent Ngorongoro Caldera.

REFERENCES

Adelsberger, K., Wirth, K. and Mabula, A., 2002. Provenance of Middle Stone Age tools of the Laetoli archaeological site, Tanzania. Geological Society of America (GSA), Abstract with programs 34, 51-7.

Bagdasaryan, G. P., Gerasimovskiy, V. I., Polyakov, A. I. and Gukasyan. R. Kh., 1973. Age of volcanic rocks in the rift zones of East Africa. Geochemistry International 10, 66-71.

Bell, K. and Tilton, G., 2001. Nd, Pb and Sr isotopic compositions of East African Carbonatites: Evidence for mantle mixing and plume inhomogeneity. Journal of Petrology 42, 1927-1945.

Bizimis M., Salters, V. J. M. and Dawson, B. D., 2003.The brevity of carbonatite Source in the mantle: evidence from Hf isotope. Contributions to Mineralogy and Petrology 145, 281-300.

Bolge, L., Carr, M. J., Feigenson, M., and Alvarado, G., 2006. Geochemical Stratigraphy and magmatic evolution at Arenal volcano, Costa Rica. Journal of Volcanology and Geothermal Research 157, 34-48.

Cahen, L., Snelling, J. J., Delhal, J., and Vail, J. R., 1984. The geochronology and evolution of Africa. Clarendon, Oxford.

Carr, M. J., Saginor, I., Alvarado, G. E., Bolge, L. L., Lindsay, F. N., Milidakis, K., Turrin, B., Feigenson M. D., and Swisher III, C. C., (2007). Element Fluxes from the Volcanic Front of Nicaragua and Costa Rica. Journal of Geochemistry, Geophysics, Geosystems 8, Q06001, doi:10.1029/2006GC001396.

Class, C., Altherr, R., Volker, F., Eberz, G., and McCulloch, M., 1994. Geochemistry of Pliocene to Quaternary alkali basalts from the Huri Hills, northern Kenya. Chemical Geology 113, 1-22.

Cohen, R. S., O'Nions, R. K. and Dawson, J. B., 1984. Isotope geochemistry of xenoliths from East Africa: implications for development of mantle reservoirs and the interaction. Earth and Planetary Science Letters 68, 209-220.

Cox, A., 1969. Geomagnetic reversals. Science 163, 237-245.

Cox, K. G., Bell, J. D., and Pankhurst, R. J., 1979. *The Interpretation of the Igneous Rocks*. Allen and Unwin, London.

Curtis, G. H., and Hay, R. L., 1972. Further geological studies and potassium-argon dating at Olduvai Gorge and Ngorongoro Crater. In: Bishop, W. W., and Miller, J. A. (ed.), Calibration of Hominoid Evolution. Scottish Academic Press, Edinburgh.

Dawson, J. B. Bowden, P. and Clark, G. C., 1968. Activity of the carbonatite volcano Oldoinyo Lengai, 1966. International Journal of Earth sciences 57, 865-879.

Davies, G. R., and MacDonald, R., 1987. Crustal influence in the petrogenesis of The Naivasha Basalt-Comendite Complex: Combined trace element and Sr-Nd-Pb isotope constraints. Journal of Petrology 28, 1009-1031.

Deino, A. L., and McBrearty, S., 2002. $^{40}Ar/^{39}Ar$ dating of the Kapthurin Formation, Baringo, Kenya. Journal of Human Evolution 42, 185 - 210.

Deniel, C., Vidal, P., Coulon, C., Vellutini, P. and Piguet, P., 1994. Temporal evolution of mantle sources during continental rifting: the volcanism of Djibouti (Afar). Journal of Geophysical Research 99, 2853-2869.

Drake, R., and Curtis, G., 1987. K – Ar Geochronology of the Laetoli fossil localities. In: Leakey, M. D., and Harris, J. M. (ed.), Laetoli a Pliocene site in northern Tanzania. Clarendon Press, Oxford.

Furman, T., (2007). Geochemistry of East African Rift Basalts: An overview. Journal of African Earth Sciences. doi:10.1016/j.jafrearsci.2006.06.009

Furman, T., Bryce, J., Karson, J. and Iotti, A., 2004. East African Rift System (EARS) plume structure: Insights from Quaternary Mafic lavas from Turkana, Kenya. Journal of Petrology 45, 1069-1088.

Hannah, R. S., Vogel, T. A., Patino, L. C., Alvarado, G. E., Pérez, W., and Smith, D. R., 2002. Origin of silicic volcanic rocks in Central Costa Rica: a study of a chemically variable ash-flow sheet in the Tiribí Tuff. Bulletin of Volcanology 64, 117-133.

Hart, S. R., Hauri, E. H., Oschmann, L. A., and Whitehead, J. A., 1992. Mantle plumes and entrainment: Isotopic evidence. Science 256, 517-520.

Hay, R. L., 1987. Geology of Laetoli area: Laetoli a Pliocene site in northern Tanzania. In: Leakey, M. D., and Harris, J. M. (ed.), A Pliocene site in northern Tanzania. Clarendon Press, Oxford.

Hay, R., 1976. Geology of the Olduvai Gorge*: A study of sedimentation in a semi-arid basin*. University of California Press, Berkeley.

Hofmann, A. W., Jochum, K. P., Seufert, M., and White, W. M., 1986. Nb and Pb In oceanic basalts: New constraints on mantle evolution. Earth and Planetary Science Letters, 79, 33-45.

Johnson, J. S., Gibson, S. A., Thompson, R. N., and Nowell, G. M., 2005. Volcanism in the Vitim volcanic field, Siberia: Geochemical evidence for a mantle plume beneath the Baikal rift zone. Journal of Petrology 46, 1309-1344.

Jones, A. P., Smith, J. V., Hansen, E. C., and Dawson, B. D., 1983. Metamorphism, partial melting and K-metasomatism of garnet-scapolite-kyanite granulite xenoliths from Lashaine, Tanzania. Journal of Geology 91, 143-165.

Key, R., Charsley, T., Hackman, B., Wilkinson, A. and Rundle, C., 1989. Superimposed Upper Proterozoic collision-controlled orogenies in the Mozambican Orogenic Belt of Kenya. Precambrian Research 44, 197-225.

Klaudius, J., and Keller, J., 2006. Peralkaline silicate lavas at Oldoinyo Lengai, Tanzania. Lithos 91, 173-190.

Lee, C.-T. and Rudnick, R.L., 1999, Compositionally stratified cratonic lithosphere: petrology and geochemistry of peridotite xenoliths from the Labait tuff cone, Tanzania, In: Gurney, J. J., Gurney, J. L., Pascoe, M. D. and Richardson, S. H., (ed.) *The Nixon Volume, Proc. Seventh Int. Kimberlite Conf*. pp. 503-521.

Mandeville, C. W., Webster, J. D., Rutherford, M. J., Taylor, B. E., Timbal, A., and Faure, K., 2002. Determination of molar absorptivities for infrared absorption Bands of H_2O in andesitic glasses. American Mineralogist 87, 813-821.

Manega, P. C., 1993. Geochronology, Geochemistry and Isotopic Study of the Plio-Pleistocene Hominid Sites and the Ngorongoro Volcanic Highlands in Northern Tanzania. Ph.D. Thesis, University of Colorado.

McDougall, I. and Harrison, M., 1999. Geochronology and thermochronology by the $^{40}Ar/^{39}Ar$ Method. Oxford University Press, New York.

Mertz, D. F., Weinrich, A. J., Sharp, W. D., and Renne, P. R., 2001. Alkaline intrusions in a near-trench setting, Franciscan complex, California: Constrains from geochemistry, petrology and $^{40}Ar/^{39}Ar$ chronology. American Journal of Science 301, 877-911.

Mollel, G. F., Swisher III, C. C., Feigenson, M. D., and Carr, M. J., 2005. Geochemistry and Geochronology of Ngorongoro Crater, Tanzania: Implication for magma evolution, duration of volcanic activity and age of the Ngorongoro N-R Geomagnetic Polarity Transition. Abstract, American Geophysical Union (AGU) Annual Meeting (Louisiana, May 2005).

Mollel, G., 2002. Petrology and geochemistry of the southeastern Ngorongoro Volcanic Highland (NVH); and contribution to "sourcing" of stone tools at Olduvai Gorge, Tanzania. Masters Thesis, Rutgers University.

Möller, A., Mezger, K., and Schenk, V., 1998. Crustal age domains and the evolution of continental crust in Mozambique belt of Tanzania: combined Sm-Nd, Rb-Sr, and Pb-Pb isotopic evidence. Journal of Petrology 39, 749-783.

Ndessokia, P., (1990). The mammalian fauna and archaeology of the Ndolanya and Olpiro Beds, Laetoli, Tanzania. Ph.D. Thesis, University of California, Berkeley.

Nielsen, T. F. D., and Veksler, I. V., 2002. Is natrocarbonatite a cognate fluid condensate? Contributions to Mineralogy and Petrology 142, 425-435.

Paslick, C., Halliday, A. N., James, D. and Dawson, J. B. 1995. Enrichment of Continental lithosphere by OIB melts: Isotopic evidence from the volcanic province of northern Tanzania. Earth and Planetary Science Letters 130, 109-126.

Paslick, C. and Halliday, A. N., 1996. Indirect crustal contamination: evidence from isotopic and chemical disequilibria in minerals from alkali basalts and nephelines from northern Tanzania. Contributions to Mineralogy and Petrology 125, 277-292.

Pickering, R., 1964, Endulen. Geological Survey of Tanzania, Quarter Degree Sheet 52, scale 1:125,000.

Renne, P., Swisher III, C., Deino, A., Kamer, D., Owens, T., and DePaolo, D., 1998. Intercalibration of standards, absolute ages, and uncertainties in $^{40}Ar/^{39}Ar$ dating. Chemical Geology 145**,** 117-152.

Späth, A., Le Roex, A., and Opiyo-Akech, N., 2001. Plume-Lithosphere interaction and the origin of continental rift-related alkaline volcanism of the Chyulu Hills Volcanic Province, southern Kenya. Journal of Petrology 42, 765-787.

Sun, S., and McDonough, W. F., 1989. Chemical and isotopic systematics of Oceanic basalts: implications for mantle composition and processes. In: Sounders, A. D., and Norry, M. J., (ed.), Magmatism in Ocean Basins. Geological Society Special Publication 42, 313-345.

Trua, T., Deniel, C. and Mazzuoli, R., 1999. Crustal control in the genesis of Plio-Quaternary bimodal magmatism of the main Ethiopian Rift (MER): geochemical and isotopic (Sr, Nd, Pb) evidence. Chemical Geology 155, 201-231.

Turrin, B. D., Muffler, L. J. P., Clynne, M. A. and Champion, D. E., 2007. Robust 24 ± 6 ka $^{40}Ar/^{39}Ar$ age of a low-potassium tholeiitic basalt in the Lassen Region of NE California. Quaternary Research, doi:10.1016/j.yqres.2007.02.004

Vukadinovic, D., 1994. High-field-strength elements in Javanese arc basalts and Chemical layering in the mantle wedge. Journal of Mineralogy and Petrology 55, 293-308.

Weeraratne, D. S., Forsyth, D. W., Fischer, K. M. and Nyblade, A. A., (2003). Evidence for an upper mantle plume beneath the Tanzania Craton from rayleigh wave tomography. Journal of Geophysical Research 108, 2427

CHAPTER 4

Geochemical evolution of Ngorongoro Crater: implications for crustal-magma interaction

Abstract

$^{40}Ar/^{39}Ar$ ages, major and trace element abundancies and Sr-Nd-Pb isotope ratios, and the magmatic evolutionary history of the lavas and tephra of the Pliocene Ngorongoro Caldera (Ngorongoro) in northern Tanzania are presented. The collective data allows for an accurate geochronological interpretation of the Ngorongoro caldera wall. Major and trace elements of lavas exposed in the caldera wall are consistent with a stratified magma chamber whose silicic top and basaltic bottom was inverted by sequential eruption. In general, the lower part of the exposed Ngorongoro sequence is high in silica, alkalies and High Field Strength Elements (HFSE). Zr, Nb and Hf are highly correlated with each other and decrease up section, indicating the extent of magma evolution. The upper part of the sequence is more mafic and includes olivine basalts having the highest magnesium number (~60).

The Sr and Nd isotope ratios from these lavas are widely dispersed ($^{87}Sr/^{86}Sr$ = 0.70405 to 0.70801, $^{143}Nd/^{144}Nd$ = 0.512205 to 0.512623). Pb isotope ratios are consistent with previous studies: $^{206}Pb/^{204}Pb$ = 18.73 to 19.37, $^{207}Pb/^{204}Pb$ = 15.64 to 15.69, $^{208}Pb/^{204}Pb$ = 39.52 to 39.55. Although the Sr isotopic ratios are similar to those of Oceanic Island Basalt (OIB), the more radiogenic lower part ($^{87}Sr/^{86}Sr > 0.705$) likely resulted from crustal-magma interaction this is supported by Ce/Pb ratios ($<25 \pm 5$) which are lower than those expected from primary mantle derived liquids. Two possible contaminants are the Tanzanian Archean Craton to the west and the late Proterozoic Mozambican Belt in the east. Moderate normalized Tb/Yb ratios (2.7-2.1) of these lavas suggest lithospheric mantle melting, a finding consistent with other studies in the region.

Laser incremental-heating and single grain total fusion (anorthoclase) $^{40}Ar/^{39}Ar$ dating of samples from the bottom and top of the Ngorongoro wall section give ages of 2.28 ± 0.02 Ma and 2.02 ± 0.01 Ma respectively, constraining a duration of volcanism of the order of 260 ky. A Normal to Reverse geomagnetic polarity transition recorded in the Ngorongoro wall was correlated with the Gauss-Matuyama transition by Grommé *et al.* (1970). The revised ages for Ngorongoro in conjunction with revised ages for this portion of the geomagnetic polarity timescale suggest possible correlation with the (N-R) 2.14 Ma Réunion-Matuyama transition.

BACKGROUND

Ngorongoro Caldera is the largest volcano of the Plio-Pleistocene volcanic complex situated at the southern end of the Gregory Rift, near the southern bifurcation of the eastern branch of the East African Rift System (Figure 1.1 & 1.2). Its present day caldera is 3000 m high, approximately 20 km in diameter and exposes about 350 meters of section; trachydacite at the bottom, to trachyandesite, basalt and rhyolite at the top (Grommé *et al.* 1970; Manega, 1993; Mollel, 2002). Ngorongoro is the only volcano of the highland complex that exposes a thick stratigraphical section. The volcanic highland is collectively referred to as the Ngorongoro Volcanic Highland Complex (NVHC) consisting of at least 10 major volcanic centers stretching about 80 km from the 1.6 myr old Oldeani volcano in the south to the active Oldoinyo Lengai in the north. The oldest NVHC volcanic activity is about 8.1 Ma for the centrally located Essimingor volcano (Bagdasaryan *et al.* 1973), although this K-Ar age may be anomalously old due to problems with inherited or excess ^{40}Ar.

The NVHC is superimposed on two major geologic provinces: the Tanzanian Archean Craton basement rocks (Figure 1.1 and 1.2; Cahen *et al.* 1984) to the west and the late-Proterozoic Mozambican belt basement rocks to the east (Key *et al.,* 1989, Möller *et al.* 1998). The present day rift in northern Tanzania began about 1.2 Ma and is superimposed on an earlier episode of faulting that began at about 3 Ma (Macintyre *et al.*, 1974; Dawson, 1992, Foster *et al.* 1997).

Most of the East African Rift volcanoes are erupting through thick and old (Precambrian) crustal rocks. This may result in longer residence time for magma batches crossing the crust and if the magma chamber is large enough, latent heat from the magmas could partially melt the crust and incorporate portions of it into the magma. Magma-crust interaction is a common occurance in EAR volcanics, e.g. in the Naivasha Complex, Central Kenya (Davies and MacDonald, 1987).

Previous studies of Ngorongoro have been limited to some K-Ar dating and paleomagnetic studies that showed a polarity reversal from normal (N) to reverse (R) in the 350 m caldera wall section (Grommé *et al.,* 1970; Figure 2.1). K-Ar dates for Ngorongoro ranged from about 2.45 to 2.0 Ma, a duration of about 450 ka (Grommé *et al.,* 1970; Curtis and Hay, 1972; Hay 1976). The N-R transition that occurs near the base of the section was suggested to correlate with the Gauss-Matuyama boundary considered at that time to be 2.43 Ma (Cox, 1969). Volcaniclastic materials of the Olduvai Gorge lower section are considered to have erupted from the Ngorongoro (Hay, 1976). Stratigraphy of the lower Olduvai Bed I, from oldest to youngest, includes the Naabi Ignimbrite, Coarse-Feldspar-Crystal-Tuff (CFCT), Tuff IA and the Mafic Tuff (Hay, 1976, McHenry, 2004). The Naabi ignimbrite is 5 m thick at Olduvai Locality 66 (Hay, 1976), and is geochemically correlated to a Ngorongoro source. The Naabi Ignimbrate composes of anorthoclase, aenigmatite and augite, minor quartz and rare amphibole; it may relate be related to the development of the Ngorongoro caldera following a catastrophic collapse (Hay, 1976; McHenry, 2004; Mollel and McHenry, 2004).

The objectives of this chapter are two fold: (1) provide a geochemical evolution as recorded on the Ngorongoro caldera wall and evaluate the extent of crustal contamination during Ngorongoro volcanism (2) provide $^{40}Ar/^{39}Ar$ dates for the Ngorongoro activity and the age of the magnetic reversal recorded on the caldera wall.

METHODS

Field methods

Sample selection

Ngorongoro samples were collected from the well-exposed caldera wall sections adjacent to the western descending (WDR) and Lerai ascending roads (LAR), part of the Ngorongoro Wildlife Conservation road that loops into the caldera. The LAR section represents the same section studied by Grommé *et al.* (1970). Nine lava samples and one tuff were collected from the LAR section (Figure 2.1); a second tuff sample was collected from WDR. Sample locations are shown on Figure 2.1 and GPS UTM coordinates of the two tuffs are given in Table 4.1.

Table 4.1: UTM coordinate locations of Ngorongoro Caldera tuff.

NGAS	0780006E	9641230N
NGDS	0775363E	9651332N

Laboratory methods

Major and trace element analyses

Whole rock samples were powdered in an alumina mill and analyses were determined in the Department of Geological Sciences at Michigan State University. The powders were fused into glass discs using the high dilution fusion technique which involves the mixing of rock powder with lithium tetraborate and ammonium nitrate Hannah *et al.* (2002). Major and minor element concentrartions were determined by X-ray fluorescence (XRF) using a SMAX Rigaku X-ray spectrograph. Trace element abundances were determined using laser ablasion mass spectrometry (LA-ICP MS) following procedures of Hannah *et al.* (2002). Analytical data were monitored using co-analyzed USGS rock standards. Major element oxides are provide in weight percent (wt %) and trace elements in parts per million (ppm); (Table 4.2).

Sr-Nd-Pb isotopes

Sr and Nd isotopic analyses were done in the Department of Geological Sciences at Rutgers University using a multi-collector VG Isoprobe TIMS. Sample preparation followed that of Bolge *et al.* (2006). Measured values for SRM-987 Sr and La Jolla-Nd standards were $^{87}Sr/^{86}Sr = 0.710237 \pm 5$ and $^{144}Nd/^{143}Nd = 0.511846 \pm 2$, respectively. Pb isotopes were measured at the University of Rochester, NY, following methods similar to those outlined in Basu *et al.* (1991) and Tatsumoto *et al.* (1992). Analyses are reported in Table 4.2.

$^{40}Ar/^{39}Ar$ dating

Four samples, a trachydacite (NG2), olivine basalt (NG8), and tuff (NGAS and NGDS) were prepared for $^{40}Ar/^{39}Ar$ analysis. Lavas were analyzed using laser incremental-heating techniques, whereas tuff anorthoclase grains were analyzed by laser total fusion techniques. Samples were crushed, sieved between 0.425 to 0.250 mm meshes, and washed in ultrasonic baths of distilled water. The purified samples were loaded in Al sample disks along with aliquots of the standard Fish Canyon Sanidine (FC2 = 28.02 ± 0.16 Ma; Renne *et al.* 1998), wrapped in Al foil, and sealed in quartz glass tubes. Samples were irradiated in the cadmium-lined, in-Core Irradiation Tube [CLICIT] facility of the Oregon State University Triga Research Reactor [OSTR] for one and four hours for the lavas and anorthoclase grains respectively. The following interference corrections were used: $^{36}Ar/^{37}Ar_{Ca} = 2.72 \pm 0.01(x10^{-4})$, $^{39}Ar/^{37}Ar_{Ca} = 7.11 \pm 0.024\ (10^{-4})$, and $^{40}Ar/^{39}Ar_{K} = 7 \pm 3\ (10^{-4})$ (Deino and McBrearty, 2002).

Incremental heating was accomplished in step-wise heating increments for 60 seconds each using a 40 Watt CO_2 laser defocused though a 6 mm integrator lens at the Rutgers University Ar-lab. For total fusion analyses a 2 mm integrator lens is used and the grains fused for 9 seconds. The released argon isotopes were measured on a MAP215-50 mass spectrometer and the $^{40}Ar/^{39}Ar$ ages were calculated using automated software by A. Deino following procedures similar to those outlined in Renne *et al.* (1998) and references therein. J values ($2.5922 \times 10^{-4} \pm 2.9231 \times 10^{-7}$ and $1.0586 \times 10^{-3} \pm 1.61 \times 10^{-6}$ for the lava, and anorthoclase grains respectively) were calculated from replicate analyses of the co-irradiated FC2. Mass discrimination was monitored during the analyses from replicate aliquots delivered from an on-line air pipette system.

RESULTS

Major and trace element chemistry

Major and trace element abundances of the nine lava samples from the LAR section are given in Table 4.2. The two rhyolitic tuffs are welded and often contain lithic fragments. No clean sample was found for bulk chemistry, however mineral separate compositions from sample NGDS are reported in McHenry *et al.* (2007). The LAR section (Figure 2.1) is trachydacite at its base, basalt-trachyandesite in mid-section and basalt at the top. The nomenclature is based on the variation of total alkali versus silica content plot of Le Bas *et al.* (1986; Figure 4.1). MgO content of the lavas is typically 3.16 – 0.42 wt%, (except for one sample NG8 (MgO = 11.01 wt %), is holocrystalline and my represent a cumulate. Trachydacite at the bottom of the section has the lowest Mg# (~13), and comprises plagioclase, anorthoclase, minor augite, titanomagnetite, rare biotite and altered olivine. The most basaltic lava near top section has the highest Mg# (~60) and is primarily composed of olivine, titaniaugite, plagioclase, titanomagnetite and rare apatite and biotite.

The entire section is however, thought to be capped by two rhyolitic ignimbrites that are preserved on streams draining the volcano. The “Red” and “Green” Ignimbrites are found in stratigraphic superposition on the northwestern flanks, on fault scarps north of Lemagurut, in stream channels at the foot of northwestern slopes of Olmoti and on the western part of the Olduvai main Gorge (Hay, 1976). The ignimbrites are coarse grained and generally similar in composition to the NGDS tuff on the WDR, consisting of anorthoclase, augite, quartz, aenigmatite, titanomagnetite, ilmenite and rare weathered fayalite (Hay, 1976; McHenry *et al.,* 2007).

Table 4.2: Major element oxides (wt %), other elements (ppm), and Sr, Nd, and Pb isotope analyses of the LAR lavas. n.d. = not determined

Elevation (m)	1896	1904	1923	1962	1972	2064	2122	2138	2174
Sample Id	NG-01	NG-02	NG-03	NG-04	NG-05	NG-7	NG-08	NG-09	NG-10
XRF analyses									
SiO2	53.96	63.25	62.08	53.91	53.32	53.49	45.51	49.12	52.57
TiO2	2.59	1.29	1.19	2.03	2.32	2.12	2.96	3.72	2.84
Al2O3	14.93	16.43	14.95	15.79	15.43	16.45	9.49	14.81	14.62
Fe2O3	11.79	5.17	6.42	9.9	10.73	9.48	14.56	13.82	11.83
MnO	0.16	0.11	0.11	0.09	0.13	0.13	0.19	0.17	0.16
MgO	1.49	0.42	0.7	1.24	3.16	2.87	11.01	3.61	3.08
CaO	4.68	2.6	2.83	4.75	6.27	6.51	11.26	7.42	6.6
Na2O	4.58	5.82	4.93	4.71	4.47	4.53	2.56	3.97	4.18
K2O	2.57	3.18	3.48	2.65	2.05	2.02	0.95	1.38	1.85
P2O5	0.64	0.36	0.32	0.65	0.5	0.48	0.42	0.46	0.59
Total	97.39	98.63	97.01	95.72	98.38	98.08	98.91	98.48	98.32
Rb	27.7	52.4	55.9	40.3	18.8	17.7	-3.5	2.9	20.1
Sr	555.5	528.2	417.2	531.9	622.7	637.1	426.1	511.2	469.9
Zr	477	568.6	563.1	477.4	338.9	309.5	215.5	320.2	372.3
V	68.01	9.22	8.6	70.32	125.05	104.5	216.88	172.71	104.21
Cr	11.36	12.68	10.37	9.89	47.91	41.75	537.4	10.22	9.62
Y	44.15	48.34	37.06	33.45	45.8	22.18	18.34	36.14	31.62
Nb	74	75.1	73.21	63.15	50.87	49.92	37.76	43.89	49.64
Ba	704.07	843.18	733.96	655.48	580.62	558.03	267.2	344.93	434.26
ICP-MS analyses									
La	83.98	133.84	73.74	64.94	107.52	46.24	32.65	46.5	44.83
Ce	127.69	157.93	132.13	123.36	95.95	89.67	62.41	67.25	87.39
Pr	19.69	28.05	16.96	15.21	23.62	10.8	7.57	11.52	10.66
Nd	76.39	106.98	63.53	58.53	89.63	40.65	30.02	47.71	41.78
Sm	13.69	18.24	11.4	10.65	15.18	7.39	6	9.47	8.22
Eu	3.73	4.46	3.04	3	3.97	2.29	1.71	2.86	2.43
Gd	12.12	16.13	9.91	9.26	12.8	6.52	5.1	8.83	7.56
Tb	1.64	2.12	1.41	1.27	1.76	0.89	0.72	1.26	1.08
Dy	8.18	10.83	6.86	6.36	8.56	4.12	3.63	6.66	5.44
Ho	1.58	1.89	1.39	1.25	1.57	0.81	0.66	1.23	1.05
Er	3.91	4.56	3.35	3.07	3.66	2	1.55	2.95	2.6
Yb	3.33	4.03	3.08	2.67	2.97	1.76	1.35	2.52	2.3
Lu	0.45	0.51	0.46	0.44	0.43	0.25	0.2	0.36	0.36
Hf	8.12	10.42	9.51	7.57	5.61	5.13	3.45	5.3	6.07
Ta	4.24	4.37	4.22	3.53	2.85	2.67	2.34	2.61	2.88
Pb	8.49	14.82	10.78	8.14	6.5	7.14	2.65	3.38	7.03
Th	9.84	10.6	10.4	8.9	6.64	6.21	3.32	4.23	5.53
U	1.88	2.97	2.28	1.9	1.54	1.26	0.86	0.96	1.09
TIMS analyses									
87/86Sr	0.70530	0.70801	n.d	0.70634	0.70533	0.70509	0.70405	0.70418	0.70449
143/144Nd	n.d	0.51221	n.d	0.51225	0.51228	0.51227	0.51262	0.51254	
206/204Pb	18.23	18.73	n.d	18.2	n.d	18.46	19.37	19.06	18.63
207/204Pb	15.52	15.64	n.d	15.54	n.d	15.6	15.69	15.6	15.56
208/204Pb	39.52	39.52	n.d	39.38	n.d	39.1	39.55	39.45	39.54

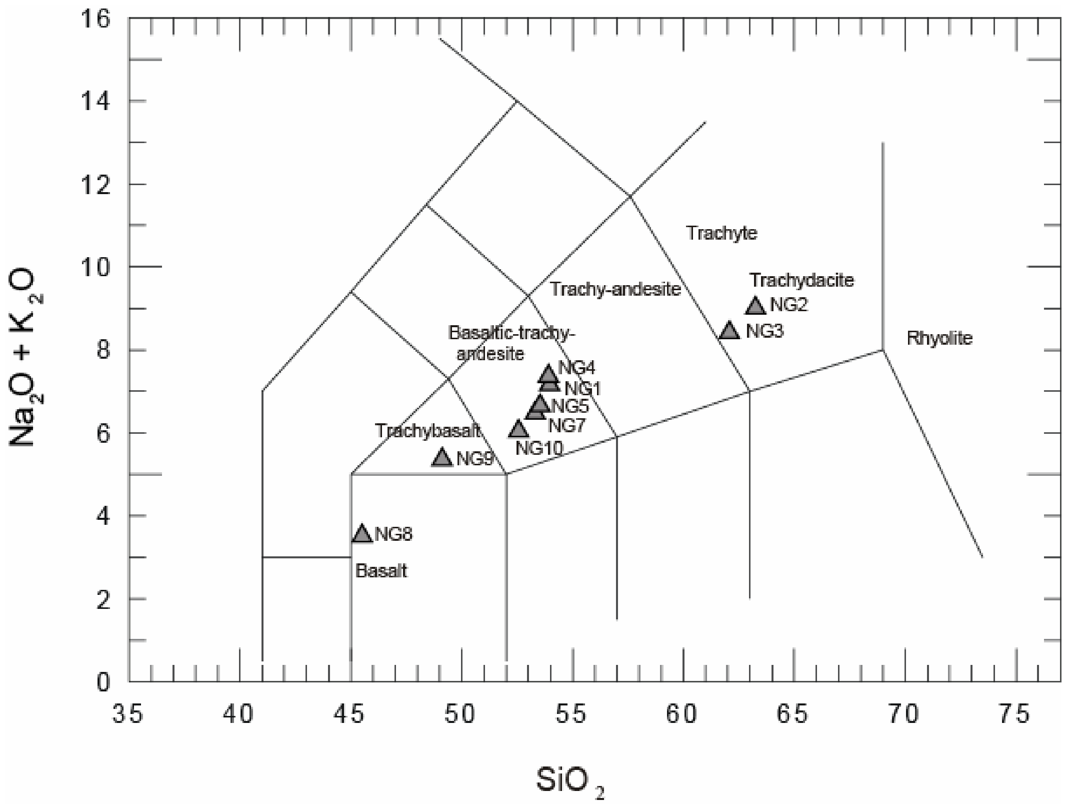

Figure 4.1. Total alkali versus silica nomenclature diagram of Le Bas *et al.* (1986) for Ngorongoro lavas.

Major elements vary systematically with increase in silica content consistent with fractionation. MgO and CaO decrease with increase SiO_2 whereas Na_2O increase and Al_2O_3 shows a diffused pattern consistent with feldspar fractionation (Figure 4.2a). Trace elements show a similar pattern. Highly incompatible elements that are well determined weathering resistant e.g. Zr, Nb, and Hf are positively correlated with each other consistent with a single magma batch (Figure 4.2b). Several high field strength element (HFSE) ratios show a narrow range e.g. Hf/Nb (0.1 – 0.13), U/La (~0.025) and Zr/Nb is (6.2 – 7.7, with one outlier at 5.7).

Elevation versus major and trace elements plot (Figures 4.3) show the LAR section become more mafic up-section. The lower part of the LAR section is high in silica and alkalies (Figure 4.3a and Table 4.2) whereas the upper section is generally more mafic and less evolved, furthermore, the upper LAR section is higher in MgO, CaO, FeO, MnO, and TiO_2 (Figure 4.3a and Table 4.2) compared to the lower part of the section. The higher concentration of TiO_2 in the upper section compared to the bottom reflects the increased abundance of titaniaugite in the basalt and trachybasalt. The lower part of the LAR section is also characterized by higher concentrations of HFSE e.g. Zr, Nb, Pb and U than the upper part (Figure 4.3b).

Primitive mantle-normalized plots of all lavas show enrichments in incompatible elements and negative Sr and P anomalies (Figure 4.4a). In general, all lavas show REE patterns similar to OIB with the most basaltic lava (NG8) at the bottom and the most evolved (trachydacite NG2) at the top (Figure 4.4b).

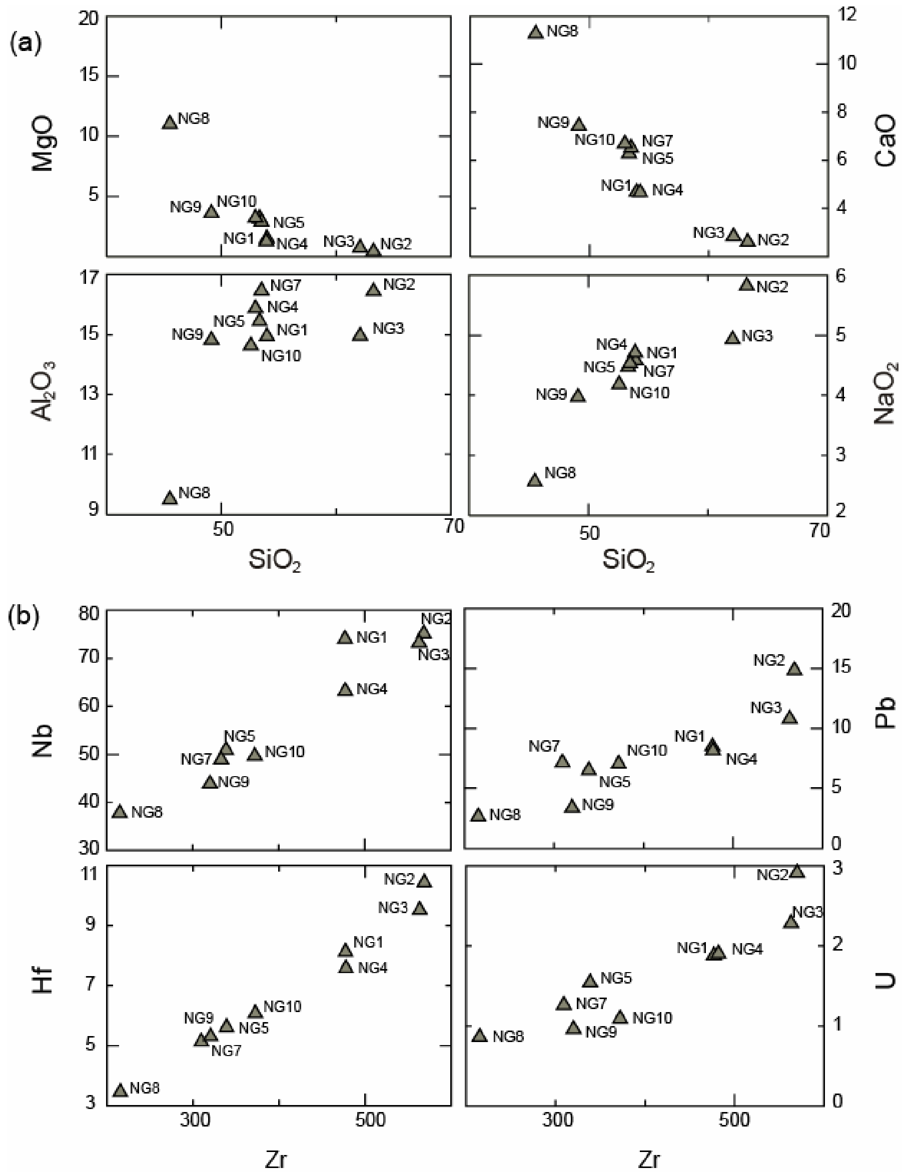

Figure 4.2: Variation of (a) Silica against major elements. SiO_2 is negatively correlated with major elements (with the exception of Na_2O), Al_2O_3 shows a diffused pattern, and all are consistent with crystal-liquid fractionation. (b) Zr against trace elements. Zr is positively correlated to most trace elements also indicating fractionation of Ngorongoro lavas.

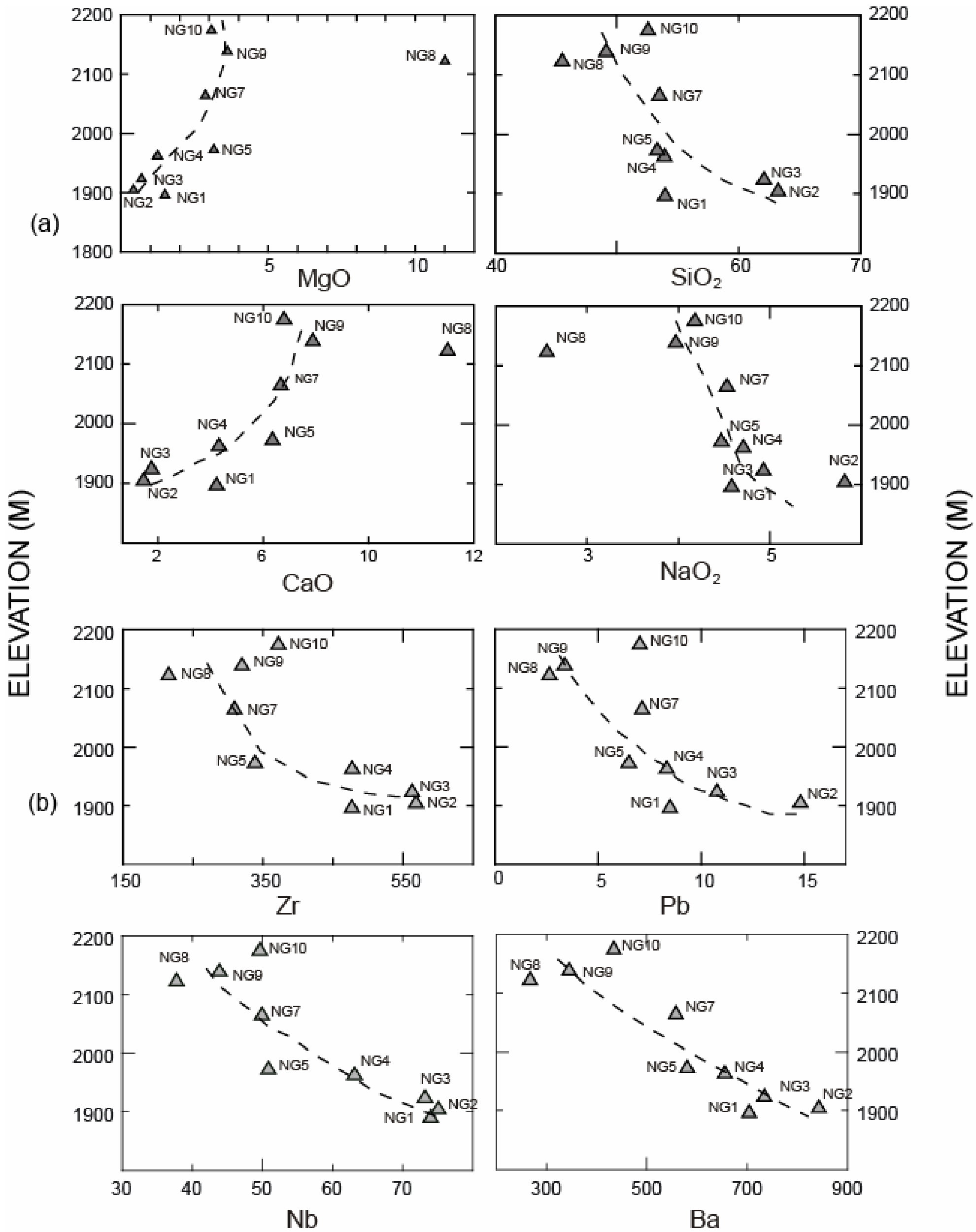

Figure 4.3 Elevation (m) versus (a) major elements (wt %) plots for Ngorongoro section showing high MgO and CaO (upper part of the section) and high SiO_2 and Na_2O (lower part of the section). (b) Trace elements (ppm) plots for Ngorongoro section indicating decreasing trace element concentration with increasing elevation. The more evolved lower section was at the top in the magma chamber. Sample numbers increase up-section, dashed lines indicate evolution trends.

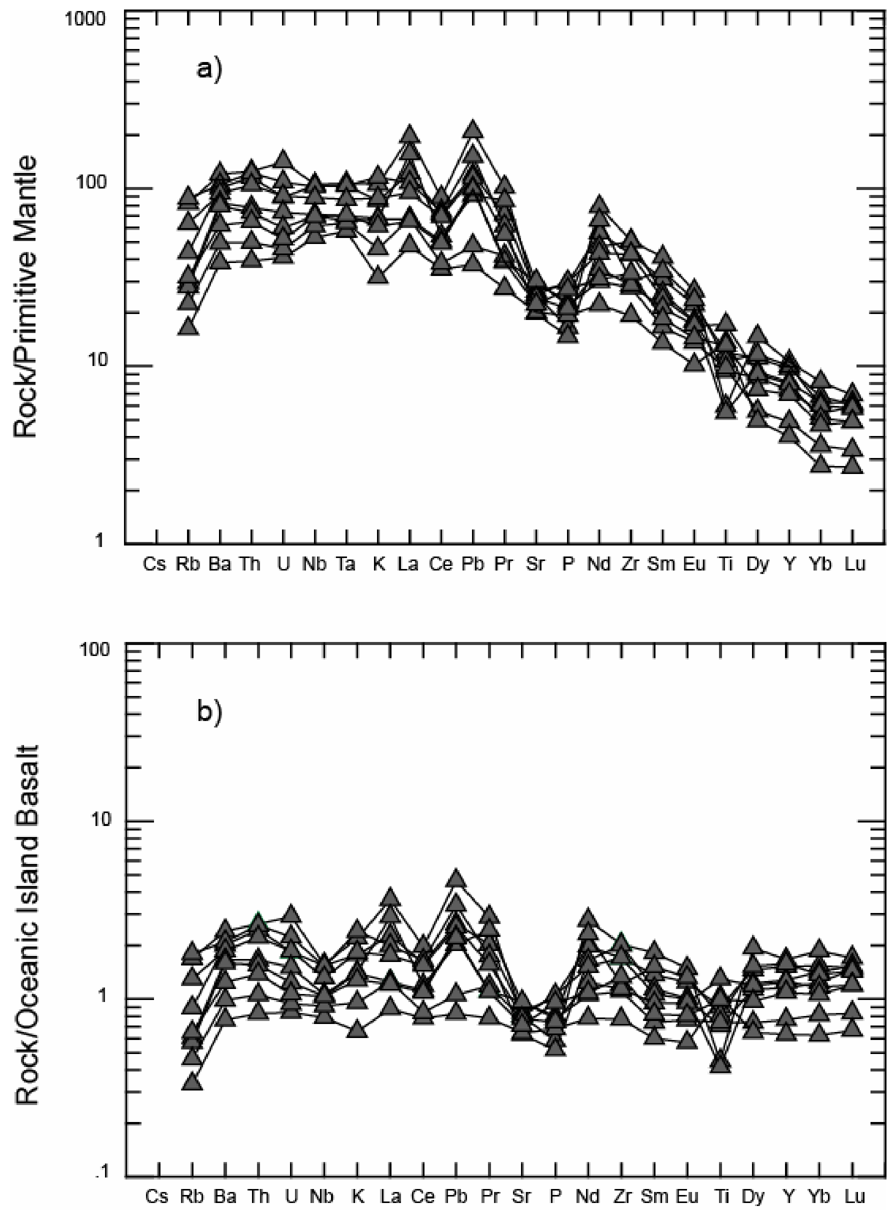

Figure 4.4 (a) Compared to primitive mantle, the Ngorongoro is elevated in trace and REE elements. Troughs of Sr and P indicate crystal-liquid fractionation into plagioclase and apatite. (b) Oceanic Island Basalt (OIB) normalized ratio close to 1 indicates chemistry similarity of Ngorongoro lava with OIB type source. Normalization values of Sun and McDonough, (1989).

Isotope data

The Sr, Nd and Pb isotope measurements are given in Table 4.2. The lower part of the section is more radiogenic in $^{87}Sr/^{86}Sr$ than the upper section and records the lowest $^{143}Nd/^{144}Nd$ isotope ratios whereas upper has the highest. The Pb isotopes are relatively consistent throughout the section and are similar to ratios reported by others in the region (Paslick *et al.,* 1995; Manega, 1993).

DISCUSSION

Major and trace elements

The positive correlation of highly immobile elements, Zr versus other trace elements especially Nb, Hf, Pb (Figure 4.2b) suggests little or no mobilization of trace elements. Sr and P troughs in the spider diagrams (Figures 4.4b) are indicative of feldspar and apatite fractionation, whereas Ti and Rb troughs are attributed to titanomagnetite and K-feldspar fractionation, respectively. The negative K-anomaly could also reflect a source character (e.g. Späth *et al*., 1996, 2001). Negative Sr and P anormalies become more pronounced with increased degree of fractionation (e.g., trachydacite samples, NG2 and NG3). This is consistent with petrographic observations, which show higher modal abundance of anorthoclase in the trachydacite.

Plots of major and trace elements versus elevation (Figures 4.3) show an inverted pattern. The more evolved lavas (trachydacites) of the lower part of the section give way to intermediate composition (basaltic trachyandesite) in mid-section to basalt at the top. The increase in the concentrations of compatible elements, TiO_2, FeO, MgO, MnO and CaO up-section, and the decrease in the concentrations of incompatible elements SiO_2,

Na_2O, K_2O as well as incompatible trace elements such as Zr, suggests that the magma chamber erupted sequenctially from top to bottom and now is exposed in a roughly inverted position.

Although about a third of the Ngorongoro elevation is thought to have been lost during a final catastrophic eruption and subsequent caldera collapse (Hay, 1976), the remaining section (about 95% of the total volume) shows inversely stratified volcanism. The small, overall section missing as final ignimbrites associated with the caldera collapse correlate with those preserved on the lower flanks of Ngorongoro (e.g. Naabi) and are dated at 2.029 ± 0.005 Ma (Walter *et al.,* 1991, 1992). The inverted geochemical signature of Ngorongoro is typical of stratified magma chambers. Inversely stratified volcanism has also been observed in Satsuma-Iwajima Volcano, Japan (Saito *et al.,* 2002), and in La Pacana Caldera, Northern Chile (Schmitt *et al.,* 2003).

Crustal influence

There is an overall negative correlation between Nd and Sr isotope ratios, typical of most volcanic areas and silica content is positively correlated with Sr isotope ratios whereas Nd isotope ratio is negatively correlated. A plot of SiO_2 versus $^{87}Sr/^{86}Sr$ isotope ratio (Figure 4.5a) indicate significant increases in radiogenic Sr with increasing fractionation from NG8 to NG2, an increase that can not be reconciled by fractionation.The $^{87}Sr/^{86}Sr$ is also negatively correlated to Mg# (not illustrated) and produce nonlinear trend when plotted against 1/Sr (not shown) suggesting that Sr isotope ratio as well as Sr concentration from LAR section may have been modified by secondary processes, e.g. crustal assimilation during magma ascent**.** The Ce/Pb ratios in lavas have been shown to be sensitive to crustal contamination, e.g. (Hofmann, 1986; Furman, 2007). Large ion lithophile elements (LILE) such as Pb and Rb are commonly enriched in magmas that have undergone crustal assimilation. Measured ratios of Ce/Pb for primary mantle derived liquids are 25 ± 5 (Hofmann *et al.,* 1986; Sun and McDonough, 1989). The least mobile HFSE (e.g., Zr) is positively correlated to Pb and Ce, suggesting that these elements have not been mobilized by others processes such as weathering. The Ce/Pb ratios for most of the Ngorongoro lavas (Figure 4.5b) are < 25 ± 5, suggesting that magmas of Ngorongoro underwent copious crustal contamination similar to the Naivasha volcanic complex in the southern Kenya Rift (Davies and MacDonald, 1987).

The Nd isotopes demonstrate a similar trend, $^{143}Nd/^{144}Nd$ is lowest (0.512205) in the trachydacite (at the bottom of the sequence) and is highest (0.512623) in the most basaltic lava (near top of the section; Table 4.2).The pattern shown by trachydacite and basaltic trachyandesite in the lower part of the section (Figures 4.5a and 4.5b) suggests crust-magma mixing (e.g., Briquet *et al.,* 1979; Depaolo, 1981 and Carlson *et al.,* 1981). The high $^{87}Sr/^{86}Sr$ ratios of 0.716654 and 0.727279 from metapelite and gneiss of the Mozambican belt in northeastern Tanzania (bordering NVHC to the east) and the Tanzanian Craton (bordering NVHC to the west; Möller *et al.,* 1998) may represent possible contaminants. The high Sr-isotope values measured in the Ngorongoro sequence are most likely the result of entrainment of partially melted crustal material, as no obvious crustal xenocrysts have been observed under optical microscopy. Moreover, any crustal xenocrysts may have resulted in anomalously old NG2 (the most Sr radiogenic) whole rock ages.

Paslick *et al.* (1996) have suggested from their study on alkali basalts and nephelinites of northern Tanzania, that there is chemical and isotopic disequilibrium between the minerals and their host rocks, which can be explained by up to 10% assimilation of upper crust. Assuming that the most magnesium rich sample (NG8) is pristine, modeling of mixing using the Sr and Nd isotopes from the Ngorongoro samples with tonalitic gneiss from Tanzania craton (Möller *et al.,* 1998) suggests that the assimilation may have been up to 15% in the lower part of the Ngorongoro section (Figure 4.5c).

The Pb isotope ratios are similar throughout the section and are within the range of values reported by Paslick *et al.* (1995) and Manega (1993) for volcanic rocks of northern Tanzania. These Pb values are well within the range of OIB, indicating that Pb was not affected by crustal contamination, an observation similar to that of Paslick *et al.* (1995).

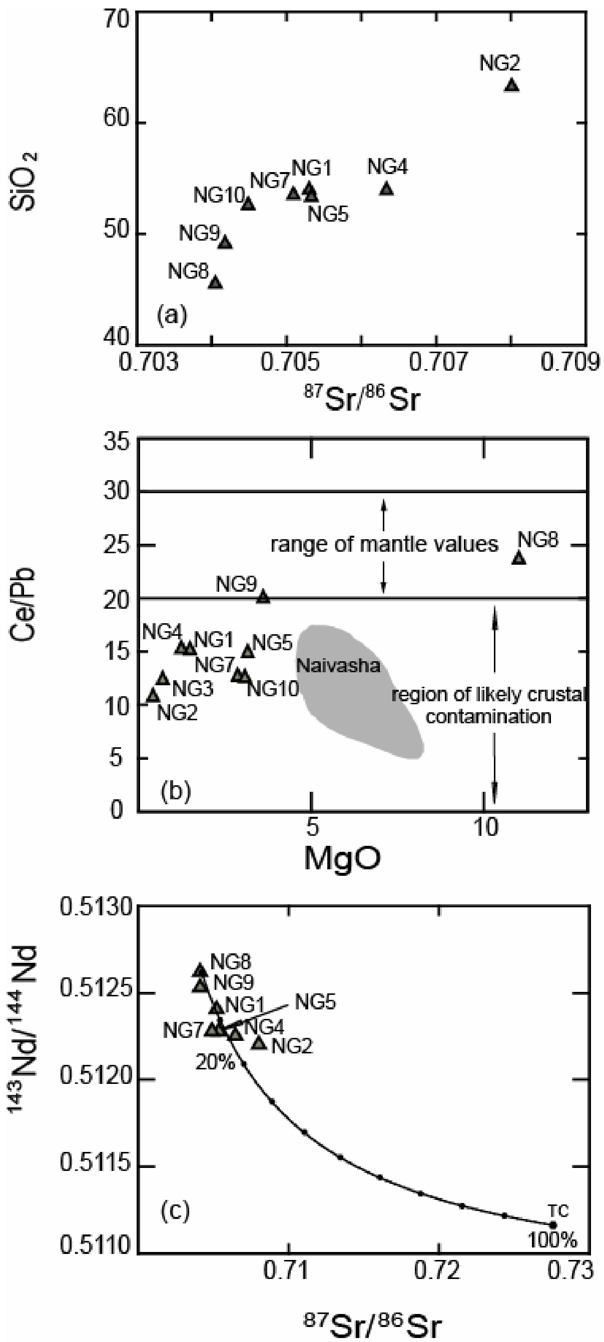

Figure 4.5(a) Variation of SiO_2 content (wt %) versus $^{87}Sr/^{86}Sr$ for Ngorongoro lavas indicating increasing crustal assimilation with fractionation. (b) Values of Ce/Pb sensitive to crustal contamination as inferred from Naivasha (shaded) area (Davies and MacDonald, 1987; Furman, 2007). Most of the NC lavas fall within the region of crustal contamination. NG-8 is within the range of mantle-derived melts (Hofmann *et al.* 1986; Sun and McDonough, 1989). (c) Modeling of $^{143}Nd/^{144}Nd$ versus $^{87}Sr/^{86}Sr$ by mixing NG8 basalt form the LAR section with tonalitic gneiss from Tanzania Craton (TC) Möller *et al.* (1998) suggests crustal assimilation of up to 15% in the LAR lower section.

Source

Geochemical and geophysical data suggests that the origin of the East African Rift volcanics are attributable to a plume or multiple plumes (Marty *et al.,* 1996; Burke, 1996; Mechie *et al.*, 1997; Ebinger and Sleep, 1998; George *et al.*, 1998; Rogers *et al.,* 2000). Geophysical data show a decrease in S-wave velocity between the 410 km and 660 km discontinuities across the eastern rift and has been interprited to be the result of rising mantle plumes (Owens *et al.*, 1995, 2000) and rayleigh wave tomography data from northeastern Tanzania by Nyblade *et al.* (2000) and Weeraratne *et al.* (2003) established the likelihood of the presence of an upper mantle plume head beneath the Tanzania Craton. Nyblade *et al.* 2000 and Weeraratne *et al.* (2003) argue that their results are supported by petrography and isotopic studies of Paslick *et al.* (1995) and others, who show that lavas from volcanics in north Tanzania are similar to OIB.

OIB-normalized trace and REE ratios for lavas from the LAR are close to one (Figure 4.4b) supporting an OIB type source as suggested by Paslick *et al.* (1995) and Cohen *et al.* (1984). The REE ratios are slightly higher for the more evolved Ngorongoro trachydacites due to magma fractionation. Isotopic variation of Nd versus Sr for Ngorongoro lavas (Figure 4.6) plots within or near the field defined by lava from northern Tanzania. The less contaminated lavas from the upper part of the LAR section (e.g. NG8) plot within the field defined by the East African Carbonatite, [EAC; Bell and Tilton, 2001] specifically Oldoinyo Lengai. A source for the EAC as well as for lavas from northern Tanzania, is thought to be a result of mixing between high-μ (HIMU) and enriched mantle (EMI) reservoirs (Paslick *et al.*, 1995; Bell and Tilton, 2001; Bizimis *et al.*, 2003), suggesting that Ngorongoro likely originated from a similar source. The Pb-Pb plots (Figure 4.7) shows similar results, the less contaminated lavas from the LAR section occupy fields defined by lavas from Turkana, Chyulu and Huri Hills (which are also thought to have originated from a source defined by a binary mixture of HIMU and EMI; Späths *et al.,* 2001; Furman *et al.*, 2004, 2006). Although the REE enrichment patters of the lavas from the LAR are similar to those portrayed by a garnet-rich source, moderate $(Tb/Yb)_n$ = 2.7-2.1 [chondrite normalized; Sun and McDonough, 1989] are within the range of values obtained from Turkana volcanic province in northern Kenya (Furman *et al.,* 2006) considered to indicate melting in the lithospheric mantle (depth greater than the garnet-spinel stability field).

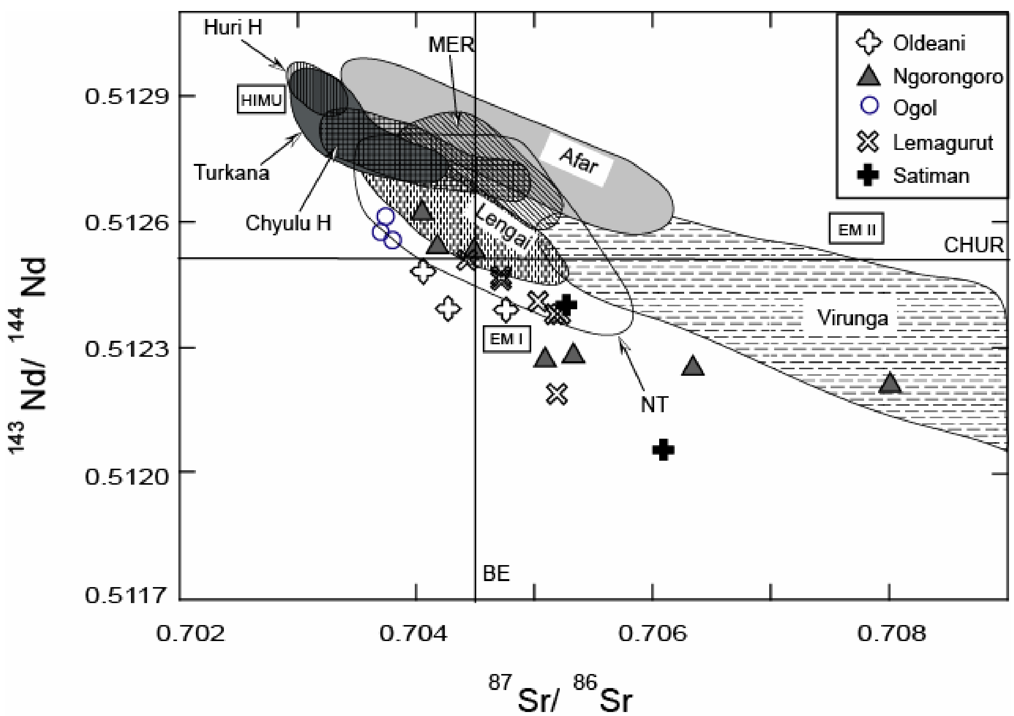

Figure 4.6: Sr and Nd radiogenic variations for Ngorongoro lavas compared to other lavas from the East African Rift System (EARS) as well as hypothetic mantle endmember compositions. BE, Bulk Earth; CHUR, Chondritic Uniform Reservoir; Huri H., Huri Hills; Chyulu H., Chyulu Hills; MER, Main Ethiopian Rift; NT, Northern Tanzania; Lengai, Oldoinyo Lengai. Source of data: Class et *al*., 1994; Deniel *et al.,* 1994; Paslick *et al.*, 1995; Bell and Simonetti, 1996; Kalt et al., 1997; Rogers et al., 1998; Trua et *al*., 1999; Bell and Tilton, 2001; Späths *et al*., 2001; Furman *et al*., 2004, 2006; Keller *et al*., 2006. HIMU, EMI, and EM II fields from Hart *et al*., 1992).

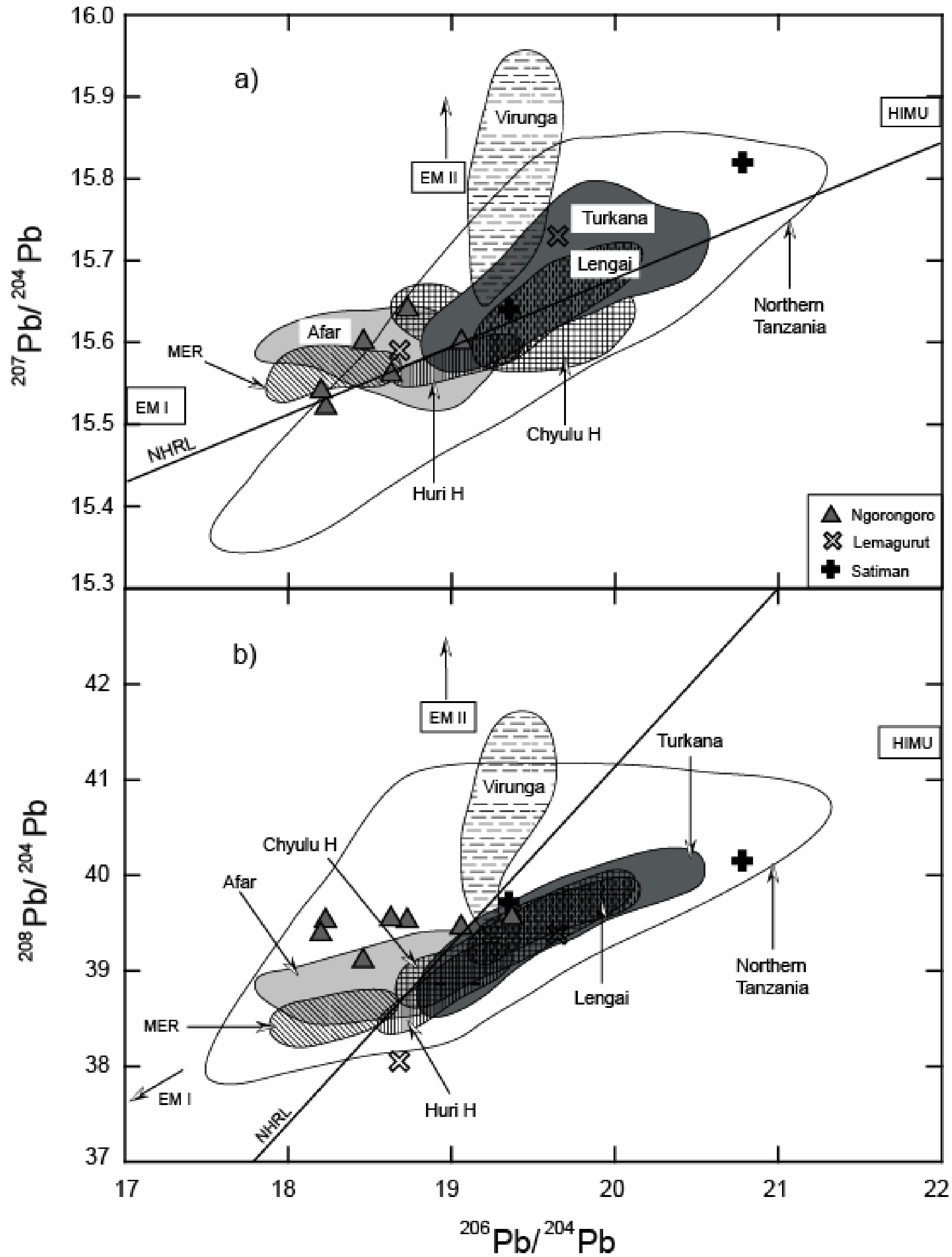

Figure 4.7: Pb-Pb radiogenic variations for Ngorongoro lavas compared to other lavas from the East African Rift System (EARS) as well as hypothetic mantle endmember compositions. BE, Bulk Earth; CHUR, Chondritic Uniform Reservoir; Huri H., Huri Hills; Chyulu H., Chyulu Hills; MER, Main Ethiopian Rift; NT, Northern Tanzania; Lengai, Oldoinyo Lengai. (a) $^{207}Pb/^{204}Pb$ versus $^{206}Pb/^{204}Pb$ and (b) $^{208}Pb/^{204}Pb$ versus $^{206}Pb/^{204}Pb$. Source of data: Class et *al*., 1994; Deniel *et al.*, 1994; Paslick *et al.*, 1995; Bell and Simonetti, 1996; Kalt et al., 1997; Rogers et al., 1998; Trua et *al.*, 1999; Bell and Tilton, 2001; Späths *et al.*, 2001; Furman *et al.*, 2004, 2006; Keller *et al.*, 2006. HIMU, EMI and EM II fields from Hart *et al.*, 1992).

GEOCHRONOLOGY

Anorthoclase from the two welded tuffs, NGAS collected below NG1 of the LAR section (Figure 2.1) and NGDS from the rim top of the WDR section, have been dated by single crystal laser total fusion $^{40}Ar/^{39}Ar$ techniques. Twenty six single crystal total fusion analyses of the NGAS anorthoclase grains yield a weighted mean age of 2.22 ± 0.05 Ma, whereas 24 analyses of the NGDS anorthoclase grains give an average weighted mean age of 2.023 ± 0.008 Ma (Table 4.3 and Figure 4.8a). Feldspar from the two samples shows very distinct Ca/K values (Table 4.3), clearly representing different ignimbrites.

The matrix of lava sample NG2 yielded a total fusion age of 2.28 ± 0.02 Ma (Figure 4.8b), that is indistinguishable from its isochron age of 2.25 ± 0.02 Ma (Figure 4.8c). The matrix of lava NG8 yielded a plateau ages of 2.19 ± 0.03 Ma (three incremental-heating steps, 53% $^{39}Ar^*$ total release between 750°C and 960°C; Figure 4.8b). Its isochron age of 2.22 ± 0.04 Ma is indistinguishable from the plateau age, and the $^{40}Ar/^{36}Ar$ intercept is indistinguishable from the atmospheric air at 295 ± 2. The ages of NGAS and NG2 are indistinguishable within the experimental errors and NG8 falls well within the stratigraphic interval. These dates imply that the eruptive history of Ngorongoro was very short in duration.

Table 4.3: $^{40}Ar/^{39}Ar$ single grain total fusion age data for NGAS and NGDS

Run ID	Sample ID	Ca/K	Mol^{39}Ar	%^{40}Ar*	Age (Ma)	± (Ma)
3008-1	NG-AS	10.729	0.006	16.70	2.31	0.63
3008-2	NG-AS	7.484	0.006	69.40	2.07	0.48
3008-3	NG-AS	4.436	0.010	88.20	2.28	0.3
3008-4	NG-AS	5.106	0.011	92.00	2.33	0.29
3008-5	NG-AS	5.620	0.010	78.40	2.17	0.31
3008-6	NG-AS	7.836	0.006	86.50	2.07	0.53
3008-7	NG-AS	6.271	0.016	93.80	2.25	0.35
3008-8	NG-AS	6.027	0.018	89.80	2.22	0.31
3008-9	NG-AS	5.970	0.031	47.00	2.27	0.18
3008-10	NG-AS	8.408	0.030	82.80	2.22	0.18
3008-11	NG-AS	6.167	0.024	87.80	2.34	0.23
3008-12	NG-AS	7.998	0.018	70.80	2.09	0.31
3008-13	NG-AS	5.932	0.023	60.30	2.27	0.25
3008-14	NG-AS	8.056	0.022	53.70	2.16	0.25
3008-15	NG-AS	7.342	0.015	86.80	2.12	0.22
3008-16	NG-AS	5.714	0.012	91.30	2.21	0.26
3008-17	NG-AS	4.292	0.010	95.70	2.28	0.31
3008-18	NG-AS	5.406	0.013	90.10	2.31	0.23
3008-19	NG-AS	4.074	0.018	82.10	2.22	0.17
3008-20	NG-AS	3.447	0.016	72.30	2.07	0.19
3008-21	NG-AS	3.945	0.010	93.90	2.22	0.3
3008-22	NG-AS	4.449	0.022	84.70	2.18	0.14
3008-23	NG-AS	5.341	0.013	84.80	2.33	0.24
3008-24	NG-AS	3.985	0.035	97.10	2.3	0.73
3008-25	NG-AS	0.791	0.034	92.60	2.28	0.76
3008-26	NG-AS	1.658	0.034	98.20	2.26	0.75

Weighted Mean = **2.219 ± 0.05** Ma, Arithmetic Mean = 2.225 ± 0.05 Ma.

Table 4.3 continued

Run ID	Sample ID	Ca/K	Mol^{39}Ar	%^{40}Ar*	Age (Ma)	± (Ma)
30010-1	NG-DS	0.139	0.067	92.20	2.02	0.05
30010-2	NG-DS	0.039	0.063	96.50	1.97	0.05
30010-3	NG-DS	0.025	0.127	90.70	2.06	0.03
30010-4	NG-DS	0.086	0.071	98.10	2.04	0.04
30010-5	NG-DS	-0.007	0.034	97.40	2.06	0.09
30010-6	NG-DS	0.019	0.126	97.30	2.02	0.03
30010-7	NG-DS	0.052	0.041	99.80	2.01	0.07
30010-8	NG-DS	0.061	0.060	91.60	1.95	0.05
30010-9	NG-DS	0.078	0.143	95.60	2.13	0.02
30010-10	NG-DS	0.011	0.052	94.40	2.05	0.06
30010-11	NG-DS	0.017	0.084	95.90	2.08	0.04
30010-12	NG-DS	0.009	0.092	83.50	2.04	0.04
30010-13	NG-DS	0.063	0.061	91.10	1.99	0.05
30010-14	NG-DS	0.089	0.063	83.70	2.13	0.05
30010-15	NG-DS	0.071	0.159	94.20	1.90	0.04
30010-16	NG-DS	0.070	0.111	91.50	1.91	0.05
30010-17	NG-DS	0.199	0.092	96.50	2.02	0.06
30010-18	NG-DS	0.055	0.053	95.60	1.93	0.11
30010-19	NG-DS	-0.122	0.047	82.80	2.06	0.12
30010-20	NG-DS	0.053	0.392	93.70	2.00	0.02
30010-21	NG-DS	0.113	0.096	89.10	1.91	0.06
30010-22	NG-DS	0.077	0.059	93.50	1.93	0.10
30010-23	NG-DS	0.384	0.047	56.00	1.93	0.12
30010-24	NG-DS	0.136	0.059	93.30	1.93	0.10

Weighted Mean = **2.023 ± 0.008** Ma, Arithmetic Mean = 2.003 ± 0.008 Ma.

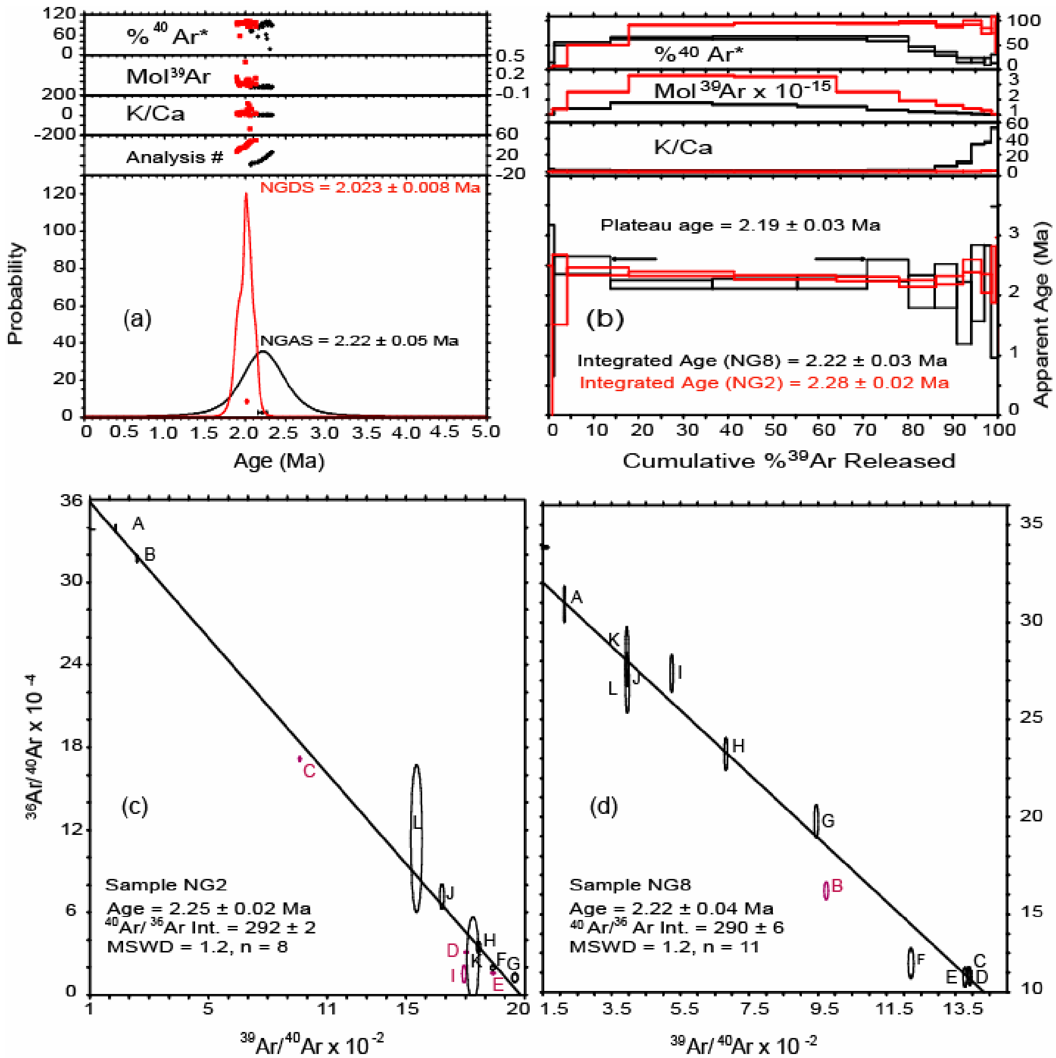

Figure 4.8 (a) Age probability spectrum for anorthoclase grains from samples NGDS (lighter lines, n = 24) and NGAS (darker lines, n = 26) indicating weighted mean ages calculated following procedures similar to those outlined in Renne *et al.* (1998). (b) $^{40}Ar/^{39}Ar$ Incremental-heating spectra for NG2 (lighter lines) and NG8 (darker lines). The plateau age of 2.19 ± 0.03 Ma for NG8 is indistinguishable from its total fusion age of 2.22 ± 0.03 Ma. NG2 yielded a total fusion age of 2.28 ± 0.02 Ma that is indistinguishable from its isochron age (c) An isochron age of 2.25 ± 0.02 Ma for NG2 is indistinguishable from its total fusion age. (d) NG8 isochron age of 2.22 ± 0.04 Ma is analytically indistinguishable from the plateau age.

The duration of basaltic activity appears to have been very short (lasting ~90 -100 kyrs from 2.28 to 2.19 Ma) if we include the two basaltic lavas above NG8. This duration is about a third of the overall time of volcanic activity at Ngorongoro and suggests that there was a pause of about 170 ka prior to the final rhyolitic eruptions and subsequent caldera formation. This hiatus was likely sufficiently long to allow for this large system (pre-caldera) to mix and fractionate rhyolite. Due to geochemical similarites in these lavas, it is plausible that the final eruption was induced by the addition of the new lava (more mafic NG8) from beneath.

The NGDS is geochemically similar to the Naabi ignimbrite (McHenry *et al.* 2007) and its age is identical to the 2.02 ± 0.02 Ma age obtained on anorthoclase of a tuff collected from the same section (Manega, 1993). It is also indistinguishable from an age of 2.029 ± 0.005 Ma obtained from the Naabi Ignimbrite (Walter *et al.*, 1991, 1992). The Ca/K ratios from NGDS are also similar to those obtained from the Naabi Ignimbrite by Walter *et al.* (1991, 1992). The Naabi ignimbrite is the thickest and most widespread unit reported from Ngorongoro (Hay, 1976; McHenry, 2004; McHenry *et al.* 2007) and appears to have been erupted during or near the end of Ngorongoro activity. Such a large and catastrophic eruption may be associated with the collapse of Ngorongoro. The Naabi Ignimbrite is still as thick as 5m at Hay (1976) Locality 66, some 40 km to the west of Ngorongoro.

Combined ages from both single grain total fusion and incremental-heating analyses indicate that Ngorongoro was active between 2.28 ± 0.02 Ma and 2.02 ± 0.01 Ma with a hiatus which lasted about 170 kyrs. The new data suggests that the duration of the eruption was much shorter (about 260 kyrs) than previous estimates of 450 kyrs and about 170 kyrs younger than previously considered (Grommé *et al.,* 1970). Previous correlations of the Ngorongoro Normal to reverse geomagnetic polarity transition with the Gauss-Matuyama (Grommé *et al.*1970) now needs to be reconsidered. The ages presented here in conjunction with revised ages for the Geomagnetic Polarity Timescale (Cande and Kent, 1995; Gradstein *et al.,* 2004), better correlate the Ngorongoro N-R with the upper Réunion-Matuyama boundary of 2.14 Ma.

The older ages obtained by the K-Ar total fusion method can be explained either by incorporation of older crustal material in to the magma or by excess argon. These problems are common in the Ngorongoro Volcanic Highland and have been reported by Evernden and Curtis (1965); Grommé and Hay (1971); and Curtis and Hay (1972) and Mollel *et al.* (in press). Old ages from Ngorongoro lower section suggest overlapping volcanic activity with the Lemagurut volcano that was active between 2.40 ± 0.01 Ma and 2.22 ± 0.10 Ma.

CONCLUSIONS

The inverted geochemical signature observed on the Ngorongoro LAR section implies a stratified magma chamber. OIB-normalized trace element concentrations of close to one and moderate $(Tb/Yb)_n$ = 2.7-2.1, suggests an OIB-type source and melting of garnet-free source rock.

The Sr, Nd and Pb data from the less contaminated Ngorongoro lavas plot within the range of the East African Carbonatites (EAC) can be explained by mixing between enriched mantle and high-μ reservoirs. The Sr isotope data from the LAR section varies widely ($^{87}Sr/^{86}Sr$ from 0.70405 to 0.70801). The increasing radiogenic character of Sr and the decreasing Nd isotope ratio down section implies increasing crustal contamination. This is also supported by Ce/Pb values ($<25 \pm 5$) lower than those expected for primary mantle derived liquids.

The new $^{40}Ar/^{39}Ar$ ages indicate that Ngorongoro was active between 2.28 ± 0.02 Ma and 2.023 ± 0.008 Ma. These new dates suggest a duration of volcanic activity of Ngorongoro of 260 kyrs which contrast previous estimates of 450 kyrs on the basis of K-Ar dating. The Ngorongoro normal to reverse geomagnetic transition at the lower part of the LAR section best correlates with the upper Réunion-Matuyama boundary at 2.14 Ma.

The Ngorongoro upper age limit of 2.02 ± 0.01 Ma from the WDR section ignimbrite is indistinguishable from the age of the Naabi Ignimbrite (Olduvai Lower Most Bed I).The similarities in age and geochemistry of these ignimbrites (McHenry *et al.*, 2007) strongly suggests that they represent the same eruptive units. As such, Ngorongoro remains the most probable source for Olduvai Lower Most Bed I.

REFERENCES

Bagdasaryan, G.P., Gerasimovskiy, V.I., Polyakov, A.I., Gukasayan, R.K., Vernadskiy, V.I., 1973. Age of volcanic rocks in the rift zones of East Africa. Geochemistry International 10, 66-71.

Basu, A., Junwen, W., Wankang, H., Guanghong, X. and Tatsumoto, M., 1991. Major, elements, REE, and Pb, Nd and Sr isotopic geochemistry of Cenozoic volcanic rocks of eastern China: implications for their origin from suboceanic-type mantle reservoirs. Earth and Planetary Science Letters 105, 149-169.

Bell, K. and Simonetti, A., 1996. Carbonatite magmatism and plume activity: Implications from the Nd, Pb and Sr isotope systematics of Oldoinyo Lengai. Journal of Petrology, 37(6): 1321-1339.

Bell, K. and Tilton, G., 2001. Nd, Pb and Sr isotopic compositions of East African Carbonatites: Evidence for mantle mixing and plume inhomogeneity. Journal of Petrology 42, 1927-1945.

Bizimis M., Salters, V. J. M. and Dawson, B. D., 2003. The brevity of carbonatite Source in the mantle: evidence from Hf isotope. Contributions to Mineralogy and Petrology 145, 281-300.

Bolge, L., Carr, M. J., Feigenson, M. and Alvarado, G., 2006. Geochemical Stratigraphy and magmatic evolution at Arenal volcano, Costa Rica. Journal of Volcanology and Geothermal Research 157, 34-48.

Briquet, L. and Lancelot, J. R., 1979. Rb-Sr systematics and crustal contamination models for calc-alkaline igneous rocks. Earth and Planetary Sciences Letters 43, 385-496.

Burke, K., 1996. The African plate. South African Journal of Geology 99, 339-410.

Cahen, L., Snelling, J. J., Delhal, J., and Vail, J. R., 1984. The Geochronology and Evolution of Africa. Clarendon, Oxford.

Cande, S. C. and Kent, D. V., 1995. Revised calibration of the geomagnetic polarity time scale for the Late Cretaceous and Cenozoic. Journal of Geophysical Research
100, 6093-6095.

Carlson R. W., Lugmair, G. W, and MacDougall, J. D., 1981. Colombia river volcanism: the question of mantle heterogeneity or crustal contamination. Geochemical et Cosmochimica Acta 45, 2483-2499.

Class, C., Altherr, R., Volker, F., Eberz, G., and McCulloch, M., 1994. Geochemistry of Pliocene to Quaternary alkali basalts from the Huri Hills, northern Kenya. Chemical Geology 113, 1-22.

Cohen, R. S., O'Nions, R. K. and Dawson, J. B., 1984. Isotope geochemistry of xenoliths from East Africa: implications for development of mantle reservoirs and the interaction. Earth and Planetary Science Letters 68, 209-220.

Cox, A., 1969. Geomagnetic reversals. Science 163, 237-245.

Curtis, G. H. and Hay, R. L., 1972. Further geological studies and potassium-argon dating at Olduvai Gorge and Ngorongoro Caldera. In: W. W. Bishop and J. A. Miller (ed), Calibration of Hominoid Evolution. Scottish Academic Press: Edinburgh.

Davies, G. R., and MacDonald, R., 1987. Crustal influence in the petrogenesis of the Naivasha Basalt-Comendite Complex: Combined trace element and Sr-Nd-Pb isotope constraints. Journal of Petrology 28, 1009-1031.

Dawson, J. B., 1992. Neogene tectonics and volcanicity in the North Tanzania sector of the Gregory Rift Valley: contrasts with the Kenya sector. Tectonophysics 204, 81-92.

Deino, A.L., McBrearty, S., 2002. $^{40}Ar/^{39}Ar$ dating of the Kapthurin Formation, Baringo, Kenya. Journal of Human Evolution 42, 185-210.

Deniel, C., Vidal, P., Coulon, C., Vellutini, P. and Piguet, P., 1994. Temporal evolution of mantle sources during continental rifting: the volcanism of Djibouti (Afar). Journal of Geophysical Research 99, 2853-2869.

Depaolo, D. J, 1981. Trace elements and isotopic effects of combined wall-rock assimilation and fractional crystallization. Earth and Planetary Science Letter 53, 189-202.

Ebinger, C. J. and Sleep, N. H., 1998, Cenozoic magmatism throughout east Africa resulting from impact of a single plume. Nature 395, 788-791.

Evernden, J. F. and Curtis, G. H., 1965. The potassium-argon dating of late Cenozoic rocks in East Africa and Italy. Current Anthropology 6, 343-364.

Foster, A., Ebinger, C., Mbede, E., Rex, D., 1997. Tectonic development of the northern Tanzanian sector of the East African Rift system. Journal of the Geological Society of London 154, 689-700.

Furman, T., (2007). Geochemistry of East African Rift Basalts: An overview. Journal of African Earth Sciences. doi:10.1016/j.jafrearsci.2006.06.009.

Furman, T., Bryce, J., Karson, J. and Iotti, A., 2004. East African Rift System (EARS) plume structure: Insights from Quaternary Mafic lavas from Turkana, Kenya. Journal of Petrology 45, 1069-1088.

Furman, T., Kaleta, K. M., Bryce, J. G., and Hanan, B. B., 2006. Tertiary mafic lavas of Turkana, Kenya: constraints on the East African plume structure and the occurrence of high-μ volcanism in Africa. Journal of Petrology 47, 1221 – 1244.

George, R., Rogers, N. and Kelley, S., 1998, Earliest magmatism in Ethiopia: Evidence for two mantle plumes in one flood basalt province. Geology 26, 923-926.

Gradstein, F.M., Ogg, J.G., Smith, A.G., Bleeker, W., Lourens, L.J., 2004. A new geologic time scale, with special reference to Precambrian and Neogene. Episodes 27, 83-100.

Grommé, C. S. and Hay, R. L. 1971. Geomagnetic polarity epochs: Age and duration of the Olduvai normal polarity events. Earth and Planetary Science Letters 10, 179-185.

Grommé, C. S., Reilley, T. A., Mussett, A. E and Hay, R. L., 1970. Paleomagnetism and Potassium-Argon Ages of Volcanic Rocks of Ngorongoro Caldera, Tanzania. Geophysical Journal Royal Astronomical Society 22, 101-115.

Hannah, R. S., Vogel, T. A., Patino, L. C., Alvarado, G. E., Pérez, W. and Smith, D. R.,

2002. Origin of silicic volcanic rocks in Central Costa Rica: a study of a chemically variable ash-flow sheet in the Tiribí Tuff. Bulletin of Volcanology 64, 117-133.

Hart, S. R, Hauri, E. H., Oschmann, L. A., and Whitehead, J. A., 1992. Mantle plumes and entrainment: Isotopic evidence. Science 256, 517-520.

Hay, R., 1976. Geology of the Olduvai Gorge: A Study of Sedimentation in a Semi-arid Basin. University of California Press, Berkeley.

Hofmann, A. W., Jochum, K. P., Seufert, M., and White, W. M., 1986. Nb and Pb in oceanic basalts: New constraints on mantle evolution. Earth and Planetary Science Letters 79, 33-45.

Kalt, A., Hegner, E. and Satir, M., 1997. Nd, Sr, and Pb isotopic evidence for diverse lithospheric mantle sources of East African Rift carbonatites. Tectonics 278, 31 – 4 5.

Keller, J., Zaitsev, A. N. and Wiedenmann, D., 2006. Primary magmas at Oldoinyo Lengai: The role of olivine melilitites. Lithos 91, 150-172.

Key, R., Charsley, T., Hackman, B., Wilkinson, A. and Rundle, C., 1989. Superimposed Upper Proterozoic collision-controlled orogenies in the Mozambican Orogenic Belt of Kenya. Precambrian Research 44, 197-225.

Le Bas, M. J., LeMaitre, R. W., Streckeisen, A. and Zanettin, B., 1986. A chemical classification of volcanic rocks based on the total alkali-silica diagram. Journal of Petrology 27, 745-750.

Macintyre, R. M., Mitchell, J. G., and Dawson, J. B., 1974. Age of the fault movements in the Tanzania sector of the East African Rift system. Nature 247, 354-356.

Manega, P. C., 1993. Geochronology, Geochemistry and Isotopic Study of the Plio- Pleistocene Hominid Sites and the Ngorongoro Volcanic Highlands in Northern Tanzania. Ph.D. Dissertation, University of Colorado, Boulder.

Marty, B., Pik, R., and Yirgu G., 1996. Helium isotopic variations in Ethiopian plume lavas: nature of magmatic sources and limit on lower mantle contribution. Earth and Planetary Science Letters 144, 223-237.

McHenry, L., 2004. Characterization and correlation of altered Plio-Pleistocene tephra using a multiple technique approach: Case study at Olduvai Gorge, Tanzania. Ph.D. Dissertation, Rutgers University, New Jersey.

McHenry, L., Mollel, G and Swisher III, C., 2007. Direct compositional correlations between Olduvai Gorge Bed I tephra and volcanic sources in the Ngorongoro Volcanic Highlands, Tanzania. Quaternary International doi:10.1016/j.quaint.2007.01.004.

Mechie, J., Keller, G. R., Prodehl, C., Kahn, M. A., Gaciri, S. J., 1997. A model for the structure, composition and evolution of the Kenya Rift. Tectonophysics 236, 409-438.

Mollel, G., 2002. Petrology and geochemistry of the southeastern Ngorongoro Volcanic Highland (NVH); and contribution to “sourcing” of stone tools at Olduvai Gorge, Tanzania. Masters Thesis, Rutgers University, New Jersey.

Mollel, G. F. and McHenry, L. J., 2004. Temporal evolution of the Ngorongoro Volcanic Highland (NVH) in relation to Bed I of Olduvai Gorge, Tanzania: A progress report. Paleoanthropology Society Annual Meeting, Montreal, April, 2004.

Mollel, G. F., Swisher III, C. C., Feigenson, M. D. and Carr, M. J., (in press). Petrology, geochemistry, and age of Satiman, Lemagurut and Oldeani: sources of the volcanic deposits of the Laetoli area. In: T. Harrison (Ed.) *Paleontology and Geology of Laetoli: Human Evolution in Context Volume 1*, Springer, Dordrecht

Möller, A, Mezger, K. and Schenk, V., 1998. Crustal age domains and the evolution of continental crust in Mozambique belt of Tanzania: combined Sm-Nd, Rb-Sr, and Pb-Pb isotopic evidence. Journal of Petrology 39, 749-783.

Nyblade, A. A., Owens, J. T., Gurrola, H., Ritsema, J. and Langston, C. A., 2000. Seismic evidence for a deep upper mantle thermal anomaly beneath East Africa. Geology 28, 599-602.

Owens, J. T., Nyblade, A. A. and Langston, C. A., 1995.The Tanzania broadband experiment, IRIS News Letters, XIV, 1.

Owens, J. T., Nyblade, A. A., Gurrola, H. and Langston, C. A., 2000. Mantle transition zone structure beneath Tanzania, East Africa. Geophysical Research Letters 7, 827-830.

Paslick, C., Halliday, A. N., James, D. and Dawson, J. B. 1995. Enrichment of Continental lithosphere by OIB melts: Isotopic evidence from the volcanic province of northern Tanzania. Earth and Planetary Science Letters 130, 109-126.

Paslick, C., Halliday, A. N., Lange, R. A., James, D. J. and Dawson, J. B., 1996. Indirect crustal contamination: evidence from isotopic and chemical disequilibria in minerals from alkali basalts and nephelines from northern Tanzania. Contributions to Mineralogy and Petrology 125, 277-292.

Renne, P., Swisher III, C., Deino, A., Kamer, D., Owens, T., DePaolo, D., 1998. Intercalibration of standards, absolute ages, and uncertainties in $^{40}Ar/^{39}Ar$ dating. Chemical Geology 145**,** 117-152.

Rogers, W. M., James, D., Kelley, S. P., De Mulder, M, 1998. The generation of potassic lavas from eastern Virunga province, Rwanda. Journal of Petrology 39, 1223-1247.

Rogers, N., Macdonald, R., Fitton, J. G., George, R., Smith, M. and Barreiro, B., 2000. Two mantle plumes beneath the East African rift system: Sr, Nd and Pb isotope evidence from Kenya Rift basalts. Earth and Planetary Science Letters 176, 38-400.

Saito, G., Stimac, J. A., Kawanabe, Y. and Goff, F., 2002. Mafic-felsic magma interaction at Satsuma-Iwojima Volcano, Japan; evidence from mafic inclusion in rhyolite. Earth, Planets and Space 54, 303-325.

Schimitt, A. K., Lindsay, J. M., de Silva, S. and Trumbull, R. B., 2003. U-Pb zircon chronostratigraphy of early Pliocene ignimbrites from La Pacana, North Chile; implications for formation of stratified magma chambers.

Journal of Volcanology and Geothermal Research 120, 43-53.
Späth, A., Le Roex, A., and Opiyo-Akech, N., 2001. Plume-Lithosphere interaction and the origin of continental rift-related alkaline volcanism-the Chyulu Hills Volcanic Province, southern Kenya. Journal of Petrology 42, 765-787.
Späth, A., Le Roex, A., and Duncan, A. R., 1996. The geochemistry of lavas from The Comores Archipelago, western Indian Ocean: petrogenesis and mantle source region characteristics. Journal of Petrology 37, 961-991.
Sun, S,-s. and McDonough, W. F., 1989, Chemical and isotopic systematics of oceanic basalts: Implications for mantle compositions and processes. In: A. D. Sauders and M. J. Norry (ed.), Magmatism in the Oceanic Basins. Geological Society Special Publication 42, 313-345.
Tatsumoto, M., Basu, A., Wangkang, H., Junwen, W. and Guanghong, X., 1992. Sr, Nd, and Pb isotopes of ultramafic xenoliths in volcanic rocks of Eastern China: enriched components EMI and EMII in subcontinental lithosphere. Earth and Planetary Science Letters 113, 107-128.
Trua, T., Deniel, C. and Mazzuoli, R., 1999. Crustal control in the genesis of Plio-Quaternary bimodal magmatism of the main Ethiopian Rift (MER): Geochemical and isotopic (Sr, Nd, Pb) evidence. Chemical Geology 155, 201-231.
Walter, R.C., Manega, P.C. and Hay, R.L., 1992. Tephrochronology of Bed I, Olduvai Gorge: An application of laser fusion $^{40}Ar/^{39}Ar$ dating to calibrating biological and climatic change. Quaternary International 13, 37-46.
Walter, R.C., Manega, P.C., Hay, R.L., Drake, R.E. and Curtis, G.H., 1991. $^{40}Ar/^{39}Ar$ dating of Bed I, Olduvai Gorge, Tanzania. Nature 354, 145-149.
Weeraratne, D. S., Forsyth, D. W., Fischer, K. M. and Nyblade, A. A., (2003). Evidence for an upper mantle plume beneath the Tanzania Craton from rayleigh wave tomography. Journal of Geophysical Research 108 (B9), 2427

CHAPTER 5

Petrogenesis of basalt-trachyte lavas from Olmoti Crater

Abstract

Plio-Pleistocene Olmoti Crater is part of the Ngorongoro Volcanic Highland Complex (NVHC), situated at the southern divergence of the Gregory Rift, in northern Tanzania. It is considered the source of the volcaniclastic deposits at the proximal hominid-bearing Olduvai Gorge. Here, I report on the petrology, geochemistry, and geochronology of lavas from Olmoti Crater and its relationships with the NVHC and Olduvai Gorge.

Major and trace element data show a compositional range from basalt to trachyandesite for the Olmoti Lower Section (OLS) lavas and include trachyte in the Olmoti Upper Section (OUS). The elemental data are consistent with derivation from a single parental magma. The mineral assemblage includes sodic ferroan augite, plagioclase, anorthoclase, titanomagnetite, kaersutite, katophorite, aenigmatite and rare olivine and biotite. High Field Strength Element (HFSE) ratios (e.g., Zr and Nb) are fractionated within the lava types and the ratios appear to decrease with increasing fractionation. The cause of the fractionated Zr/Nb is crystallization of Ti-bearing minerals (titanomagnetite, aenigmatite, amphibole, and biotite) that are a repository for HFSE (LaTourrette et al. 1995; Vannucci et al. 1995). The Zr/Nb ratios are higher lower in the section and decrease up-section, consistent with increased modal abundance of Ti-bearing phases as well as a decrease in the amphibole magnesium number.

The Sr and Nd isotope ratios of OLS and OUS overlap and vary between 0.70454 to 0.704930 and 0.512144 to 0.512760, respectively. These ratios can be explained by mixing of enriched mantle and high-μ reservoirs; however, their wider variability reflects

crust-magma interaction. The isotope ratios are within the range of values defined by OIB globally, and moderate normalized Tb/Yb ratios (2.3-1.6) in these lavas suggest melting in the lithospheric mantle consistent with other studies in the region.

The $^{40}Ar/^{39}Ar$ laser incremental-heating analyses of matrix and anorthoclase from representative samples indicate that Olmoti activity was short in duration lasting ~200 ka from 2.01 ± 0.03 Ma to 1.80 ± 0.01 Ma. These dates are compatible with ages on tephra interbedded in Olduvai Bed I (Hay, 1976; Walter *et al.,* 1992) and are in agreement with the top of the Olduvai Subchron. The older ages for Olmoti are significant because they overlap with volcanism from Ngorongoro caldera, implying that multiple volcanoes were contemporaneously active.

BACKGROUND

Olmoti Crater is part of the Plio-Pleistocene Ngorongoro Volcanic Highland Complex (NVHC), situated at the southern divergence of the Gregory Rift of the East African Rift System (EARS) in northern Tanzania (Figures 1.1 and 1.2). Olmoti is among the largest volcanoes of the NVHC and is considered the source of the bulk of the volcanic and volcaniclastic deposits of the proximal hominin and archaeological bearing deposits of Olduvai Gorge Bed I.

The NVHC is superimposed on two major geologic provinces: the Tanzanian Archean Craton basement rocks (Cahen *et al.*, 1984) to the west and the late-Proterozoic Mozambican Belt basement rocks to the east (Key *et al.*, 1989). Present day rifting in northern Tanzania developed at about 1.2 Ma as a result of major faulting that began at about 3 Ma (Dawson, 1992; Foster *et al*., 1997). Pre-rift volcanism produced large shield volcanoes of basalt-trachyte-phonolite association. The earliest reported volcanic activity along the NVHC is 8.1 Ma for phonolitic lavas at Essimingor (Bagdasaryan *et al.*, 1973), although this age might be anomalously old due to excess argon (Mollel *et al.*, in press). Volcanism after the main phase of rift faulting produced volatile and alkali-rich explosive centers, some of which (e.g. Oldoinyo Lengai) are active today (Dawson, 1992, Foster *et al.*, 1997).

Olmoti Crater has a summit diameter of about 6 km and a maximum elevation of 3100 m (Hay, 1976). Previous studies indicate that it is primarily composed of basalt and trachyandesite (Hay, 1976). Lava and tephra interbedded in the artifact, hominin and vertebrate fossil bearing Bed I strata (ca 1.9 to 1.78 Ma) of Olduvai Gorge (Leakey *et al.*, 1971; Hay, 1976; Ashley and Driese, 2000; Ashley and Hay, 2002; Blumenschine *et al.*,

2003) are considered to come from nearby Olmoti Crater (McHenry *et al.*, 2007; Hay, 1976). This correlation is based on K-Ar and paleomagnetics data obtained from Olduvai lava and general similarity in compositions of volcanic material (Hay, 1976; McHenry, 2004; Mollel and McHenry, 2004). Further support of this correlation was provided by McHenry *et al.* (2007) through geochemical fingerprinting of mineral suites, textures, and $^{40}Ar/^{39}Ar$ dating, linking Olduvai Bed I tephra to Olmoti.

The objectives of this Chapter are twofold: 1) characterize the chemistry and mineral compositions of lavas from Olmoti Crater and 2) provide precise $^{40}Ar/^{39}Ar$ ages delimiting Olmoti activity. The evolutionary history of Olmoti is important for understanding factors controlling rift-related magmatism along the EARS and in particular northern Tanzania. Moreover, dates obtained from lavas and volcaniclastic materials exposed in fault escarpments help constrain fault movements (e.g. Macintyre *et al.*, 1974; Hay, 1976; Dawson, 1992) and the tectonic development of the region (e.g. Foster *et al.*, 1997). Better chronological control is also important for determining sources for Olduvai Bed I volcanic material. Olduvai Bed I lavas and Tuff IF, both interpreted to have originated from Olmoti, are useful marker units for Olduvai stratigraphy (Hay, 1976; McHenry, 2004; McHenry *et al.*, 2007). Sources of these volcanics have been of great interest to both geologists and archaeologists working at Olduvai, as Tuff IF has been a focus of study of hominin landscape usage during a time of major faunal turnover (Blumenschine *et al.*, 2005).

PREVIOUS WORK

On his regional maps of the Ngorongoro Volcanic Highland areas, Pickering (1965) shows Olmoti composed primarily of basalt and phonolite, whereas Hay (1976) and Manega (1993) indicate primarily basalt and trachyandesite.

The K-Ar dating of basalt and tephra at Olduvai Gorge following the discovery of the Zinjanthropus fossil by Louis and Mary Leakey in 1959 represents one of the first age determinations for hominin fossil calibration (Koenigswald *et al.*, 1961; Leakey *et al.*, 1962). Subsequently, there have been a series of attempts to refine the age of the Olduvai sequence and of the volcanoes of the NVHC using K-Ar methods (Curtis and Hay, 1972; Bagdasaryan *et al.*, 1973; Drake and Curtis, 1987; Manega, 1993), and more recently (in the 1990s) using $^{40}Ar/^{39}Ar$ techniques in the 1990s (Walter *et al.*, 1991, 1992; Manega, 1993). Available K-Ar dates for the NVHC are of mixed quality and accuracy. This is, in part, due to the incorporation of detrital minerals in the tephra resulting in ages that are anomalously old (e.g. Grommé *et al.*, 1970; Curtis and Hay, 1972). Excess ^{40}Ar in some dated mineral phases such as nepheline have also resulted in ages that are too old (Mollel *et al.*, in press). In some cases, poor sample site documentation has hampered the use of some analyses because it is difficult to interpret or correlate with any particular volcanic center (e.g. Manega, 1993). For example, K-Ar dates reported by Manega (1993) for Olmoti crater were obtained by dating lava flows and ignimbrites collected from slopes or lavas that align with Olmoti crater, rather than from the volcano itself. Existing K-Ar and $^{40}Ar/^{39}Ar$ ages for Olmoti range from 1.85 to 1.09 Ma, suggesting that Olmoti was active between about 1.85 and 1.1 Ma.

METHODS

Field methods

To assure correct assignment of lavas to Olmoti, samples for this study were collected from inside the crater wall. Sample selection was based on availability of outcrops and sample freshness (none of the samples show significant weathering), as well as the presence of datable mineral phases. Three samples of the Olduvai Bed I lava were also collected and are discussed separately (section 11) because their relative position in the Olmoti sequence is unclear. UTM coordinates of the sampled sites are provided in Table 5.1.

Laboratory methods

Samples were pulverized using a jaw crusher and powdered in a mill-grinder before being sent to the Department of Geological Sciences at Michigan State University (MSU). At MSU, rock powders were made into glass disks using the high dilution fusion (HDF) technique by mixing the powder with lithium tetraborate as a flux and ammonium nitrate as an oxidizer. The proportions used were 1 gm rock, 9 gm lithium tetraborate and 0.25 gm ammonium nitrate. These materials were mixed, fused at 1000 $^{\circ}$C in a platinum crucible in an oxidizing flame for 30 minutes and then poured into platinum molds (Hannah *et al*., 2002). Major elements were determined using an SMAX Rigaku X-ray spectrometer and data was reduced using the fundamental parameter method (Criss, 1980) using XRFWIN software (Omni Instruments).

Trace and rare earth element concentrations were determined on the same glass disks by laser ablation using a Platform Inductively Coupled Plasma Mass Spectrometer

(ICP-MS). The procedures followed are similar to those outlined by Hannah *et al*. (2002). Data quality was monitored by co-analyzed USGS rock standards. Compared to the USGS, AGV-1 standard (Gladney *et al.*, 1988) the error was $< \pm 3$ % for all major oxides. Compared to the USGS, AGV-1 standard (Eggins *et al*., 1997), error was $< \pm 6$ % for all trace and REE elements except for Pt, Eu, Gd and Rb where error is ± 8 %. Major element oxides in weight percent (wt %) and trace elements in parts per million (ppm) are given in Table 5.1.

The Sr and Nd isotopic analyses of selected samples were conducted at Rutgers University using a multi-collector VG Isoprobe TIMS. Sample preparation procedures followed those of Bolge *et al.* (2006). Measured values for the SRM-987 Sr and La Jolla-Nd standards were $^{87}Sr/^{86}Sr = 0.710237 \pm 5$ and $^{143}Nd/^{144}Nd = 0.511846 \pm 2$, respectively. Analyses of the selected samples are reported on Table 5.1.

Mineral phases of selected samples were determined using a Cameca XS50 electron microprobe at the University of Wisconsin-Madison, following the procedures and standards of McHenry *et al.* (2007). Running conditions were 15 KV and 15 nA with a focused beam. A few samples were also analyzed at Rutgers University (RU) using JEOL JXA-8600 SuperProbe (Mollel, 2002). At RU, the same beam current was used; accelerating voltage was set at 20 KV with a beam diameter of one micrometer. Microprobe analyses (point counts) of selected samples are reported in Table 5.2 as oxides in wt %

Seven lava samples from the OLS and OUS sections were prepared for $^{40}Ar/^{39}Ar$ incremental heating analyses. Samples were crushed using a Sepor mini-jaw crusher, sieved between 0.425 to 0.250 mm meshes, and washed in ultra sonic baths of distilled water. The purified samples were loaded into Al sample disks along with aliquots of the Alder Creek Sanidine (ACs = 1.194Ma), wrapped in Al foil, sealed in quartz glass tubes, and then irradiated in the Cadmium-Lined, In-Core Irradiation Tube [CLICIT] facility of the Oregon State University Triga Research Reactor [OSTR] for 40 - 60 minutes. The interference corrections used are $^{36}Ar/^{37}Ar_{Ca}$ = 2.72 ± 0.01(x10^{-4}), $^{39}Ar/^{37}Ar_{Ca}$ = 7.11 ± 0.024 (10^{-4}), and $^{40}Ar/^{39}Ar_{K}$ = 7 ± 3 (10^{-4}) (Deino and McBrearty, 2002). Mass discrimination was monitored during the analyses from replicate aliquots delivered from an on-line air pipette system, and J was calculated from replicate analyses of the co-irradiated AC mineral standards. At the Rutgers University Ar-lab, samples were heated in step-wise increments for 60 seconds each using a 40-Watt CO_2 laser defocused though a 6 mm integrator lens. The released argon isotopes were measured on a MAP215-50 mass spectrometer and $^{40}Ar/^{39}Ar$ ages were calculated using automated software by A. Deino following procedures similar to those outlined in Renne et al. (1998 and references therein). Plateau, isochron, and total fusion ages are reported in Table 5.3. All plateau ages constitute at least three contiguous steps, and at least 50 % of the total radiogenic argon ($^{39}Ar^*$) released. A more detailed evaluation of the analytical data can be found in Carr *et al.* (2007) and Turrin *et al.* (2007).

RESULTS

Petrography and mineral chemistry

Based on stratigraphic position and chemistry, the Olmoti lavas are here divided into two groups: those with SiO_2 content < 55 wt % are classified as mafic and those with SiO_2 content > 59 wt % are defined as silicic. The mafic lavas include basalt and trachyandesite and come exclusively from the OLS whereas the silicic lavas are trachytic and come exclusively from the OUS. The two groups have distinctive mineral assemblages, related to their differing chemistry.

The mafic lower group (Figure 5.1) is medium-grained and composed of augite, plagioclase, anorthoclase, and amphibole. Ilmenite is the main oxide mineral. The groundmass is made up of plagioclase, anorthoclase and augite and the phenocrysts are of the same composition but also include amphibole. Plagioclase and anorthoclase are trachytoid and glomeroporphyritic in texture. The plagioclase compositions from different grains range from An_{55} to An_{14} and have ophitic and subophitic textures with augite. Augite composition ranges from $En_{39}Fs_{20}Wo_{41}$ to $En_{30}Fs_{29}Wo_{40}$. The augite is very sodium and iron rich, hence the name sodic ferroan augite. The TiO_2, Na_2O, and FeO contents of the augite are as high as 2.5, 3.0, and 13.8 wt % respectively. Typical Na_2O and FeO contents for augites and ferroan augites are < 1 wt % and 8 wt % and < 1 wt % and 27 wt % respectively (Deer *et al.,* 1992).

Amphibole is present as phenocryst and is mainly kaersutitic. In general, kaersutite is chemically characterized by high titanium contents ranging between 5 and 10 wt % (Deer *et al*., 1992). For the Olmoti samples, one grain has a TiO_2 content of 10.7 wt % (Table 5.2).

Ilmenite occurs in subhedral prisms, one grain has a TiO_2 content of ~45 wt %

Table 5.1: UTM coordinates, major oxides (wt %), trace elements (ppm) and Sr and Nd isotope data for Olmoti lavas, na = not analyzed

Sample	OLT-1	OLT-2	OLT3	OLT4	OLT5	OLT6	OLT7	03-OLT1	03-OLT2	03-OLT3	04-OLT1	04-OLT2	04-OLT3	04-OLT4	OLD1	OLD2	OLD3
UTM E	797524	797524	797532	797484	797679	797894	798302	794697	794651	794811	796201	796201	796201	795796	774955	768273	767160
UTM S	9665626	9665626	9665615	9665556	9665686	9665678	9664913	9664264	9664218	9664266	9664130	9664130	9664130	9664272	9675092	9671216	9671182
SiO2	48.50	48.85	47.79	48.46	53.80	53.34	53.22	59.72	59.67	60.24	62.80	63.87	60.43	60.33	48.62	49.03	48.69
TiO2	2.74	2.78	2.84	2.88	2.50	2.58	2.19	0.59	0.64	0.66	0.54	0.53	1.04	0.58	2.76	3.01	2.94
Al2O3	14.83	14.88	14.91	16.56	15.88	15.53	17.46	17.13	17.29	17.24	15.92	14.94	17.93	17.32	15.23	15.03	14.91
FeO	13.83	14.39	15.28	13.61	10.95	11.16	9.44	6.15	6.15	6.27	7.04	6.98	6.66	6.24	12.11	12.9	12.35
MnO	0.18	0.13	0.13	0.19	0.16	0.16	0.12	0.21	0.23	0.24	0.25	0.29	0.14	0.25	0.19	0.19	0.15
MgO	3.97	3.66	3.42	2.74	2.71	2.49	1.93	0.78	0.76	0.54	0.26	0.25	0.61	0.59	3.06	3.59	4.4
CaO	8.00	7.66	7.15	7.58	5.82	5.68	6.44	1.18	1.60	1.10	0.51	0.63	1.80	1.08	8.89	7.94	9.06
Na2O	3.63	3.65	3.68	3.86	4.36	4.49	4.70	6.97	6.56	6.97	6.60	6.48	6.75	6.89	4.45	4.52	3.95
K2O	1.31	1.31	1.36	1.52	2.04	2.01	1.78	5.08	5.14	4.70	4.34	4.41	3.69	5.02	2	1.86	1.66
P2O5	0.40	0.41	0.42	0.45	0.54	0.56	0.53	0.07	0.09	0.09	0.05	0.05	0.23	0.05	0.6	0.54	0.46
Total	97.39	97.72	96.98	97.85	98.76	98.00	97.81	97.88	98.13	98.05	98.31	98.43	99.28	98.35	97.91	98.61	98.57
Rb	8.5	8.9	9.9	32.5	44.0	37.5	42.4	131.0	146.9	120.2	80.0	123.0	91.0	130.0	40	42	46
Sr	467	479	452	745	665	689	892	365	764	121	50	35	415	313	1344	778	909
Zr	254	252	265	280	362	391	359	689	652	647	1005	949	601	698	322	314	258
Ba	409	404	410	674	1010	1127	1371	380	786	2047	468	493	1143	2919	658	622	572
La	43	44	44	73	104	134	87	167	188	211	112	161	109	411	72	74	61
Ce	75	77	80	130	167	176	159	279	268	336	303	487	140	375	120.28	124.13	103.59
Pr	8.99	9.49	9.61	15.72	19.28	24.41	17.91	30.16	30.53	38.40	22.26	32.59	20.14	62.79	14.93	15.67	12.8
Nd	35	36	37	60	70	88	65	102	102	133	69	111	68	212	58.41	61.49	50.33
Sm	nd	6.54	nd	11.24	12.33	15.43	12.12	16.96	16.53	24.08	9.88	18.40	10.54	32.91	10.64	11.77	9.36
Eu	1.90	1.99	2.04	3.11	3.59	4.34	3.52	3.42	3.57	5.32	1.92	3.64	3.55	6.53	2.99	3.27	2.72
Gd	5.82	6.15	6.25	9.72	11.50	14.69	10.32	15.29	14.81	22.65	14.29	26.59	11.50	39.47	10.32	11.01	9.26
Tb	0.83	0.86	0.88	1.36	1.59	2.03	1.45	2.20	2.10	3.63	1.18	2.58	1.35	5.47	1.42	1.54	1.26
Y	21.47	21.39	22.12	35.17	51.45	58.14	37.40	64.74	70.93	124.30	17.63	42.98	37.10	179	37.59	37.33	32.52
Dy	4.40	4.16	4.37	6.97	8.15	10.68	7.15	11.68	11.32	21.40	4.63	11.62	6.65	29.82	7.08	7.36	6.23
Ho	0.80	0.77	0.81	1.30	1.63	2.07	1.33	2.32	2.21	4.31	0.83	2.09	1.32	6.20	1.37	1.43	1.18
Er	2.01	1.86	1.97	3.07	4.16	5.15	3.41	6.06	5.83	11.18	2.23	4.74	3.11	14.45	3.37	3.59	2.76
Yb	1.76	1.69	1.71	2.81	3.72	4.42	3.06	6.22	5.97	10.58	3.23	6.09	3.42	15.01	4.48	4.66	3.67
Lu	0.24	0.24	0.24	0.39	0.56	0.62	0.43	0.77	0.70	1.37	0.46	0.84	0.47	2.06	0.41	0.45	0.33
V	187	192	189	275	153	156	132	1.03	1.11	1.29	3.82	13.51	4.43	0.00	239.11	240.91	264.1
Cr	17.28	17.31	16.43	22.86	14.77	14.30	19.64	2.62	2.37	2.72	4.29	5.36	4.19	4.14	1.92	9.54	136.44
Nb	45	45	46	72	97	104	90	276	252	263	386	351	199	314	88	89	77
Hf	4.35	4.26	4.53	6.62	8.35	8.80	7.17	18.06	15.93	16.20	26.61	28.61	13.15	16.93	7.37	7.67	6.3
Ta	2.45	2.43	2.59	3.97	5.12	5.29	4.41	17.18	15.36	15.35	20.99	19.33	10.17	16.97	4.79	4.93	4.22
Pb	3.80	4.18	3.91	6.86	10.71	9.17	14.14	19.78	17.98	18.39	26.74	35.68	13.36	22.40	3.96	4.13	4.42
Th	5.74	5.82	6.07	9.94	11.94	12.19	9.68	33.95	29.81	30.07	51.13	55.66	24.66	34.46	12.79	11.43	9.46
U	0.40	0.50	0.53	1.11	2.40	2.16	2.30	5.71	2.47	5.03	2.90	3.37	2.45	4.72	2.15	2.71	3.05
87Sr/86Sr	nd	0.70458	nd	nd	0.70473	nd	0.70508	0.70493	nd	0.70454	0.70473	0.70412	nd	0.70463	0.70498	0.70490	0.70502
143Nd/144Nd	0.51214	0.51246	nd	nd	nd	nd	0.51255	nd	nd	0.51276	0.51265	0.51247	nd	0.51269	nd	nd	0.51267

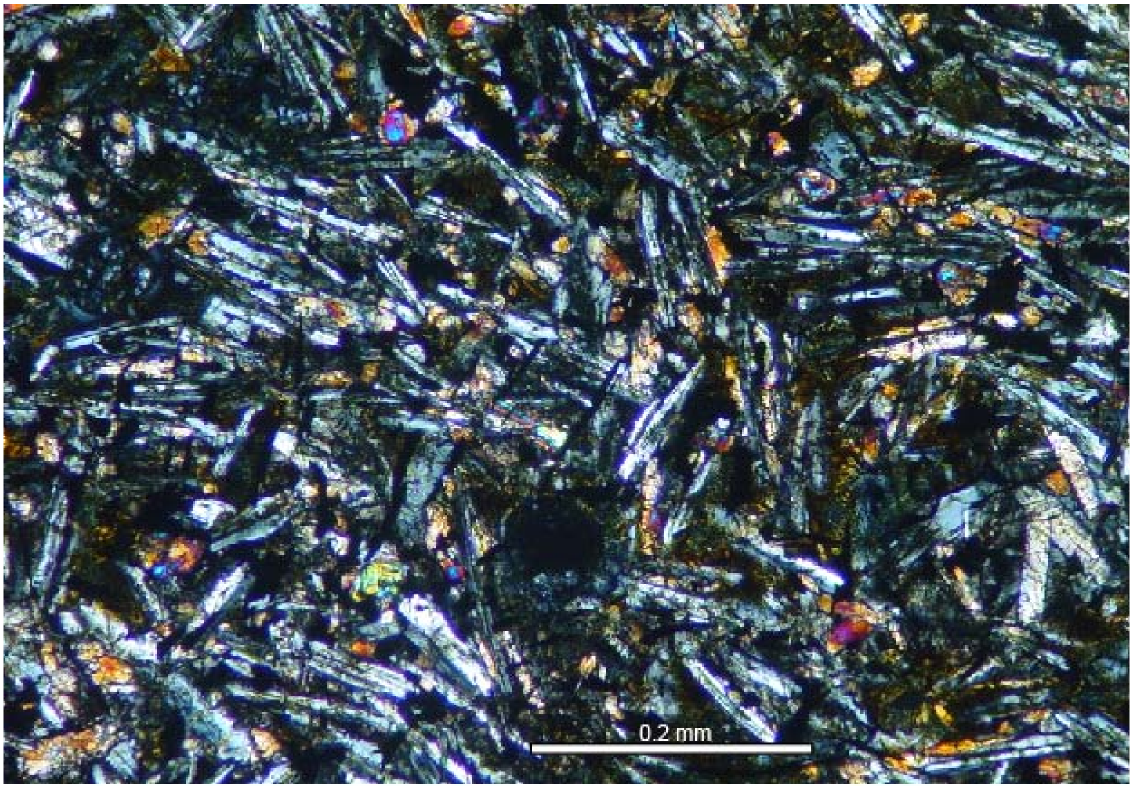

Figure 5.1: Microphotograph of medium-grained Olmoti basalt (00-OLT3) from OLS showing ophitic augite (green and rainbow colors) and albite twinned plagioclase.

Table 5.2: Olmoti mineral compositions (electron microprobe data)

Lower Section											
00-OLT4											
Augite	SiO2	TiO2	Al2O3	FeO	MnO	MgO	CaO	Na2O	K2O	BaO	SUM
1	49.57	2.48	6.78	13.41	0.29	8.31	13.55	3.01	0.83	0.00	98.23
2	51.86	0.94	4.97	13.02	0.38	10.33	15.51	1.92	0.40	0.00	99.34
3	50.35	1.32	2.84	11.82	0.29	12.82	18.56	0.73	0.16	0.00	98.90
Mean	**50.59**	**1.58**	**4.87**	**12.75**	**0.32**	**10.49**	**15.87**	**1.89**	**0.46**	**0.00**	**98.82**
Feldspar											
1	56.27	0.16	26.98	0.59	0.02	0.09	9.03	6.55	0.55	0.00	100.23
2	58.52	0.18	24.56	0.89	0.00	0.07	6.80	7.59	0.85	0.00	99.45
3	62.92	0.21	22.69	1.09	0.02	0.04	5.13	7.68	1.69	0.00	101.46
4	56.01	0.13	26.31	0.53	0.02	0.08	9.81	5.91	0.45	0.00	99.23
Mean	**58.43**	**0.17**	**25.13**	**0.77**	**0.01**	**0.07**	**7.69**	**6.93**	**0.88**	**0.00**	**100.09**
Kaersutite											
1	40.03	7.88	3.62	27.47	0.30	9.37	10.64	1.10	0.40	0.00	100.81
2	38.07	7.95	3.87	27.20	0.41	8.13	10.68	1.21	0.52	0.00	98.04
3	37.67	9.04	5.49	27.27	0.39	6.59	10.45	2.00	0.32	0.00	99.23
4	49.92	4.81	11.74	15.76	0.22	4.03	7.66	4.97	1.84	0.00	100.94
00-OLT7											
Augite											
1	54.06	0.72	4.38	13.83	0.30	8.09	14.94	1.35	0.43	0.08	98.18
2	52.12	0.79	2.40	12.24	0.45	12.02	18.44	0.66	0.13	0.12	99.37
3	52.40	1.10	7.15	9.77	0.31	9.00	15.47	2.99	0.78	0.08	99.03
4	51.04	0.84	1.39	12.54	0.46	12.58	18.89	0.52	0.08	0.03	98.37
Mean	**52.40**	**0.86**	**3.83**	**12.09**	**0.38**	**10.42**	**16.93**	**1.38**	**0.35**	**0.07**	**98.74**
Feldspar											
1	53.30	0.13	29.65	0.52	0.01	0.18	11.00	4.89	0.26	0.02	99.96
2	63.14	0.12	22.30	0.61	0.00	0.15	2.94	8.00	2.62	0.12	99.98
3	61.29	0.17	23.04	0.92	0.04	0.12	4.25	7.48	2.01	0.14	99.46
4	61.91	0.21	22.61	0.64	0.01	0.27	3.77	8.09	2.50	0.17	100.18
Kaersutite											
1	35.50	8.13	12.24	32.30	0.20	1.66	2.59	5.54	1.90	0.75	100.82
2	31.19	10.74	10.73	37.11	0.22	0.38	2.20	4.18	1.99	0.87	99.61
3	45.73	4.88	13.99	22.92	0.23	0.92	3.40	5.51	3.31	0.47	101.35
Oxides											
1	1.55	44.55	0.12	46.64	0.55	1.67	1.44	0.27	0.03	3.59	100.39

Table 5.2 continued

Upper section
03-OLT1

Fayalite	SiO2	TiO2	Al2O3	FeO	MnO	MgO	CaO	Na2O	K2O	BaO	SUM
1	29.80	0.05	0.04	55.34	4.04	7.60	0.89	0.05	0.00	0.00	97.80
2	29.85	0.05	0.08	56.54	4.07	6.55	0.91	0.08	0.00	0.00	98.14
3	30.00	0.07	0.16	55.45	3.92	7.28	0.94	0.08	0.00	0.00	97.89
4	30.94	0.05	0.16	54.28	4.01	8.70	0.73	0.08	0.00	0.00	98.96
5	31.09	0.02	0.06	55.51	4.00	7.86	0.81	0.04	0.00	0.00	99.38
6	31.05	0.08	0.07	56.32	4.13	6.99	1.01	0.07	0.00	0.00	99.71
Mean	**30.45**	**0.05**	**0.09**	**55.57**	**4.03**	**7.50**	**0.88**	**0.07**	**0.00**	**0.00**	**98.65**
Augite											
1	47.96	2.57	1.18	21.67	0.68	3.12	14.12	5.00	0.07	0.15	96.52
2	49.08	1.49	1.28	19.94	0.81	4.76	17.47	3.18	0.10	0.00	98.10
3	49.70	2.07	0.88	24.29	0.90	1.47	11.43	6.47	0.07	0.18	97.46
4	51.04	0.24	0.90	25.35	0.86	1.25	9.31	7.46	0.06	0.00	96.47
Mean	**49.44**	**1.59**	**1.06**	**22.81**	**0.81**	**2.65**	**13.08**	**5.53**	**0.08**	**0.08**	**97.14**
Feldspar											
1	67.12	0.00	18.85	0.71	0.00	0.02	0.33	8.47	4.45	0.06	100.00
2	66.34	0.00	18.08	0.57	0.00	0.01	0.20	7.13	6.54	0.00	98.86
3	65.53	0.00	19.57	0.67	0.00	0.04	0.88	8.63	3.56	0.00	98.88
4	64.63	0.00	19.56	0.68	0.00	0.05	1.00	8.07	4.46	0.56	99.00
5	65.98	0.00	17.99	0.85	0.00	0.09	0.29	6.52	6.90	0.09	98.72
Mean	**65.92**	**0.00**	**18.81**	**0.70**	**0.00**	**0.04**	**0.54**	**7.76**	**5.18**	**0.14**	**99.09**
Katophorite											
1	50.66	0.49	1.44	24.38	0.93	5.72	2.79	7.49	1.76	0.02	95.67
2	46.14	1.81	4.60	20.33	1.00	7.62	6.94	4.74	1.58	0.00	94.75
3	49.54	1.55	2.38	22.05	0.97	7.38	3.77	7.18	1.36	0.00	96.17
4	47.37	1.30	3.34	19.61	0.87	9.31	7.00	4.95	1.59	0.00	95.33
Mean	**48.43**	**1.29**	**2.94**	**21.59**	**0.94**	**7.50**	**5.13**	**6.09**	**1.57**	**0.00**	**95.48**
Aenigmatite											
1	39.56	6.81	0.84	40.97	1.27	1.05	0.50	7.25	0.00	0.00	98.24
2	39.27	7.24	0.98	40.63	1.30	0.76	0.58	7.01	0.00	0.00	97.76
3	40.62	3.90	0.56	43.21	1.26	0.86	0.42	7.13	0.05	0.06	98.06
Mean	**39.82**	**5.98**	**0.79**	**41.60**	**1.27**	**0.89**	**0.50**	**7.13**	**0.02**	**0.02**	**98.02**
Biotite											
1	38.26	4.00	10.71	13.12	0.38	15.82	0.01	0.81	8.80	0.20	92.09
2	39.09	3.78	10.61	13.38	0.38	15.61	0.01	0.88	8.81	0.00	92.56
3	39.99	3.16	9.50	11.68	0.28	17.40	0.01	1.03	9.24	0.00	92.28
Mean	**39.11**	**3.64**	**10.27**	**12.73**	**0.34**	**16.28**	**0.01**	**0.91**	**8.95**	**0.07**	**92.31**
Oxides											
1	0.13	15.77	0.56	78.23	1.31	0.17	0.05	0.00	0.00	0.00	96.22
2	0.16	16.83	0.52	76.22	1.37	0.18	0.02	0.00	0.00	0.00	95.30
3	0.16	15.59	0.61	78.46	1.52	0.19	0.01	0.00	0.00	0.00	96.54
4	0.15	16.54	0.45	76.92	1.61	0.08	0.03	0.00	0.00	0.00	95.77
Mean	**0.15**	**16.18**	**0.53**	**77.46**	**1.45**	**0.15**	**0.02**	**0.00**	**0.00**	**0.00**	**95.95**

Table 5.2 continued

03-OLT3											
Augite	SiO2	TiO2	Al2O3	FeO	MnO	MgO	CaO	Na2O	K2O	BaO	SUM
1	48.36	2.00	1.02	20.45	0.84	4.14	15.74	3.64	0.05	0.00	96.24
2	50.73	0.66	0.51	27.26	0.64	0.90	7.93	8.56	0.03	0.00	97.22
3	49.16	0.93	1.64	13.57	0.75	10.41	19.92	0.98	0.03	0.00	97.39
4	50.08	1.54	2.11	12.45	0.78	11.12	19.58	1.02	0.00	0.05	98.73
Mean	**49.58**	**1.28**	**1.32**	**18.43**	**0.75**	**6.64**	**15.79**	**3.55**	**0.03**	**0.01**	**97.40**
Feldspar											
1	67.77	0.00	19.47	0.49	0.00	0.00	0.06	5.88	8.41	0.00	102.08
2	70.33	0.00	19.55	0.80	0.00	0.01	0.04	4.11	7.77	0.25	102.84
3	71.36	0.00	19.66	0.46	0.00	0.00	0.14	1.96	6.54	0.03	100.15
4	70.28	0.00	20.33	0.66	0.00	0.01	0.12	2.96	6.92	0.09	101.36
5	64.75	0.00	19.23	0.63	0.00	0.01	0.61	8.69	3.95	0.28	98.14
Mean	**68.90**	**0.00**	**19.65**	**0.61**	**0.00**	**0.01**	**0.19**	**4.72**	**6.72**	**0.13**	**100.92**
Katophorite											
1	48.46	2.65	1.99	21.53	0.95	7.79	5.38	5.79	1.55	0.00	96.10
2	48.06	2.41	1.98	24.15	0.95	6.69	5.21	6.01	1.52	0.00	96.98
3	49.40	1.54	0.79	22.62	0.81	2.97	13.73	5.22	0.07	0.00	97.14
4	49.73	0.84	0.71	25.82	0.64	1.73	11.11	6.73	0.03	0.10	97.44
5	48.12	2.04	2.08	23.76	0.80	6.59	5.11	6.12	1.43	0.13	96.18
Mean	**48.76**	**1.90**	**1.51**	**23.58**	**0.83**	**5.15**	**8.11**	**5.97**	**0.92**	**0.05**	**96.77**
Aenigmatite											
1	38.17	6.77	1.73	42.17	1.68	0.64	0.66	6.86	0.07	0.21	98.96
2	40.73	5.45	1.48	41.68	1.52	0.72	0.65	6.29	0.04	0.04	98.59
3	39.03	6.41	0.94	41.43	1.52	1.02	0.48	7.38	0.08	0.04	98.31
4	40.45	7.35	1.67	39.37	1.36	0.80	0.45	7.03	0.19	0.00	98.67
5	38.81	5.78	0.78	42.32	1.63	0.71	0.26	7.67	0.05	0.00	98.01
Mean	**39.44**	**6.35**	**1.32**	**41.39**	**1.54**	**0.78**	**0.50**	**7.05**	**0.08**	**0.06**	**98.51**
Oxides											
1	0.35	20.35	0.30	71.85	2.26	0.12	0.01	0.00	0.00	0.00	95.23
2	0.09	18.32	0.21	74.60	1.81	0.09	0.02	0.00	0.00	0.00	95.15
3	0.14	20.42	0.20	75.39	1.93	0.06	0.03	0.00	0.00	0.00	98.18
4	0.11	16.95	0.14	77.33	1.64	0.04	0.00	0.00	0.00	0.00	96.22
5	0.90	18.78	0.20	75.52	1.92	0.06	0.03	0.00	0.00	0.00	97.40
Mean	**0.32**	**18.97**	**0.21**	**74.94**	**1.91**	**0.07**	**0.02**	**0.00**	**0.00**	**0.00**	**96.44**

The silicic upper group (Figure 5.2) is holocrystalline, phaneritic, fine-grained, and composed of trachytic textured feldspar, augite, aenigmatite, amphibole, olivine, and biotite. Titanomagnetite is the main oxide phase. Feldspar varies in composition from oligoclase to anorthoclase with average compositions ranging from $An_1Ab_{71}Or_{28}$ to $An_3Ab_{67}Or_{30}$ (Table 5.2). Anorthoclase makes up most of the groundmass as well as the phenocrysts, although oligoclase appears to be dominant in the latter. Some grains have localized Ba-rich areas.

One silicic lava (03-OLT1) contains a few phenocrysts of fayalitic olivine occurring in a subophitic texture with anorthoclase and augite. The average olivine composition is $Fa_{85}Fo_{15}$ and some grains have MnO content as high as 4.13 wt % (Table 5.2).

Augite in the silicic samples (e.g., 03-OLT3) is greenish brown, makes up part of the groundmass, and is subophitic with anorthoclase. The augite is very sodic and iron rich, with Na_2O and FeO contents up to 8.6 and 27.3 wt %, respectively (Table 5.2). Compositions for the Olmoti sodic ferroan augite ranges from $En_4Fs_{70}Wo_{26}$ to $En_{34}Fs_{22}Wo_{44}$.

The amphiboles in the trachytes are different in composition from those found in the mafic OLS. These have lower TiO_2 (0.5 to 2.65 wt %) compared to the kaersutite. They occur in subophitic textures with feldspar and in minor abundance as phenocrysts. Their FeO and Na_2O content range from 19.6 to 25.8 and 4.7 to 7.50 wt %, respectively (Table 5.2). This composition appears to be of the katophorite series also found in Baie-des-Moutons syenite complex, La Tabatiére, Québec, Canada (Lalonde and Martin, 1983).

Reddish brown prisms of aenigmatite occur as phenocrysts. Its TiO_2 and Na_2O content range from 3.9 to 7.4 and 6.3 to 7.7 wt % respectively and appears to fall within the range of aenigmatite found in trachyte from Puu Koae, West Maui, Hawaii (Velde, 1978).

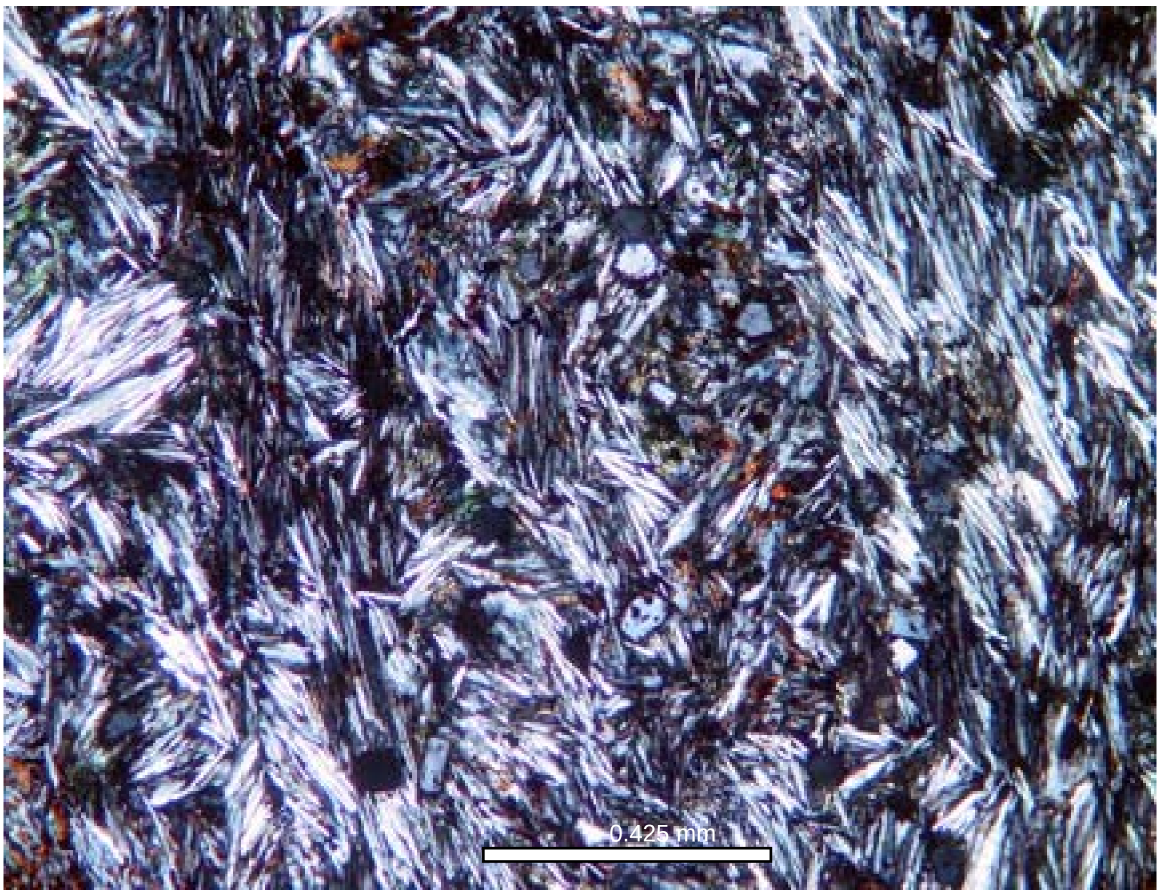

Figure 5.2: Microphotograph of fine-grained trachyte (04-OLT4) from OUS showing abundant alkali feldspar (elongated lath-shaped grains). Brown specks are of augite and olivine.

Biotite is present in minor abundance. TiO_2 content of three analyzed flakes is nearly constant and is between 3.2 and 4.0 wt % (Table 5.2), and the overall composition falls within the range of biotite from mantle xenoliths (Delaney *et al*., 1980; Deer *et al.*, 1992; Dawson, 2002).

Titanomagnetite is the main oxide phase. Its average composition is $Usp_{34}Mg_{66}$. One sample (03-OLT3) contains trace amounts of sodalite.

Major elements

Major element analyses of all lavas are summarized in Table 5.1. According to the classification diagram of Cox *et al.* (1979), the Olmoti lavas vary in composition from basalt to trachyte and include trachyandesites (Figure 5.3). All of the Olmoti lavas are alkaline with SiO_2 content varying from 47.8 to 63.9 wt % and peraluminous using the alumina index of Shand (1927). The mafic lavas differ from the silicic lavas, with higher concentrations of TiO_2, FeO_t, MgO, CaO, and P_2O_5 (Table 5.1). The silicic lavas are characterized by high concentrations of Al_2O_3, MnO, Na_2O, and K_2O. The Mg # is higher in the mafic lavas (~36-27) compared to the silicic lavas (~20-7).

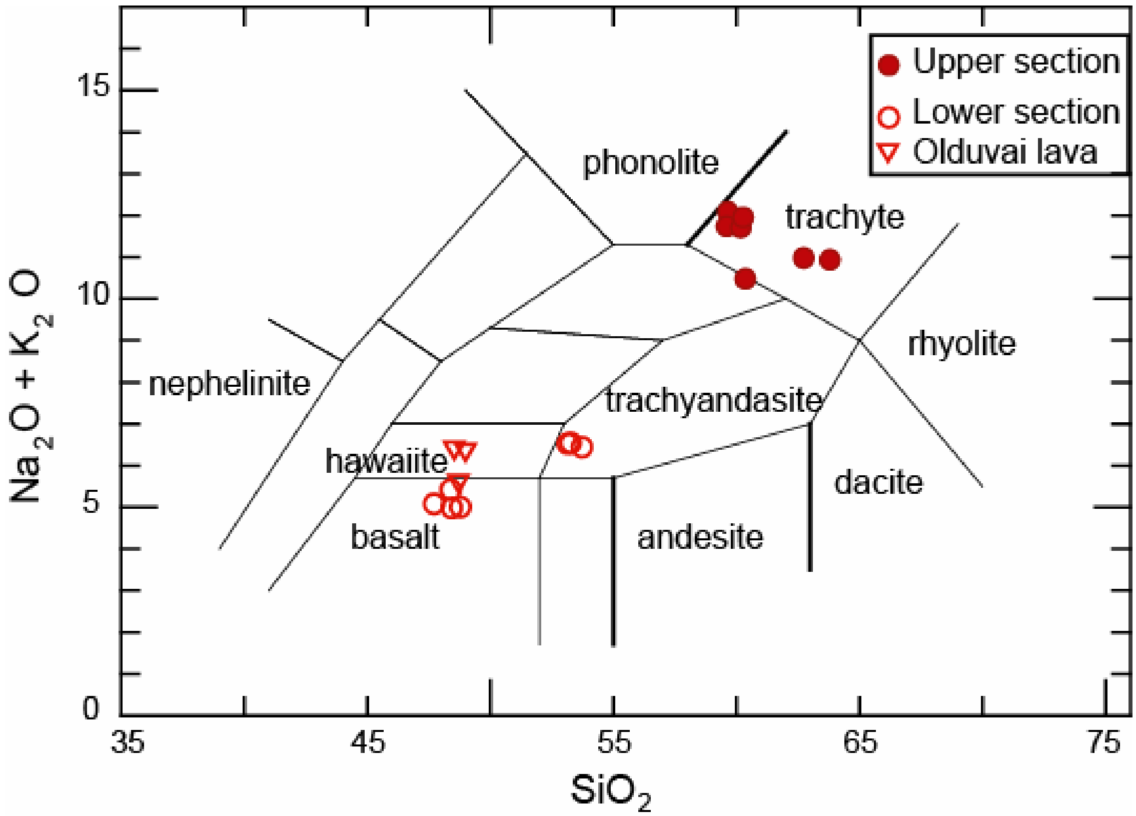

Figure 5.3: Total Alkali versus Silica classification of Cox *et al.* (1979) for Olmoti and Olduvai Bed I lavas.

Trace elements

Highly compatible trace elements such as Cr and V are more concentrated in the mafic lavas (14.3 – 22.9 ppm and 131.5 – 274.8 ppm, respectively), than in the trachyte (2.4 – 5.4 ppm and > 14 ppm, respectively, Table 5.1). Compared to ordinary chondrites all lavas are enriched in rare earth elements (REEs, not illustrated). When compared to primitive mantle, all of the lavas are enriched and show negative Rb, U, K, and Ce anomalies. The trachytes also show negative Sr, P, and Ti anomalies (Figure 5.4). In all lavas, Large Ion Lithophile Elements (LILE) and REEs decrease with increasing Mg#, and High Field Strength Elements (HFSE, e.g. Nb and Zr) clearly separate the mafic lavas from the trachytes. Nb is > 200 ppm in the trachytes and < 100 ppm in the mafic lavas, while Zr is > 600 ppm in the trachytes and is < 400 ppm in the mafic lavas (Table 5.1).

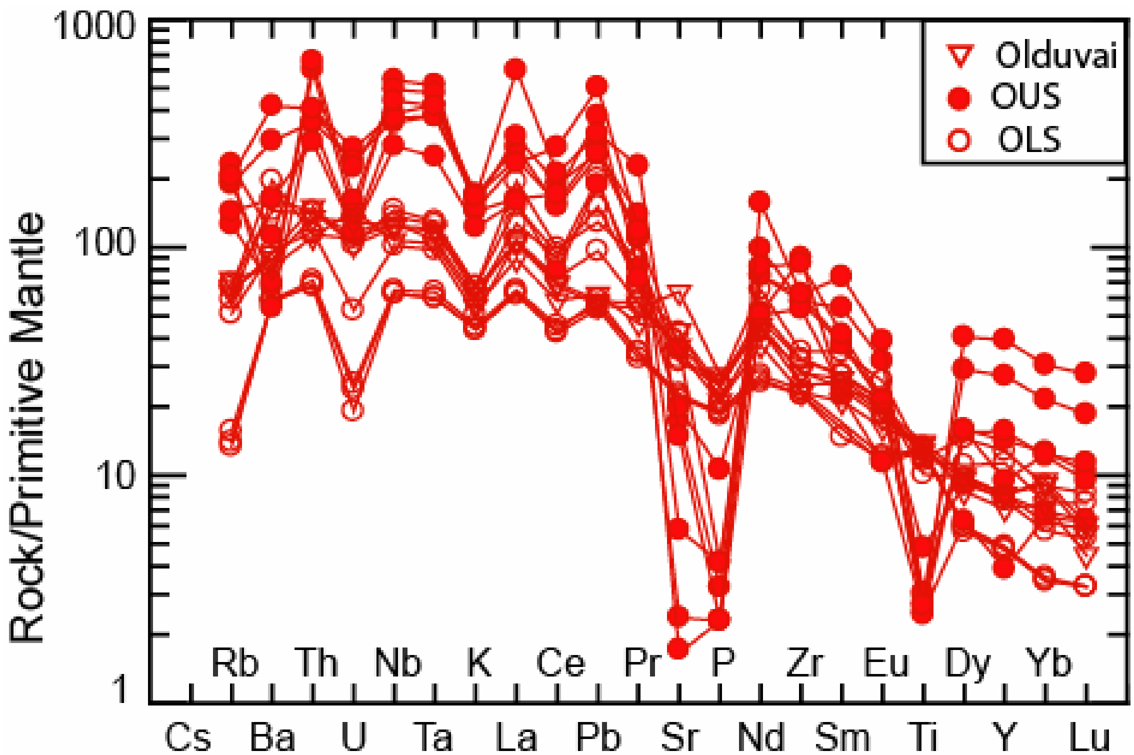

Figure 5.4: Primitive mantle normalized incompatible elements plot indicate that Olmoti lavas are enriched in incompatible elements. Troughs of Sr, P, and Ti indicate fractionation of feldspar, apatite and Ti-rich phases (titanomagnetite, aenigmatite, amphibole, titanian augite, and biotite) respectively. Normalizing values of Sun and McDonough 1989.

Sr and Nd isotope

Isotopic ratios of Sr and Nd from selected lavas are shown in Table 5.1. The mafic lavas are characterized by slightly lower $^{143}Nd/^{144}Nd$ (0.512144 – 0.512550) compared to the trachyte (0.512470 – 0.512760) and are slightly higher in $^{87}Sr/^{86}Sr$

(0.70458 – 0.7050730 compared to 0.70454 – 0.704930 in the trachyte). Overall the isotope data for the trachytes are indistinguishable from and overlap with those of the mafics. There is no simple relationship between Mg# and SiO_2 against the Sr isotope ratio. While the Sr isotope ratio is negatively correlated to SiO_2 in the OUS, a positive correlation is observed in the OLS (not illustrated).

Weathering and sample exclusion

Petrographic study of thin sections indicated minor alteration of the feldspar to clays, particularly in the samples from the upper section (OUS). This is not surprising given the wet and warm East African climate. Since weathering is likely to have disturbed fluid mobile elements, it was necessary to identify and eliminate samples that have suffered significant alteration before any geochemical interpretation. Large cations (e.g. Ce, Rb and K) are fluid mobile and are easily mobilized and either concentrated or depleted in weathered rocks (e.g. Boulange and Colin, 1994; Cotton *et al.,* 1995; Yang and Holland, 2003; Patino *et al.*, 2004). Under oxidizing conditions, Ce can change from its normal trivalent to a tetravalent state, which allows it to be preferentially fractionated from other REEs (e.g. Boulange and Colin, 1994). A plot of Ce verses Ce* (Figure 5.5) has been used by Bolge *et al.* (2006) and Braun *et al.* (1998) to identify samples enriched or depleted in Ce due to weathering. Ce* is the calculated concentration that Ce should have if the REE pattern follows a smooth transition from La to Pr. Samples 04-OLT1, 04-OLT2, and 04-OLT4 do not appear to fall on a coherent line defined by the rest of the samples. Trace element data from these three samples are thus treated with caution during data interpretation.

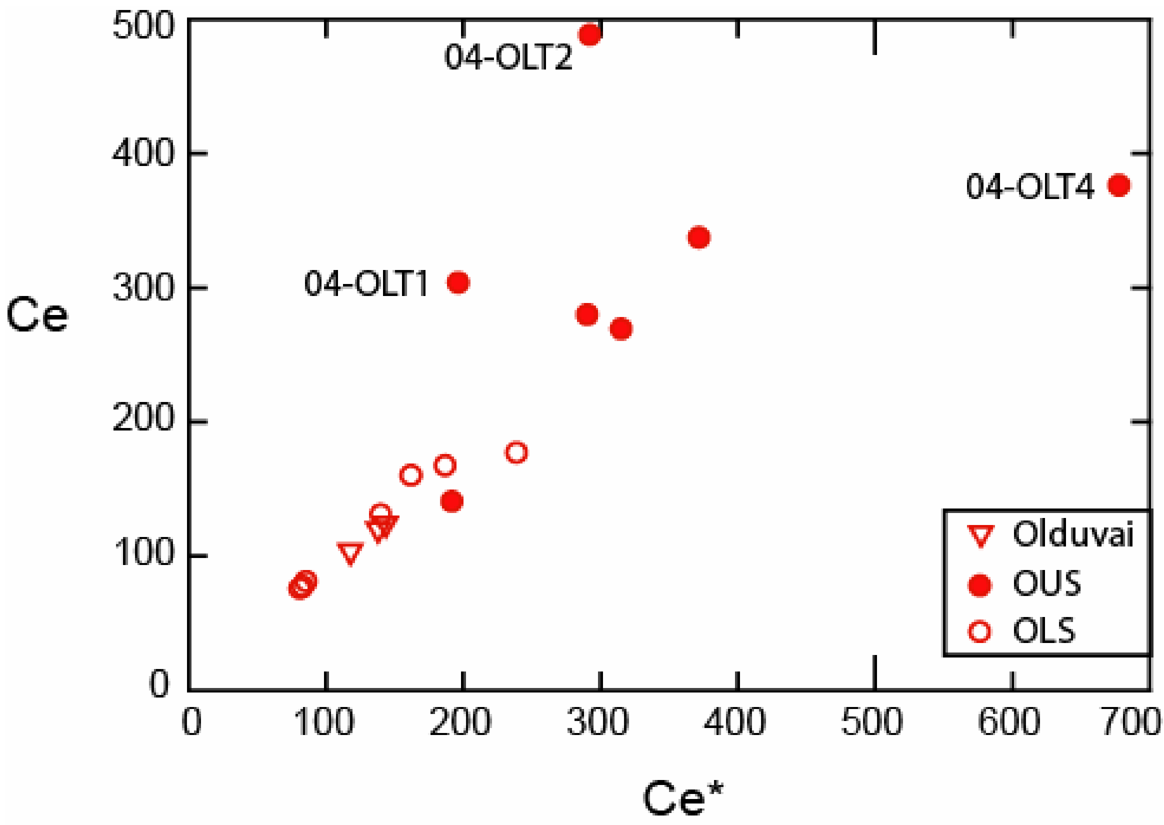

Figure 5.5: Ce* is the extrapolated value for Ce calculated from normalized La and Pr values. Samples 04-OLT1, 04-OLT2, and 04-OLT4 plot off the 1:1 line displaying Ce anomalies cause by weathering, thus their LILE concentrations should be treated with caution during data interpretation.

DISCUSSION

Fractional crystallization

Previously reported Olmoti lava compositions have been restricted to basalt and trachyandesite (Hay, 1976; Manega, 1993). These compositions were mainly based on a few lava flows collected at Olduvai Gorge and interpreted to have originated from Olmoti. Earlier work by Mollel (2002) and recent exploration on the far western corner of the crater revealed that Olmoti lavas are bimodal in composition ranging from basalt to trachyte (Figure 5.3). The mineral assemblage of the basalt and trachyandesite in OLS is similar to that of the trachyte, although aenigmatite appears to be absent in the basalt and trachyandesite. The basalts are composed of sodic ferroan augite, plagioclase, titanomagnetite, kaersutite, and while olivine was not observed, it cannot be ruled out. The trachytes are mainly composed of alkali feldspar, augite, aenigmatite, katophorite, minor biotite, and fayalite.

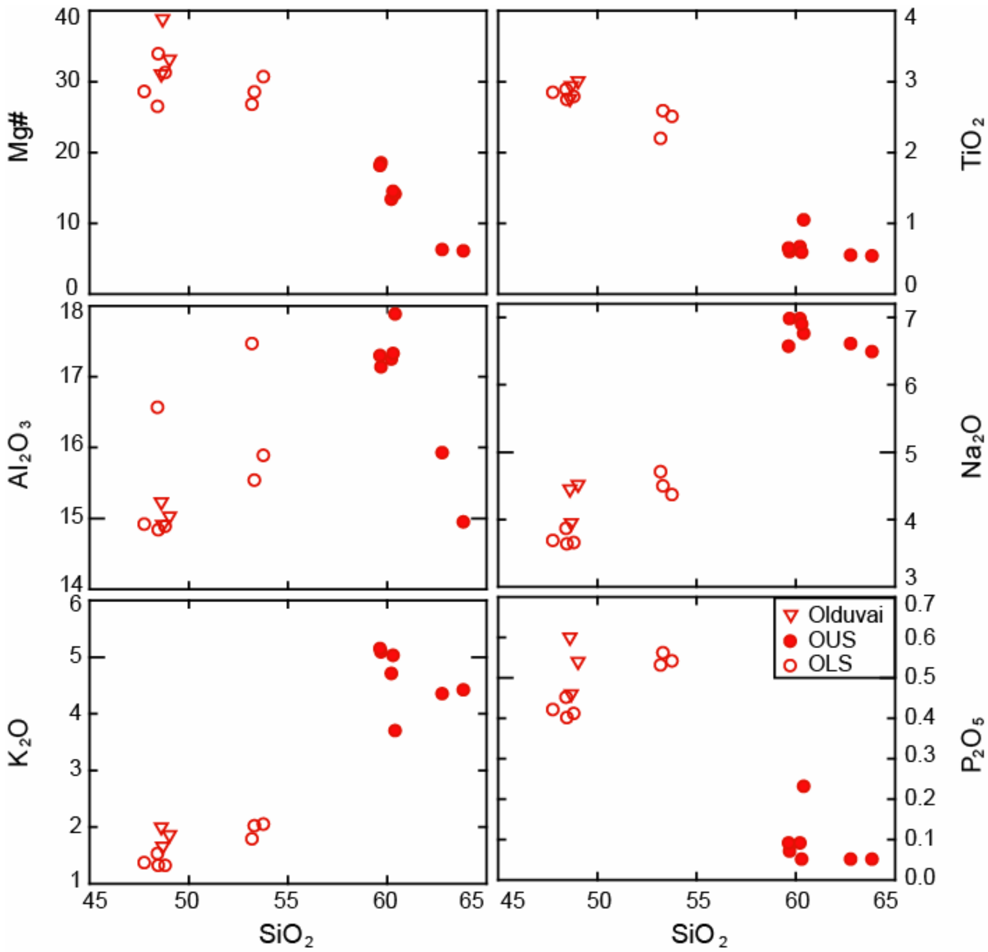

Figure 5.6: Major elements versus silica Harker diagrams. Decreasing Mg# and TiO_2 with increasing SiO_2 is consistent with fractional crystallization. Fractionating phases are titanian augite, plagioclase, Fe-Ti oxides and amphibole in rocks with SiO_2 < 59 wt % and include aenigmatite, alkali feldspar, biotite, olivine, and apatite in rocks with SiO_2 > 59 wt %.

Bivariate plots of major elements (e.g. TiO_2 and Mg# versus SiO_2, Figure 5.6) suggest that fractional crystallization was a key process in producing Olmoti lavas. FeO is negatively correlated to SiO_2 (not shown), indicating fractionation of olivine and augite lower in the fractionation sequence (below 59 wt % silica content). Al_2O_3, Na_2O, and K_2O show an inflection in the fractionation trend at 59 wt % silica content (Figure 5.6c, and 5.6d), indicating fractionation of alkali feldspar higher in the sequence. This is also in agreement with the observed negative Eu anomaly. The typical Eu/Eu* value for the trachyte is 0.5 – 0.7 compared to 0.9 – 1.0 for the basalt and trachyandesite suggesting that trachyte formed subsequent to plagioclase fractionation. Removal of aenigmatite, amphiboles and biotite is also more significant above 59 wt % silica content. This is indicated by the increasing negative anomaly of K, Sr, and Ti from basalt to trachyte. The strong negative P anomaly observed in the trachytes reflects apatite fractionation. La is positively correlated with most trace elements consistent with fractional crystallization except for Sr and the HFSE (not shown). Troughs for Rb, U, K and Ce in spider diagram (Figure 5.7) appear for all Olmoti lavas as well as in lavas from Oldeani and Lemagurut (Mollel *et al.*, in press) and may reflect source character. The negative K anomaly may also indicate the presence of a K-rich phase in the source (e.g., Späth *et al.,* 2001).

HFSE, such as Ta, Nb, Zr, and Hf, are negatively correlated to Mg# (not shown) but when plotted against silica content (Figure 5.9), they show an inflection above the 59 wt % silica content, mimicking the fractionation trends displayed by the major incompatible elements (Na, K, and P, in Figure 5.6). This is consistent with petrographic observations that indicated a higher modal abundance of amphibole, aenigmatite and biotite higher in the fractionation sequence.

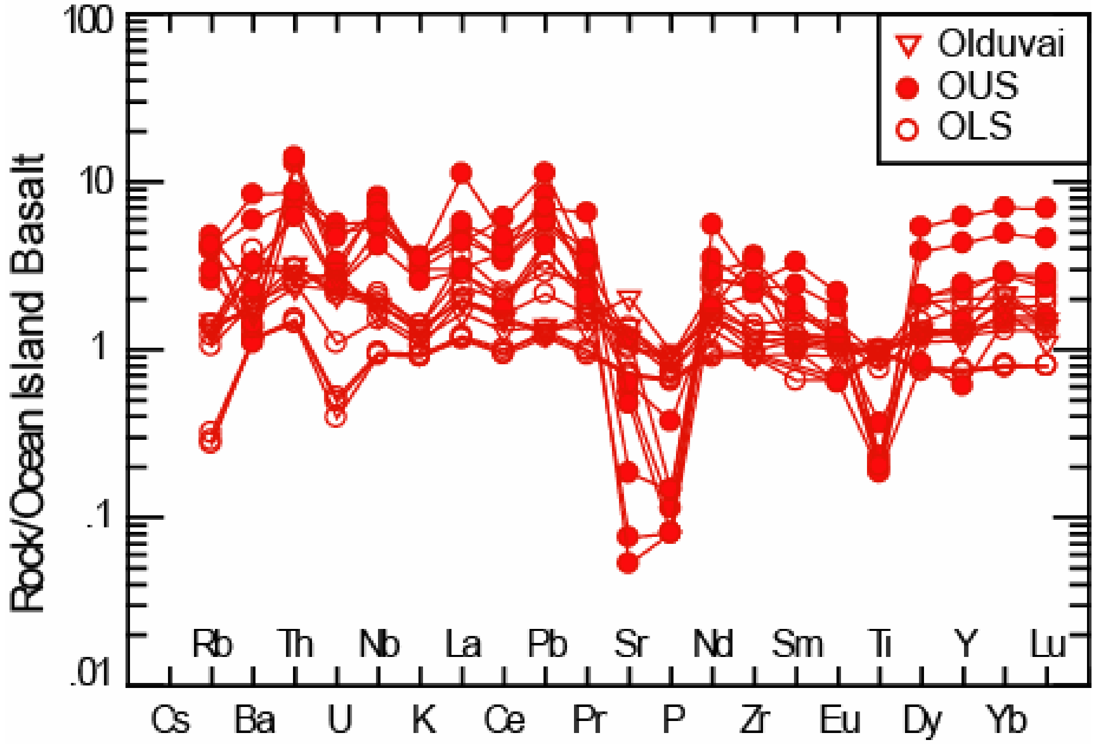

Figure 5.7: The Oceanic Island Basalt (OIB) normalized trace element ratios for Olmoti and Olduvai lavas are close to one, suggesting an IOB type source. Troughs in Sr, P, and Ti indicate fractionation of feldspars, apatite, and Ti-bearing minerals, respectively. Normalizing values of Sun and McDonough 1989.

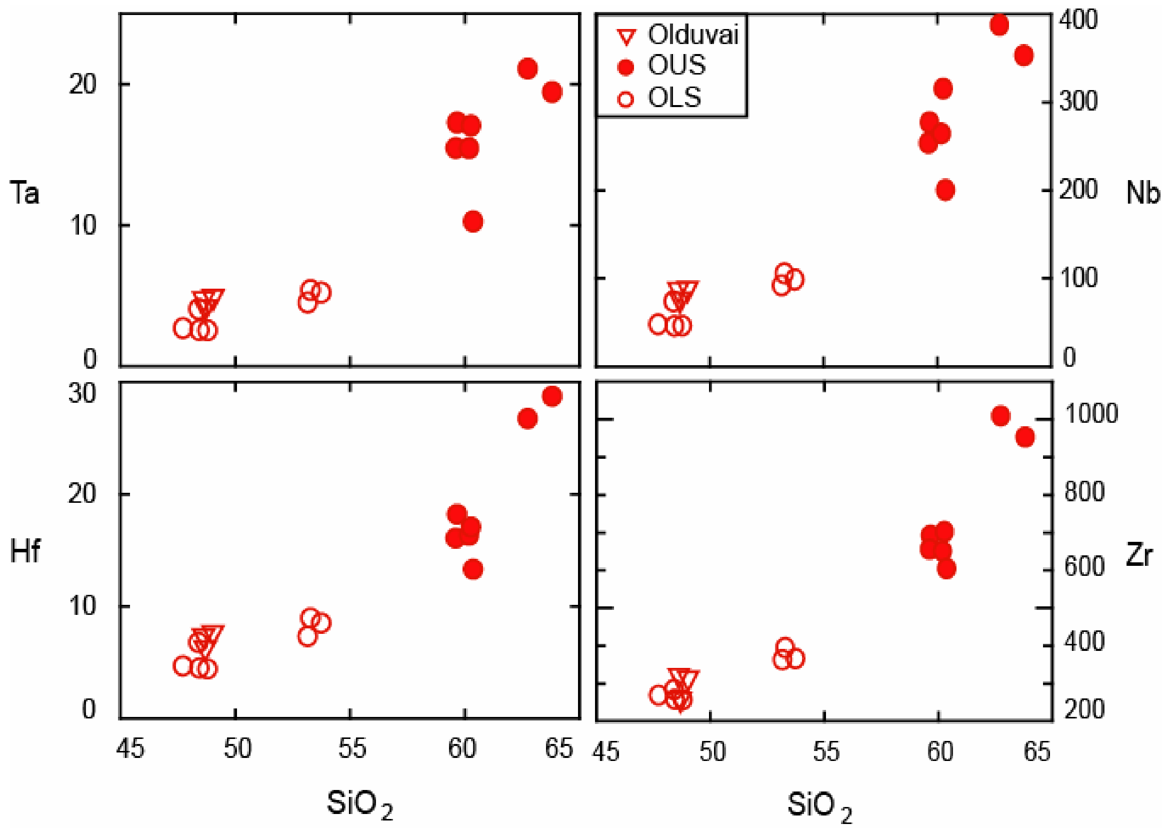

Figure 5.8: High Field Strength Elements (HFSE) are more concentrated in OUS compared to OLS and Olduvai lava and increase with increasing SiO_2 contents, consistent with fractional crystallization.

Zr and Nb fractionation

Volatile-bearing minerals such as amphibole and phlogopite are important repositories for HFSE (Brenan *et al.*, 1995; Ionov and Hofmann, 1995; LaTourrette *et al.*, 1995; Vannucci *et al.*, 1995). Site preference of incorporated HFSE in pargasite and kaersutite is provided by Farges *et al.* (1994), Oberti *et al.* (2000), and Tiepolo *et al.* (1999, 2000). Brenan and Watson (1991) and Keppler (1996) have also shown that the clinopyroxene-hydrous fluid partition coefficients for HFSE (Ta, Nb, Zr, and Hf) are significantly > 1 while they are < 1 for LILE. Moreover, the partition coefficient for

HFSE between amphibole and clinopyroxene are >> 1 (Witt-Eickschen and Hart, 1994; Charot *et al.*, 1995; Vannucci *et al.*, 1995; Ionov *et al.*, 1997; Grégoire *et al.*, 2000) suggesting that HFSE partition coefficients between amphibole and fluid are also much greater than 1. In Olmoti lavas, Zr/Nb is commonly unaffected by fractionation or secondary processes such as weathering, which is unique for the basalt, trachyandesite, and trachyte (Figure 5.9a). This suggests that the lavas were either derived by different degrees of partial melting of a cogenetic source or from distinct magma sources. There is an apparent temporal progression from high Zr/Nb in the basalt to a low value of this ratio in the trachyte. The unique Zr/Nb ratios in these lavas appear to be related to the removal of Ti-bearing minerals that commonly incorporate HFSE in their structures. An experimental study on fractionation of HFSE by Tiepolo *et al.* (2001) showed that Nb can be decoupled from Zr during mantle processes and that the Zr partition coefficient between amphibole and liquid depends on the type of amphibole that crystallizes. Higher Mg# amphiboles crystallizing from melts more easily incorporate Zr relative to Nb, leading to lower Zr/Nb ratios in the residual melt. Indeed, kaersutite in the basalt sample (00-OLT4) lower in the section (OLS) has higher MgO (4.0 wt %) content compared to < 1.7 wt % in the kaersutite from a trachyandesite sample (00-OLT7) also in the OLS (Table 5.2). This is consistent with the decreasing Zr/Nb ratio from the basalt to the trachyandesite. The Mg # from katophorite in the trachyte is higher than that of the kaersutite from the basalt (Figure 5.9b) suggesting that the trachyte did not evolve from these basalts.

In a study of the structural environment of Zr in two inosilicates from the Cameroon Line (Fitton, 1987) alkali lavas consisting of basanite, trachyte, and phonolite, Farges *et al*. (1994) concluded that the inosilicates (amphiboles) crystallizing from the melt provided six fold-coordination sites similar to those occupied by Zr in the melt. HFSE also become compatible late in the fractionation sequence (Tiepolo *et al.*, 2000). Crystallization of Zr minerals involving alternating stages of compatibility and incompatibility have been documented in nepheline syenites and peralkaline granites from Motzfeldt, Greenland (Jones and Peckette, 1980) and in amphibole-rich mantle xenoliths from the Kerguelen Islands (Moine *et al.*, 2001).

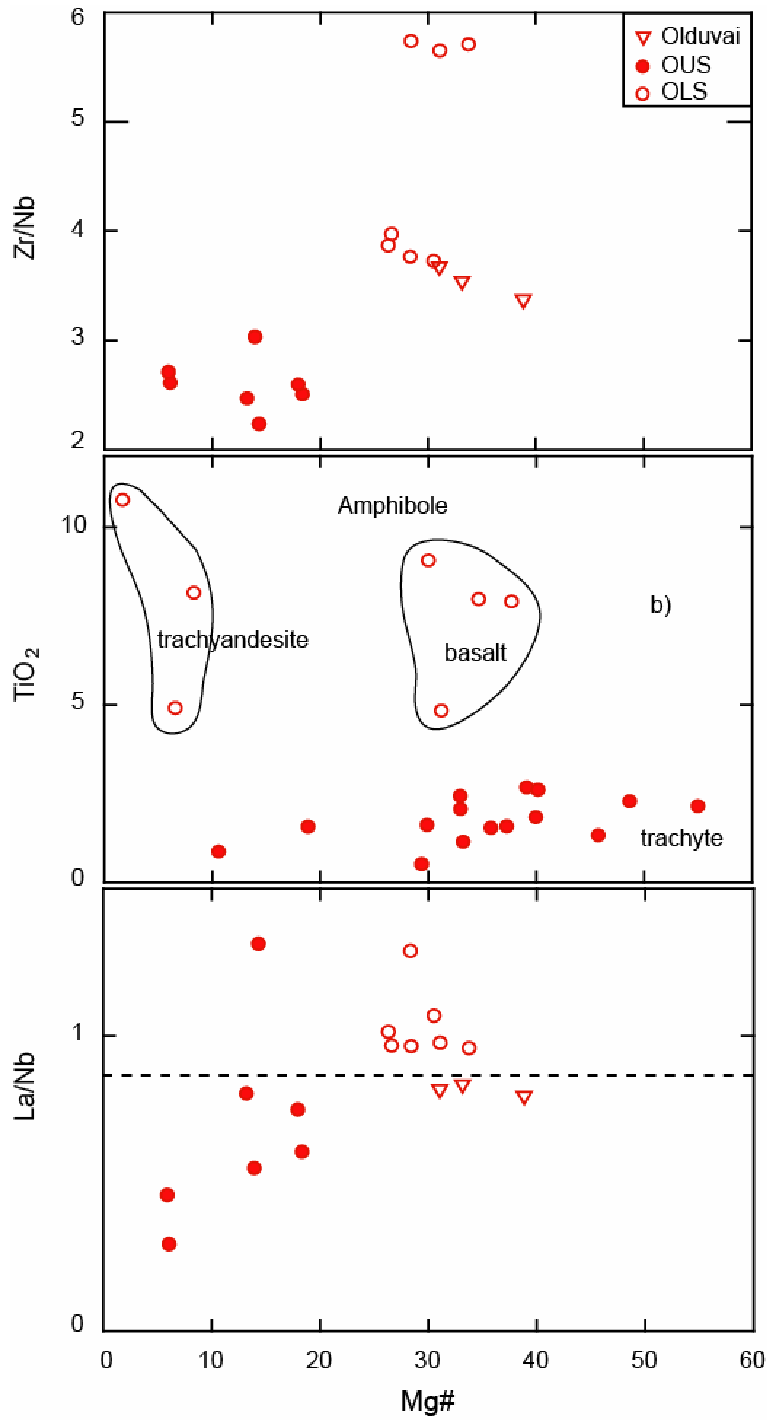

Figure 5.9 a): HFSE ratios verses Mg#. The Zr/Nb ratio is unique for basalt, trachyandesite and trachyte. Olmoti trachyandesite and Olduvai trachybasalt share similar ratio. b) TiO_2 versus Mg# for amphiboles from lavas 00-OLT4, 00-OLT7, 03-OLT1, and 03-OLT3 from Table 2 (microprobe data). Higher Mg# in amphiboles from the trachytes indicates that the trachytes did not evolve from these basalts or trachyandesites. c) The La/Nb ratio for trachytes is lower compared that of basalt and trachyandesite suggesting that the trachytes were derived by small degree partial melts compared to the basalt.

Trachytes

Many studies (DePaolo, 1981; Macdonald *et al.*, 1995; Panter et al. 1997; Ngounouno *et al.*, 2000; Kabeto *et al.*, 2001), invoke processes such as fractional crystallization and assimilation of continental crust for the generation of evolved magmas in continental extensional settings. Partial melting of earlier under-plated mafic magmas through further fractional crystallization can also generate evolved magmas (Trua *et al.*, 1997). The MgO content in the katophorite from the trachyte in OUS is surprisingly similar and in some cases higher than that of the kaersutite from the basalt and much higher than that of the trachyandesite (Table 5.2). This suggests that the trachytes did not evolve from the basalt or the trachyandesite because later amphibole (katophorite) would be expected to have lower MgO content compared to that of the earlier amphibole. Another possible explanation for the formation of these trachytes involves a lower degree partial melt, presumably from the same parent as the basalt because no signs of multiple sources are seen from the isotope data. Magma mixing is another possibility. Typical signs for magma mixing include zoned crystals and resorbed textures. Microscope study of the trachytes and detailed microprobe work on the selected samples did not reveal any magma-mixing signature. Excluding one outlier from OUS (Figure 5.9c), La/Nb is slightly higher and similar in the basalt and trachyandesite but unique and lower for the trachytes, perhaps suggesting that the trachyte was derived from a lower degree melt of the parent of the basalt.

Apart from magma fractionation, higher concentrations of LILE in lavas can also be achieved by a smaller degree of partial melt (Johnson *et al.*, 2005; Mertz *et al.*, 2001). This would seem to suggest that the trachytes were derived by small degree partial melting of underplated basalt, however this mechanism alone cannot explain the fractionation of Zr/Nb which is already accounted for through fractionation of Ti bearing minerals, especially amphibole. High concentrations of incompatible elements common in differentiated alkali lavas (especially Zr) can be used as a crude index of fractionation (Weaver *et al.*, 1972; Baker *et al.*, 1977). In Olmoti the Zr is likely hosted in the aenigmatite, titanomagnetite, amphibole, and titaniaugite since no zircon was observed in thin sections. The trachyte has the highest concentrations of Zr (646 to 1005 ppm), while the basalt and trachyandesite have the lowest (252 to 390 ppm). Overall, this suggests the derivation of trachyandesite from basalt through fractional crystallization. The discrepancy in the mineral data between the OLS and OUS does not support the derivation of the trachyte from either the basalt or the trachyandesite. The La/Nb ratio supports derivation of the trachyte by small degree partial melts of the same parent as the basalt. Higher concentrations of SiO_2, Na_2O, K_2O, and other incompatible elements in the trachyte require fractional crystallization subsequent to partial melting. Derivation of silicic lavas by protracted fractional crystallization of alkali basalt is well documented elsewhere (Barberi *et al.*, 1975; McDonough and Nelson, 1984; Mungall and Martin, 1995; Kar *et al.*, 1998; Ayalew *et al.*, 2002).

In a recent study of phase relationships in peralkaline silicic magmas from the Kenya Rift, Scaillet and MacDonald, (2001, 2003) showed that titanian aenigmatite, sodic amphibole and biotite are stable at low oxygen fugacity between a Ni-NO solid buffer, a fayalite-magnetite-quartz solid buffer, and temperatures below 800 ºC. The similarity in mineral assemblage between the Olmoti trachyte (fayalite, alkali feldspar, aenigmatite, sodic ferroan augite, amphibole, and biotite) and that of the Kenya Rift peralkaline lava may suggest that Olmoti trachytes were produced under similar conditions.

Source and crustal influence

There is a general consensus from geophysical and geochemical data that a mantle plume/s is responsible for the production of large volumes of lava along the EARS (Hart *et al.,* 1989; Smith, 1994; Burke, 1996; Mechie *et al.*, 1997; Ebinger and Sleep, 1998; George *et al.*, 1998; Rogers *et al*. 2000; Nyblade *et al*. 2000; Weeraratne *et al*. 2003; Furman *et al.*, 2004, 2006). The Sr, Nd, and Pb isotopic study on basalts and phonolites by Paslick *et al*. (1995), concluded that Oceanic Island Basalt (OIB) is the source for lavas from northern Tanzania. OIB normalized trace element ratios (Figure 5.7) for all Olmoti lavas are close to one, in agreement with results from previous workers in the region. The fractionated trachyandesite and trachytes have higher ratios of most trace elements and are depleted in Sr, P, and Ti as a result of fractional crystallization. The Sr and Nd isotope data from selected basalt, trachyandesite and trachyte samples are indistinguishable and overlap between lava types (Table 5.1). The data are within the range of values defined by OIB lavas globally and $^{87}Sr/^{86}Sr$ versus $^{143}Nd/^{144}Nd$ values for most of the selected Olmoti lava (Figure 5.10) fall within or near the field defined by lavas from northern Tanzania. Some of the lavas also fall within fields defined by lavas from other volcanic provinces in the EARS (e.g. Chyulu Hills and Virunga). In general the Olmoti lavas are consistent with an origin from a source defined by a mixture between enriched mantle (EMI) and high-μ (HIMU) reservoirs similar to lavas from Chyulu Hills (Späths *et al*., 2001) and from northern Tanzania (Paslick *et al.*, 1995; Bell and Tilton, 2001; Bizimis *et al.*, 2003). Moderate chondritic normalized (Tb/Yb)n ~2.3-1.6 for Olmoti lavas [normalizing values of Sun and McDonough, 1989], are within the range of values obtained in Turkana lavas (Furman *et al.*, 2006) implied to indicate a melting depth in the lithospheric mantle, greater than the garnet-stability field.

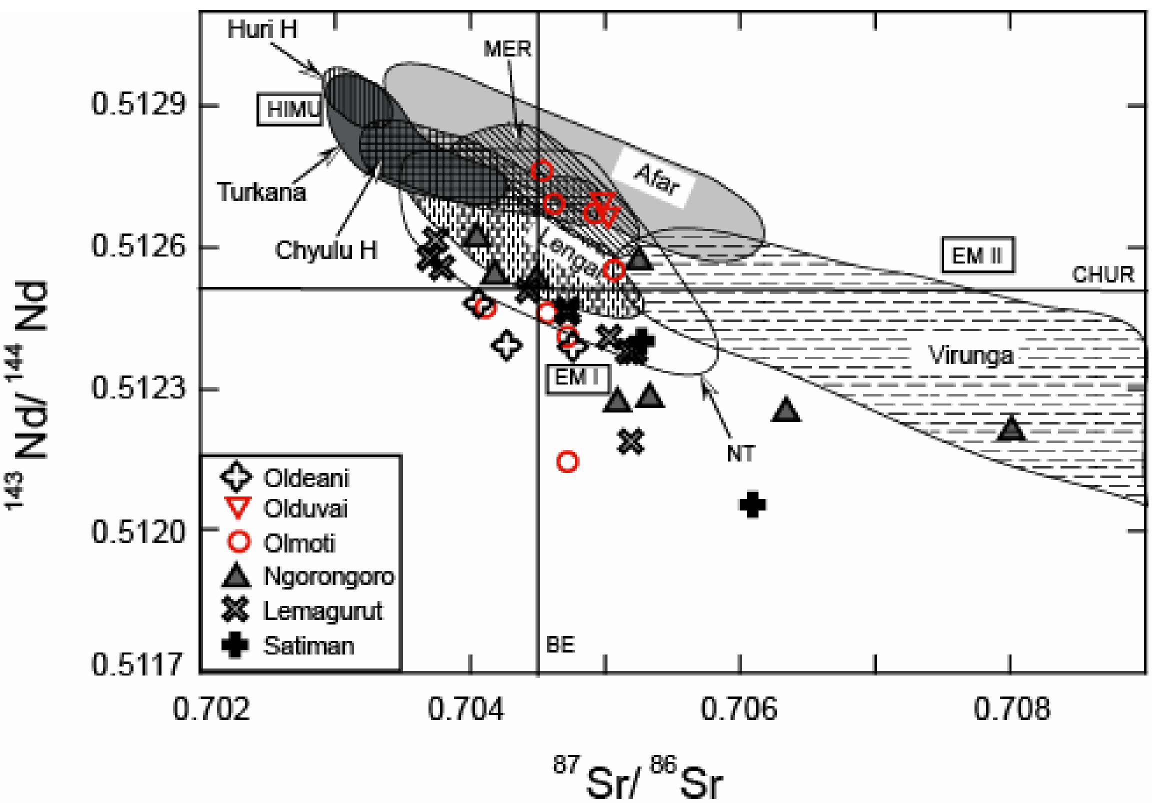

Figure 5.10: $^{143}Nd/^{144}Nd$ versus $^{87}Sr/^{86}Sr$ variation for lavas from Olmoti and Olduvai Bed I compared to other lavas from the East African Rift System (EARS) as well as hypothetic mantle endmember compositions. BE, Bulk Earth; CHUR, Chondritic Uniform Reservoir; Huri H., Huri Hills; Chyulu H., Chyulu Hills; MER, Main Ethiopian Rift; NT, Northern Tanzania; Lengai, Oldoinyo Lengai. Source of data: Class et *al*., 1994; Deniel *et al.,* 1994; Paslick *et al.*, 1995; Bell and Simonetti, 1996; Kalt et al., 1997; Rogers et al., 1998; Trua et *al*., 1999; Bell and Tilton, 2001; Späths *et al*., 2001; Furman *et al*., 2004, 2006; Keller *et al.*, 2006; Mollel *et al.*, in press. HIMU, EMI, and EM II fields from Hart *et al*., 1992).

Compared to Ngorongoro lavas (in Chapter 4) that have yielded a wide range of $^{87}Sr/^{86}Sr$ (0.70405 – 0.70801), Olmoti appears to be restricted in range suggesting a lesser degree of crustal assimilation compared to Ngorongoro. The Ce/Pb ratios are 20 ± 5 for mantle-derived fluids (Hofmann *et al.*, 1986; Sun and McDonough, 1989). Most of the Olmoti samples plot below the range of mantle values suggesting that these lavas have undergone variable degrees of crustal assimilation (Figure 5.11), similar to lavas from Naivasha province in southern Kenya Rift (Davies and MacDonald, 1987).

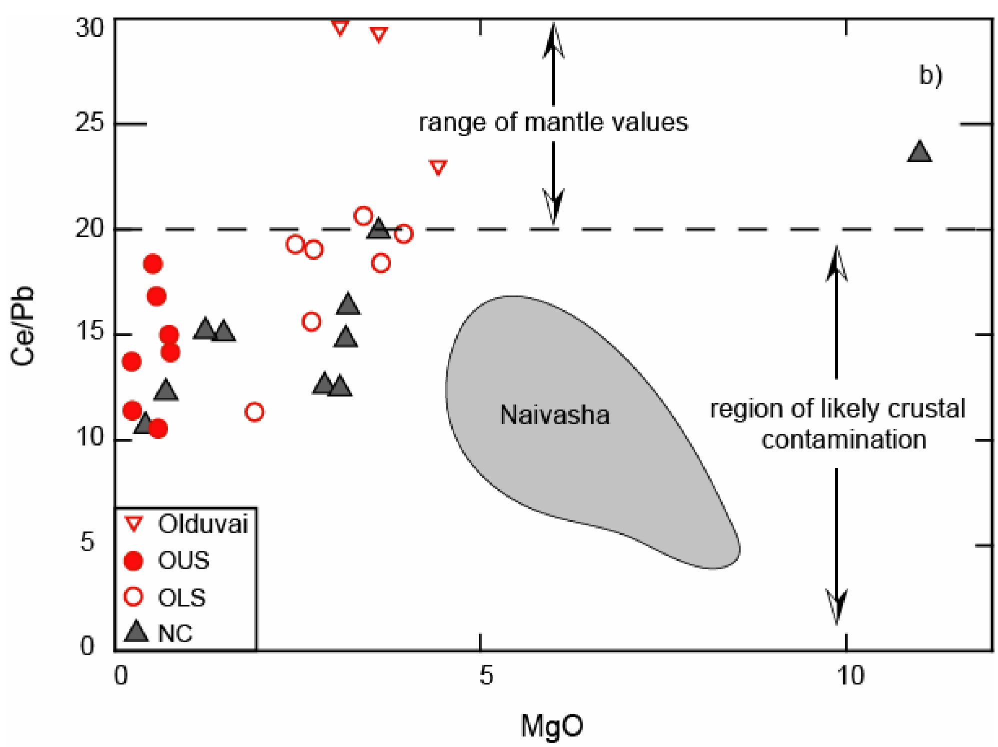

Figure 5.11: Variation of Ce/Pb is sensitive to crustal contamination as inferred from Naivasha (shaded) area (Davies and MacDonald, 1987; Furman, 2007). Most of the Olmoti lavas fall within the region of crustal contamination similar to lavas from lower Ngorongoro (NC) section (Chapter 4). Only one sample is within the range of mantle values whereas all the Olduvai Bed I lavas are relatively uncontaminated (Hofmann *et al.*, 1986; Sun and McDonough 1989).

GEOCHRONOLOGY

Using the $^{40}Ar/^{39}Ar$ method, I dated lavas from the mafic OLS and the silicic OUS. Incremental-heating analysis of matrix from two OLS lavas (00-OLT2 and 00-OLT5) yielded plateau ages of 2.01 ± 0.04 Ma and 1.90 ± 0.02 Ma respectively (Figure 5.12a and Table 5.3). The cumulative %$^{39}Ar^*$ on the plateau for 00-OLT2 and 00-OLT5 are 69.1% and 80.7% respectively. Total fusion and plateau ages for both samples are indistinguishable from their isochron ages and the $^{40}Ar/^{36}Ar$ intercept for both samples are within the range of the atmospheric ratio (295.5) suggesting that these dates are good age estimates for the Olmoti lower section.

Dates on anorthoclase from 04-OLT2 and matrix material from four OUS trachytes were determined by the same method. Three of the five samples yielded plateau ages ranging from 1.85 ± 0.01 Ma to 1.80 ± 0.01 Ma (Figure 5.12b). The plateau, isochron, and integrated ages from 03-OLT1 and 04-OLT2 (Table 5.3) are indistinguishable from each other and the $^{40}Ar/^{36}Ar$ intercept for both samples are within atmospheric ratios suggesting that the 1.85 ± 0.01 Ma date is the best age estimate for these lavas. Plateau, isochron, and integrated ages from sample 03-OLT3 are also indistinguishable, suggesting that 1.80 ± 0.01 Ma (Table 5.3) is a good age estimate for this sample. Matrix from samples 03-OLT2 and 04-OLT4 did not yield plateau ages. The total fusion ages of 1.92 ± 0.01 Ma and 1.97 ± 0.01 Ma from 03-OLT3 and 04-OLT4 are much older than their isochron ages of 1.87 ± 0.02 Ma and 1.83 ± 0.04 respectively. Isochron ages from these two samples are indistinguishable from each other and the $^{40}Ar/^{36}Ar$ intercepts for both samples (Table 5.3) are within error of the atmospheric ratio suggesting good age estimates.

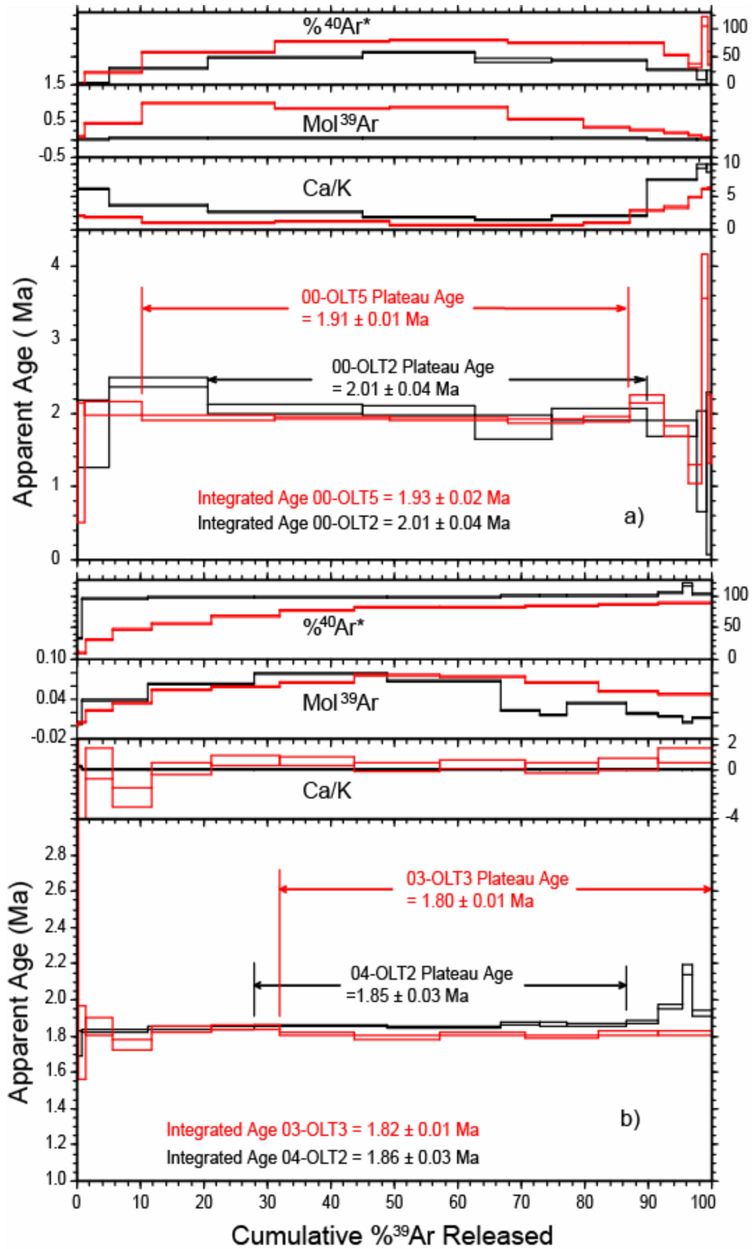

Figure 5.12 (a) $^{40}Ar/^{39}Ar$ incremental-heating spectra for lavas from OLS. Four and five-step plateau ages for matrix from 00-OLT2 and 00-OLT5 are 2.01 ± 0.04 Ma and 1.91 ± 0.01 Ma, respectively. Integrated ages for both samples are indistinguishable from plateau ages. Cumulative % $^{39}Ar^*$ released on the plateau steps are 69 and 80 for 00-OLT2 and 00-OLT5 and the plateau temperatures are ~650 - 800 ºC and 750 - 1000 ºC, respectively. (b) Five and six-step plateau ages for anorthoclase and matrix from 04-OLT2 and 03-OLT3 (OUS) are 1.85 ± 0.01 Ma and 1.80 ± 0.01 Ma, respectively. Integrated ages for both samples are indistinguishable from plateau ages. Cumulative % $^{39}Ar^*$ released on the plateau steps are 58 and 68 for 04-OLT2 and 03-OLT3 and the plateau temperatures are ~ 800 - 1000 ºC and 950 - 1300 ºC respectively.

These ages are also indistinguishable from the age of 1.85 ± 0.01 Ma obtained from samples 03-OLT1 and 04-OLT2 (Table 5.3), suggesting that lower age estimate for OUS is 1.85 ± 0.01 Ma.

These ages imply that Olmoti activity began much earlier than previously thought (the new ages are about 140 kyr older) and much shorter in duration (~200 kyr compared to 740 kyr) than previously estimated by K-Ar and $^{40}Ar/^{39}Ar$ dating (Manega, 1993).

Table 5.3: $^{40}Ar/^{39}Ar$ ages for Olmoti and Olduvai lavas, bolded indicate preferred ages

Sample Id	Material	Integrated Age (Ma)	Plateau Age (Ma)	Isochron Age (Ma)	$^{40}Ar/^{36}Ar$ Intercept	MSWD	% $^{39}Ar^*$ on Plateau
00-OLT2	matrix	2.01 ± 0.04	**2.01 ± 0.04**	2.01 ± 0.05	292 ± 3	1.1	69.1
00-OLT5	matrix	1.91 ± 0.02	**1.90 ± 0.02**	1.92 ± 0.01	295 ± 2	0.82	80.7
03-OLT1	matrix	1.88 ± 0.01	**1.85 ± 0.01**	1.84 ± 0.01	299 ± 1	1.2	65
03-OLT2	matrix	1.92 ± 0.01		**1.87 ± 0.02**	298 ± 2	1.9	
03-OLT3	matrix	1.82 ± 0.01	**1.80 ± 0.01**	**1.80 ± 0.01**	296 ± 3	1.7	68.0
04-OLT2	anorthoclase	1.86 ± 0.03	**1.85 ± 0.03**	**1.85 ± 0.03**	285 ± 8	1.7	58.6
04-OLT4	matrix	1.97 ± 0.01		**1.83 ± 0.04**	296 ± 5	1.7	
OLD1	matrix	1.88 ± 0.02	**1.86 ± 0.02**	**1.86± 0.02**	294.2 ± 1.5	1.4	100
OLD2	matrix	1.87 ± 0.02	**1.86 ± 0.02**	**1.84± 0.02**	296.2 ± 0.8	1.1	90.3

Irradiation parameter (J) calculated from co-irradiated Alder Creek (AC) sanidine:

Sample #	J value
00-OLT2	$7.119 \times 10^{-5} \pm 2.238 \times 10^{-7}$
00-OLT5	$2.5816 \times 10^{-4} \pm 1.5286 \times 10^{-7}$
03-OLT1, 03-OLT2, & 03-OLT3	$1.791 \times 10^{-4} \pm 7.7782 \times 10^{-7}$
04-OLT2, 04-OLT4	$1.804 \times 10^{-4} \pm 3.2873 \times 10^{-6}$
OLD1 & OLD2	$1.753 \times 10^{-4} \pm 1.6971 \times 10^{-7}$

Implications for NVHC and Olduvai and Laetoli deposits

Olduvai Bed I lava

Three lava samples (from different lava flows) collected from lower Olduvai Bed I (Hay, 1976; McHenry, 2004) are hawaiite in composition (Figure 5.3). The hawaiite composition is the same as trachy-basalt following the total alkali versus silica classification of Le Bas et al. (1986), only that these are slightly more alkaline. The lavas are holocrystalline fine to medium grained with two of them (OLD1 and OLD3) showing flow banding. Their mineral assemblage consists of plagioclase, alkali feldspar, olivine and amphibole phenocrysts in a ground mass of augite, alkali feldspar and plagioclase, and Fe-Ti is the main oxide phase.

Major element data (Table 5.1) shows that the Olduvai lavas are less evolved similar to lavas from lower part of the OLS and their silica content is restricted between 48 and 49 wt %. Similar to lavas from OLS the Olduvai lavas show a continuous decrease in TiO_2 and Mg# (Figure 5.6), FeO and CaO (not illustrated) and an increase in Na_2O, Al_2O_3 and K_2O (Figure 5.6) with increasing silica content that is consistent with fractional crystallization. They are also characterized by slightly lower MnO and higher P_2O_5 contents compared to OUS (Table 1).

Compatible trace elements (e.g. Cr) are within the range of those from OLS (2-10, ppm), but one lava (OLD3) is more mafic and has the higher Cr content of 136 ppm (Table 1). Compared to primitive mantle the three Olduvai lavas are enriched (Figure 5.4) and show negative K and P anomaly. Most LILE (e.g. Hf, Zr, Nb and Ta) are positively correlated with silica (Figure 5.8). HFSE ratios such as Zr/Nb and La/Nb (Figure 5.9) do not compare with one particular portion of the Olmoti section. While the Zr/Nb ratio

(~3.5) is similar to that obtained on trachyandesite from upper part of OLS, the La/Nb ratio is lower than 0.9, similar to OUS and other lavas of the NVH that are considered derived by low degree partial melt of the source rock (Mollel et al., in press).

The Sr isotope data (Table 1) from the three Olduvai lavas overlap with those from Olmoti and are restricted in range from 0.704902 to 0.705021. A single Nd isotope ratio of 0.512670 from one of the lava is also within the range of Olmoti lavas, together with the Sr data, and trace element [e.g. normalized OIB ~ 1, Figure 5.7; $(Tb/Yb)_n$ 1.6 – 1.4] suggests same parental lineage with the Olmoti. The Ce/Pb ratio >20 (Figure 5.12) for the Olduvai lavas suggest limited crustal contamination compared to the Olmoti.

Matrix from all three Olduvai lavas were dated by $^{40}Ar/^{39}Ar$ laser incremental-heating method. Analyses from two samples (OLD1 and OLD2) yielded well behaved plateaus, and same plateau ages of 1.86 ± 0.02 Ma that are comparable with their integrated ages, and indistinguishable from a combined isochron age of 1.85 ± 0.02 Ma (Figure 5.13; Table 5.3). Analysis of multiple aliquots from the third sample OLD3 yielded spurious age spectra suggesting that the K-Ar system may have been disturbed. The new $^{40}Ar/^{39}Ar$ age of 1.85 ± 0.02 Ma is indistinguishable from that of 1.87 ± 0.01 Ma, obtained by dating the same material, using the same method (Walter *et al*., 1991, 1992) and is comparable to the ages of 1.85 ± 0.01 to 1.80 ± 0.01 Ma obtained from OUS suggesting a correlation between the Olduvai Bed I lava and the OUS.

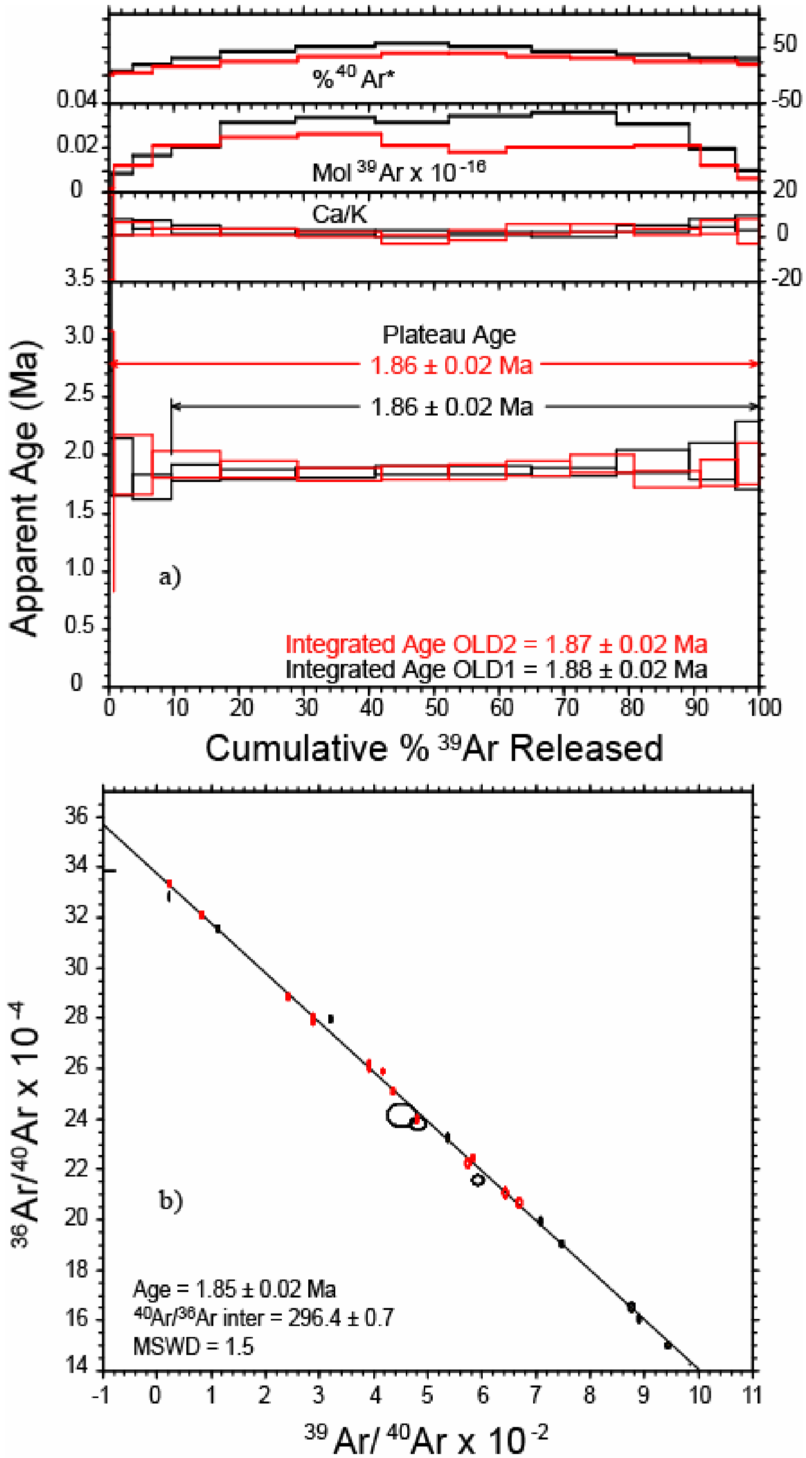

Figure 5.13(a) $^{40}Ar/^{39}Ar$ incremental-heating spectra for Olduvai lavas. Plateaus and integrated ages of the two samples are indistinguishable. Cumulative % ^{39}Ar* on the plateaus ages > 90, obtained at temperatures between ~500ºC - 1200 ºC. (b) Inverse isochron spectrum for combined analyses on OLD1 and OLD2.

The new $^{40}Ar/^{39}Ar$ ages for Olmoti are consistent with the Olduvai Bed I chronology (2.01 – 1.79 Ma; Hay 1976; Walter et al., 1992; Blumenschine et al., 2003), lending support to Hay's 1976 suggestion that Olmoti was the source for the Olduvai Bed I lavas and upper Bed I tuff. All Bed I tuff and lava compositions compare well with Olmoti compositions. Ages from the OUS section are consistent with the Olduvai magnetic transition at 1.785 Ma (Berggren et al., 1995; Cande and Kent, 1995; Tamrat et al., 1995) and the mineral and textural compositions of the lavas compares well with that of rock fragments from tuff IF (McHenry et al., 2007).

The age of 2.01 ± 0.04 Ma from OLS suggests that Olmoti may be a partial source for Olduvai lower Bed I as it overlaps in activity with that of Ngorongoro caldera (Mollel et al., in prep) the source for the more silicic lower Bed I tuffs (Hay, 1976; McHenry et al., 2007). This is the first convincing evidence for contemporaneous multiple source activity from the NVH during Pleistocene.

Olpiro Beds

Hay (1976) suggested a correlation between the phonolitic Olpiro tuff (2.00 ± 0.01 Ma; Ndessokia, 1990; Manega, 1993) in the Laetoli area (southwest of Olduvai Gorge, Figure 1) and the Olduvai lower Bed I, a correlation supported by age data from Ndessokia (1990) and Manega (1993). Ndessokia and Manega further correlated this tuff with Olduvai Coarse Feldspar Crystal Tuff (CFCT) which consists of three different compositions: basaltic, trachytic, and rhyolitic (McHenry, 2004, in press). Olmoti is basaltic to trachytic in composition, and one trachytic lava (03-OLT3) contains trace amounts of a silica-undersaturated mineral (sodalite). This undersaturated composition may suggest an Olmoti source for the Olpiro Beds. The fine-grained nature of the Olpiro beds (Hay, 1987) also supports a distal source. The silica undersaturated centers near Laetoli are either too old (Satiman and Engelosin; Mollel et al., in press) or too young (Embagai, Chapter 6; Manega, 1993). Although Ngorongoro appears to be within reasonable age range (2.29 ± 0.02 to 2.02 ± 0.01 Ma; Mollel et al., in prep), its silicic composition makes it an unlikely source.

REFERENCES

Ashley, G. and Driese, S., 2000. Paleopedology and paleohydrology of a volcaniclastic paleosol interval: implication for Early Pleistocene stratigraphy and paleoclimate record, Olduvai Gorge, Tanzania. Journal of Sedimentary Research 70, 1065-1080.

Ashley, G. M. and Hay, R. L., 2002. Sedimentation patterns in an early Plio-Pleistocene volcaniclastic rift-platform basin, Olduvai Gorge, Tanzania. In: R. W. Renaut and G. M. Ashley (ed.) Continental Rift Sedimentation SEPM Special Publication 73, 107-122.

Ayalew, D., Barbey, P., Marty, B., Reisberg, L., Yirgu, G., and Pik, R., 2002. Source, genesis and timing of the giant ignimbrite deposits associated with Ethiopian continental flood basalts. Geochimica et Cosmochimica Acta 66, 1429-1448.

Bagdasaryan, G. P., Gerasimovskiy, V. I., Polyakov, A. I. and Gukasyan. R. Kh., 1973. Age of volcanic rocks in the rift zones of East Africa. Geochemistry International 10, 66 - 71.

Barberi, F., Santacroce, R., Ferrara, G., Treuil, M., and Varet, J., 1975. A transitional basalt – pantellerite sequence of fractional crystallization, in the Boina centre (Afar Rift, Ethiopia). Journal of Petrology 16, 22-56.

Bell, K. and Simonetti, A., 1996. Carbonatite magmatism and plume activity: implications from the Nd, Pb and Sr isotope systematics of Oldoinyo Lengai. Journal of Petrology, 37(6): 1321-1339.

Bell, K. and Tilton, G., 2001. Nd, Pb and Sr isotopic compositions of East African Carbonatites: Evidence for mantle mixing and plume inhomogeneity. Journal of Petrology 42, 1927-1945.

Berggren, W. A., Hilgen, H. J., Langereis, C. G., Kent, D. V., Obradovich, J. D., Raffi, I., Raymo, M. E. and Shackleton, N. J., 1995. Late Neogene chronology: new perspectives in high-resolution stratigraphy. Geological Society of America Bulletin 107, 1272-1287.

Bizimis M., Salters, V. J. M. and Dawson, B. D., 2003.The brevity of carbonatite source in the mantle: evidence from Hf isotopes. Contributions to Mineralogy and Petrology 145, 281-300.

Blumenschine, R. J., Peters, C. R., Masao, F. T., Hay, R. L., Stanistreet, I. G., Stollhofen, H., Bamford, M., Albert, R. M., Andrews, P., Ebert, J. I. and Njau, J. K., 2005. Traces of Oldowan hominid landuse during the Lowermost Bed II landscape succession in the Paleo-Olduvai basin, Tanzania. Program and Abstracts, Human Evolution, Paleoecology and Paleolithic Archaeology, 2005 Meeting.

Blumenschine, R., Peters, C., Masao, F., Clarke, R., Deino, A., Hay, R., Swisher, C., Stanistreet, I., Ashley, G., McHenry, L., Sikes, N., Van Der Merwe, N., Tactikos, J., Cushing, A., Deocampo, D., Njau, J. and Ebert, J., 2003. Late Pliocene *homo* and hominid land use from western Olduvai Gorge, Tanzania. Science 299, 1217-1221.

Bolge, L., Carr, M. J., Feigenson, M., and Alvarado, G., 2006. Geochemical stratigraphy and magmatic evolution at Arenal volcano, Costa Rica. Journal of Volcanology and Geothermal Research 157, 34-48.

Boulange, B., and Colin, F., 1994. Rare earth mobility during conversion of nephelinite into lateritic bauxite at Passa Quatro Minas Gerais, Brazil. Applied Geochemistry 9, 701-711.

Braun, J. J, Viers, J., Dupre, B., Polve, M., Ndam, J. and Muller, J. P., 1998. Solid/liquid REE fractionation in lateritic system of Goyoum, East Cameroon: the implication for the present dynamics of soil covers of the humid tropical regions. Geochimica Cosmochimica Acta 62, 273-299.

Brenan, J. M. and Watson, E. B., 1991. Partitioning of trace elements between olivine and aqueous fluids at high P-T conditions: implications for the effect of fluid composition on trace element transport. Earth and Planetary Science Letters 107, 672-688.

Brenan, J. M., Shaw, H. F., Ryerson, F. J., and Phinney, D. L., 1995. Experimental determination of trace element partitioning between pargasite and a synthetic hydrous andesitic melt. Earth and Planetary Science Letters 135, 1 –11.

Burke, K., 1996. The African plate. South African Journal of Geology 99, 339-410.

Cahen, L., Snelling, J. J., Delhal, J., and Vail, J. R., 1984. The Geochronology and Evolution of Africa. Clarendon, Oxford.

Cande, S. C. and Kent, D. V., 1995. Revised calibration of the geomagnetic polarity time scale for the Late Cretaceous and Cenozoic. Journal of Geophysical Research 100, 6093-6095.

Carr, M. J., Saginor, I., Alvarado, G. E., Bolge, L. L., Lindsay, F. N., Milidakis, K., Turrin, B., Feigenson M. D., and Swisher III, C. C., (2007). Element fluxes from the volcanic front of Nicaragua and Costa Rica. Journal of Geochemistry, Geophysics, Geosystems 8, Q06001, doi:10.1029/2006GC001396..

Chazrot, G., Menzies, M. A. and Harte, B., 1995. Determination of partition coefficients between apatite , clinopyroxene, amphibole and melt in natural spinel lherzolites from Yemen: implications for wet melting of lithospheric mantle. Geochimica et Cosmochimica Acta 60, 423-437.

Class, C., Altherr, R., Volker, F., Eberz, G., and McCulloch, M., 1994. Geochemistry of Pliocene to Quaternary alkali basalts from the Huri Hills, northern Kenya. Chemical Geology 113, 1-22.

Cotton, J., Le Dez, A., Bau, M., Caroff, M., Maury, R. C., Dulski, P., Fourcade, S., Bohn, M., and Brousse, R., 1995. Origin of anomalous rare-earth element and yttrium enrichments in subaerially exposed basalts: evidence from French Polynesia. Chemical Geology 119, 115-138.

Cox, K. G., Bell, J. D. and Pankhurst, R.J., 1979. The interpretation of igneous rocks. London, George Allen and Unwin.

Criss, J. W., 1980. Fundamental parameters calculations on a laboratory microcomputer. Advances in X-ray Analysis 23, 93-97

Curtis, G. H. and Hay, R. L., 1972. Further geological studies and potassium-argon dating at Olduvai Gorge and Ngorongoro Caldera. In: W. W. Bishop and J. A. Miller (ed), Calibration of Hominoid Evolution. Scottish Academic Press: Edinburgh.

Davies, G. R., and MacDonald, R., 1987. Crustal influence in the petrogenesis of the

Naivasha Basalt-Comendite Complex: Combined trace element and Sr-Nd-Pb isotope constraints. Journal of Petrology 28, 1009-1031.

Dawson, J. B., 1992. Neogene tectonics and volcanicity in the North Tanzania sector of the Gregory Rift Valley: contrasts with the Kenya sector. Tectonophysics 204, 81-92.

Dawson, J. B., 2002. Metasomatism and partial melting in upper-mantle peridotite xenoliths from the Lashaine volcano, northern Tanzania. Journal of Petrology 43, 1749-1777.

Deer, W. A., Howie, R. A. and Zussman, J., 1992. An Introduction to Rock-forming Minerals: 2nd ed. Pearson Education Limited, Harlow, London.

Deino, A. L., McBrearty, S., 2002. $^{40}Ar/^{39}Ar$ dating of the Kapthurin Formation, Baringo, Kenya. Journal of Human Evolution 42, 185 - 210.

Delaney, J. S., Carswell, D. A., and Dawson, J. B., 1980. Chemistry of micas from kimberlites and xenoliths. Primary- and secondary-textured micas from peridotite xenoliths. Geochimica et Cosmochimica Acta 44, 857-872.

Deniel, C., Vidal, P., Coulon, C., Vellutini, P. and Piguet, P., 1994. Temporal evolution of mantle sources during continental rifting: the volcanism of Djibouti (Afar). Journal of Geophysical Research 99, 2853-2869.

Depaolo, D. J, 1981. Trace elements and isotopic effects of combined wall-rock assimilation and fractional crystallization. Earth and Planetary Science Letter 53, 189-202.

Drake, R. and Curtis, G., 1987. K – Ar Geochronology of the Laetoli fossil localities. In: M.D. Leakey and J.M. Harris (ed). *Laetoli a Pliocene Site in Northern Tanzania*. Clarendon Press. Oxford, 48 - 52.

Ebinger, C. J. and Sleep, N. H., 1998. Cenozoic magmatism throughout east Africa resulting from impact of a single plume. Nature 395, 788-791.

Eggins, S. M, Woodhead, J. D, Kinsley, L. P. J, Sylvester, P., McCulloch, M. T., Hergt, J. M., and Handler, M. R., (1997) A simple method for the precise determination of 40 or more trace elements in geological samples by ICPMS using enriched isotope internal standardization. Geochemical Geology 134, 311-326.

Farges, F., Brown, G. E., and Velde, D., 1994. Structural environment of Zr in two inosilicates from Cameroon: mineralogical and geochemical implications. American mineralogist 79, 838-847.

Fitton, J. G., 1987. The Cameroon line West Africa: A comparison between oceanic and continental alkaline volcanism. In J. G. Fitton and B.G. Upton (Ed.) Alkaline Igneous Rocks, volume 30, 273 – 291. Geological Society Special Publications, Washington, DC.

Foster, A., Ebinger, C., Mbede, E., Rex, D., 1997. Tectonic development of the northern Tanzanian sector of the East African Rift system. Journal of the Geological Society of London 154, 689-700.

Furman, T., (2007). Geochemistry of East African Rift Basalts: An overview. Journal of African Earth Sciences doi:10.1016/j.jafrearsci.2006.06.009.

Furman, T., Bryce, J., Karson, J., and Iotti, A., 2004. East African Rift System (EARS) plume structure: Insights from Quaternary Mafic lavas from Turkana, Kenya. Journal of Petrology 45, 1069-1088.

Furman, T., Kaleta, K. M., Bryce, J. G., and Hanan, B. B., 2006. Tertiary mafic lavas of

Turkana, Kenya: constraints on the East African plume structure and the occurrence of high-μ volcanism in Africa. Journal of Petrology 47, 1221-1244.

George, R., Rogers, N., and Kelley, S., 1998. Earliest magmatism in Ethiopia: Evidence for two mantle plumes in one flood basalt province. Geology 26(10), 923-926.

Gladney, E. S., Jones, E. A., and Nickell, E. J., 1988. Compilation of elemental concentration data for USGS AGV-1, GSP-1 and G-2. Geostandards Newsletter 16, 111 – 300.

Gradstein, F.M., Ogg, J.G., Smith, A.G., Bleeker, W., Lourens, L.J., 2004. A new geologic time scale, with special reference to Precambrian and Neogene. Episodes 27, 83-100.

Grégoire, Moine, B. N., O'Reilly, S. Y., Cottin, J. Y. and Giret, A., 2000. Element residence and partitioning in mantle xenoliths metasomatized by high alkaline silicate and carbonate-rich melts (Kerguelen Island, Indian Ocean). Journal of Petrology 41, 477 – 509.

Grommé, C. S., Reilley, T. A., Mussett, A. E and Hay, R. L., 1970. Paleomagnetism and Potassium-Argon Ages of Volcanic Rocks of Ngorongoro Caldera, Tanzania. Geophysical Journal Royal Astronomical Society 22, 101-115.

Hannah, R. S., Vogel, T. A., Patino, L. C., Alvarado, G. E., Pérez, W., and Smith, D. R., 2002. Origin of silicic volcanic rocks in Central Costa Rica: a study of a chemically variable ash-flow sheet in the Tiribí Tuff. Bulletin of Volcanology 64, 117-133.

Hart, W. K., WoldeGabrie, G., Walter, R. C. and Mertzman, S. A., 1989. Basalt volcanism in Ethiopia: Constraints on continental rifting and mantle interaction. Journal of Geophysical Research 94, 7731-7748.

Hart, S. R., Hauri, E. H., Oschmann, L. A., and Whitehead, J. A., 1992. Mantle plumes and entrainment: Isotopic evidence. Science 256, 517-520.

Hay, R., 1976. Geology of the Olduvai Gorge*: A study of sedimentation in a Semi-arid Basin*. University of California Press, Berkeley.

Hay, R., 1987. Geology of Laetoli area. In: M. D. Leakey and J. M. Harris (Ed.) *Laetoli: A Pliocene site in northern Tanzania*. Oxford: Clarendon Press, 23 – 47.

Hofmann, A. W., Jochum, K. P., Seufert, M., and White, W. M., 1986. Nb and Pb in oceanic basalts: New constraints on mantle evolution. Earth and Planetary Science Letters, 79, 33-45.

Ionov, D. A., and Hofmann, A. W., 1995. Nb-Ta-rich mantle amphiboles and micas: Implications for subduction-related metasomatic trace element fractionations. Earth and Planetary Science Letters 131, 341-356.

Ionov, D. A., Griffin, W. L., and O'Railley, S. Y., 1997. Volatile bearing minerals and Lithophile trace elements in the upper mantle. Chemical Geology 141, 153 – 184.

Johnson, J. S., Gibson, S. A., Thompson, R. N., and Nowell, G. M., 2005. Volcanism in the Vitim volcanic field, Siberia: Geochemical evidence for a mantle plume beneath the Baikal rift zone. Journal of Petrology 46(7), 1309-1344.

Jones, A. P. and Peckette, A., 1980. Zirconium-bearing aegirines from Motzfeldt, South Greenland. Contributions to Mineralogy and Petrology 75, 251-255.

Kabeto, K., Sawada, Y., Iizumi, S. and Wakatsuki, T., 2001. Mantle sources and magma-crust interactions in volcanic rocks from the northern Kenya rift: geochemical evidence. Lithos 56, 111-139.

Kalt, A., Hegner, E. and Satir, M., 1997. Nd, Sr, and Pb isotopic evidence for diverse lithospheric mantle sources of East African Rift carbonatites. Tectonics 278, 31 – 4 5.

Kar, A., Weaver, B., Davidson, J., and Colucci, M., 1998. Origin of differentiated volcanic and plutonic rocks from Ascension Island, South Atlantic Ocean. Journal of Petrology 39, 1009-1024.

Keller, J., Zaitsev, A. N. and Wiedenmann, D., 2006. Primary magmas at Oldoinyo Lengai: The role of olivine melilitites. Lithos 91, 150-172.

Keppler, H., 1996. Constraints from partitioning experiments on the composition of subduction-zone fluids. Nature 380, 237-240.

Key, R., Charsley, T., Hackman, B., Wilkinson, A., and Rundle, C., 1989. Superimposed Upper Proterozoic collision-controlled orogenies in the Mozambican Orogenic Belt of Kenya. Precambrian Research 44, 197-225.

Koenigswald, G. H., Von Genter, W. and Lippolt, H. J., 1961. Age of the basalt flow at Olduvai, East Africa. Nature 192, 720-721

Lalonde, A. E., and Martin, R. F., 1983. The Baie-des-Moutons syenitic complex, La Tabatiére, Québec, II. The ferromagnesian minerals. Canadian Mineralogist 21, 81-91.

LaTourrette, T. Z., Hervig, R. L., and Holloway, J. R., 1995. Trace element partitioning between amphibole, phlogopite, and basanite melt. Earth and Planetary and Science Letters 135, 13-30.

Leakey, L. S. B., Curtis, G. H. and Evernden, J. F., 1962. Age of basalt underlying Bed I, Olduvai. *Nature* 194, 610-612.

Leakey, M., 1971. *Olduvai Gorge: excavations in Beds I and II; 1960-1963*. Cambridge University Press: Cambridge, UK.

LeBas, M. J., LeMaitre, R. W., Streckeisen, A., Zanettin, B., 1986. A chemical classification of volcanic rocks based on the total alkali-silica diagram. Journal of Petrology 27, 745-750.

Macdonald, R., Davies, G. R. Upton, B. G. J. Dunkley, P. N., Smith, M. and Leat, P. T., 1995. Petrogenesis of the Silali volcano, Gregory Rift, Kenya. Journal of Geological Society London 152, 703-720.

Macintyre, R. M., Mitchell, J. G., and Dawson, J. B., 1974. Age of the fault movements in the Tanzania sector of the East African Rift system. Nature 247, 354-356.

Manega, P. C., 1993. Geochronology, Geochemistry and Isotopic Study of the Plio-Pleistocene Hominid Sites and the Ngorongoro Volcanic Highlands in Northern Tanzania. Ph.D. Dissertation, University of Colorado.

McDonough, W. F., and Nelson, D. O., 1984. Geochemical constraints on magma processes in a peralkaline system: the Paisano volcano, West Texas. Geochimica et Cosmochimica Acta 48, 2443-2455.

McHenry, L.J., 2005. Phenocryst composition as a tool for correlating fresh and altered tephra, Bed I, Olduvai Gorge, Tanzania. Stratigraphy 2, 101-115.

McHenry, L.J., 2004. Characterization and correlation of altered Plio-Pleistocene tephra using a ‘‘multiple technique’’ approach: case study at Olduvai Gorge, Tanzania. Ph.D. Dissertation, Rutgers University, New Brunswick, New Jersey, 381pp.

McHenry, L. J., (in press). Geochemistry and mineralogy of Laetoli area tuffs: Lower Laetoli through Naibadad Beds. In: Harrison, T (Ed.), Paleontology and

Geochronology of Laetoli: Human Origin in Context 1, Springer, Dordrecht.
McHenry, L.J., Mollel, G.M., Swisher, C.C. III. Compositional and textural correlations between Olduvai Gorge Bed I tephra and volcanic sources in the Ngorongoro Volcanic Highlands, Tanzania, Quaternary International (2007), doi:10.1016/j.quaint.2007.01.004.
Mechie, J., Keller, G. R., Prodehl, C., Kahn, M. A., and Gaciri, S. J., 1997. A model for the structure, composition and evolution of the Kenya Rift. Tectonophysics 236, 409-438.
Mertz, D. F., Weinrich, A. J., Sharp, W. D., and Renne, P. R., 2001. Alkaline intrusions in a near-trench setting, Franciscan complex, California: Constrains from geochemistry, petrology and $^{40}Ar/^{39}Ar$ chronology. American Journal of Science 301, 877-911.
Moine, B. N., Grégoire, M., O'Reilly, S. Y., Sheppard, S. M. F., and Cottin, J. Y., 2001. High field strength element fractionation in the upper mantle: Evidence from amphibole-rich composite mantle xenoliths from the Kerguelen Islands (Indian Ocean). Journal of Petrology 42, 2145-2167.
Mollel, G., 2002. Petrology and geochemistry of the southeastern Ngorongoro Volcanic Highland (NVH); and contribution to "sourcing" of stone tools at Olduvai Gorge, Tanzania. Masters Thesis, Rutgers University, New Brunswick, New Jersey.
Mollel, G.F., McHenry, L.J., 2004. Temporal evolution of the Ngorongoro Volcanic Highland (NVH) in relation to Bed I of Olduvai Gorge, Tanzania: a progress report. Abstract: 2004 Paleoanthropology Society Annual Meeting, Montreal, April, 2004.
Mollel, G. F., Swisher, C. C., Feigenson, M. D., and Carr, M. J., (in press). Petrology, geochemistry, and age of Satiman, Lemagurut, and Oldeani: sources of the volcanic deposits of the Laetoli area. In T. Harrison (Ed.): Paleontology and Geology of Laetoli: Human Evolution in Context Volume 1, Springer, Dordrecht.
Mungall, J. E., and Martin, R. F., 1995. Petrogenesis of basalt - comendite and basalt – pantellerite suites, Terceira, Azore and some implications for the origin of ocean-island rhyolites. Contribution to Mineralogy and Petrology 119, 43-55.
Ndessokia, P., (1990). The mammalian fauna and archaeology of the Ndolanya and Olpiro Beds, Laetoli, Tanzania. Ph.D. Dissertation, University of California,
Berkeley. Ngounouno, I., Déruelle, B. and Demaiffe, D., 2000. Petrology of bimodal Cenozoic volcanism of the Kapsiki plateau (northernmost Cameroon, Central Africa). Journal of Volcanology and Geothermal Research 102, 21-44.
Nyblade, A. A., Owens, J. T., Gurrola, H., Ritsema, J. and Langston, C. A., 2000. Seismic evidence for a deep upper mantle thermal anomaly beneath East Africa. Geology 28, 599-602.
Oberti, R., Vannucci, R., Zenetti, A., Tiepolo, M., and Brumm, R. C., 2000. A crystal-chemical re-evaluation of amphibole/melt and amphibole/clinopyroxene D_{Ti} in petrogenic studies. American Mineralogist 85, 407-419.
Panter, K. S., Kyle, P. R. and Smellie, J. L., 1997. Petrogenesis of a phonolite-trachyte succession at Mount Sidley, Marie Byrd Land, Antarctica. Journal of Petrology 38(9), 1225 - 1253
Paslick, C., Halliday, A. N., James, D. and Dawson, J. B. 1995. Enrichment of

continental lithosphere by OIB melts: Isotopic evidence from the volcanic province of northern Tanzania. Earth and Planetary Science Letters 130, 109-126.
Patino, L. C., Velbel, M. A., Price, J. R., and Wade, J. A., 2004. Trace element mobility during spheroidal weathering of basalts and andesites in Hawaii and Guatemala. Chemical Geology 202, 343-364.
Pickering, R., 1965. Ngorongoro. Geological Survey of Tanzania, Quarter degree sheet 53, scale 1:125,000.
Renne, P., Swisher III, C., Deino, A., Kamer, D., Owens, T., and DePaolo, D., 1998. Intercalibration of standards, absolute ages, and uncertainties in $^{40}Ar/^{39}Ar$ dating. Chemical Geology 145**,** 117-152.
Rogers, W. M., James, D., Kelley, S. P., De Mulder, M, 1998. The generation of potassic lavas from eastern Virunga province, Rwanda. Journal of Petrology 39, 1223-1247.
Rogers, N., Macdonald, R., Fitton, J. G., George, R., Smith, M., and Barreiro, B., 2000. Two mantle plumes beneath the East African rift system: Sr, Nd and Pb isotope evidence from Kenya Rift basalts. Earth and Planetary Science Letters 176, 38-400.
Scalliet, B. and McDonald, R., 2001.Phase relations of peralkaline silicic magmas and petrogenetic implications. Journal of Petrology 42, 825-845.
Scalliet, B. and McDonald, R., 2003. Experimental constraints on the relationships between peralkaline rhyolites of the Kenya Rift Valley. Journal of Petrology 44(10), 1867-1894.
Shand, S. J., 1927. The Eruptive Rocks. John Wiley. New York.
Smith, M., 1994. Stratigraphic and structural constraints on mechanisms of active rifting in Gregory rift Kenya. In: Prodehl, C., Keller, G. R. and Khan, M. A. (Ed.): Crustal and Upper Mantle Structure of the Kenya Rift. Tectonophysics, 3-22.
Späth, A., Le Roex, A., and Opiyo-Akech, N., 2001. Plume-Lithosphere interaction and the origin of continental rift-related alkaline volcanism-the Chyulu Hills Volcanic Province, southern Kenya. Journal of Petrology 42, 765-787.
Sun, S., and McDonough, W. F., 1989. Chemical and isotopic systematics of oceanic basalts: implications for mantle composition and processes. In: Sounders, A. D., and Norry, M. J., (Eds.), Magmatism in Ocean Basins. Geological Society Special Publication 42, 313-345.
Tamrat, E., Thouveny, N., Taïeb, M., and Opdyke, N. D., (1995). Revised magnetostratigraphy of the Plio-Pleistocene sedimentary sequence of the Olduvai Formation (Tanzania). Palaeogeography, Palaeoclimatology, Palaeoecology 114, 273-283.
Tiepolo, M., Zanetti, A., and Oberti, R., 1997. Detection, crystal-chemical mechanism and petrological implications of Ti^{4+} partitioning in pargasite and kaersutite. European Journal of Mineralogy 11, 345-354.
Tiepolo, M., Bottazzi, P., Foley, S., Oberti, R., Vannucci, R., and Zanetti, A., 2001. Fractionation of Nb and Ta from Zr and Hf at mantle depths: the role of titanian pargasite and kaersutite. Journal of Petrology 42, 221-232.
Tiepolo, M., Vannucci, R., Oberti, R., Foley, S., Bottazzi, P., and Zanetti, A., 2000. Nb and Ta incorporation and fractionation in titanian pargasite and kaersutite: crystal-chemical constrains and implications for natural systems. Earth and Planetary

Science Letters 176, 185-201.
Trua, T., Deniel, C. and Mazzuoli, R., 1999. Crustal control in the genesis of Plio-Quaternary bimodal magmatism of the Main Ethiopian Rift (MER): geochemical and isotopic (Sr, Nd, Pb) evidence. Chemical Geology 155, 201-231.
Turrin, B. D., Muffler, L. J. P., Clynne, M. A. and Champion, D. E., 2007. Robust 24 ± 6 ka $^{40}Ar/^{39}Ar$ age of a low-potassium tholeiitic basalt in the Lassen Region of NE California. Quaternary Research, doi:10.1016/j.yqres.2007.02.004
Vannucci, R., Piccardo, G. B., Rivalenti, G., Zanetti, A., Rampone, E., Ottolini, L., Oberti, R., Muzzucchelli., M., and Bottazzi, P., 1995. Origin of LREE-depleted amphiboles in the subcontinental mantle. Geochimica et Cosmochimica Acta 59, 1763-1771.
Velde, D., 1978, An aenigmatite-richterite-olivine trachyte from Puu Koae, West Maui, Hawaii. American Mineralogist 63, 771- 778.
Walter, R.C., Manega, P.C. and Hay, R.L., 1992. Tephrochronology of Bed I, Olduvai Gorge: An application of laser fusion $^{40}Ar/^{39}Ar$ dating to calibrating biological and climatic change. Quaternary International 13, 37-46.
Walter, R.C., Manega, P.C., Hay, R.L., Drake, R.E. and Curtis, G.H., 1991. $^{40}Ar/^{39}Ar$ dating of Bed I, Olduvai Gorge, Tanzania. Nature 354, 145-149.
Weaver, S. D., Seal, J. S. and Gibson, I. L., 1972. Trace element data relevant to the origin of trachytes and pantelleritic lavas in the East African Rift System. Contributions to Mineralogy and Petrology 36, 181-194.
Weeraratne, D. S., Forsyth, D. W., Fischer, K. M. and Nyblade, A. A., (2003). Evidence for an upper mantle plume beneath the Tanzania Craton from rayleigh wave tomography. Journal of Geophysical Research 108 (B9), 24-27
Witt-Eickschen, G. and Harte, B., 1994. Distribution of trace elements between amphibole and clinopyroxene from mantle peridotites of Eifel (West Germany). Chemical Geology 117, 235-250.
Yang, W., and Holland, H. D., 2003. The Hekpoort paleosol profile in strata 1 at Gaborone, Botswana: Soil formation during the great oxidation event. American Journal of Science 303, 187-220.

CHAPTER 6

Other silica undersaturated centers

RESULTS

An introduction and description of the lava types found in Embagai and Engelosin by previous workers was given in Chapter 1. Analytical procedures were also provided in chapter 2. Petrography, result of major and trace element analyses, and Sr-Nd-Pb isotopes as well as whole rock $^{40}Ar/^{39}Ar$ are provided below.

Petrography and mineral chemistry

Embagai

Based on major element chemistry of four samples, and the classification scheme of Cox *et al*. (1979), Embagai lavas are nephelinite and foidite (Figure 6.1). Petrographic studies of the four thin sections using an optical microscope and one sample EMB-4 using an electron microprobe indicates that Embagai rocks are phaneritic, porphyritic, coarse to fine-grained in texture, and that one lava (03-EMB2) has a glassy groundmass.

Detailed study of sample 03-EMB4 indicates that the rock is holocrystalline porphyritic, coarse to fine-grained, and composed of nepheline, augite, andradite, melilite, apatite, and titanomagnetite (Figure 6.2). The phenocrysts are of nepheline, augite, garnet and occasionally melilite and apatite in a groundmass of nepheline and augite. The nepheline is tabular, colorless to white, highly fractured and ranges in composition from $Na_{4.23}K_{1.65}(Al_{5.25}Fe_{0.51})Si_{6.3}O_{24}$ to $Na_{4.14}K_{1.62}(Al_{5.55}Fe_{0.48})Si_{6.15}O_{24}$ (Table 6.1). The Embagai nephelines are Fe-rich, the FeO content ranges from 2.7 - 4.8 wt % (Table 6.1). Typical FeO content in nepheline is < 2 wt % (Deer *et al.*, 1992).

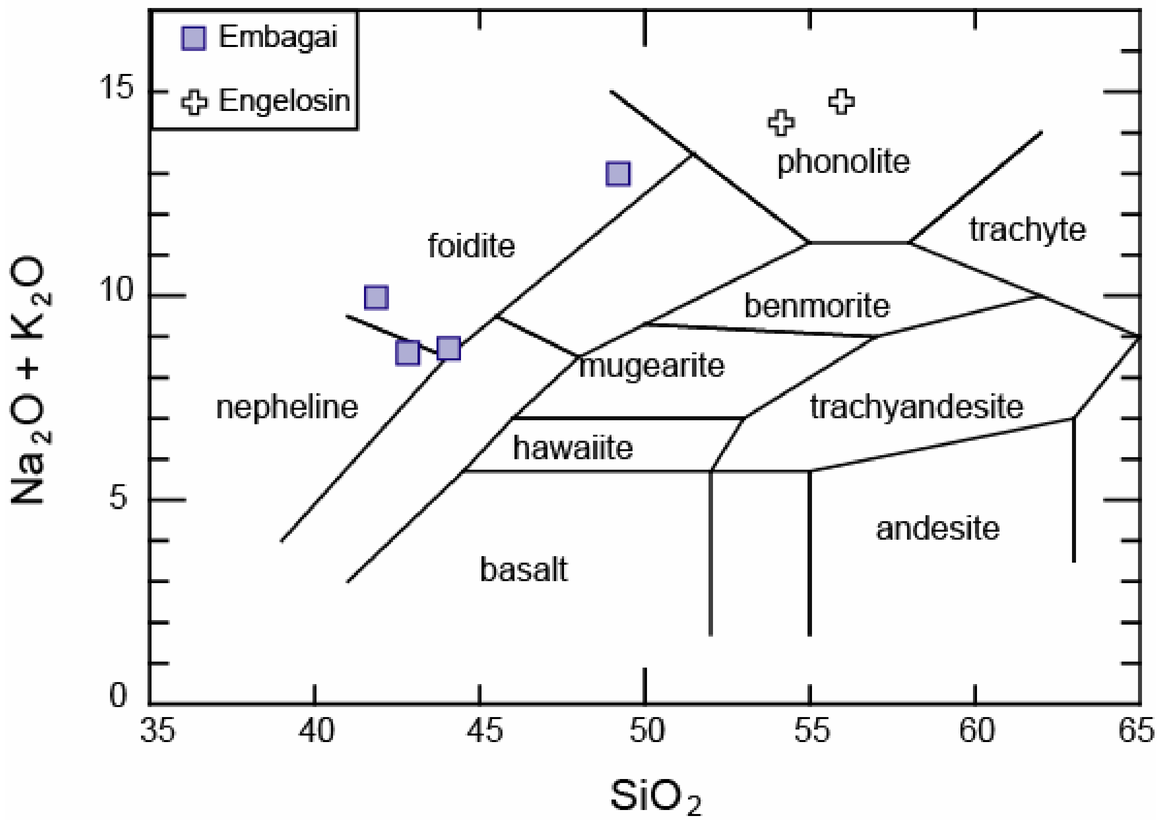

Figure 6.1: Total Alkali versus Silica classification of Cox *et al.*, (1979) for lavas from Embagai and Engelosin.

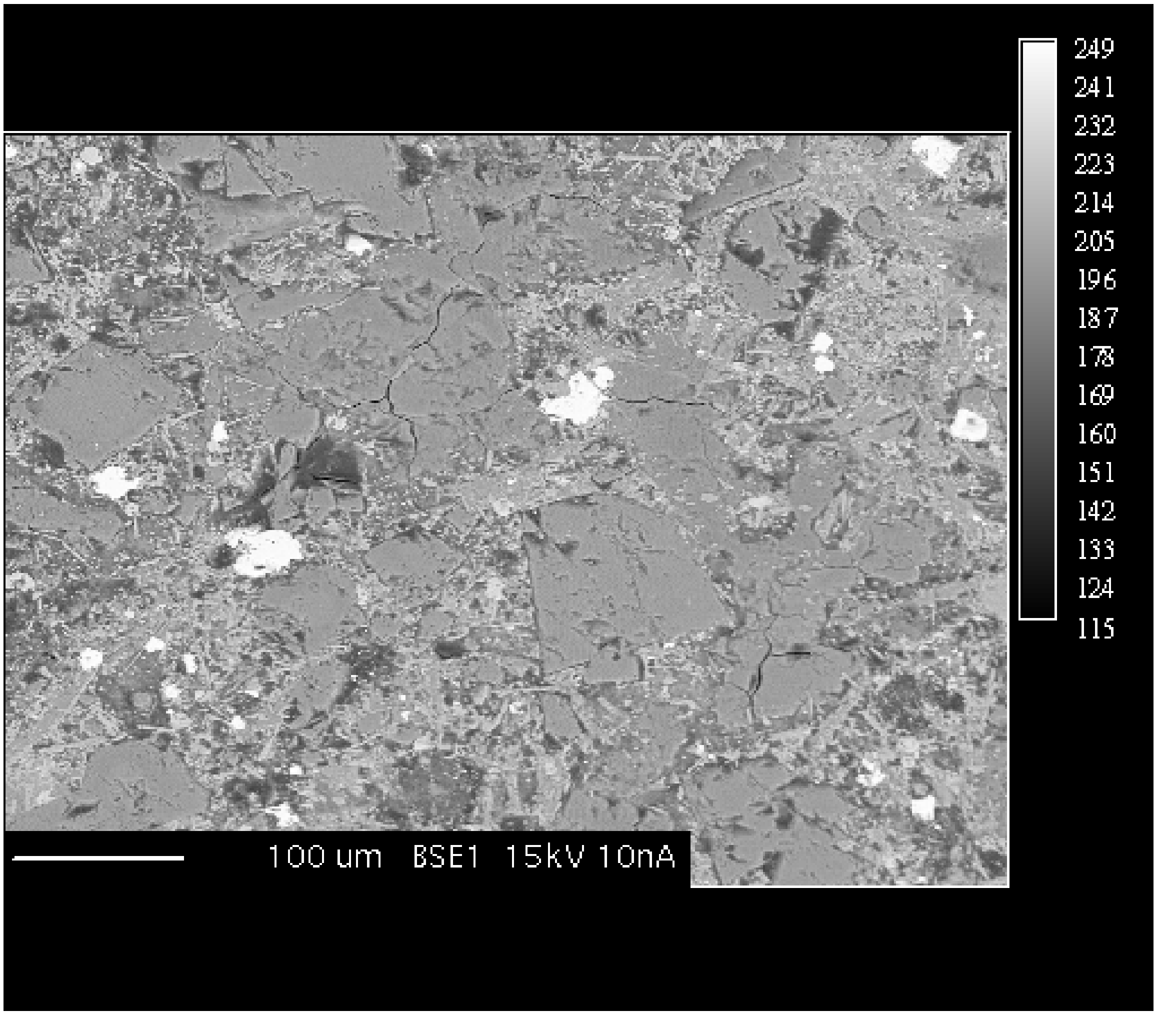

Figure 6.2: Back Scatter Electron Image of foidite (EMB-4) showing large tabular crystals of nepheline sitting on fine-grained lath-shaped augite. The bright specks are of titanomagnetite.

Table 6.1. Embagai mineral compositions (%wt), electron microprobe data.

Pyroxene	SiO2	TiO2	Al2O3	MgO	MnO	FeO	CaO	Na2O	K2O	P2O5	Total
1	51.84	1.47	2.16	14.02	0.17	7.91	24.06	0.73	0.03	0.03	102.41
2	50.88	1.92	2.52	14.78	0.14	8.23	23.17	0.36	0.01	0.12	102.13
3	50.88	1.89	2.40	14.94	0.17	8.02	23.31	0.33	0.00	0.00	101.93
4	48.69	2.74	4.37	13.49	0.09	7.81	23.79	0.57	0.00	0.04	101.59
5	48.33	3.08	4.78	12.74	0.14	8.39	23.76	0.66	0.03	0.15	102.04
6	51.87	0.91	0.43	10.62	0.54	12.54	22.67	2.07	0.02	0.00	101.67
7	51.95	1.21	1.24	12.75	0.31	24.88	9.40	1.12	0.03	0.01	102.90
8	52.58	0.96	0.82	11.74	0.42	10.23	23.16	1.72	0.04	0.00	101.67
9	51.74	1.21	0.65	10.97	0.46	11.83	23.31	1.84	0.00	0.01	102.02

Nepheline	SiO2	TiO2	Al2O3	MgO	MnO	FeO	CaO	Na2O	K2O	P2O5	Total
1	42.92	0.04	31.49	0.25	0.00	3.07	0.07	15.08	8.41	0.01	101.32
2	41.13	0.00	31.46	0.19	0.00	3.81	0.11	14.34	8.52	0.00	99.57
3	42.82	0.04	30.28	0.32	0.00	4.10	0.19	14.89	8.79	0.03	101.46
4	41.73	0.07	29.87	0.22	0.01	3.66	0.16	14.64	8.44	0.01	98.81
5	41.47	0.00	30.79	0.12	0.04	4.28	0.17	14.90	9.21	0.00	100.97
6	42.04	0.11	29.93	0.25	0.00	2.71	0.16	14.72	8.54	0.03	98.47
7	42.30	0.01	29.14	0.39	0.01	4.83	0.60	14.36	8.67	0.01	100.34
8	41.56	0.03	31.48	0.14	0.00	3.57	0.09	14.74	9.17	0.00	100.78

Andradite	SiO2	TiO2	Al2O3	MgO	MnO	FeO	CaO	Na2O	K2O	P2O5	Total
1	27.27	19.19	0.36	1.02	0.39	19.35	33.61	0.62	0.02	0.03	101.86
2	26.23	18.84	0.53	1.04	0.31	20.10	33.81	0.36	0.02	0.05	101.30
3	25.53	25.34	0.10	1.06	0.47	13.78	33.24	1.32	0.07	0.03	100.94
4	26.83	19.41	0.36	1.06	0.40	19.10	33.40	0.59	0.01	0.00	101.14

Melalite	SiO2	TiO2	Al2O3	MgO	MnO	FeO	CaO	Na2O	K2O	P2O5	Total
1	43.90	0.05	6.53	4.90	0.16	7.44	33.53	4.59	0.18	0.03	101.30
2	43.81	0.01	6.60	4.83	0.22	7.58	33.24	4.73	0.16	0.03	101.21

Apatite	SiO2	TiO2	Al2O3	MgO	MnO	FeO	CaO	Na2O	K2O	P2O5	Total
1	0.34	0.02	0.00	0.03	0.02	0.22	58.94	0.03	0.03	40.78	100.40
2	0.36	0.00	0.00	0.01	0.00	0.24	58.74	0.01	0.01	39.76	99.12

Oxide	SiO2	TiO2	Al2O3	MgO	MnO	FeO	CaO	Na2O	K2O	P2O5	Total
1	0.02	9.96	0.38	0.93	1.58	81.55	0.28	0.00	0.02	0.02	94.73
2	0.03	10.49	0.81	1.13	1.70	80.01	0.33	0.00	0.03	0.05	94.57

Augite is mostly lath-shaped, fine-grained, and makes up part of the groundmass as well as the phenocrysts. It is green to greenish brown, and is sodium and titanium rich. The augite composition ranges from $En_{35}Fs_{50}Wo_{15}$ to $En_{32}Fs_{19}Wo_{49}$ and its Na_2O and TiO_2 content is $\leq$ 2.1 %wt and $\leq$ 3.1 wt% respectively (Table 6.1). Augite containing 3-6 wt % TiO_2 is known as *titanian augite* (Deer e*t al.*, 1992).

Melilite phenocrysts are lath-shaped and Na and Fe rich (Table 6.2). The composition of two grains ranges from $Ca_{1.64}Na_{0.41}K_{0.01})(Mg_{0.33}Fe_{0.28}Mn_{0.01}Al_{0.35}Si_2)O_7$ to $Ca_{1.62}Na_{0.42}K_{0.01})(Mg_{0.33}Fe_{0.29}Mn_{0.01}Al_{0.35}Si_2)O_7$

Apatite is colorless, has high relief, and is hexagonal in shape. Accessory apatite occurs subophitic with nepheline and the composition from two grains range from $Ca_{5.53}(PO_4)_3(OH, F, Cl)$ to $Ca_{5.46}(PO_4)_3(OH, F, Cl)$ (Table 6.1). It is worth noting that neither OH, F nor Cl were analyzed, making it impossible to tell the exact apatite type. Fluoro-apatite is however the most common type in igneous rocks (Deer *et al.*, 1992).

Andradite phenocrysts occur in cubes, are dark brown or black, and Ti- and Na-rich. The composition of the Embagai andradite ranges from $Ca_{3.12}(Na_{0.1}Mn_{0.03}Mg_{0.14}Fe_{0.78}Ti_{1.27})(Fe_{0.61}Al_{0.04}Si_{2.34})O_{12}$ to $Ca_{3.06}(Na_{0.22}Mn_{0.03}Mg_{0.14}Fe_{0.35}Ti_{1.64})(Fe_{0.64}Al_{0.01}Si_{2.19})O_{12}$ and its TiO_2 and Na_2O contents vary from 18.8 – 25.3 wt % and 0.4 – 1.3 wt % respectively (Table 6.1). Andradite with such high Ti composition ($TiO_2 \geq 15$ wt %) is referred to as *schorlomite* (Deer *et al.*, 1992). Embagai garnets are similar in composition to those found in Satiman (Chapter 3) and are different from pyrope garnet found in Lashaine and Labait xenolith in northern Tanzania that are characterized by relatively low TiO_2 contents < 8.5 wt % (Jones et al., 1983, Lee and Rudnick, 1999). Unlike other groups of garnet, the titanian andradite and *schorlomite* are exclusively found in alkaline igneous rocks, e.g., phonolite, nephelinite and ijolite (Deer *et al.,* 1992).

The main oxide phase is titanomagnetite that occurs as subhedral prisms. If all the Ti is assumed to be ulvospinel, the average oxide composition is $Usp_{23}Mg_{77}$ (Table 6.1). In summary, the Embagai crater is composed primarily of porphyritic, fine to coarse-grained foidite and nephelinite (Figure 6.1). The mineral assemblage includes nepheline, titaniaugite, andradite, apatite, melilite, titanomagnetite, ± amphibole.

Engelosin

Petrographic study of two thin sections using an optical microscope indicates that Engelosin is composed primarily of aphanitic greenish fine-grained phonolitic lavas (Figure 6.1). Engelosin mineral assemblage includes alkali feldspar, sodic augite, nepheline, titanite, apatite and rare Fe-Ti oxide. The groundmass is made up of alkali feldspar and sodic augite and the phenocrysts are of nepheline, augite, titanite and apatite.

Major and trace elements

Major element analyses of all lavas are given in Table 6.2. Engelosin lava has higher incompatible element concentrations than Embagai lavas (Figure 6.1). Engelosin has the highest SiO_2 content ranging from 54.13 – 55.96 wt % compared to Embagai with a relatively wider range from 41.86 to 49.20 wt %. Harker diagrams (Figure 6.3) show continuous decrease in TiO_2, FeO, MgO, and CaO and an increase in Na_2O and Al_2O_3 with increasing silica content. MnO and P_2O_5 also decrease with increasing silica content (not shown). K_2O content is slightly higher in Embagai ranging from 2.35 – 5.49 wt %

compared to 4.93 – 5.19 wt % in Engelosin (Table 6.1), and in overall decreases with increasing silica content (not shown).

Compatible trace elements (e.g. Cr) are low (<10 ppm) in Embagai as well as Engelosin (Table 6.1). In all lavas, the abundances of most of the trace elements and rare earth elements (REEs) are positively correlated with La, except in Embagai lavas were Sr decreases and Ba shows almost no change (Figure 6.4). Overall Engelosin and Embagai have high concentrations of Large Ion Lithophile Elements (LILE). All lavas are enriched compared to primitive mantle (Figure 6.5), and show negative anomalies in K and P. In addition, Engelosin shows Ba, U, La, Ce and Ti negative anomalies.

Table 6.2. UTM coordinate of locations, major and trace elements, and Sr, Nd and Pb isotope analyses of lavas from Embagai and Engelosin; na = not analyzed

Sample Id	EMB3	EMB4	EMB5	EMB6	EGA	EGB
UTME	815752	817397	818014	818100	764947	764955
UTMS	9680922	9677440	9678326	9678276	9678188	9678150
XRF data						
SiO2	44.06	41.86	42.82	49.2	54.13	55.96
TiO2	2.81	2.47	3.18	1.85	0.64	0.62
Al2O3	15.73	14.1	12.34	17.18	19.7	20.35
FeO	10.55	12.2	13.56	8.24	4.75	4.54
MnO	0.29	0.46	0.41	0.26	0.14	0.12
MgO	2.21	3.5	4.02	1.29	0.74	0.48
CaO	8.73	8.68	9.15	4.76	2.05	1.36
Na2O	6.36	5.7	5.11	7.5	9.31	9.57
K2O	2.35	4.26	3.49	5.49	4.93	5.19
P2O5	0.8	0.74	1.13	0.38	0.17	0.09
Total	93.89	93.97	95.21	96.15	96.56	98.28
ICP MS LA data						
Rb	209	100	111	146	111	119
Sr	1346	2298	2248	2018	1532	870
Zr	548	415	653	555	650	688
Ba	3098	2967	3913	2726	1135	978
La	164	95	96	146	66	47
Ce	271	117	137	233	119	82
Pr	30	12	15	25	12	9
Nd	107	39	54	85	37	27
Sm	18	8	11	14	7	4
Eu	5	3	3	4	2	1
Gd	16	8	10	12	7	5
Tb	2	1	1	2	1	1
Y	54	40	46	48	18	17
Dy	10	7	8	9	4	3
Ho	2	1	2	2	1	1
Er	5	3	4	4	3	2
Yb	5	4	4	5	4	3
Lu	1	0	1	1	0	0
V	176	296	400	98	54	47
Cr	3	2	2	3	3	2
Nb	265	237	187	260	320	322
Hf	11	8	15	12	13	12
Ta	13	7	7	11	16	17
Pb	9	10	4	14	32	29
Th	26	4	8	28	34	33
U	4	4	3	2	2	4
Zr/Nb	2.07	1.75	3.49	2.13	2.03	2.14
TIMS data						
87Sr/86Sr	0.704160	na	0.704380	0.704140	na	0.705695
143Nd/144Nd	0.512658	na	0.512750	0.512590	na	0.511826
206Pb/204Pb	19.77	na	na	19.02	na	20.9
207Pb/204Pb	15.66	na	na	15.56	na	15.87
208Pb/204Pb	39.84	na	na	39.42	na	42.08

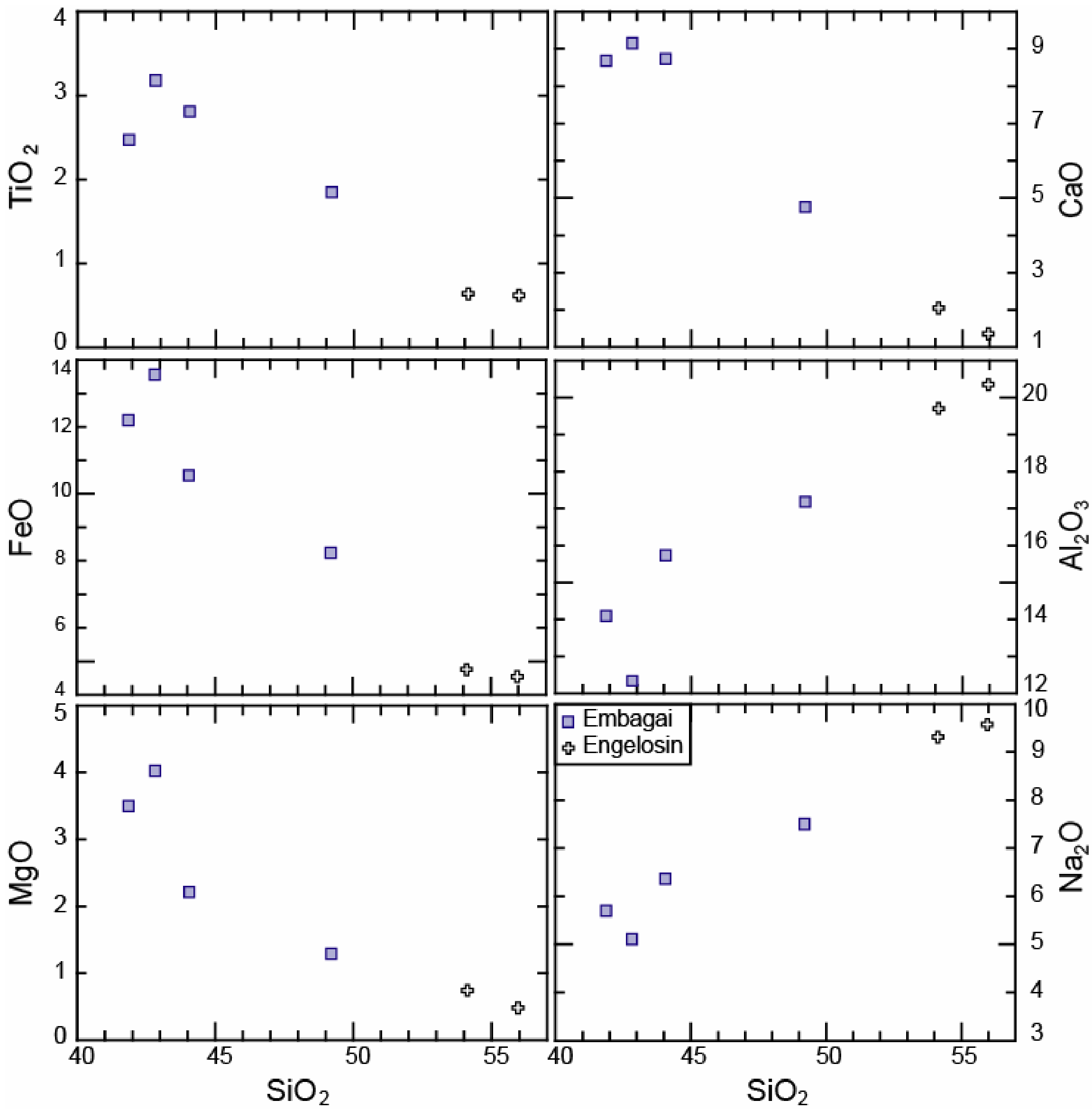

Figure 6.3: Major elements versus Silica (wt %) Harker diagrams for lavas from Embagai and Engelosin. Decreasing TiO_2, FeO, MgO and CaO is consistent with fractionation of augite, andradite, titanomagnetite and melilite.

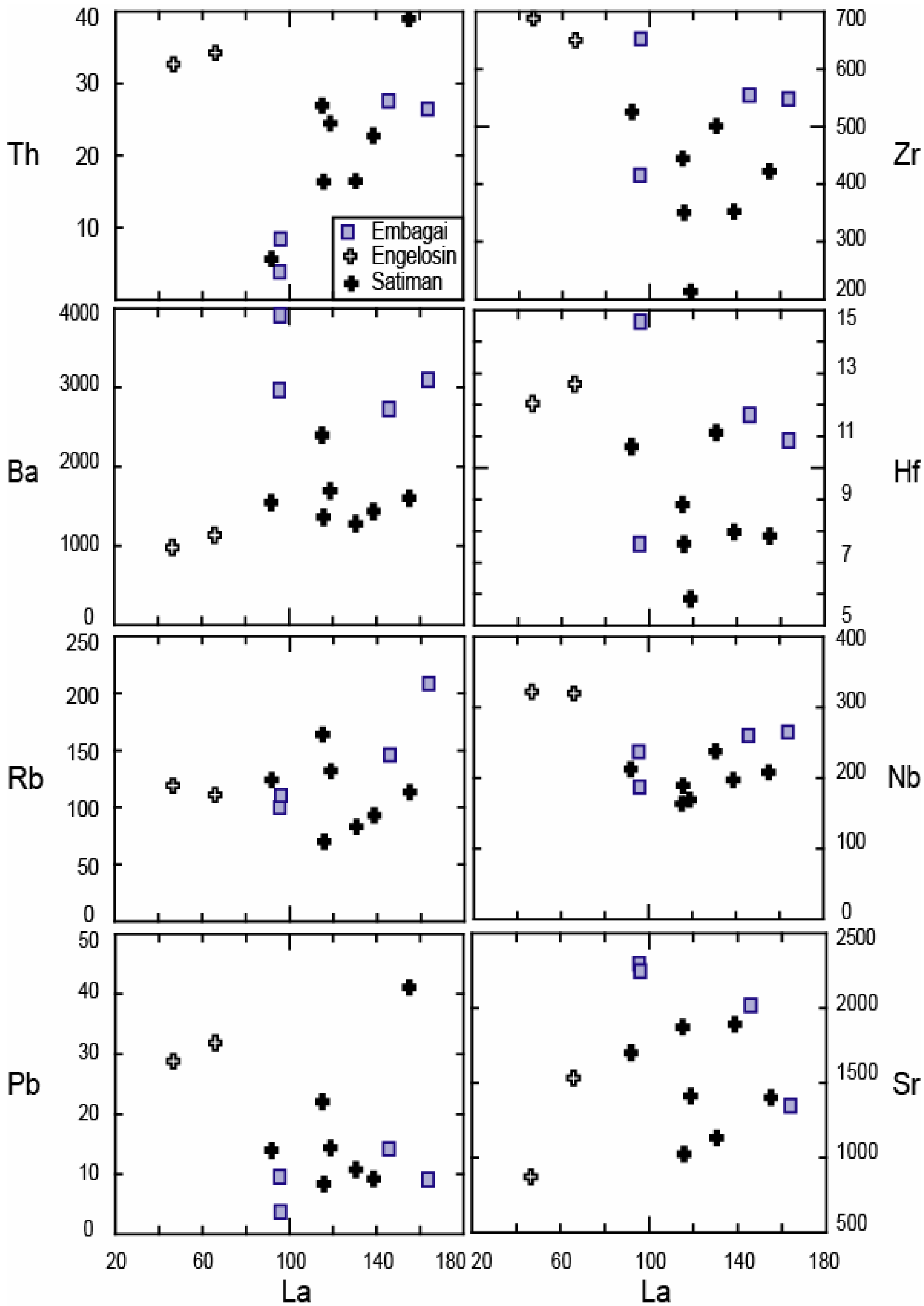

Figure 6.4: Trace and REEs correlate positively with La for Embagai and Engelosin. Sr decreases with increasing La and Ba and Pb shows almost no change. Similar to the Satiman volcano located to the west, Engelosin and Embagai have higher concentrations of LILE.

Sr-Nd-Pb isotopes

The Sr-Nd-Pb isotopes for selected samples from Embagai and Engelosin are shown in Table 6.1. Sr and Nd analyses were done on three lavas from Embagai and one from Engelosin. Two Embagai lavas and one Engelosin were analyzed for Pb. The ^{143}Nd/^{144}Nd ratio of 0.511826 on a phonolite from Engelosin recorded the lowest value in the entire NVHC and Embagai values vary from 0.512590 – 0.512750. The ^{87}Sr/^{86}Sr value of the Engelosin phonolite, 0.705695 is also higher than values from Embagai that varies from 0.70414 to 0.704380. Low Nd isotope ratios from Engelosin were also reported by Manega (1993). The Engelosin phonolite also recorded the highest Pb isotope ratios in the entire NVHC i.e. ^{206}Pb/^{204}Pb = 20.9, ^{207}Pb/^{204}Pb = 15.87 and ^{208}Pb/^{204}Pb = 42.08 (Appendix 1). Compared to Engelosin, the Pb isotope values from two Embagai lavas are relatively less radiogenic ([^{206}Pb/^{204}Pb = 19.02 – 19.77, ^{207}Pb/^{204}Pb = 15.56 – 15.66 and ^{208}Pb/^{204}Pb = 39.42 – 39.84]; Appendix 1). The ^{206}Pb/^{204}Pb and ^{208}Pb/^{204}Pb correlates positively with U/Pb, and these ratios decrease with increasing silica content (not illustrated).

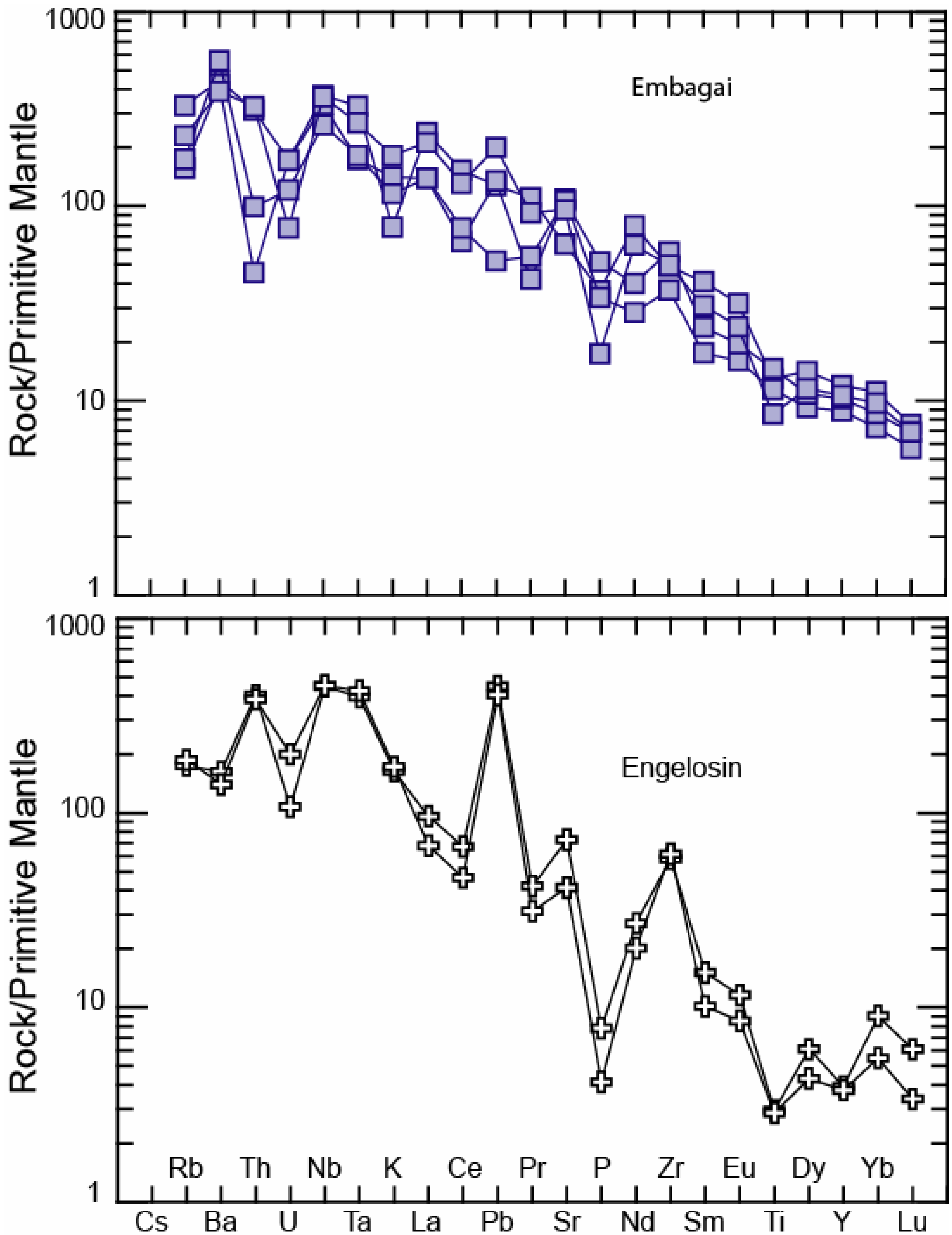

Figure 6.5: Primitive mantle normalized trace elements diagram for Embagai and Engelosin indicating enrichment in incompatible elements. Troughs of P and Ti suggest apatite and titanite fractionation. The positive Pb anomaly is attributed to crustal assimilation.

DISCUSSION

Engelosin and Embagai are composed of silica undersaturated lavas and are here compared to the silica-poor Satiman (Chapter 3) to see if they share similar chemical and magma evolution processes. Variation of major elements versus silica (Figure 6.3) suggests that fractional crystallization was part of the process that created the observed chemical variations. The decrease in TiO_2, FeO, MgO, and CaO suggests augite and titanite fractionation in Embagai. The decrease in MnO and CaO is consistent with melilite fractionation, P_2O_5 and CaO with apatite, and that of K_2O with nepheline fractionation. Fractionation of apatite and titanite is also supported by the negative P and Ti anomaly seen in the spider diagrams (Figure 6.4). Both the Engelosin and Embagai lavas have high concentrations of LILE similar to Satiman (Figure 6.4) suggesting that they were derived either from an enriched source or by small degree partial melt of parent rock (Mertz *et al*., 2001; Johnson *et al*., 2005). Variation of Pb, Ce, Th, Ta, Nd, Eu and Sm shows positive trends with silica (Figure 6.6), the rest of LILE show no change or trends (not shown). The concentration of HFSE such as Zr, Nb, and Ta are almost constant for the Embagai lavas suggesting that magma fractionation was not significant compared to other centers in the NVHC (e.g. Ngorongoro in chapter 4). The higher concentration of LILE together with variation of major elements against silica suggests that the Engelosin and Embagai lavas were derived by low degree partial melting of parent followed by magma fractionation. HFSE ratios e.g. Zr/Nb, Hf/Nb and La/Nb are low and similar between Engelosin and Embagai (Figure 6.7). One Embagai sample (EMB5) has higher ratios of these elements, excluding the one sample, Engelosin and Embagai share a Zr/Nb ratio of ~2.1, which is similar to that obtained from the silica-poor Satiman volcano. The La/Nb ratios for the Engelosin and Embagai are lower than 0.9, consistent with other lavas that are thought to have been derived by relatively lower degree partial melt of the source rock i.e., Satiman and Oldoinyo Lengai (Chapter 3).

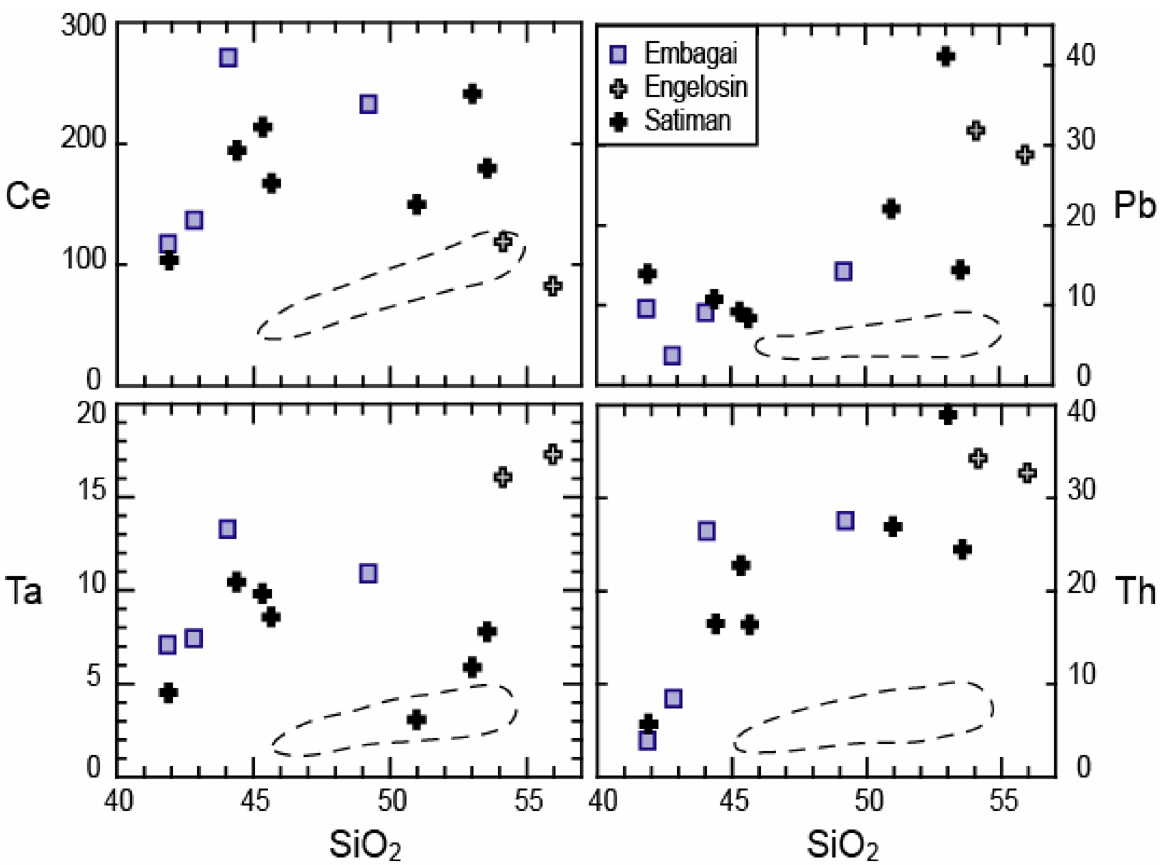

Figure 6.6: Variation of LILE (Ce, Ta, Pb and Th in ppm) with SiO_2 content (wt %). The concentrations in these lavas are higher compared to concentrations measured on lavas from other basaltic center in the NVHC e.g. Ngorongoro and Oldeani (dashed fields).

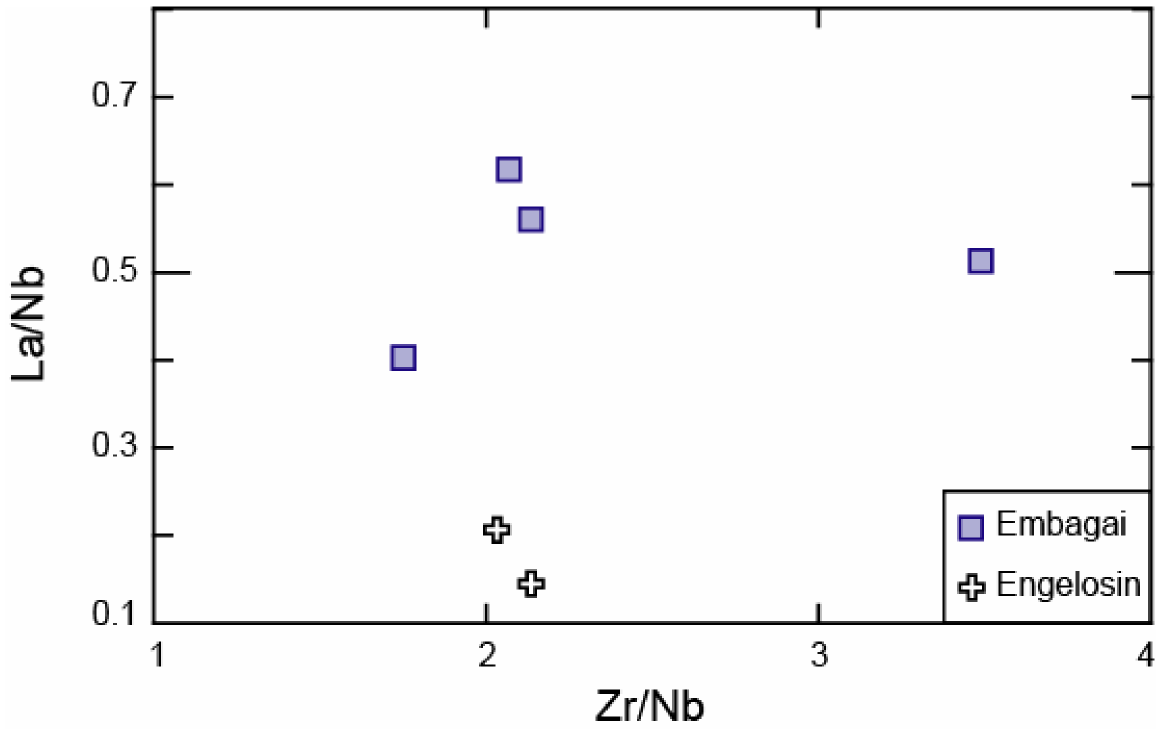

Figure 6.7: La/Nb versus Zr/Nb for Embagai and Engelosin lavas. The Zr/Nb ratio for Engelosin and Embagai lava (except EMB5) are similar ~2.1 and unique from that of Olduvai ~3.5. La/Nb ratio sensitive to the degree of partial melting is lower than 0.9, consistent with ratios obtained from other centers in the NVHC that are though to have been derived from lower degree partial melt of the parent rock (Mollel *et al.*, in press).

The Sr and Nd data from Engelosin and Embagai reported here are within the range of values defined by Oceanic Island Basalt (OIB) globally (Hart, 1984; Hart *et al.*, 1986) and together with their trace elements that gave a ratio of ~1 when normalized to OIB (Figure 6.8), suggests an OIB source for these lavas. The Ce/Pb ratio sensitive to crustal contamination is 3.7 - 2.85 for Engelosin lava, the lowest in the entire NVHC, suggesting that the Engelosin was more crustal contaminated than others.

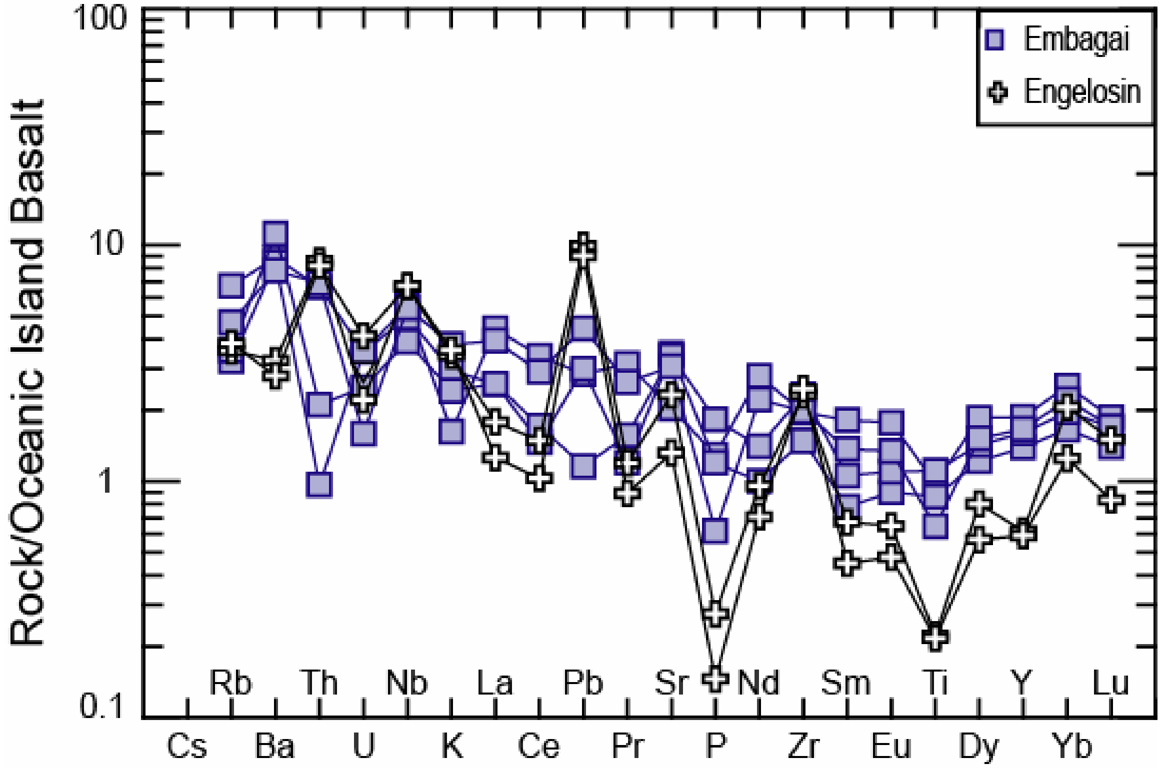

Figure 6.8: Oceanic Island Basalt (OIB) normalized trace element ratio close to 1 for Embagai and Engelosin lavas suggest an OIB source. The higher concentrations of these elements suggest derivation from an enriched source or resulted from low degree partial melt of the sourcerock. Engelosin lava shows a positive Pb anomaly likely from crustal contamination.

A Sr-Nd isotope plot for the relatively less contaminated Embagai with Ce/Pb = 12.2 – 36.9 fall within the field defined by lavas from northern Tanzania (Figure 6.9; Paslick *et al.*, 1995). These data closely fallow the field defined by the East African Carbonatite [EAC] of Bell and Tilton, (2001) that includes lavas from Oldoinyo Lengai, Kerimasi and Homa Mountains, among others (Kalt *et al.*, 1997). Most of the less contaminated NVHC lavas plot close to the intersection of Bulk Earth (BE) and Chondritic Uniform Reservoir (CHUR) hypothetical mantle endmembers (Figure 6.9).

The Engelosin lava with the lowest $^{143}Nd/^{144}Nd$ ratio of 0.511826 (Figure 6.9) clearly indicates crustal contamination.

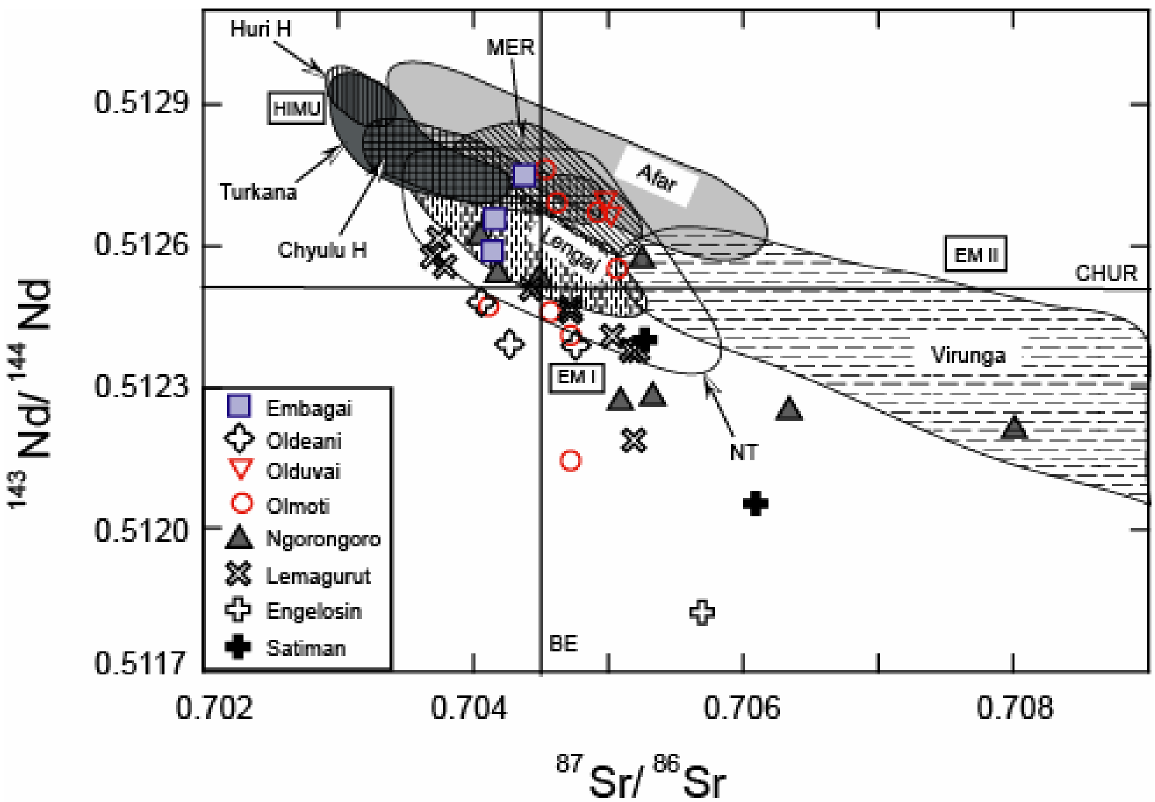

Figure 6.9. Nd-Sr isotope variation for NVHC lavas compared with other lavas from the East African Rift System, as well as hypothetic mantle endmember compositions. BE, Bulk Earth; CHUR, Chondritic Uniform Reservoir; Huri H., Huri Hills; Chyulu H., Chyulu Hills; MER, Main Ethiopian Rift; NT, Northern Tanzania, Lengai, Oldoinyo Lengai. Source of data: Class et *al*., 1994; Bell and Simonetti, 1995; Paslick *et al*., 1995; Deniel *et al.,* 1994; Kalt *et al.*, 1997; Rogers *et al.,* 1998; Trua et *al.*, 1999; Bell and Tilton, 2001; Späths *et al*., 2001; Furman *et al*., 2004, 2006; Keller *et al*., 2006. DMM, HIMU, EM I and EMII fields from Hart *et al*., 1992).

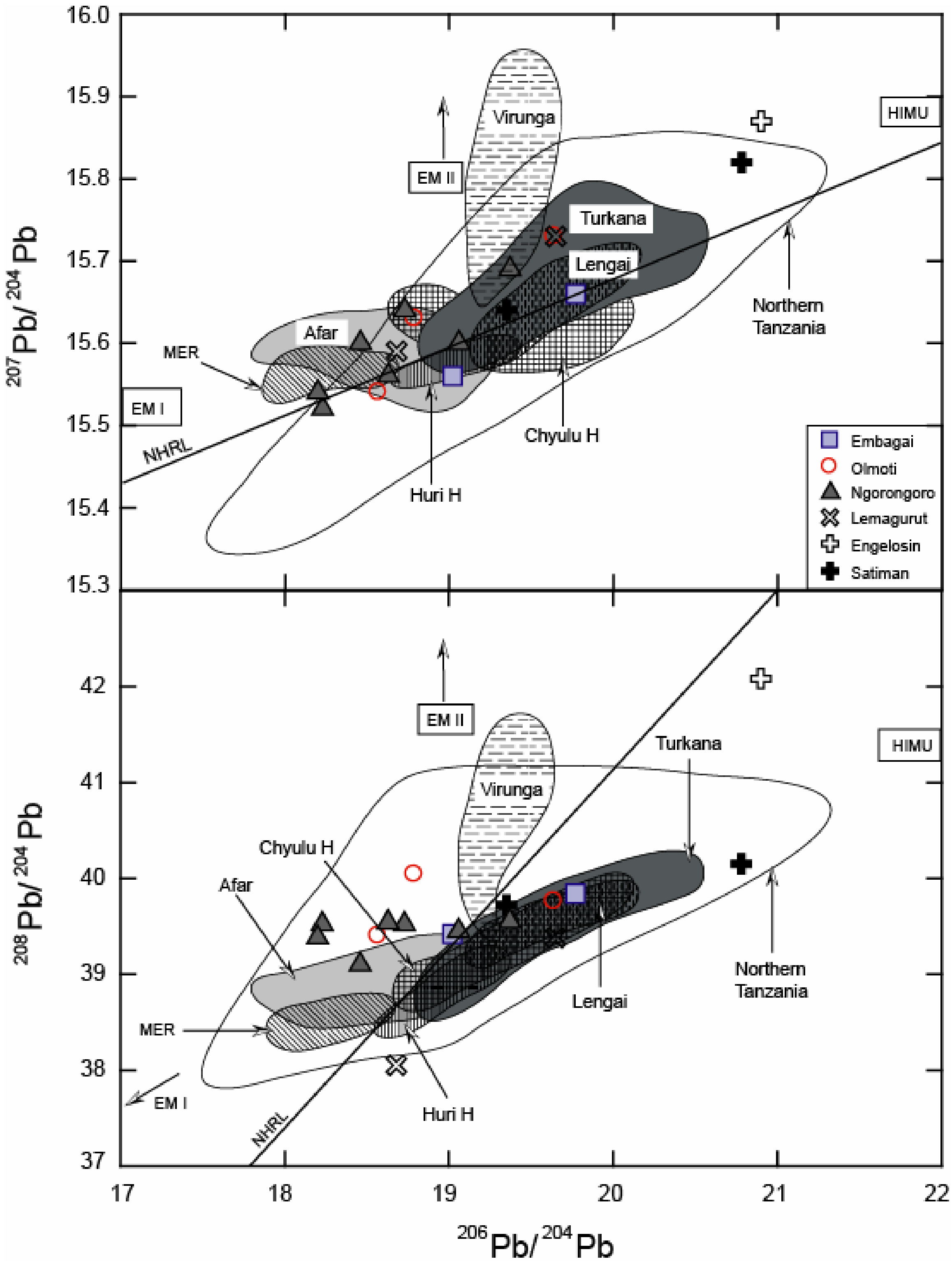

Figure 6.10. Pb-Pb isotope diagram comparing lavas from the NVHC with lavas from the East African Rift System. NHRL, Northern Hemisphere Reference Line (Hart, 1984).

The Pb isotope data from Embagai as well as from the rest of NVHC varies widely: $^{206}Pb/^{204}Pb$ = 18.20 – 20.90, $^{207}Pb/^{204}Pb$ = 15.52 – 15.87 and $^{208}Pb/^{204}Pb$ = 39.10 – 42.08 (Appendix 1), but are within the range of values reported by Paslick *et al*., (1995) for volcanics in northern Tanzania. On their study, evidence from volcanic province of northern Tanzania for enrichment of continental lithosphere by OIB melts, Paslick *et al.*, concluded that the wide range of Pb isotope values reflects a source character and are not a result of crustal contamination. On the $^{207}Pb/^{204}Pb$ - $^{206}Pb/^{204}Pb$ diagram, the NVHC lavas plot slightly above the Northern Hemisphere Reference Line (NHRL) although on the $^{208}Pb/^{204}Pb$ - $^{206}Pb/^{204}Pb$ diagram, they slightly trend above and below this line (Figure 6.10). The radiogenic Pb similar to HIMU and relatively unradiogenic Nd coupled with radiogenic Sr (> 0.704) similar to EM I is a common feature of lavas from the East African Rift (Paslick *et al*. 1995, Kalt *et al*., 1997, Bell and Tilton, 2001, Späth *et al.*, 2001). There is a general agreement that lithospheric mantle is the source for these lavas, e.g. Chyulu Hills located northeast of the NVHC (Späth *et al.*, 2001). On their study on plume-lithosphere interaction and the origin of continental rift-related alkaline volcanism, Späth *et al.* concluded that the Chyulu lavas in southern Kenya were generated by plume-derived metasomatic fluids. Support for their argument came from the presence of metasomatized mantle peridotite xenolith in northern Tanzania and other parts of East Africa (Cohen *et al.*, 1984; Rudnick *et al*., 1993; Lee and Rudnick, 1999, Aulbach *et al.,* in review).

From these geochemical data, it can be concluded that: (1) Embagai and Engelosin lavas shares chemical similarities (e.g. La/Nb, Zr/Nb) with Satiman suggesting that they were all derived by relatively low degree partial melt of parent rock compared to the basaltic lavas in Chapter 3. (2) Fractionation was among processes involved in producing the Embagai lavas. The crystallizing phases are augite, nepheline, apatite, melilite, and andradite (3) All the NVHC lavas experienced variable degrees of crustal contamination. This conclusion is supported by the wide dispersion of Sr and Nd isotope ratios from these rocks as well as lower Ce/Pb ratios than expected from mantle derived melts. Engelosin lavas appear to have experienced the most contamination.

GEOCHRONOLOGY

Embagai

Matrix from three Embagai lavas (EMB3, EMB5 and EMB6) as well as nepheline separated from samples EMB3 and EMB6 were analyzed by $^{40}Ar/^{39}Ar$ laser incremental-heating technique. Analysis of matrix from sample EMB3 gave a plateau age of 1.15 ± 0.02 Ma that is indistinguishable from an isochron age of 1.14 ± 0.04 Ma (obtained from plateau steps). This age is also indistinguishable from an isochron age of 1.16 ± 0.04 Ma (Figure 6.11, Table 3) obtained from all steps. The slightly younger integrated age of 1.09 ± 0.03 Ma could be due to K loss during low temperature alteration of the lava. An MSWD of 1.4 and $^{40}Ar/^{36}Ar$ intercept of 294.1 ± 0.8 similar to atmospheric ratio suggests that this is a good age estimate for sample EMB3.

Table 6.3. $^{40}Ar/^{39}Ar$ ages for Embagai, Engelosin and Olduvai Bed I lava. Bold indicate preferred ages.

Sample Id	Material	Total Fusion Age (Ma)	Plateau Age (Ma)	Isochron Age (Ma)	$^{40}Ar/^{36}Ar$ Intercept	MSWD	%^{39}Ar* on Plateau
EMB3	Matrix	1.09 ± 0.03	1.15 ± 0.02	**1.16 ± 0.04**	294.1 ± 0.8	1.4	89.7
EMB5	Matrix	0.70 ± 0.03		**0.81 ± 0.02**	296.4 ± 1.0	1.3	
EMB6	Nepheline	1.32 ± 0.01		**1.13 ± 0.01**	303.6 ± 1.3	0.92	
EMB6	Matrix	1.12 ± 0.01		**1.06 ± 0.01**	312 ± 2.0	1.5	
ENGB	Matrix	2.96 ± 0.01	2.97 ± 0.01	**2.97 ± 0.02**	300 ± 5.0	1.7	56.4

Irradiation parameter (J) calculated from co-irradiated standard:

Sample #	J-value	Standard used
EMB3 & EMB5	$1.785 \times 10^{-4} \pm 2.1524 \times 10^{-6}$	Alder Creek Sanidine
EMB6	$1.753 \times 10^{-4} \pm 1.6971 \times 10^{-6}$	Alder Creek Sanidine
ENGB	$2.5906 \times 10^{-4} \pm 3.267 \times 10^{-7}$	Fish Canyon Sanidine

Nepheline separate from the same sample yielded an integrated age of 1.18 ± 0.11 Ma which is indistinguishable from the isochron age of the matrix. This age however, is significantly younger than its plateau age of 1.56 ± 0.8 Ma. An isochron from plateau steps gave an age of 1.88 ± 0.08 Ma significant older than the plateau age and is indistinguishable from an isochron of 1.87 ± 0.07 Ma derived from all the steps. Although both isochron ages gave a reasonable MSWD ≤ 1.9, the $^{40}Ar/^{36}Ar$ intercept of ≤ 285 ± 2 from both isochron is lower than that of atmospheric air, probably suggesting that the K-Ar system of the nepheline has been disturbed. Because the integrated, plateau and isochron ages from the nepheline separate are inconsistent from each other, only the matrix age is considered reliable.

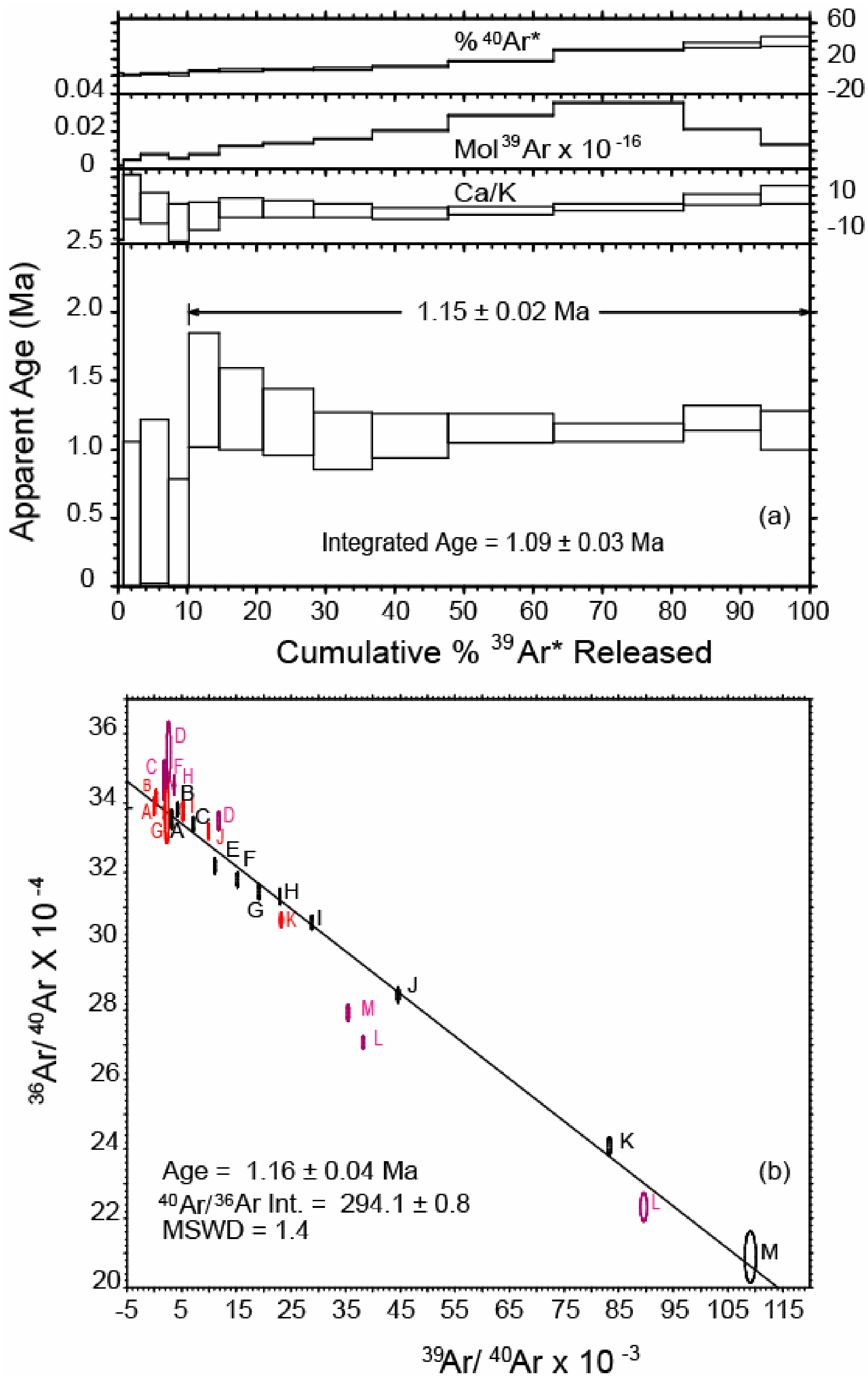

Figure 6.11(a). ^{40}Ar/^{39}Ar incremental-heating spectrum for Embagai sample EMB3. Lower temperature steps yielded relatively younger ages compared to the plateau, a typical sign for low temperature alteration of the sample. Cumulative % ^{39}Ar* on the plateau age is 89.7 Released between ~900ºC - 1200 ºC (b) Inverse isochron for sample EMB3 yielded an age of 1.16 ± 0.04 Ma that is indistinguishable from the plateau age.

Analysis of matrix from sample EMB5 gave an integrated age of 0.70 ± 0.03 Ma that is younger than its isochron age of 0.81 ± 0.02 Ma (Figure 6.12, Table 3). The younger integrated age in this sample is also likely a result of low temperature alteration of the sample. An MSWD of 1.3 and $^{40}Ar/^{36}Ar$ intercept of 296.4 ± 1.0 suggests that the isochron age is a better age estimate for the sample.

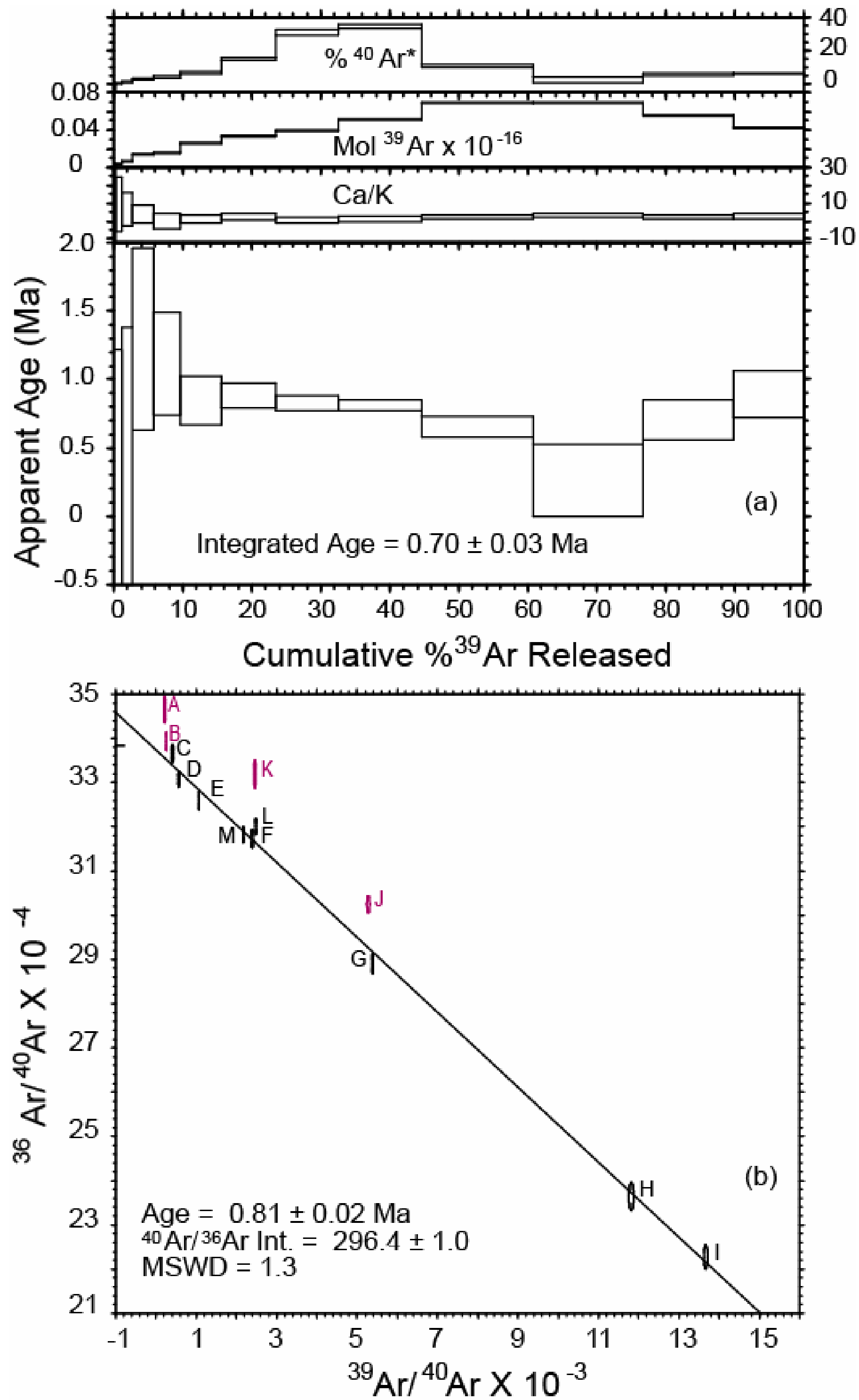

Figure 6.12(a). $^{40}Ar/^{39}Ar$ incremental-heating spectrum for Embagai sample EMB5. The younger integrated age suggests low temperature alteration of the sample. (b) Inverse isochron for sample EMB5.

Analysis of nepheline separate from sample EMB6 gave an integrated age of 1.32 ± 0.01 Ma that is older than its isochron age of 1.13 ± 0.01 Ma. The isochron age gave an MSWD = 0.92 and $^{40}Ar/^{36}Ar = 303.6 \pm 1.3$, indicating that these nepheline grains have excess argon. Analysis of matrix from the same sample gave an integrated age of 1.12 ± 0.01 Ma that is older than its isochron age of 1.06 ± 0.01 Ma, with MSWD = 1.5 and $^{40}Ar/^{36}Ar = 31 \pm 2$.

The age information obtained from analyzing the matrix is consistent with that from the nepheline separate, all indicating that excess argon is a problem in sample EMB6, and that the ages obtained from these analyses are unreliable. However isochron ages from both analyses fall within the range of ages obtained from samples EMB3 and EMB5, suggesting that Embagai volcano was active between 1.16 ± 0.04 Ma and 0.81 ± 0.02 Ma.

The duration for Embagai activity, as suggested by these new dates, is within the range of 1.2 to 0.6 Ma reported by Manega (1993) using a similar method. The K-Ar dates of similar age range (1.2 ± 0.06 Ma to 0.8 ± 0.4 Ma) were reported from basalt collected from top of the Kitete and Engaruka escarpments (Macintyre *et al.*, 1974; Foster *et al.*, 1997). These dates were interpreted to record major faulting episode in the region. Olduvai Bed II – Bed III times recorded major changes in the drainage and sedimentation direction that resulted from such faulting (Hay, 1976). The drainage direction is now from the basement rocks in the west to the fault-bounded Olbalbal Depression in the east compared to the previous east-west direction recorded lower in the Olduvai stratigraphy (Hay, 1976). Embagai eruption therefore started as part of major faulting episode in northern Tanzania. Other volcanoes that were associated with this faulting episode includes Loolmalasin, Buko, Gelai, Kwaraha, and Hanang (Macintyre *et al.*, 1974; Dawson, 1992)

Engelosin

Matrix from one lava, sample ENGB collected from Engelosin cone was dated by the $^{40}Ar/^{39}Ar$ laser incremental-heating technique. The analysis produced a plateau age of 2.97 ± 0.01 Ma (Figure 6.13, Table 6.3) that is analytically indistinguishable from its integrated age of 2.96 ± 0.01 Ma. An isochron derived from all increment-steps gave an age of 2.97 ± 0.02 Ma, with MSWD = 1.7 and $^{40}Ar/^{36}Ar$ intercept similar to that of atmospheric air ratio. The isochron age is indistinguishable from the plateau and integrated age suggesting that this is a good age estimate for Engelosin activity.

The age of 2.97 ± 0.02 Ma is older than a K-Ar date of 2.68 ± 0.07 Ma obtained by dating the same material (Manega, 1993). The cause for the age discrepancy is unclear, and may suggest differential cooling ages on the Engelosin plug or the two ages are dating different parts of the plug. Hay (1976) noted fine- and coarse-grained lava from Engelosin that could be a result of differential cooling or indicating different parts of the plug. Although the Ce/Pb as well as the Sr-Nd-Pb isotope data indicates that Engelosin is highly contaminated by crustal material, the $^{40}Ar/^{39}Ar$ spectra (Figure 6.13) indicate that K-Ar system has not been disturbed.

Manega also reported a K-Ar age of 2.99 ± 0.09 Ma obtained by dating an alkali basalt collected from Natron-Manyara escarpment in the Natron area (sample NATM89-01). Isaac and Curtis (1974) reported a similar the K-Ar age of 3.18 ± 0.08 Ma on biotite extracted from biotite-rich lava collected from Mosonik volcano. These ages are coeval with the new $^{40}Ar/^{39}Ar$ presented here, and suggest that Engelosin is likely part of a larger event, probably linked to the nephelinitic Mosonik volcanism located about 30 km northeast of Engelosin.

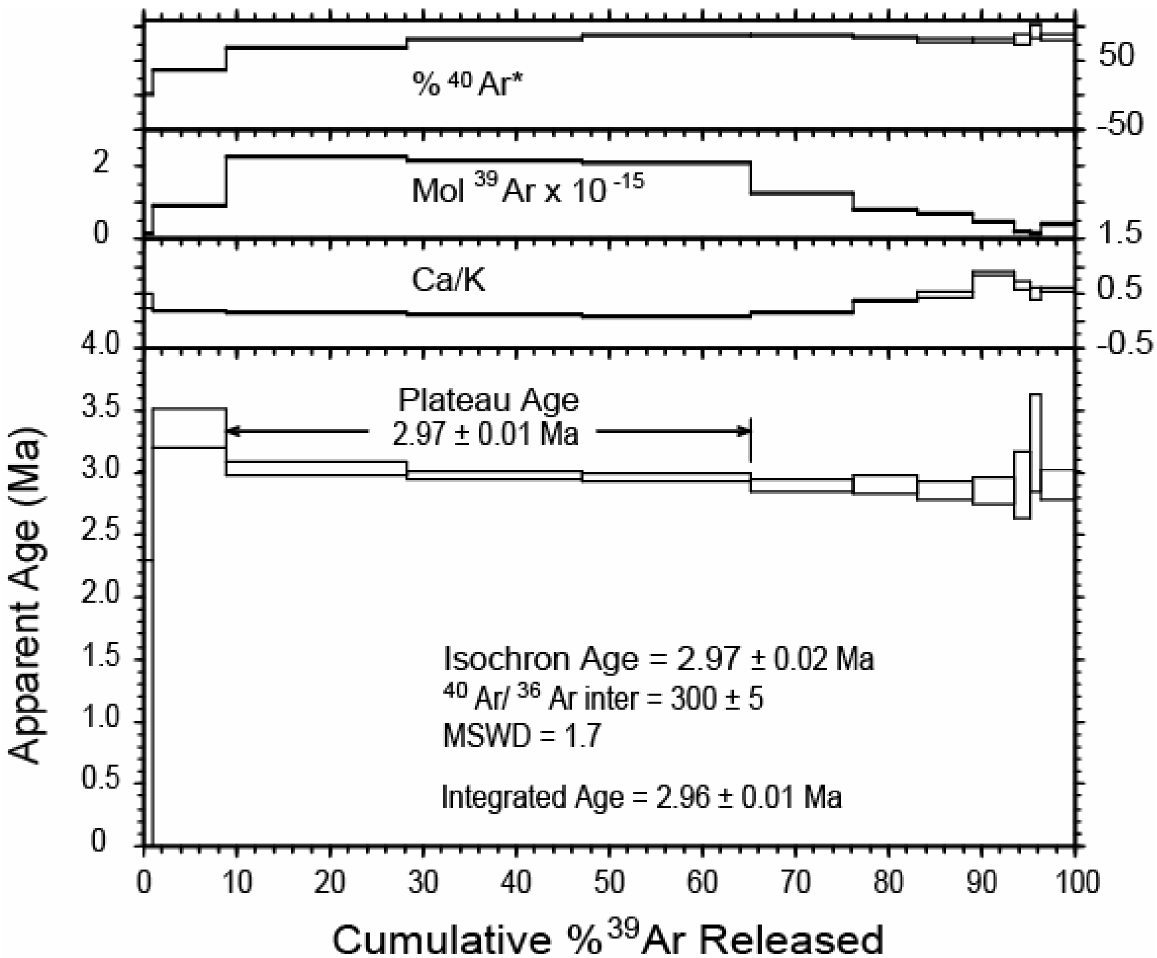

Figure 6.13. $^{40}Ar/^{39}Ar$ incremental-heating spectrum for Engelosin sample ENGB. The plateau, isochron and integrated ages are indistinguishable. Cumulative % $^{39}Ar^*$ on the three-step plateau age is 56.4 obtained at temperatures between ~650ºC - 900 ºC.

CHAPTER 7

NGORONGORO VOLCANIC HIGHLAND COMPLEX OVERVIEW

INTRODUCTION

An overview of basalt chemistry for the East African Rift System (EARS) was recently given by Furman (2007). This review was warranted by the increasing number of publications on the geochemistry and petrology of volcanics along the entire EARS (e.g. Class *et al.*, 1994; Furman, 1995; Rogers *et al.*, 1998; Furman and Graham, 1999; Bell and Tilton, 2001; Macdonald *et al.,* 2001; Le Roex *et al.*, 2001; Späth *et al.*, 2001; Scaillet and Macdonald, 2003; Furman et *al.*, 2004, 2006). However, no comments were made on lavas of the NVHC in northern Tanzania due to the paucity of published research from this part of the rift. Petrological, geochemical and geochronological data presented in the previous chapters (Chapter 3, 4, 5 and 6) together with data from previous studies (Foster *et al.,* 1997; Paslick *et al.*, 1995, 1996; Manega, 1993; Dawson, 1992; Drake and Curtis, 1987; Hay, 1976, 1987; Macintyre *et al.*, 1974; Bagdasaryan *et al.,* 1972; Grommè *et al.,* 1970) permits further insights on the general understanding of the nature and relationship of lava type erupting in the NVHC and provides a geochronological framework. Finally, a model for NVHC volcanism is proposed which constrains both the nature of the source melting at depth and the actual depth of melting.

NVHC lava type variability in time and space

The earliest extension in the EARS is documented in the northeastern Turkana area at ~35 Ma (McDougall and Watkins, 2006). Faulting propagated north and south reaching northern Tanzania at about 1.2 Ma (Foster *et al.*, 1997; Dawson, 1992; Macintyre *et al.*, 1974). Volcanism in northern Tanzania appears to have started much later than in the north (Kenya and Ethiopia) with the eruption of phonolitic Essimingor at about 8.1 ± 1 Ma (Bagdasaryan *et al*., 1972). Published data (Manega, 1993; Drake and Curtis, 1987; Hay, 1976) and that from previous chapters (Chapter 3, 4, 5 and 6) shows that the main phase of volcanism at the NVHC occurred from 4.63 ± 0.05 Ma to present. The age of 8.1 ± 1 Ma may be inaccurate (too old) due to excess argon (see Mollel *et al.*, in press; Curtis and Hay, 1972). Overall, volcanism appears to have been continuous with activities overlapping between volcanic centers: Satiman 4.63 to 2.5 Ma, Engelosin ~2.97 Ma, Lemagurut 2.4 to 2.22 Ma, Ngorongoro 2.29 to 2.02 Ma, Olmoti 2.01 to 1.1 Ma, Oldeani 1.61 to 1.52 Ma; Embagai 1.20 to 0.60, Kerimasi 0.50 to 0.22 Ma and Oldoinyo Lengai 0.1 Ma to present (Mollel *et al.*, in press; Manega, 1993; Drake and Curtis, 1987; Hay, 1976). These eruptions also overlap in age with volcanic activity in Meru 2.1 to 0.06 Ma, and Kilimanjaro ~0.22 Ma to the east (Wilkinson *et al.*, 1986).

Lava types appear to be mostly silica poor (Figure 7.1) for most part of the 4.65 Ma to Present NVHC history. Basaltic to silicic lavas appear restricted to an interval between about 2.40 ± 0.01 Ma and 1.52 ± 0.02 Ma. For the most part, age data are in agreement with a northward younging direction (Manega, 1993) from Satiman in the south to Oldoinyo Lengai in the north. An exception is the 1.61 Ma Oldeani eruption interpreted as a satellite vent following the collapse of the Ngorongoro Caldera. Low LILE ratios (e.g., La/Nb in the silica poor lavas), supports formation by small-degree partial melts of parent rock relative to the silica-saturated counterparts. This is consistent with results from experimental melting studies which illustrate that silica poor lavas such as nephelinites, melanephelinites, and basanites can be generated by: (1) high-pressure, low-degree partial melting of fertile peridotite (Takahashi and Kushiro,1983; Zhang and Herzberg, 1994), (2) melting of peridotite in the presence of CO_2 or H_2O (Hirose, 1997;

Kawamoto and Holloway, (1997), (3) melting of an amphibole- or phlogopite-bearing peridotite (Mengel and Green, 1989; Thibault et al. 1992).

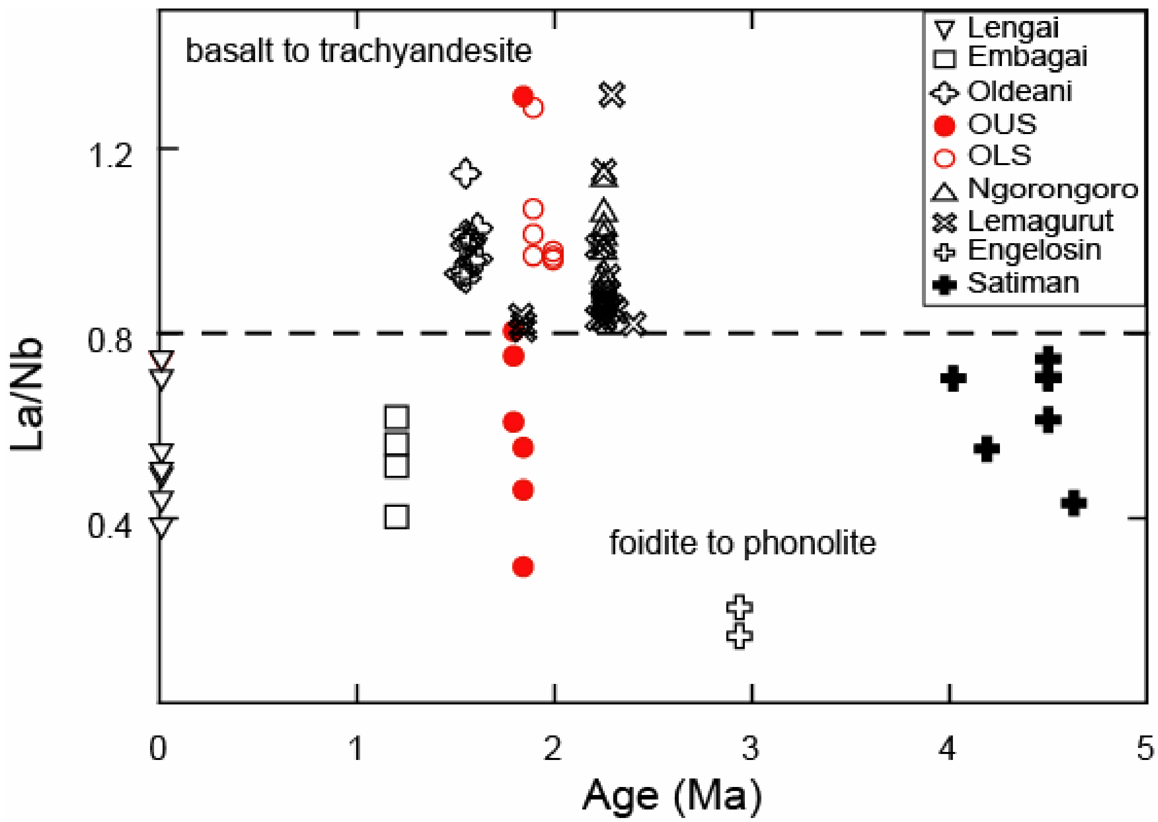

Figure 7.1: La/Nb versus age for lavas from the Ngorongoro Volcanic Highland Complex (NVHC) indicate that over time, the NVHC is dominated by silica-undersaturated lavas, derived from lower degree partial melting of the source relative to the silica-saturated. The eruption of silica-saturated lavas between 2.4 and 1.6 Ma may reflect perturbed mantle potential temperatures due to plume activity. Data source: Oldoinyo Lengai from Klaudius and Keller (2006). OLS, Olmoti Lower Section; OUS, Olmoti Upper Section.

Source rock lithology and depth of melting

Results of lithological source analysis for many Large Igneous Provinces (LIP) shows that peridotite is the dominant source for magmatism at the Azores, Cape Verda, Cook-Austral, Ascension, St. Helene and Tristan da Cunha (Herzberg, 2006a). In a study on the petrology and thermal structure of the Hawaiian plume, Herzberg (2006b) used a CaO wt% versus MgO wt% plot to discriminate a garnet peridotite source from a pyroxenite source. Employing this plot for the NVHC lavas (Figure 7.2), suggests a peridotite lithology, similar to lavas from Turkana lavas, Furman *et al.,* 2006.

The presence of garnet or a K-rich phase in the source rock is commonly used to constrain the depth at which mantle melting occurs. Amphibole has been documented to be stable at pressures ~25 Kbars (~90 km) under water-saturated conditions (Foley, 1991; Mengel and Green, 1986). Chondritic-normalized spider diagrams presented in the previous chapters indicate that all lavas from the NVHC were derived from an enriched source. Because of the higher compatibility of Yb relative to Tb, high Tb/Yb ratios are expected during melting of a garnet bearing source (Kelemen *et al.*, in review; van Westrenen *et al.*, 2001; Yogodzinski *et al.*, 1995). Moderate to low chondritic normalized $(Tb/Yb)_n$ ~2.7-1.0 [normalizing value of Sun and McDonough, 1989] from the NVHC lavas are within the range of values measured in Tertiary Turkana basalt that are thought to indicate melting at or above the garnet-spinel transition (~80 km depth; Furman *et al.*, 2006).

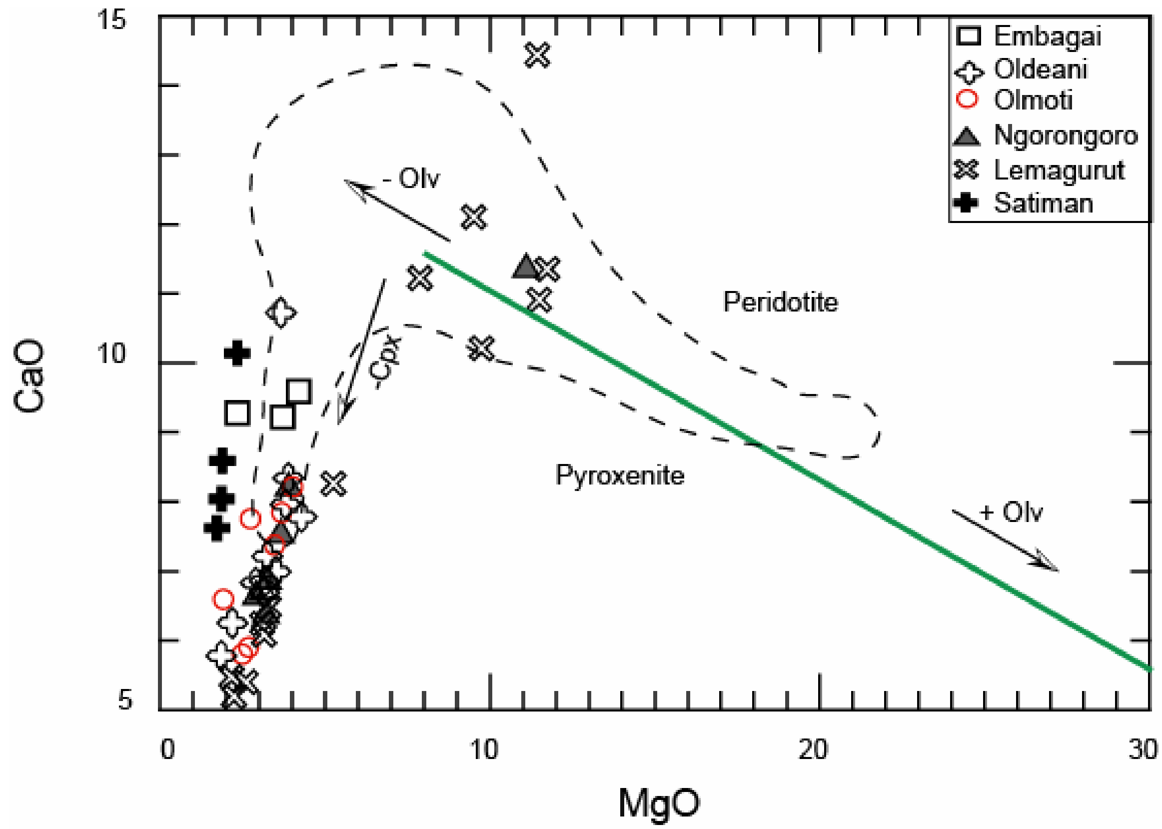

Figure 7.2: Variation of CaO versus MgO for NVHC (lava with CaO > 5 wt %) indicating a peridotite source rock for the less contaminated and Mg-rich lava, similar to Turkana lavas [dashed field], (Furman et *al.*, 2006). Arrows point to olivine addition (right hand) and subtraction (left). Decreasing CaO and MgO indicates pyroxene fractionation (Modified from Herzberg, 2006).

Another common criterion used to determine depth of mantle melting is to compare major oxides content of individual primitive lavas (back corrected to olivine fractionation (Mg# = 72)), to liquid compositions determined experimentally on peridotite melts at various pressures. PRIMELT1 software has recently been developed by Herzberg *et al.* (2007) [following procedures outlined in Herzberg and O'Hara (2002) and Herzberg (2004)] and allows one to calculate primary magma composition at any given primitive lava composition. One setback for the comparison method however is that, existing melting experiments (e.g., Walter, 1998; Kushiro, 1996; Baker and Stolper, 1994; Hirose and Kushiro, 1993; Takahashi, 1986), do not take into account the effect of CO_2 and H_2O. It is well known that the presence of CO_2 during mantle melting results in a significant lowering of the solidus (Dasgupta *et al.*, in review; Dasgupta and Hirschmann, 2006; Falloon and Green, 1989). The Sr-Nd-Pb isotope data presented in previous chapters indicate that the NVHC closely follows the field defined by the East African Carbonatite Line of Bell and Tilton, (2001). Although in trace abundances, minerals such melilite and sodalite found in the NVHC lavas suggests a carbonatitic affinitity of these rocks. The fact that the carbonatitic volcano (Oldoinyo Lengai) occurs in the same volcanic complex may also support the carbonatitic affinities of these NVHC lavas. More evidence comes from CO_2-metasomatized lithosphere as documented in mantle xenoliths from northern Tanzania (Dawson, 2002, Rudnick *et al.*, 1993; Dawson and Smith, 1988; Jones *et al.*, 1983). NVHC lavas are also characterized by low MgO (mostly < 4.5 wt %), and the phenocryst assemblage includes feldspar and augite, indicating that these lavas experienced more than simply olivine fractionation.

A lithospheric mantle source for the NVHC lavas is in agreement with the work of Paslick *et al.* (1995), who suggested a lithospheric mantle source for volcanics in northern Tanzania. Moreover, mantle xenoliths from the Lashaine volcano, Olmani cone, and Pello Hill (Dawson, 2002, Rudnick *et al.*, 1993; Dawson and Smith, 1988; Jones *et al.*, 1983) indicate that the lithosphere beneath northern Tanzania has been metasomatized. A lithospheric mantle source is not localized in the NVHC only; it is in agreement with the nearby Chyulu Hills (Späth *et al.*, 2001) located some 250 km northeast of the NVHC as well as other volcanic centers in the region (e.g. Virunga province, Rogers *et al.,* 1998; Kivu, Lloyd *et al.,* 1991; Rungwe, Furman, 1995; Turkana, Furman *et al.*, 2004, 2006).

Spider diagrams for all of the NVHC lavas indicate a negative K-anomaly. This may be the result of fractionating a K-bearing mineral phase, partial melting or residual minerals in the source rock (Späth *et al.*, 1996; 2001; Class and Goldstein, 1997; le Roex *et al*., 2001). If the reason for the anomaly is due to the fractionation of K-bearing minerals, the depletion should be more pronounced in the more evolved lavas, e.g., in the Olmoti trachytes where there is a higher modal abundance of amphibole and biotite. A spider diagram of the most basaltic lava (00-NG8 with MgO ~11 wt %), a trachyte from Olmoti (03-OLT3, MgO = 0.54 wt %) with ~1 % amphibole and biotite, and Satiman foidite (01-SM5, MgO = 1.81 wt %) that is abundant in nepheline (Figure 7.3), all show similar K-depletion levels, perhaps indicating that K-depletion is not controlled by the degree of fractionation or of partial melting. Moreover, Späth *et al.* (2001, 1996) have shown that for considerable K depletion, high K-phase fractionation is required (> 10%). Such high K-phase fractionations are inconsistent with basaltic lava 00-NG8 whose phenocrysts consist predominantly of olivine and augite. In their study on the lithospheric thickness beneath the southern Kenya Rift, le Roex *et al*. (2001) have shown that during melting of an amphibole bearing source, K will be retained in the source relative to Nb and Th. The net effect is to lower the K/Nb and K/Th ratios in the derivative melt and that the level of fractionation of these ratios will be inversely proportional to the degree of melting.

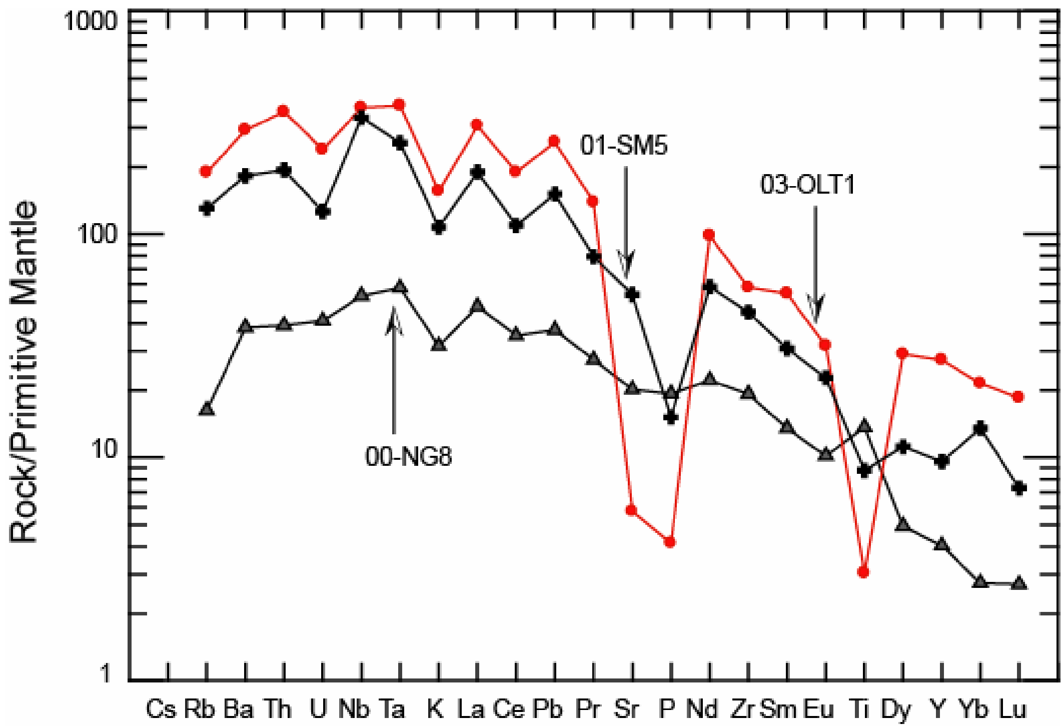

Figure 7.3: Spider diagram showing variation of incompatible trace elements for NVHC lavas: Ngorongoro basalt, 00-NG8, MgO~11 wt%; Satiman phonolite, 01-SM5, MgO~1.81 wt% and Olmoti trachyte, 03-OLT1, MgO~0.54 wt% (normalized to primitive mantle values, Sun and McDonough, 1989). All lavas show similar negative K-anomaly suggesting that the depletion is not related to the degree of fractionation of partial melting.

Indeed, a plot of K/Nb versus Nb (Figure 7.4) indicates that with the exception of two outliers from Satiman, K/Nb ratios are higher for the basalt, that were derived by relatively higher degree partial melts (shown in previous chapters) compared to the phonolites (e.g. from Satiman) and the trachytes (e.g. from Olmoti). This conclusion is in agreement with that of Furman (2007) which demonstrates that amphibole or phlogopite is present in most of the East African Rift source rocks and that its abundance is relatively smaller in the Main Ethiopia Rift (MER) compared to Kenya and Tanzania (Figure 7.5).

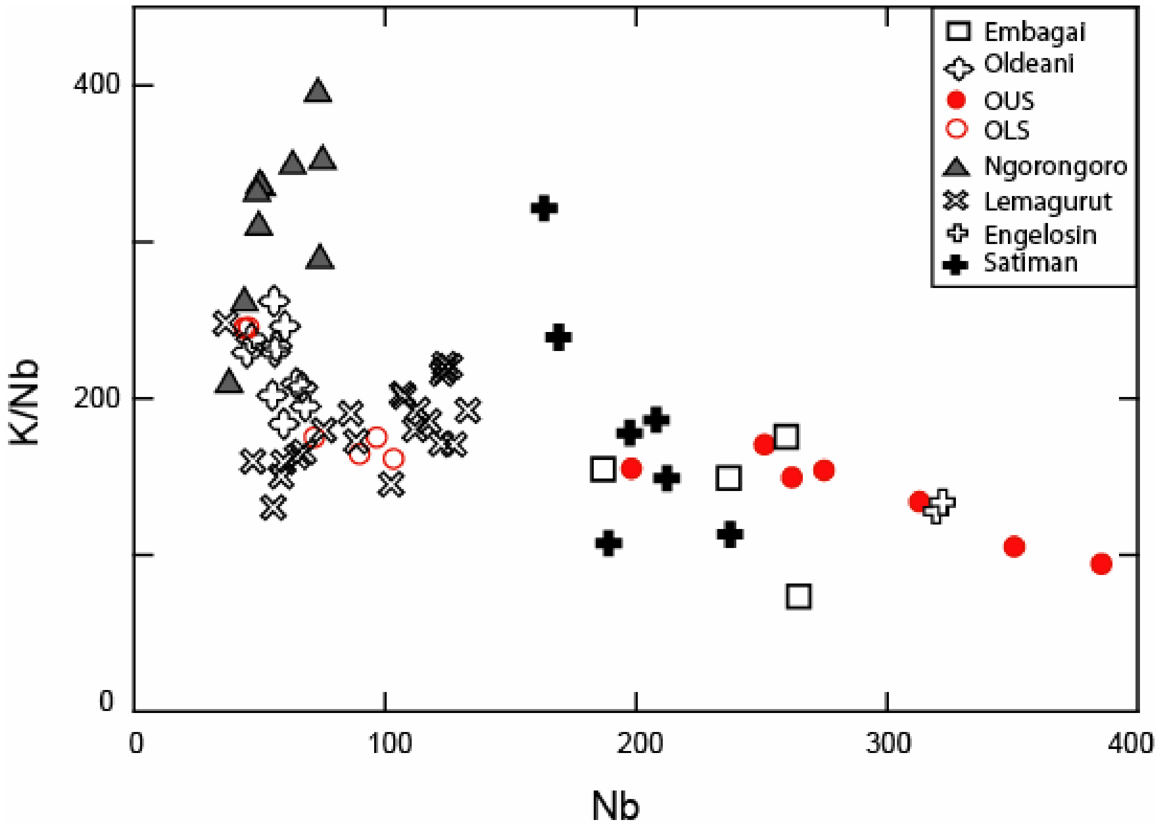

Figure 7.4: Variation of K/Nb versus Nb (ppm) for NVHC lavas indicating relatively higher K/Nb ratios for basalt (e.g. Ngorongoro and Oldeani) derived by higher degree partial melt compared to the silica poor (Satiman and Embagai). OLS, Olmoti Lower Section; OUS, Olmoti Upper Section.

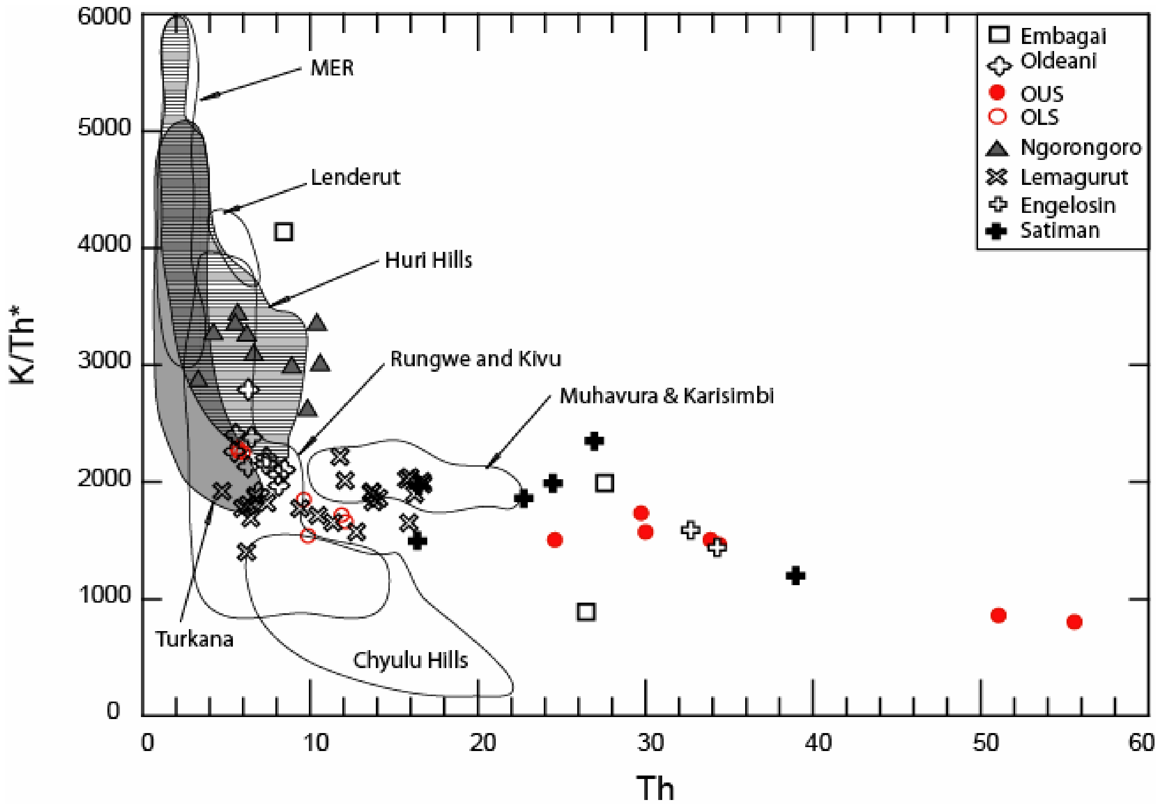

Figure 7.5: Variation of K/Th* (K_2O* 1000/Th) against Th (ppm) for the East Africa Rift lavas showing the effect of progressive melting of an amphibole- or phlogopite bearing source (Modified from Furman, 2007). Because K is an essential part of these phases, it will be retained in the source region until they are consumed through progressive melting (Späth *et al*. 2001). Within each suite, samples with highest Th and lowest K/Th* record the lowest degree of melting. Overall NVHC lavas appear to have resulted from a relatively higher degree partial melt compared to those from the Chyulu Hills in south Kenya (le Roex *et al*. 2001). OLS, Olmoti Lower Section; OUS, Olmoti Upper Section.

Overall, this indicates that an amphibole or phlogopite bearing fertile peridotite is the source rock for the NVHC lavas. Moreover, Figure 7.5 indicates that NVHC lavas were generated by relatively higher degrees of partial melting compared to those of Chyulu Hill (≤ 3%; le Roex *et al.*, 2001; Späth *et al*. 2001).

Model for NVHC volcanism

There is a general consensus from geophysical and geochemical data that the voluminous outpouring of lavas associated with the East African rift is plume(s) related. Evidence for the presence of a partially molten, low-velocity zone (LVZ) beneath northern Tanzania has been documented by many researchers (e.g., Julià *et al.*, 2005; Weeraratne *et al*. 2003; Owens *et al*. 2000; Nyblade *et al*. 2000). Weeraratne *et al*. (2003) and Nyblade *et al*. (2000) argued that the LVZ resulted from an upper mantle thermal anomaly originating from an ascending mantle plume. S-wave tomography also shows a thermal anomaly that reaches a depth of ~500 km beneath Afar (Benoit et al. 2003). These two plumes are considered part of the South African Superplume originating at the core-mantle boundary (Grand *et al.* 1997; Ritsema *et al.* 1999; Ni *et al.* 2003).

Beneath the EAR, the LVZ has been constrained to a depth of ~100 – 200 km (Julià *et al.*, 2005; Weeraratne *et al*. 2003). The minimum depth provides further support for a lithospheric source (for the NVHC lavas). A model for the NVHC volcanism therefore follows that of Späth *et al*. (2001) for the Chyulu Hills, whereby fluids/melts originating from the plume metasomatize the lithospheric mantle beneath the NVHC. Such metasomatic events cause modal infiltration of volatiles and other trace elements leading to precipitation of metasomatic minerals [e.g., amphibole] (Dawson, 2002, Rudnick *et al.*, 1993; Dawson and Smith, 1988; Jones *et al.*, 1983). Continuous conductive heating from the plume causes partial melting of the metasomatized lithosphere within the lithospheric mantle (see Fig. 13; Späth *et al*. 2001). Early low-degree partial melts reflect the geochemistry of the plume itself, while later higher-degree partial melts are mixtures of the metasomatic component (plume) and the lithospheric wall-rock. The NVHC geochemistry therefore reflects a binary mixture of these two components. It is however, clear from previous chapters, that the NVHC lavas have undergone variable degrees of crustal contamination. A third component for the NVHC chemistry therefore comes from the crust. This last component most certainly accounts for the wider variability in the isotope geochemistry displayed by these lavas.

Appendix 1: Pb isotope data for Ngorongoro Volcanic Highland Complex (NVHC)

Sample #	$^{206}Pb/^{204}Pb$	$^{207}Pb/^{204}Pb$	$^{208}Pb/^{204}Pb$
NG-01	18.23	15.52	39.52
NG-02	18.73	15.64	39.52
NG-04	18.20	15.54	39.38
NG-07	18.46	15.60	39.10
NG-08	19.37	15.69	39.55
NG-09	19.06	15.60	39.45
NG-10	18.63	15.56	39.54
OLT-2	18.79	15.63	40.04
OLT-7	18.57	15.54	39.40
04-OLT-4	19.64	15.73	39.76
01-SM-3	20.78	15.82	40.15
00-SM-5	19.35	15.64	39.72
00-LM-6	19.65	15.73	39.38
02-LM-2	18.68	15.59	38.05
EMB-3	19.77	15.66	39.84
EMB-6	19.02	15.56	39.42
ENG-B	20.90	15.87	42.08

Appendix 2: $^{40}Ar/^{39}Ar$ age data for the Ngorongoro Volcanic Highland Complex (NVH)

Lab-Id	Sample Id	$^{36}Ar/^{39}Ar$	$^{37}Ar/^{39}Ar$	$^{38}Ar/^{39}Ar$	$^{40}Ar/^{39}Ar$	$^{40}Ar^*/^{39}Ar$	$\%^{40}Ar^*$	Age (Ma)	Age Error	^{39}Ar Moles E-16	JE-5	Material	Locality	Power (W)
30138-1A	EMB-03	1.0346	13.6031	0.2150	307.67	3.056	0.984	0.98	0.90	0.1500	17.85	matrix	Embagai	2
30138-1B	EMB-03	0.7858	4.3036	0.1815	232.07	0.222	0.095	0.07	0.49	0.4715	17.85	matrix	Embagai	4
30138-1C	EMB-03	0.4623	1.0855	0.1321	138.43	1.905	1.375	0.61	0.30	0.7463	17.85	matrix	Embagai	6
30138-1D	EMB-03	0.2822	-3.0810	0.1006	84.58	0.943	1.117	0.30	0.24	0.5598	17.85	matrix	Embagai	7
30138-1E	EMB-03	0.2893	-1.2115	0.1100	90.03	4.447	4.944	1.43	0.21	0.8120	17.85	matrix	Embagai	8
30138-1F	EMB-03	0.2093	1.1702	0.0911	65.76	4.014	6.099	1.29	0.15	1.2107	17.85	matrix	Embagai	10
30138-1G	EMB-03	0.1640	0.6371	0.0790	52.12	3.721	7.137	1.20	0.12	1.3360	17.85	matrix	Embagai	12
30138-1H	EMB-03	0.1359	0.5235	0.0701	43.39	3.288	7.576	1.06	0.10	1.5837	17.85	matrix	Embagai	14
30138-1I	EMB-03	0.1057	-0.2788	0.0614	34.65	3.392	9.793	1.09	0.08	2.0511	17.85	matrix	Embagai	17
30138-1J	EMB-03	0.0638	0.4420	0.0510	22.38	3.573	15.958	1.15	0.05	2.8284	17.85	matrix	Embagai	21
30138-1K	EMB-03	0.0292	1.2977	0.0354	11.98	3.460	28.848	1.11	0.03	3.5423	17.85	matrix	Embagai	26
30138-1L	EMB-03	0.0258	3.6890	0.0222	11.12	3.798	34.056	1.22	0.05	2.0835	17.85	matrix	Embagai	32
30138-1M	EMB-03	0.0204	5.0467	0.0160	9.13	3.513	38.332	1.13	0.08	1.3060	17.85	matrix	Embagai	40
30140-1A	EMB-05	1.4832	11.0198	0.2988	427.27	-10.216	-2.372	-3.29	1.26	0.1081	17.85	matrix	Embagai	2
30140-1B	EMB-05	1.2898	4.6302	0.2558	379.78	-0.993	-0.260	-0.32	0.77	0.3949	17.85	matrix	Embagai	4
30140-1C	EMB-05	0.7877	3.2468	0.1592	233.85	1.352	0.577	0.44	0.47	0.6538	17.85	matrix	Embagai	6
30140-1D	EMB-05	0.5735	1.7177	0.1229	173.34	4.001	2.305	1.29	0.33	1.3551	17.85	matrix	Embagai	7
30140-1E	EMB-05	0.3044	-0.1347	0.0716	93.40	3.455	3.700	1.11	0.19	1.6181	17.85	matrix	Embagai	8
30140-1F	EMB-05	0.1317	0.4432	0.0373	41.48	2.607	6.283	0.84	0.09	2.5539	17.85	matrix	Embagai	10
30140-1G	EMB-05	0.0539	1.1500	0.0220	18.54	2.714	14.624	0.87	0.05	3.3288	17.85	matrix	Embagai	12
30140-1H	EMB-05	0.0199	-0.0823	0.0160	8.45	2.550	30.176	0.82	0.03	3.9018	17.85	matrix	Embagai	14
30140-1I	EMB-05	0.0164	0.4060	0.0156	7.32	2.503	34.203	0.81	0.02	5.1335	17.85	matrix	Embagai	17
30140-1J	EMB-05	0.0574	1.0376	0.0231	18.89	2.013	10.646	0.65	0.04	6.9070	17.85	matrix	Embagai	21
30140-1K	EMB-05	0.1348	1.4346	0.0376	40.52	0.804	1.981	0.26	0.13	6.8226	17.85	matrix	Embagai	26
30140-1L	EMB-05	0.1283	1.0525	0.0360	40.02	2.176	5.435	0.70	0.08	5.5490	17.85	matrix	Embagai	32
30140-1M	EMB-05	0.1465	1.1209	0.0400	45.94	2.746	5.973	0.88	0.09	4.2890	17.85	matrix	Embagai	40
30112-1A	EMB-6	0.9069	14.8939	0.1789	276.52	9.814	3.511	3.10	0.54	0.1261	17.53	nepheline	Embagai	2
30112-1B	EMB-6	0.1191	0.4830	0.0337	39.36	4.212	10.697	1.33	0.11	0.5170	17.53	nepheline	Embagai	4

Appendix 2: continued

Lab-Id	Sample Id	$^{36}Ar/^{39}Ar$	$^{37}Ar/^{39}Ar$	$^{38}Ar/^{39}Ar$	$^{40}Ar/^{39}Ar$	$^{40}Ar^{*}/^{39}Ar$	$\%^{40}Ar^{*}$	Age (Ma)	Age Error	^{39}Ar Moles E-16	JE-5	Material	Locality	Power (W)
30112-1C	EMB-6	0.0743	1.2008	0.0288	26.27	4.427	16.838	1.40	0.07	0.7012	17.53	nepheline	Embagai	6
30112-1D	EMB-6	0.0513	2.3597	0.0235	18.93	3.952	20.843	1.25	0.06	0.8625	17.53	nepheline	Embagai	8
30112-1E	EMB-6	0.0469	3.6024	0.0221	17.74	4.169	23.445	1.32	0.06	1.0588	17.53	nepheline	Embagai	10
30112-1F	EMB-6	0.0389	-0.0234	0.0202	16.11	4.622	28.697	1.46	0.05	1.1318	17.53	nepheline	Embagai	12
30112-1G	EMB-6	0.0244	0.0434	0.0175	11.88	4.674	39.358	1.48	0.03	1.6718	17.53	nepheline	Embagai	14
30112-1H	EMB-6	0.0118	0.3186	0.0153	9.34	5.892	63.071	1.86	0.02	3.2214	17.53	nepheline	Embagai	17
30112-1I	EMB-6	0.0086	0.1712	0.0141	6.58	4.062	61.702	1.28	0.01	4.5390	17.53	nepheline	Embagai	21
30112-1J	EMB-6	0.0063	0.4581	0.0133	5.68	3.855	67.834	1.22	0.01	5.8889	17.53	nepheline	Embagai	26
30112-1K	EMB-6	0.0070	0.1867	0.0134	5.66	3.607	63.708	1.14	0.01	3.4459	17.53	nepheline	Embagai	32
30112-1L	EMB-6	0.0051	-0.0652	0.0133	5.13	3.600	70.219	1.14	0.01	5.5358	17.53	nepheline	Embagai	40
30114-2A	EMB-6	0.1601	2.2085	0.0481	51.59	4.478	8.666	1.42	0.16	0.3461	17.53	matrix	Embagai	2
30114-2B	EMB-6	0.0360	0.3925	0.0249	14.57	3.954	27.138	1.25	0.03	2.5772	17.53	matrix	Embagai	4
30114-2C	EMB-6	0.0171	0.4455	0.0213	8.60	3.593	41.767	1.14	0.01	5.5287	17.53	matrix	Embagai	6
30114-2D	EMB-6	0.0087	-0.1034	0.0208	6.14	3.578	58.244	1.13	0.01	6.6904	17.53	matrix	Embagai	8
30114-2E	EMB-6	0.0063	0.0131	0.0212	5.34	3.479	65.158	1.10	0.01	9.9577	17.53	matrix	Embagai	10
30114-2F	EMB-6	0.0042	0.0344	0.0216	4.69	3.442	73.477	1.09	0.01	9.9581	17.53	matrix	Embagai	12
30114-2G	EMB-6	0.0037	0.3743	0.0227	4.49	3.437	76.599	1.09	0.01	8.3877	17.53	matrix	Embagai	14
30114-2H	EMB-6	0.0044	0.2783	0.0221	4.65	3.376	72.565	1.07	0.01	8.1503	17.53	matrix	Embagai	17
30114-2I	EMB-6	0.0065	0.4236	0.0217	5.37	3.500	65.146	1.11	0.01	9.1242	17.53	matrix	Embagai	21
30114-2J	EMB-6	0.0081	0.6747	0.0206	6.00	3.665	61.072	1.16	0.01	9.1129	17.53	matrix	Embagai	26
30114-2K	EMB-6	0.0098	0.6287	0.0191	6.45	3.607	55.891	1.14	0.01	5.3571	17.53	matrix	Embagai	32
30114-2L	EMB-6	0.0087	1.1479	0.0181	6.08	3.605	59.262	1.14	0.01	3.7514	17.53	matrix	Embagai	40
30115-2A	OLD-1	1.4345	-1.0894	0.2879	436.98	12.997	2.977	4.11	0.69	0.1478	17.53	matrix	Olduvai	2
30115-2B	OLD-1	0.2773	2.2470	0.0662	87.74	5.990	6.816	1.89	0.13	0.8610	17.53	matrix	Olduvai	4
30115-2C	OLD-1	0.0873	2.6397	0.0291	31.02	5.436	17.492	1.72	0.05	1.6731	17.53	matrix	Olduvai	6
30115-2D	OLD-1	0.0436	1.4054	0.0205	18.60	5.837	31.356	1.84	0.03	2.0518	17.53	matrix	Olduvai	8
30115-2E	OLD-1	0.0284	1.1425	0.0173	14.10	5.797	41.079	1.83	0.02	3.1536	17.53	matrix	Olduvai	10
30115-2F	OLD-1	0.0190	0.6457	0.0156	11.39	5.836	51.217	1.84	0.02	3.3890	17.53	matrix	Olduvai	12

Appendix 2: continued

Lab-Id	Sample Id	$^{36}Ar/^{39}Ar$	$^{37}Ar/^{39}Ar$	$^{38}Ar/^{39}Ar$	$^{40}Ar/^{39}Ar$	$^{40}Ar^{*}/^{39}Ar$	$\%^{40}Ar^{*}$	Age (Ma)	Age Error	^{39}Ar Moles E-16	JE-5	Material	Locality	Power (W)
30288-1K	ENGB	0.0022	0.2442	0.0217	7.53	6.900	91.665	3.22	0.20	13.3873	25.91	matrix	Engelosin	32
30288-1L	ENGB	0.0044	0.2914	0.0213	7.46	6.195	82.986	2.89	0.06	41.5989	25.91	matrix	Engelosin	40
30029-1A	00-OLT2	1.1711	3.1133	0.2173	359.06	13.286	3.692	1.71	0.46	0.8840	7.12	matrix	Olmoti	2.5
30029-1B	00-OLT2	0.1432	1.8913	0.0382	60.96	18.830	30.847	2.42	0.07	2.6970	7.12	matrix	Olmoti	3.6
30029-1C	00-OLT2	0.0574	1.3716	0.0211	32.76	15.923	48.559	2.04	0.06	4.1899	7.12	matrix	Olmoti	4.8
30029-1D	00-OLT2	0.0386	0.9806	0.0184	27.13	15.817	58.254	2.03	0.06	3.0484	7.12	matrix	Olmoti	5.5
30029-1E	00-OLT2	0.0609	0.7973	0.0229	31.98	14.058	43.936	1.80	0.17	2.1041	7.12	matrix	Olmoti	7.5
30029-1F	00-OLT2	0.0691	1.0353	0.0238	35.69	15.356	42.996	1.97	0.08	2.5790	7.12	matrix	Olmoti	9.5
30029-1G	00-OLT2	0.1263	3.9044	0.0338	50.87	13.892	27.232	1.78	0.10	1.3722	7.12	matrix	Olmoti	13
30029-1H	00-OLT2	0.1798	4.8895	0.0429	63.11	10.414	16.445	1.34	0.68	0.2549	7.12	matrix	Olmoti	16
30029-1I	00-OLT2	0.2010	4.7099	0.0458	68.07	9.084	13.301	1.17	1.11	0.1127	7.12	matrix	Olmoti	22
30303-1A	00-OLT5	0.4711	1.1352	0.1017	140.59	1.480	1.052	0.69	0.74	5.5939	25.82	matrix	Olmoti	2
30303-1B	00-OLT5	0.0283	0.9820	0.0170	12.85	4.580	35.611	2.13	0.07	41.2391	25.82	matrix	Olmoti	4
30303-1C	00-OLT5	0.0070	0.6814	0.0136	6.14	4.128	67.228	1.92	0.03	82.4694	25.82	matrix	Olmoti	6
30303-1D	00-OLT5	0.0040	0.6472	0.0128	5.14	4.005	77.925	1.86	0.07	63.8974	25.82	matrix	Olmoti	8
30303-1E	00-OLT5	0.0038	0.4115	0.0131	5.14	4.061	79.037	1.89	0.04	71.5117	25.82	matrix	Olmoti	10
30303-1F	00-OLT5	0.0040	0.5522	0.0137	5.33	4.206	78.824	1.96	0.06	42.3952	25.82	matrix	Olmoti	12
30303-1G	00-OLT5	0.0068	0.5990	0.0139	5.83	3.876	66.471	1.80	0.06	25.7795	25.82	matrix	Olmoti	14
30303-1H	00-OLT5	0.0086	1.6796	0.0147	6.60	4.186	63.336	1.95	0.07	18.9346	25.82	matrix	Olmoti	17
30303-1I	00-OLT5	0.0126	1.2061	0.0158	7.12	3.509	49.224	1.63	0.10	14.0207	25.82	matrix	Olmoti	21
30303-1J	00-OLT5	0.0031	2.9406	0.0147	7.79	7.133	91.331	3.32	0.20	6.7482	25.82	matrix	Olmoti	26
30303-1K	00-OLT5	0.0159	1.6903	0.0180	7.40	2.830	38.212	1.32	0.40	3.1507	25.82	matrix	Olmoti	32
30303-1L	00-OLT5	0.0251	2.4989	0.0100	7.82	0.592	7.554	0.28	0.63	2.1378	25.82	matrix	Olmoti	40
30127-1A	03-OLT3	0.6415	1.5604	0.1421	212.59	23.189	10.896	7.48	0.86	0.1296	17.91	matrix	Olmoti	2
30127-1B	03-OLT3	0.1858	-5.7047	0.0496	60.83	5.446	8.989	1.76	0.20	0.6320	17.91	matrix	Olmoti	4
30127-1C	03-OLT3	0.0449	0.2583	0.0228	18.97	5.721	30.161	1.85	0.05	2.4335	17.91	matrix	Olmoti	6
30127-1D	03-OLT3	0.0205	-1.1615	0.0179	11.56	5.408	46.821	1.75	0.03	3.4361	17.91	matrix	Olmoti	8

Appendix 2: continued

Lab-Id	Sample Id	$^{36}Ar/^{39}Ar$	$^{37}Ar/^{39}Ar$	$^{38}Ar/^{39}Ar$	$^{40}Ar/^{39}Ar$	$^{40}Ar^*/^{39}Ar$	$\%^{40}Ar^*$	Age (Ma)	Age Error	^{39}Ar Moles E-16	JE-5	Material	Locality	Power (W)
30127-1E	03-OLT3	0.0143	0.0335	0.0167	9.91	5.688	57.410	1.84	0.02	5.3389	17.91	matrix	Olmoti	10
30127-1F	03-OLT3	0.0096	0.3447	0.0166	8.51	5.720	67.178	1.85	0.01	5.9756	17.91	matrix	Olmoti	12
30127-1G	03-OLT3	0.0058	0.3246	0.0164	7.29	5.606	76.875	1.81	0.01	6.6091	17.91	matrix	Olmoti	14
30127-1H	03-OLT3	0.0041	0.0903	0.0166	6.76	5.543	81.993	1.79	0.01	7.5986	17.91	matrix	Olmoti	17
30127-1I	03-OLT3	0.0041	0.2244	0.0160	6.81	5.600	82.280	1.81	0.01	7.4807	17.91	matrix	Olmoti	21
30127-1J	03-OLT3	0.0035	0.0552	0.0158	6.57	5.553	84.526	1.79	0.01	6.5052	17.91	matrix	Olmoti	26
30127-1K	03-OLT3	0.0031	0.1847	0.0153	6.51	5.619	86.372	1.81	0.01	5.3191	17.91	matrix	Olmoti	32
30127-1L	03-OLT3	0.0025	0.5845	0.0146	6.32	5.613	88.847	1.81	0.01	4.6794	17.91	matrix	Olmoti	40
30125-1A	03-OLT1	0.8275	-2.0434	0.1748	258.01	13.308	5.166	4.29	0.31	0.4928	17.91	matrix	Olmoti	2
30125-1B	03-OLT1	0.2132	-0.1792	0.0542	69.53	6.519	9.377	2.11	0.06	3.0614	17.91	matrix	Olmoti	4
30125-1C	03-OLT1	0.1014	0.0479	0.0333	35.97	6.013	16.717	1.94	0.03	6.5045	17.91	matrix	Olmoti	6
30125-1D	03-OLT1	0.0610	0.1351	0.0264	23.99	5.963	24.859	1.93	0.02	7.4258	17.91	matrix	Olmoti	8
30125-1E	03-OLT1	0.0356	-0.1320	0.0223	16.33	5.790	35.470	1.87	0.01	10.1102	17.91	matrix	Olmoti	10
30125-1F	03-OLT1	0.0199	-0.0318	0.0198	11.56	5.685	49.179	1.84	0.01	10.5697	17.91	matrix	Olmoti	12
30125-1G	03-OLT1	0.0142	0.0274	0.0189	9.89	5.701	57.649	1.84	0.01	9.5979	17.91	matrix	Olmoti	14
30125-1H	03-OLT1	0.0147	0.1098	0.0193	10.02	5.702	56.886	1.84	0.01	10.0988	17.91	matrix	Olmoti	17
30125-1I	03-OLT1	0.0160	0.2022	0.0196	10.45	5.743	54.952	1.85	0.01	10.0926	17.91	matrix	Olmoti	21
30125-1J	03-OLT1	0.0174	-0.0439	0.0200	10.87	5.722	52.650	1.85	0.01	9.4967	17.91	matrix	Olmoti	26
30125-1K	03-OLT1	0.0157	0.1451	0.0194	10.44	5.822	55.747	1.88	0.01	7.1355	17.91	matrix	Olmoti	32
30125-1L	03-OLT1	0.0085	0.2079	0.0168	8.18	5.682	69.500	1.84	0.01	7.7503	17.91	matrix	Olmoti	40
30126-1A	03-OLT2	0.0714	-0.1848	0.0246	26.75	5.652	21.131	1.83	0.10	0.5521	17.91	matrix	Olmoti	2
30126-1B	03-OLT2	0.0218	-0.0358	0.0161	12.37	5.926	47.905	1.91	0.02	4.1319	17.91	matrix	Olmoti	4
30126-1C	03-OLT2	0.0199	0.1192	0.0158	11.66	5.797	49.701	1.87	0.01	8.1879	17.91	matrix	Olmoti	6
30126-1D	03-OLT2	0.0208	2.5570	0.0188	11.04	5.110	46.195	1.65	0.07	9.1641	17.91	matrix	Olmoti	8
30126-1E	03-OLT2	0.0363	-0.1088	0.0194	16.92	6.193	36.612	2.00	0.01	10.0210	17.91	matrix	Olmoti	10
30126-1F	03-OLT2	0.0528	-0.0938	0.0223	21.81	6.189	28.378	2.00	0.02	7.5572	17.91	matrix	Olmoti	12
30126-1G	03-OLT2	0.0682	-0.5370	0.0256	26.14	5.942	22.737	1.92	0.02	5.6032	17.91	matrix	Olmoti	14
30126-1H	03-OLT2	0.0700	0.0909	0.0253	26.92	6.242	23.186	2.02	0.03	6.3004	17.91	matrix	Olmoti	17

Appendix 2: continued

Lab-Id	Sample Id	$^{36}Ar/^{39}Ar$	$^{37}Ar/^{39}Ar$	$^{38}Ar/^{39}Ar$	$^{40}Ar/^{39}Ar$	$^{40}Ar^{*}/^{39}Ar$	$\%^{40}Ar^{*}$	Age (Ma)	Age Error	^{39}Ar Moles E-16	JE-5	Material	Locality	Power (W)
30126-1I	03-OLT2	0.0625	0.1423	0.0245	24.58	6.128	24.929	1.98	0.02	6.6042	17.91	matrix	Olmoti	21
30126-1J	03-OLT2	0.0591	0.0068	0.0242	23.42	5.960	25.445	1.92	0.02	6.6802	17.91	matrix	Olmoti	26
30126-1K	03-OLT2	0.0398	-0.2992	0.0206	17.96	6.161	34.317	1.99	0.02	4.4243	17.91	matrix	Olmoti	32
30126-1L	03-OLT2	0.0214	-0.3889	0.0168	12.26	5.913	48.242	1.91	0.02	4.9423	17.91	matrix	Olmoti	40
30219-1A	04-OLT2	0.0372	0.1045	0.0178	16.40	5.401	32.932	1.76	0.07	0.3087	18.04	anorthoclase	Olmoti	2
30219-1B	04-OLT2	0.0007	0.0172	0.0123	5.83	5.615	96.357	1.83	0.01	3.8889	18.04	anorthoclase	Olmoti	4
30219-1C	04-OLT2	0.0006	0.0186	0.0109	5.84	5.664	97.045	1.84	0.00	6.3298	18.04	anorthoclase	Olmoti	6
30219-1D	04-OLT2	0.0003	0.0160	0.0122	5.78	5.688	98.348	1.85	0.00	7.8806	18.04	anorthoclase	Olmoti	8
30219-1E	04-OLT2	0.0004	0.0143	0.0120	5.80	5.680	97.966	1.85	0.00	6.6856	18.04	anorthoclase	Olmoti	10
30219-1F	04-OLT2	-0.0001	0.0132	0.0124	5.71	5.731	100.393	1.86	0.01	2.3679	18.04	anorthoclase	Olmoti	12
30219-1G	04-OLT2	-0.0001	0.0131	0.0111	5.70	5.730	100.556	1.86	0.01	1.5644	18.04	anorthoclase	Olmoti	14
30219-1H	04-OLT2	-0.0001	0.0178	0.0122	5.68	5.703	100.355	1.86	0.01	3.5516	18.04	anorthoclase	Olmoti	17
30219-1I	04-OLT2	0.0000	0.0165	0.0113	5.76	5.756	99.927	1.87	0.01	1.8890	18.04	anorthoclase	Olmoti	21
30219-1J	04-OLT2	-0.0009	0.0144	0.0108	5.77	6.031	104.589	1.96	0.01	1.3895	18.04	anorthoclase	Olmoti	26
30219-1K	04-OLT2	-0.0032	-0.0045	0.0087	5.71	6.654	116.627	2.16	0.03	0.6135	18.04	anorthoclase	Olmoti	32
30219-1L	04-OLT2	-0.0004	0.0164	0.0110	5.81	5.917	101.878	1.92	0.02	1.1222	18.04	anorthoclase	Olmoti	40
30218-1A	04-OLT4	0.3556	0.0728	0.0869	118.24	13.163	11.132	4.28	0.13	1.3987	18.04	matrix	Olmoti	2
30218-1B	04-OLT4	0.0428	0.0392	0.0229	19.00	6.349	33.413	2.06	0.02	9.1613	18.04	matrix	Olmoti	4
30218-1C	04-OLT4	0.0118	0.0305	0.0173	9.12	5.624	61.660	1.83	0.01	13.9789	18.04	matrix	Olmoti	6
30218-1D	04-OLT4	0.0085	0.0310	0.0175	8.15	5.650	69.359	1.84	0.01	5.6442	18.04	matrix	Olmoti	8
30218-1E	04-OLT4	0.0063	0.0586	0.0167	8.30	6.426	77.459	2.09	0.02	7.4351	18.04	matrix	Olmoti	10
30218-1F	04-OLT4	0.0087	0.1053	0.0168	8.23	5.680	69.022	1.85	0.01	5.8759	18.04	matrix	Olmoti	12
30218-1G	04-OLT4	0.0070	0.1354	0.0157	7.65	5.607	73.251	1.82	0.01	4.3802	18.04	matrix	Olmoti	14
30218-1H	04-OLT4	0.0054	0.1683	0.0145	7.25	5.681	78.371	1.85	0.01	3.6930	18.04	matrix	Olmoti	17
30218-1I	04-OLT4	0.0039	0.1615	0.0140	6.75	5.618	83.211	1.83	0.01	2.4591	18.04	matrix	Olmoti	21
30218-1J	04-OLT4	0.0029	0.1584	0.0139	6.42	5.580	86.925	1.82	0.02	1.1636	18.04	matrix	Olmoti	26
30218-1K	04-OLT4	-0.0002	0.1466	0.0115	6.71	6.782	101.026	2.21	0.04	0.4905	18.04	matrix	Olmoti	32
30218-1L	04-OLT4	0.0031	0.1612	0.0145	6.69	5.785	86.444	1.88	0.02	1.3450	18.04	matrix	Olmoti	40

Appendix 2: continued

Lab-Id	Sample Id	$^{36}Ar/^{39}Ar$	$^{37}Ar/^{39}Ar$	$^{38}Ar/^{39}Ar$	$^{40}Ar/^{39}Ar$	$^{40}Ar^{*}/^{39}Ar$	$\%^{40}Ar^{*}$	Age (Ma)	Age Error	^{39}Ar Moles E-16	JE-5	Material	Locality	Power (W)
30292-1A	00-NG2	1.0807	0.1919	0.2211	318.74	-0.603	-0.189	-0.28	1.39	9.4294	25.91	matrix	Ngorongoro	2
30292-1B	00-NG2	0.2261	0.1655	0.0568	71.29	4.480	6.283	2.09	0.29	37.5369	25.91	matrix	Ngorongoro	4
30292-1C	00-NG2	0.0178	0.1110	0.0156	10.37	5.127	49.432	2.39	0.03	150.8846	25.91	matrix	Ngorongoro	6
30292-1D	00-NG2	0.0017	0.1284	0.0122	5.54	5.045	91.006	2.36	0.02	258.2704	25.91	matrix	Ngorongoro	8
30292-1E	00-NG2	0.0008	0.1024	0.0121	5.15	4.915	95.458	2.30	0.01	249.8045	25.91	matrix	Ngorongoro	10
30292-1F	00-NG2	0.0010	0.0837	0.0124	5.16	4.859	94.231	2.27	0.02	152.7043	25.91	matrix	Ngorongoro	12
30292-1G	00-NG2	0.0006	0.1545	0.0129	4.87	4.698	96.435	2.19	0.03	92.9731	25.91	matrix	Ngorongoro	14
30292-1H	00-NG2	0.0019	0.1208	0.0129	5.35	4.805	89.766	2.24	0.04	64.9529	25.91	matrix	Ngorongoro	17
30292-1I	00-NG2	0.0009	0.2054	0.0132	5.57	5.324	95.519	2.49	0.05	43.7260	25.91	matrix	Ngorongoro	21
30292-1J	00-NG2	0.0043	0.2965	0.0139	5.95	4.698	79.017	2.19	0.08	26.9145	25.91	matrix	Ngorongoro	26
30292-1K	00-NG2	0.0015	0.2885	0.0135	5.44	5.028	92.492	2.35	0.24	9.3423	25.91	matrix	Ngorongoro	32
30292-1L	00-NG2	0.0074	0.2108	0.0149	6.44	4.278	66.429	2.00	0.48	4.4185	25.91	matrix	Ngorongoro	40
30289-2A	00-NG8	0.1453	1.4466	0.0440	46.89	4.077	8.686	1.91	0.63	4.4998	25.92	matrix	Ngorongoro	2
30289-2B	00-NG8	0.0168	0.9623	0.0180	10.25	5.353	52.187	2.50	0.07	43.6838	25.92	matrix	Ngorongoro	4
30289-2C	00-NG8	0.0087	0.5200	0.0164	7.19	4.653	64.696	2.17	0.04	78.6626	25.92	matrix	Ngorongoro	6
30289-2D	00-NG8	0.0086	0.5566	0.0154	7.17	4.682	65.251	2.19	0.04	65.6147	25.92	matrix	Ngorongoro	8
30289-2E	00-NG8	0.0086	0.4181	0.0145	7.25	4.731	65.264	2.21	0.05	53.9235	25.92	matrix	Ngorongoro	10
30289-2F	00-NG8	0.0104	0.7531	0.0147	8.18	5.165	63.132	2.41	0.09	32.2250	25.92	matrix	Ngorongoro	12
30289-2G	00-NG8	0.0211	0.9736	0.0173	10.58	4.408	41.650	2.06	0.14	20.6061	25.92	matrix	Ngorongoro	14
30289-2H	00-NG8	0.0347	3.0521	0.0191	14.61	4.603	31.436	2.15	0.18	16.7114	25.92	matrix	Ngorongoro	17
30289-2I	00-NG8	0.0534	5.7305	0.0240	18.94	3.649	19.185	1.71	0.26	11.4334	25.92	matrix	Ngorongoro	21
30289-2J	00-NG8	0.0735	16.9637	0.0287	25.00	4.705	18.593	2.20	0.35	9.5636	25.92	matrix	Ngorongoro	26
30289-2K	00-NG8	0.0761	18.3190	0.0291	25.00	4.049	15.983	1.89	0.49	5.4389	25.92	matrix	Ngorongoro	32
30289-2L	00-NG8	0.0734	26.9267	0.0268	24.72	5.286	20.974	2.47	0.55	5.0006	25.92	matrix	Ngorongoro	40
30128-1A	03-OLDI-1	4.5083	-13.0372	0.8795	1330.10	-3.103	-0.235	-1.00	2.65	0.1206	17.91	matrix	Oldeani	2
30128-1B	03-OLDI-1	0.8324	4.8071	0.1706	248.89	3.324	1.331	1.07	0.52	0.5314	17.91	matrix	Oldeani	4
30128-1C	03-OLDI-1	0.3520	2.3445	0.0810	107.44	3.622	3.366	1.17	0.23	1.0561	17.91	matrix	Oldeani	6
30128-1D	03-OLDI-1	0.1724	0.7083	0.0467	54.39	3.503	6.437	1.13	0.15	0.8900	17.91	matrix	Oldeani	7

Appendix 2: continued

Lab-Id	Sample Id	$^{36}Ar/^{39}Ar$	$^{37}Ar/^{39}Ar$	$^{38}Ar/^{39}Ar$	$^{40}Ar/^{39}Ar$	$^{40}Ar^{*}/^{39}Ar$	$\%^{40}Ar^{*}$	Age (Ma)	Age Error	^{39}Ar Moles E-16	JE-5	Material	Locality	Power (W)
30128-1E	03-OLDI-1	0.1421	2.1505	0.0417	46.42	4.616	9.929	1.49	0.13	1.0347	17.91	matrix	Oldeani	8
30128-1F	03-OLDI-1	0.0974	1.3174	0.0311	33.06	4.403	13.305	1.42	0.08	1.6081	17.91	matrix	Oldeani	10
30128-1G	03-OLDI-1	0.0715	1.0432	0.0264	25.44	4.399	17.283	1.42	0.07	1.9797	17.91	matrix	Oldeani	12
30128-1H	03-OLDI-1	0.0528	1.5932	0.0231	20.20	4.734	23.404	1.53	0.06	2.2623	17.91	matrix	Oldeani	14
30128-1I	03-OLDI-1	0.0395	0.9345	0.0202	16.37	4.777	29.168	1.54	0.04	2.8208	17.91	matrix	Oldeani	17
30128-1J	03-OLDI-1	0.0352	1.5263	0.0191	15.13	4.842	31.976	1.56	0.04	3.2772	17.91	matrix	Oldeani	21
30128-1K	03-OLDI-1	0.0298	2.0699	0.0130	13.41	4.788	35.655	1.55	0.13	3.6257	17.91	matrix	Oldeani	26
30128-1L	03-OLDI-1	-0.2023	-2490.33	0.1268	-7.18	-53.258	2055.1	-17.29	5.36	0.0243	17.91	matrix	Oldeani	32
30128-1M	03-OLDI-1	-0.4837	-5844.89	-0.1315	-17.34	-66.770	1984.9	-21.70	6.81	0.0104	17.91	matrix	Oldeani	40
30136-1A	03-OLDI-2	12.8489	73.5216	2.4570	3889.36	103.868	2.531	33.14	9.16	0.0405	17.85	matrix	Oldeani	2
30136-1B	03-OLDI-2	5.8960	9.6162	1.1180	1742.86	1.382	0.079	0.44	3.28	0.1951	17.85	matrix	Oldeani	4
30136-1C	03-OLDI-2	1.4265	3.5035	0.2814	427.50	6.252	1.459	2.01	0.81	0.6440	17.85	matrix	Oldeani	6
30136-1D	03-OLDI-2	0.5647	0.6386	0.1178	173.31	6.492	3.744	2.09	0.35	0.7035	17.85	matrix	Oldeani	7
30136-1E	03-OLDI-2	0.3735	1.0294	0.0828	113.96	3.669	3.217	1.18	0.24	0.9209	17.85	matrix	Oldeani	8
30136-1F	03-OLDI-2	0.1753	2.1252	0.0437	56.53	4.904	8.663	1.58	0.12	1.6797	17.85	matrix	Oldeani	10
30136-1G	03-OLDI-2	0.0788	1.0915	0.0267	28.01	4.805	17.141	1.55	0.07	2.2368	17.85	matrix	Oldeani	12
30136-1H	03-OLDI-2	0.0353	0.9989	0.0186	15.38	5.033	32.690	1.62	0.04	2.6634	17.85	matrix	Oldeani	14
30136-1I	03-OLDI-2	0.0157	0.8543	0.0150	9.37	4.802	51.197	1.55	0.03	3.2948	17.85	matrix	Oldeani	17
30136-1J	03-OLDI-2	0.0075	1.8932	0.0137	7.05	5.000	70.827	1.61	0.03	3.5243	17.85	matrix	Oldeani	21
30136-1K	03-OLDI-2	0.0093	1.4635	0.0145	7.34	4.713	64.128	1.52	0.03	3.6921	17.85	matrix	Oldeani	26
30136-1L	03-OLDI-2	0.0144	3.0080	0.0165	8.67	4.669	53.750	1.50	0.05	2.2222	17.85	matrix	Oldeani	32
30136-1M	03-OLDI-2	0.0215	3.8788	0.0176	11.63	5.620	48.177	1.81	0.13	0.6657	17.85	matrix	Oldeani	40
30137-1A	03-OLDI-4	7.8776	35.3313	1.4446	2288.25	-37.681	-1.605	-12.18	5.79	0.0570	17.85	matrix	Oldeani	2
30137-1B	03-OLDI-4	3.4419	3.5920	0.6706	1022.00	5.227	0.510	1.68	1.97	0.2384	17.85	matrix	Oldeani	4
30137-1C	03-OLDI-4	0.8896	-0.0011	0.1826	267.77	4.889	1.826	1.57	0.51	0.8010	17.85	matrix	Oldeani	6
30137-1D	03-OLDI-4	0.4343	1.2939	0.0959	131.69	3.466	2.630	1.12	0.28	0.7682	17.85	matrix	Oldeani	7
30137-1E	03-OLDI-4	0.2858	-0.0926	0.0655	89.62	5.169	5.768	1.66	0.19	1.2493	17.85	matrix	Oldeani	8
30137-1F	03-OLDI-4	0.1651	0.2900	0.0428	54.32	5.546	10.207	1.78	0.11	2.1625	17.85	matrix	Oldeani	10

Appendix 2: continued

Lab-Id	Sample Id	$^{36}Ar/^{39}Ar$	$^{37}Ar/^{39}Ar$	$^{38}Ar/^{39}Ar$	$^{40}Ar/^{39}Ar$	$^{40}Ar^{*}/^{39}Ar$	$\%^{40}Ar^{*}$	Age (Ma)	Age Error	^{39}Ar Moles E-16	JE-5	Material	Locality	Power (W)
30137-1G	03-OLDI-4	0.1141	0.8037	0.0331	38.56	4.909	12.724	1.58	0.08	2.6728	17.85	matrix	Oldeani	12
30137-1H	03-OLDI-4	0.0755	1.0007	0.0262	27.44	5.218	19.004	1.68	0.06	2.9854	17.85	matrix	Oldeani	14
30137-1I	03-OLDI-4	0.0357	0.9029	0.0191	15.42	4.940	32.015	1.59	0.04	3.7993	17.85	matrix	Oldeani	17
30137-1J	03-OLDI-4	0.0144	0.9951	0.0150	9.17	5.007	54.546	1.61	0.02	4.3964	17.85	matrix	Oldeani	21
30137-1K	03-OLDI-4	0.0133	1.2687	0.0145	8.78	4.960	56.462	1.60	0.03	3.8918	17.85	matrix	Oldeani	26
30137-1L	03-OLDI-4	0.0169	1.3286	0.0155	9.69	4.810	49.571	1.55	0.03	3.0386	17.85	matrix	Oldeani	32
30137-1M	03-OLDI-4	0.0308	2.3494	0.0186	13.41	4.514	33.596	1.45	0.06	1.8315	17.85	matrix	Oldeani	40
30141-1A	03-OLDI-5	6.6449	30.8938	1.2828	1982.09	21.483	1.060	6.90	4.84	0.0502	17.85	matrix	Oldeani	2
30141-1B	03-OLDI-5	2.2065	3.1629	0.4236	637.58	-14.227	-2.226	-4.59	1.46	0.2625	17.85	matrix	Oldeani	4
30141-1C	03-OLDI-5	0.5249	3.1602	0.1139	160.69	5.856	3.636	1.88	0.33	0.8394	17.85	matrix	Oldeani	6
30141-1D	03-OLDI-5	0.2421	0.0235	0.0587	76.49	4.952	6.473	1.59	0.17	1.1230	17.85	matrix	Oldeani	7
30141-1E	03-OLDI-5	0.0777	2.5881	0.0271	27.62	4.888	17.666	1.57	0.09	1.3138	17.85	matrix	Oldeani	8
30141-1F	03-OLDI-5	0.0327	1.1946	0.0185	14.30	4.724	33.010	1.52	0.05	2.3468	17.85	matrix	Oldeani	10
30141-1G	03-OLDI-5	0.0173	0.0967	0.0155	10.01	4.900	48.970	1.58	0.04	2.4439	17.85	matrix	Oldeani	12
30141-1H	03-OLDI-5	0.0144	0.9294	0.0152	9.12	4.955	54.307	1.59	0.04	2.3930	17.85	matrix	Oldeani	14
30141-1I	03-OLDI-5	0.0174	-0.0460	0.0155	9.87	4.717	47.792	1.52	0.04	2.6211	17.85	matrix	Oldeani	17
30141-1J	03-OLDI-5	0.0249	1.3401	0.0171	12.10	4.858	40.123	1.56	0.04	2.5351	17.85	matrix	Oldeani	21
30141-1K	03-OLDI-5	0.0387	1.6904	0.0198	15.94	4.661	29.199	1.50	0.05	2.1076	17.85	matrix	Oldeani	26
30141-1L	03-OLDI-5	0.0462	2.4556	0.0212	18.37	4.930	26.792	1.59	0.07	1.5283	17.85	matrix	Oldeani	32
30141-1M	03-OLDI-5	0.0987	2.1359	0.0334	33.55	4.566	13.590	1.47	0.14	0.7635	17.85	matrix	Oldeani	40
30215-1A	04-OLDI-3	1.0742	0.9615	0.2437	355.26	37.952	10.676	12.31	0.48	0.3107	18.04	matrix	Oldeani	2
30215-1B	04-OLDI-3	0.1526	0.8827	0.0425	50.10	5.090	10.154	1.66	0.06	1.5707	18.04	matrix	Oldeani	4
30215-1C	04-OLDI-3	0.0121	0.7763	0.0141	8.21	4.709	57.346	1.53	0.01	4.5578	18.04	matrix	Oldeani	6
30215-1D	04-OLDI-3	0.0034	0.7257	0.0124	5.84	4.897	83.832	1.59	0.01	3.9268	18.04	matrix	Oldeani	8
30215-1E	04-OLDI-3	0.0038	0.8317	0.0124	5.74	4.680	81.498	1.52	0.01	3.0398	18.04	matrix	Oldeani	10
30215-1F	04-OLDI-3	0.0054	1.1220	0.0128	5.95	4.452	74.724	1.45	0.01	1.7737	18.04	matrix	Oldeani	12
30215-1G	04-OLDI-3	0.0059	1.5804	0.0149	6.22	4.608	73.990	1.50	0.02	1.2160	18.04	matrix	Oldeani	14
30215-1H	04-OLDI-3	0.0065	2.0384	0.0143	6.67	4.904	73.470	1.60	0.02	1.0626	18.04	matrix	Oldeani	17

Appendix 2: continued

Lab-Id	Sample Id	$^{36}Ar/^{39}Ar$	$^{37}Ar/^{39}Ar$	$^{38}Ar/^{39}Ar$	$^{40}Ar/^{39}Ar$	$^{40}Ar^{*}/^{39}Ar$	$\%^{40}Ar^{*}$	Age (Ma)	Age Error	^{39}Ar Moles E-16	JE-5	Material	Locality	Power (W)
30215-1I	04-OLDI-3	0.0077	2.3557	0.0145	6.91	4.830	69.790	1.57	0.05	0.3848	18.04	matrix	Oldeani	21
30215-1J	04-OLDI-3	0.0074	2.5173	0.0192	6.52	4.557	69.726	1.48	0.14	0.1340	18.04	matrix	Oldeani	26
30215-1K	04-OLDI-3	0.0082	2.3271	0.0218	6.21	3.999	64.252	1.30	0.16	0.1139	18.04	matrix	Oldeani	32
30215-1L	04-OLDI-3	0.0050	2.0476	0.0162	6.03	4.727	78.284	1.54	0.04	0.5599	18.04	matrix	Oldeani	40
30217-1A	04-OLDI-4	0.8662	1.7784	0.1834	255.23	-0.591	-0.231	-0.19	0.48	0.1238	18.04	matrix	Oldeani	2
30217-1B	04-OLDI-4	0.2299	1.5327	0.0626	75.19	7.391	9.819	2.40	0.20	0.5058	18.04	matrix	Oldeani	4
30217-1C	04-OLDI-4	0.0223	1.0946	0.0164	11.46	4.954	43.183	1.61	0.01	5.1766	18.04	matrix	Oldeani	6
30217-1D	04-OLDI-4	0.0043	0.9054	0.0128	6.14	4.928	80.276	1.60	0.01	4.5079	18.04	matrix	Oldeani	8
30217-1E	04-OLDI-4	0.0043	0.9034	0.0131	5.97	4.782	80.064	1.56	0.01	3.7477	18.04	matrix	Oldeani	10
30217-1F	04-OLDI-4	0.0069	1.1586	0.0140	6.70	4.764	71.074	1.55	0.02	1.9602	18.04	matrix	Oldeani	12
30217-1G	04-OLDI-4	0.0119	1.9223	0.0155	8.39	5.033	59.907	1.64	0.03	1.2456	18.04	matrix	Oldeani	14
30217-1H	04-OLDI-4	0.0230	3.1197	0.0176	11.32	4.780	42.113	1.55	0.04	0.7932	18.04	matrix	Oldeani	17
30217-1I	04-OLDI-4	0.0353	4.1147	0.0175	15.34	5.251	34.131	1.71	0.12	0.2008	18.04	matrix	Oldeani	21
30217-1J	04-OLDI-4	0.0676	3.9615	0.0240	23.93	4.278	17.829	1.39	0.22	0.0939	18.04	matrix	Oldeani	26
30217-1K	04-OLDI-4	0.0332	4.2469	0.0126	15.22	5.775	37.822	1.88	0.39	0.0525	18.04	matrix	Oldeani	32
30217-1L	04-OLDI-4	0.0505	3.7706	0.0213	21.53	6.943	32.157	2.26	0.10	0.2419	18.04	matrix	Oldeani	40
30304-2A	00-LM6	0.1112	0.7920	0.0320	36.94	4.154	11.240	1.94	0.68	3.9095	25.85	matrix	Lemagurut	2
30304-2B	00-LM6	0.0187	0.4577	0.0159	10.33	4.837	46.814	2.25	0.07	40.2710	25.85	matrix	Lemagurut	4
30304-2C	00-LM6	0.0050	0.4063	0.0131	6.30	4.854	77.001	2.26	0.02	157.0419	25.85	matrix	Lemagurut	6
30304-2D	00-LM6	0.0029	0.3527	0.0125	5.66	4.824	85.229	2.25	0.01	201.5042	25.85	matrix	Lemagurut	8
30304-2E	00-LM6	0.0023	0.3286	0.0124	5.51	4.870	88.308	2.27	0.01	207.1264	25.85	matrix	Lemagurut	10
30304-2F	00-LM6	0.0027	0.3668	0.0126	5.55	4.790	86.306	2.23	0.02	128.5840	25.85	matrix	Lemagurut	12
30304-2G	00-LM6	0.0037	0.5081	0.0125	5.79	4.731	81.715	2.21	0.04	76.1613	25.85	matrix	Lemagurut	14
30304-2H	00-LM6	0.0052	0.9377	0.0135	6.28	4.814	76.617	2.24	0.05	57.7775	25.85	matrix	Lemagurut	17
30304-2I	00-LM6	0.0082	2.0000	0.0140	7.08	4.827	68.116	2.25	0.06	45.6569	25.85	matrix	Lemagurut	21
30304-2J	00-LM6	0.0102	1.6196	0.0141	7.46	4.586	61.420	2.14	0.11	22.7620	25.85	matrix	Lemagurut	26
30304-2K	00-LM6	0.0102	3.0191	0.0149	8.09	5.332	65.814	2.48	0.22	11.4008	25.85	matrix	Lemagurut	32
30304-2L	00-LM6	0.0186	3.9116	0.0158	9.72	4.532	46.520	2.11	0.28	8.9092	25.85	matrix	Lemagurut	40

Appendix 2: continued

Lab-Id	Sample Id	$^{36}Ar/^{39}Ar$	$^{37}Ar/^{39}Ar$	$^{38}Ar/^{39}Ar$	$^{40}Ar/^{39}Ar$	$^{40}Ar^{*}/^{39}Ar$	$\%^{40}Ar^{*}$	Age (Ma)	Age Error	^{39}Ar Moles E-16	JE-5	Material	Locality	Power (W)
30266-1E	04-OS1	0.0018	5.3121	0.0120	0.95	0.849	89.280	2.42	0.32	86.9836	158	anorthoclase	Lemagurut	10
30266-1F	04-OS1	0.0016	5.7917	0.0121	0.95	0.944	98.759	2.69	0.36	73.6685	158	anorthoclase	Lemagurut	12
30266-1G	04-OS1	0.0022	5.9223	0.0125	0.95	0.776	81.522	2.21	0.36	76.2390	158	anorthoclase	Lemagurut	14
30266-1H	04-OS1	0.0022	6.5018	0.0124	1.01	0.871	86.092	2.48	0.35	116.6000	158	anorthoclase	Lemagurut	17
30266-1I	04-OS1	0.0027	5.9504	0.0125	0.96	0.646	66.952	1.84	0.33	124.9678	158	anorthoclase	Lemagurut	21
30266-1J	04-OS1	0.0020	6.7619	0.0124	0.86	0.825	95.900	2.35	0.40	73.9670	158	anorthoclase	Lemagurut	26
30266-1K	04-OS1	0.0022	6.6830	0.0126	0.87	0.768	87.973	2.19	0.42	61.1247	158	anorthoclase	Lemagurut	32
30266-1L	04-OS1	0.0026	5.7236	0.0121	0.90	0.603	67.063	1.72	0.35	81.9398	158	anorthoclase	Lemagurut	40
30209-1A	04-OS3	1.2221	0.4241	0.2504	372.76	11.654	3.125	3.81	0.37	0.4319	18.14	matrix	Osilale	2
30209-1B	04-OS3	0.4968	0.2864	0.1064	153.51	6.734	4.386	2.20	0.14	1.0513	18.14	matrix	Osilale	4
30209-1C	04-OS3	0.0952	0.2036	0.0318	37.22	9.100	24.450	2.98	0.03	9.5632	18.14	matrix	Osilale	6
30209-1D	04-OS3	0.0399	0.1917	0.0199	19.05	7.268	38.155	2.38	0.02	9.7521	18.14	matrix	Osilale	8
30209-1E	04-OS3	0.0279	0.2320	0.0179	15.54	7.316	47.077	2.39	0.02	5.9054	18.14	matrix	Osilale	10
30209-1F	04-OS3	0.0134	0.3654	0.0148	11.29	7.355	65.160	2.41	0.01	3.4347	18.14	matrix	Osilale	12
30209-1G	04-OS3	0.0123	0.6268	0.0143	10.75	7.180	66.773	2.35	0.02	2.1041	18.14	matrix	Osilale	14
30209-1H	04-OS3	0.0144	1.0220	0.0148	11.35	7.170	63.150	2.34	0.02	1.8901	18.14	matrix	Osilale	17
30209-1I	04-OS3	0.0188	1.3418	0.0167	12.21	6.761	55.323	2.21	0.04	0.8157	18.14	matrix	Osilale	21
30209-1J	04-OS3	0.0198	1.3280	0.0165	13.46	7.723	57.331	2.53	0.09	0.2456	18.14	matrix	Osilale	26
30209-1K	04-OS3	0.0252	1.4165	0.0207	14.34	7.002	48.793	2.29	0.12	0.1885	18.14	matrix	Osilale	32
30209-1L	04-OS3	0.0277	1.6168	0.0193	14.78	6.730	45.476	2.20	0.06	0.4274	18.14	matrix	Osilale	40
30210-1A	04-OS4	0.2619	0.4260	0.0668	89.51	12.156	13.576	3.97	0.16	0.3582	18.14	matrix	Osilale	2
30210-1B	04-OS4	0.0512	0.2932	0.0222	21.92	6.826	31.135	2.23	0.02	2.9724	18.14	matrix	Osilale	4
30210-1C	04-OS4	0.0133	0.2373	0.0147	11.15	7.242	64.962	2.37	0.01	7.8319	18.14	matrix	Osilale	6
30210-1D	04-OS4	0.0058	0.2376	0.0131	8.67	6.984	80.566	2.28	0.01	11.5571	18.14	matrix	Osilale	8
30210-1E	04-OS4	0.0042	0.2542	0.0123	8.26	7.027	85.110	2.30	0.01	6.5103	18.14	matrix	Osilale	10
30210-1F	04-OS4	0.0053	0.3367	0.0133	8.52	6.977	81.857	2.28	0.01	3.8201	18.14	matrix	Osilale	12
30210-1G	04-OS4	0.0078	0.5989	0.0130	9.39	7.142	75.994	2.34	0.01	2.3476	18.14	matrix	Osilale	14
30210-1H	04-OS4	0.0118	0.8782	0.0144	10.69	7.290	68.171	2.38	0.02	2.2056	18.14	matrix	Osilale	17

Appendix 2: continued

Lab-Id	Sample Id	$^{36}Ar/^{39}Ar$	$^{37}Ar/^{39}Ar$	$^{38}Ar/^{39}Ar$	$^{40}Ar/^{39}Ar$	$^{40}Ar^{*}/^{39}Ar$	$\%^{40}Ar^{*}$	Age (Ma)	Age Error	^{39}Ar Moles E-16	JE-5	Material	Locality	Power (W)
30210-1I	04-OS4	0.0185	1.3351	0.0146	12.39	7.023	56.655	2.30	0.03	1.0167	18.14	matrix	Osilale	21
30210-1J	04-OS4	0.0271	1.7386	0.0128	15.97	8.117	50.769	2.65	0.11	0.2003	18.14	matrix	Osilale	26
30210-1K	04-OS4	0.0070	1.7309	-0.0048	16.95	15.042	88.658	4.92	0.25	0.0873	18.14	matrix	Osilale	32
30210-1L	04-OS4	0.0267	2.0459	0.0098	18.17	10.445	57.410	3.42	0.16	0.1409	18.14	matrix	Osilale	40
30201-1A	04-OG1	0.7089	0.7665	0.1512	219.59	10.189	4.637	3.31	0.28	0.4358	18.01	matrix	Ogol	2
30201-1B	04-OG1	0.1071	0.5710	0.0340	39.10	7.514	19.205	2.44	0.04	2.1886	18.01	matrix	Ogol	4
30201-1C	04-OG1	0.0426	0.6281	0.0216	19.28	6.740	34.937	2.19	0.09	1.1272	18.01	matrix	Ogol	6
30201-1D	04-OG1	0.0168	0.7796	0.0179	12.25	7.335	59.847	2.38	0.04	1.5459	18.01	matrix	Ogol	8
30201-1E	04-OG1	0.0189	0.7667	0.0183	12.67	7.147	56.353	2.32	0.05	0.6616	18.01	matrix	Ogol	10
30201-1F	04-OG1	0.0156	0.8031	0.0173	11.63	7.086	60.896	2.30	0.02	2.1605	18.01	matrix	Ogol	12
30201-1G	04-OG1	0.0202	3.1061	0.0183	12.80	7.089	55.243	2.30	0.02	1.4609	18.01	matrix	Ogol	14
30201-1H	04-OG1	0.0244	6.3540	0.0187	13.87	7.192	51.572	2.34	0.03	1.1559	18.01	matrix	Ogol	17
30201-1I	04-OG1	0.0275	8.6043	0.0207	15.47	8.071	51.781	2.62	0.04	0.6693	18.01	matrix	Ogol	21
30201-1J	04-OG1	0.0238	9.9152	0.0184	13.56	7.336	53.621	2.38	0.05	0.5501	18.01	matrix	Ogol	26
30201-1K	04-OG1	0.0250	11.8779	0.0205	14.61	8.220	55.679	2.67	0.07	0.4057	18.01	matrix	Ogol	32
30201-1L	04-OG1	0.0925	16.8313	0.0340	34.53	8.617	24.576	2.80	0.09	0.3539	18.01	matrix	Ogol	40
30305-2A	04-OG2	1.1539	1.3882	0.2388	338.68	-2.196	-0.648	-1.02	3.52	0.7727	25.85	matrix	Ogol	2
30305-2B	04-OG2	0.2290	0.6358	0.0686	71.47	3.846	5.379	1.79	0.50	5.7146	25.85	matrix	Ogol	4
30305-2C	04-OG2	0.0628	0.4397	0.0311	23.52	4.996	21.231	2.33	0.16	17.3417	25.85	matrix	Ogol	6
30305-2D	04-OG2	0.0410	0.5091	0.0259	17.10	5.024	29.365	2.34	0.11	24.0482	25.85	matrix	Ogol	8
30305-2E	04-OG2	0.0338	0.4480	0.0229	14.62	4.674	31.967	2.18	0.10	27.0560	25.85	matrix	Ogol	10
30305-2F	04-OG2	0.0569	0.4700	0.0273	21.33	4.550	21.325	2.12	0.14	19.2981	25.85	matrix	Ogol	12
30305-2G	04-OG2	0.1000	0.5229	0.0344	34.13	4.614	13.516	2.15	0.18	16.7027	25.85	matrix	Ogol	14
30305-2H	04-OG2	0.1183	1.6122	0.0361	40.04	5.208	12.992	2.43	0.15	27.8543	25.85	matrix	Ogol	17
30305-2I	04-OG2	0.1267	3.6352	0.0373	41.75	4.620	11.038	2.15	0.13	44.0671	25.85	matrix	Ogol	21
30305-2J	04-OG2	0.1310	8.1163	0.0382	43.63	5.615	12.797	2.62	0.15	40.0891	25.85	matrix	Ogol	26
30305-2K	04-OG2	0.1114	10.1151	0.0349	36.06	3.976	10.948	1.85	0.28	10.5011	25.85	matrix	Ogol	32
30305-2L	04-OG2	0.1915	36.8916	0.0473	60.13	6.683	10.822	3.11	0.48	8.4557	25.85	matrix	Ogol	40

Appendix 2: continued

Lab-Id	Sample Id	$^{36}Ar/^{39}Ar$	$^{37}Ar/^{39}Ar$	$^{38}Ar/^{39}Ar$	$^{40}Ar/^{39}Ar$	$^{40}Ar^{*}/^{39}Ar$	$\%^{40}Ar^{*}$	Age (Ma)	Age Error	^{39}Ar Moles E-16	JE-5	Material	Locality	Power (W)
30204-1A	04-OG4	0.3068	1.0352	0.0762	105.64	15.066	14.248	4.89	0.21	0.2693	18.01	matrix	Ogol	2
30204-1B	04-OG4	0.0482	0.8564	0.0230	22.48	8.314	36.951	2.70	0.05	0.7452	18.01	matrix	Ogol	4
30204-1C	04-OG4	0.0154	0.6086	0.0155	12.69	8.186	64.481	2.66	0.02	3.4170	18.01	matrix	Ogol	6
30204-1D	04-OG4	0.0114	0.5565	0.0140	11.21	7.900	70.452	2.57	0.02	1.9850	18.01	matrix	Ogol	8
30204-1E	04-OG4	0.0132	0.6757	0.0141	11.80	7.942	67.277	2.58	0.02	1.4497	18.01	matrix	Ogol	10
30204-1F	04-OG4	0.0275	1.2308	0.0166	15.22	7.182	47.149	2.33	0.03	1.0284	18.01	matrix	Ogol	12
30204-1G	04-OG4	0.0332	2.9038	0.0187	16.43	6.853	41.595	2.23	0.03	1.2450	18.01	matrix	Ogol	14
30204-1H	04-OG4	0.0518	4.8677	0.0222	21.46	6.550	30.385	2.13	0.03	1.1711	18.01	matrix	Ogol	17
30204-1I	04-OG4	0.0540	7.4572	0.0237	22.00	6.651	30.027	2.16	0.05	0.8493	18.01	matrix	Ogol	21
30204-1J	04-OG4	0.0633	10.1254	0.0240	23.44	5.559	23.498	1.81	0.07	0.4870	18.01	matrix	Ogol	26
30204-1K	04-OG4	0.0597	11.0546	0.0272	26.83	10.131	37.384	3.29	0.11	0.3037	18.01	matrix	Ogol	32
30204-1L	04-OG4	0.0811	13.0441	0.0275	30.27	7.401	24.160	2.40	0.09	0.3573	18.01	matrix	Ogol	40
30206-1A	04-NT3	0.2076	0.0765	0.0597	80.86	19.511	24.129	6.33	0.10	0.9518	18.01	matrix	Noiti-3	2
30206-1B	04-NT3	0.0481	0.0297	0.0238	26.96	12.743	47.271	4.14	0.03	2.7462	18.01	matrix	Noiti-3	4
30206-1C	04-NT3	0.0152	0.0187	0.0190	16.77	12.283	73.238	3.99	0.01	10.8343	18.01	matrix	Noiti-3	6
30206-1D	04-NT3	0.0060	0.0371	0.0202	14.27	12.493	87.536	4.05	0.01	4.3529	18.01	matrix	Noiti-3	8
30206-1E	04-NT3	0.0078	0.1172	0.0199	14.80	12.500	84.450	4.06	0.01	3.9240	18.01	matrix	Noiti-3	10
30206-1F	04-NT3	0.0112	0.3009	0.0183	15.72	12.434	79.091	4.04	0.01	3.5825	18.01	matrix	Noiti-3	12
30206-1G	04-NT3	0.0178	0.5685	0.0182	17.13	11.913	69.530	3.87	0.02	2.9161	18.01	matrix	Noiti-3	14
30206-1H	04-NT3	0.0232	0.8038	0.0190	19.42	12.640	65.049	4.10	0.02	2.3804	18.01	matrix	Noiti-3	17
30206-1I	04-NT3	0.0140	0.7487	0.0156	19.29	15.216	78.810	4.94	0.04	0.8866	18.01	matrix	Noiti-3	21
30206-1J	04-NT3	0.0217	0.7312	0.0177	18.97	12.624	66.518	4.10	0.05	0.5604	18.01	matrix	Noiti-3	26
30206-1K	04-NT3	0.0241	0.7260	0.0169	19.65	12.579	63.989	4.08	0.06	0.4000	18.01	matrix	Noiti-3	32
30206-1L	04-NT3	0.0264	0.7390	0.0178	20.32	12.571	61.825	4.08	0.04	0.7667	18.01	matrix	Noiti-3	40
30020-1A	01-SM3	0.9872	6.7399	-5.1576	56.00	-237.220	-421.0	-30.91	7.93	-0.0423	7.16	matrix	Satiman	2.2
30020-1B	01-SM3	0.8287	31.5474	2.7571	-17.32	-267.096	1498.5	-34.84	17.68	0.0549	7.16	matrix	Satiman	3.2
30020-1C	01-SM3	0.4402	12.7051	0.7472	-7.54	-138.146	1810.3	-17.93	5.57	0.1154	7.16	matrix	Satiman	4.2
30020-1D	01-SM3	0.7506	1.6837	0.1554	251.48	29.859	11.855	3.85	0.17	1.5865	7.16	matrix	Satiman	5

Appendix 2: continued

Lab-Id	Sample Id	$^{36}Ar/^{39}Ar$	$^{37}Ar/^{39}Ar$	$^{38}Ar/^{39}Ar$	$^{40}Ar/^{39}Ar$	$^{40}Ar^{*}/^{39}Ar$	$\%^{40}Ar^{*}$	Age (Ma)	Age Error	^{39}Ar Moles E-16	JE-5	Material	Locality	Power (W)
30020-1E	01-SM3	0.6432	1.2638	0.1324	221.56	31.625	14.258	4.08	0.16	2.7880	7.16	matrix	Satiman	6.5
30020-1F	01-SM3	0.4788	0.7472	0.1057	173.02	31.627	18.267	4.08	0.16	3.4311	7.16	matrix	Satiman	8
30020-1G	01-SM3	0.4504	0.6558	0.1039	169.13	36.109	21.337	4.66	0.10	2.8812	7.16	matrix	Satiman	9.5
30020-1H	01-SM3	0.3746	0.6052	0.0875	145.57	34.945	23.993	4.51	0.09	6.3275	7.16	matrix	Satiman	12
30020-1I	01-SM3	0.2588	0.6886	0.0624	112.79	36.384	32.237	4.69	0.07	11.2514	7.16	matrix	Satiman	16
30020-1J	01-SM3	0.1894	0.7636	0.0490	94.50	38.604	40.823	4.98	0.07	10.9448	7.16	matrix	Satiman	22
30020-1K	01-SM3	-0.1312	-0.9161	-0.0450	-92.69	-53.968	58.270	-6.98	19.77	-4.7050	7.16	matrix	Satiman	29
30020-1L	01-SM3	0.0891	0.5759	0.0334	71.44	45.178	63.205	5.83	0.12	3.8481	7.16	matrix	Satiman	35
30021-1A	03-SM3	0.9931	-29.2394	4.2871	-0.96	-288.615	30931.6	-37.67	37.00	-0.0044	7.16	nepheline	Satiman	2.2
30021-1B	03-SM3	0.4644	128.2018	1.8822	0.27	-143.513	-47062	-18.63	3.29	0.0408	7.16	nepheline	Satiman	3.2
30021-1C	03-SM3	-0.0464	-86.0649	0.1581	0.17	6.788	4247.7	0.88	0.86	-0.0088	7.16	nepheline	Satiman	4.2
30021-1D	03-SM3	0.1766	-0.0272	0.0472	94.85	42.660	44.977	5.50	0.20	2.2931	7.16	nepheline	Satiman	6.5
30021-1E	03-SM3	0.0764	0.0352	0.0281	65.96	43.389	65.776	5.60	0.11	2.6875	7.16	nepheline	Satiman	8
30021-1F	03-SM3	0.0610	-0.0137	0.0253	70.22	52.178	74.308	6.73	0.10	5.2230	7.16	nepheline	Satiman	10
30021-1G	03-SM3	0.0428	-0.1049	0.0211	65.34	52.681	80.633	6.79	0.08	7.6350	7.16	nepheline	Satiman	12
30021-1H	03-SM3	0.0286	0.0127	0.0183	53.95	45.486	84.315	5.87	0.06	3.2502	7.16	nepheline	Satiman	14
30021-1I	03-SM3	0.0247	0.1238	0.0160	50.21	42.925	85.488	5.54	0.07	1.2703	7.16	nepheline	Satiman	16
30021-1J	03-SM3	0.0227	0.0107	0.0169	54.11	47.405	87.616	6.11	0.06	3.7860	7.16	nepheline	Satiman	19
30021-1K	03-SM3	0.0203	0.0199	0.0164	56.91	50.912	89.468	6.56	0.06	4.3051	7.16	nepheline	Satiman	24
30226-1A	01-SM5	1.3354	0.3886	0.3160	438.49	43.923	10.014	14.46	1.10	0.1276	18.32	matrix	Satiman	2
30226-1B	01-SM5	0.5448	0.2099	0.1339	174.78	13.802	7.895	4.56	0.14	1.7481	18.32	matrix	Satiman	4
30226-1C	01-SM5	0.1541	0.1438	0.0597	58.32	12.814	21.968	4.23	0.05	4.0621	18.32	matrix	Satiman	6
30226-1D	01-SM5	0.0581	0.1304	0.0428	32.80	15.633	47.652	5.16	0.03	3.5826	18.32	matrix	Satiman	8
30226-1E	01-SM5	0.0365	0.1714	0.0366	24.15	13.364	55.342	4.41	0.02	5.4073	18.32	matrix	Satiman	10
30226-1F	01-SM5	0.0185	0.3375	0.0305	17.39	11.952	68.694	3.95	0.03	5.8726	18.32	matrix	Satiman	12
30226-1G	01-SM5	0.0200	1.1164	0.0289	18.62	12.796	68.655	4.22	0.02	5.2830	18.32	matrix	Satiman	14
30226-1H	01-SM5	0.0232	3.1399	0.0263	19.51	12.937	66.110	4.27	0.02	3.6080	18.32	matrix	Satiman	17
30226-1I	01-SM5	0.0120	2.9824	0.0208	15.80	12.513	78.991	4.13	0.02	1.6297	18.32	matrix	Satiman	21

Appendix 2: continued

Lab-Id	Sample Id	$^{36}Ar/^{39}Ar$	$^{37}Ar/^{39}Ar$	$^{38}Ar/^{39}Ar$	$^{40}Ar/^{39}Ar$	$^{40}Ar^{*}/^{39}Ar$	$\%^{40}Ar^{*}$	Age (Ma)	Age Error	^{39}Ar Moles E-16	JE-5	Material	Locality	Power (W)
30226-1J	01-SM5	0.0107	3.0444	0.0191	15.56	12.670	81.207	4.18	0.02	1.2523	18.32	matrix	Satiman	26
30226-1K	01-SM5	0.0063	2.1312	0.0174	14.35	12.684	88.228	4.19	0.03	1.0682	18.32	matrix	Satiman	32
30226-1L	01-SM5	0.0174	3.2185	0.0192	17.35	12.476	71.719	4.12	0.03	1.1019	18.32	matrix	Satiman	40
30023-1A	01-SM5	1.1097	0.7982	0.2119	326.21	-1.661	-0.509	-0.21	0.45	0.0502	7.16	nepheline	Satiman	2.2
30023-1B	01-SM5	0.3186	0.4470	0.0682	125.78	31.690	25.184	4.09	0.09	0.5266	7.16	nepheline	Satiman	4
30023-1C	01-SM5	0.2503	-0.2522	0.0503	112.50	38.515	34.243	4.97	0.17	0.2156	7.16	nepheline	Satiman	5.5
30023-1D	01-SM5	0.1093	0.2741	0.0324	69.80	37.518	53.739	4.84	0.16	0.6235	7.16	nepheline	Satiman	6.5
30023-1E	01-SM5	0.1480	0.1515	0.0414	92.77	49.053	52.868	6.33	0.18	1.6969	7.16	nepheline	Satiman	8
30023-1F	01-SM5	0.0309	0.0418	0.0188	49.49	40.355	81.547	5.21	0.06	6.1945	7.16	nepheline	Satiman	10
30023-1G	01-SM5	0.0155	0.0534	0.0146	43.30	38.717	89.420	4.99	0.05	4.6084	7.16	nepheline	Satiman	12
30023-1H	01-SM5	0.0310	0.0535	0.0183	48.02	38.855	80.914	5.01	0.06	4.7956	7.16	nepheline	Satiman	14
30023-1I	01-SM5	0.0090	0.0429	0.0148	37.41	34.744	92.882	4.48	0.04	2.2846	7.16	nepheline	Satiman	16
30023-1J	01-SM5	0.0105	0.1057	0.0147	38.33	35.254	91.958	4.55	0.05	1.6847	7.16	nepheline	Satiman	19
30023-1K	01-SM5	0.0101	0.1918	0.0136	37.43	34.455	92.038	4.45	0.04	1.7813	7.16	nepheline	Satiman	24

REFERENCES

Adelsberger, K., Wirth, K. and Mabula, A. 2002. Provenance of Middle Stone Age tools of the Laetoli archaeological site, Tanzania. *Geological Society of America (GSA),* Abstract with programs 34, 51-7.

Allègre, C. J., Staudacher, T., and Sarda, P., 1987. Rare gas systematics: formation of the atmosphere, evolution and structure of the Earth's mantle. Earth and Planetary Science Letters 81, 127-150.

Ashley, G., 2000. Geologists Probe Hominid Environments, GSA Today, Geological society of America, 10, 24-29.

Ashley, G. and Driese, S., 2000. Paleopedology and paleohydrology of a volcaniclastic paleosol interval: implication for Early Pleistocene stratigraphy and paleoclimate record, Olduvai Gorge, Tanzania. Journal of Sedimentary Research 70, 1065-1080.

Ashley, G. M. and Hay, R. L., 2002. Sedimentation patterns in an early Plio-Pleistocene volcaniclastic rift-platform basin, Olduvai Gorge, Tanzania. In: R. W. Renaut and G. M. Ashley (ed.) Continental Rift Sedimentation SEPM Special Publication 73, 107-122.

Aulbach, S., Rudnick, R. L., and McDonough, W. F., (in review). Li-Sr-Nd isotope signatures of the plume and cratonic lithospheric mantle beneath the margin of the rifted Tanzanian Craton (Labait). Contributions to Mineralogy and Petrology

Bagdasaryan, G. P., Gerasimovskiy, V. I., Polyakov, A. I. and Gukasyan. R. Kh., (1973). Age of volcanic rocks in the rift zones of East Africa. Geochemistry International, 10, 66-71.

Baker, B. H., 1987. Outline of the petrology of the Kenya rift alkaline province. In J. G. Fitton and B. G. J. Upton (eds.), *Alkaline Igneous Rocks*. Geological Society (London) Special Publication 30, 293-311.

Baker, B. H. and Wohlenberg, J., 1971. Structure and evolution of the Kenya Rift Valley. Nature 229, 538-541.

Baker, B. H., Willims, L. A., Miller, J. A. and Fitch, F. J., 1971. Sequence and geochronology of the Kenya rift volcanics. Tectonics 11, 191-215.

Baker, M. B. and Stolper E. M., 1994. Determining the composition of high-pressure mantle melts using diamond aggregates. Geochimica et Cosmochimica Acta 58, 2811-2827.

Basu, A., Junwen, W., Wankang, H., Guanghong, X. and Tatsumoto, M., 1991. Major, elements, REE, and Pb, Nd and Sr isotopic geochemistry of Cenozoic volcanic rocks of eastern China: implications for their origin from suboceanic-type mantle reservoirs. Earth and Planetary Science Letters 105, 149-169.

Bedini, R. M., Bodinier, J. -L., Dautria, J. -M. and Morten, L., 1997. Evolution of LILE-enriched small melt fractions in the lithospheric mantle: a case study from the East African Rift. Earth and Planetary Science Letters 153, 67-83.

Bell, K. and Simonetti, A., 1996. Carbonatite magmatism and plume activity: Implications from the Nd, Pb and Sr isotope systematics of Oldoinyo Lengai. Journal of Petrology, 37(6): 1321-1339.

Bell, K. and Tilton, G., 2001. Nd, Pb and Sr isotopic compositions of East African Carbonatites: Evidence for mantle mixing and plume inhomogeneity. Journal of

Petrology 42, 1927-1945.
Beloussov, V. V., 1966. Modern concepts of the structure and development of the earth's crust and upper mantle of continents. Journal of Geological Society, London 122, 293 - 314.
Berhe, S. M., Desta, B., Nicoletti, M. and Teferra, M., 1987. Geology, geochronology and geodynamic of Cenozoic magmatic province in W and SE Ethiopia. Journal of Geological Society of London 144, 213-226.
Bevington, P. R., 1969. Data Reduction and Error analysis for Physical Sciences. McGraw-Hill, New York.
Bizimis M., Salters, V. J. M. and Dawson, B. D., 2003. The brevity of carbonatite source in the mantle: evidence from Hf isotope. Contributions to Mineralogy and Petrology 145, 281-300.
Blumenschine, R. and Masao, F., 1991. Living sites at Olduvai Gorge, Tanzania? Preliminary landscape archaeology results in the basal Bed II lake margin zone. Journal of Human Evolution, 21, 451-462.
Blumenschine, R. and Peters, C., 1998. Archaeological predictions for hominid land use in the paleo-Olduvai Basin, Tanzania, during lower most bed II times: Journal of Human Evolution 34, 565-607.
Blumenschine, R., Peters, C., Masao, F., Clarke, R., Deino, A., Hay, R., Swisher, C., Stanistreet, I., Ashley, G., McHenry, L., Sikes, N., Van Der Merwe, N., Tactikos, J., Cushing, A., Deocampo, D., Njau, J. and Ebert, J., 2003. Late Pliocene *homo* and hominid land use from western Olduvai Gorge, Tanzania. Science 299, 1217-1221.
Bolge, L., Carr, M. J., Feigenson, M., and Alvarado, G., 2006. Geochemical stratigraphy and magmatic evolution at Arenal volcano, Costa Rica. Journal of Volcanology and Geothermal Research 157, 34-48.
Briquet, L. and Lancelot, J. R., 1979. Rb-Sr systematics and crustal contamination models for calc-alkaline igneous rocks. Earth and Planetary Sciences Letters 43, 385-496.
Burke, K., 1996. The African plate. South African Journal of Geology 99, 339-410.
Cahen, L., Snelling, J. J., Delhal, J., and Vail, J. R., 1984. The Geochronology and Evolution of Africa. Clarendon, Oxford.
Cande, S. C. and Kent, D. V., 1995. Revised calibration of the geomagnetic polarity time scale for the Late Cretaceous and Cenozoic. Journal of Geophysical Research, 100, 6093-6095.
Carlson, R. W., Lugmair, G. W. and MacDougall, J. D., 1981. Columbia River volcanism: the question of mantle heterogeneity or crustal contamination. Geochemical et Cosmochimica Acta 45, 2483-2499
Carr, M. J., Saginor, I., Alvarado, G. E., Bolge, L. L., Lindsay, F. N., Milidakis, K., Turrin, B., Feigenson M. D., and Swisher III, C. C., (2007). Element Fluxes from the Volcanic Front of Nicaragua and Costa Rica. Journal of Geochemistry, Geophysics, Geosystems 8, Q06001, doi:10.1029/2006GC001396.
Class, C. and Goldstein, S. L., 1997. Plume-lithospheric interaction in ocean basins: constraints from the source mineralogy. Earth and Planetary Science Letters 150, 245-260.
Class, C., Altherr, R., Volker, F., Eberz, G., and McCulloch, M., 1994. Geochemistry of

Pliocene to Quaternary alkali basalts from the Huri Hills, northern Kenya. Chemical Geology 113, 1-22.

Cohen, R. S., O'Nions, R. K. and Dawson, J. B., 1984. Isotope geochemistry of xenoliths from East Africa: implications for development of mantle reservoirs and the interaction. Earth and Planetary Science Letters, 68**,** 209-220.

Craig, H., 1990. Helium isotope distribution in mantle hotspots. EOS, Transactions American Geophysical Union 71, 1669.

Criss, J. W., 1980. Fundamental parameters calculations on a laboratory microcomputer. Advances in X-ray Analysis 23, 93-97

Coulié, E., Quidelleur, X., Gillot, P. -Y., Courtillot, V., Lefèvre, J. -C. and Chiesa, S., 2003. Comparative K-Ar and Ar/Ar dating of Ethiopia and Yemenite Oligocene volcanism: implication for timing and duration of the Ethiopian traps. Earth and Planetary Science Letters 206, 477-492.

Courtillot, V., Achache, J., Landre, F., Bonhommet, N., Montigny, R. and Féraud, G., 1984. Episodic spreading and rift propagation: new paleomagnetic and geochronologic data from the Afar nascent passive margin. Journal of Geophysical Research 89, 3315-3333.

Cox, A., 1969. Geomagnetic reversals. Science 163, 237-245.

Cox, K. G., Bell, J. D., and Pankhurst, R. J., 1979. *The Interpretation of the Igneous Rocks*. Allen and Unwin, London.

Curtis, G. H. and Hay, R. L., 1972. Further geological studies and potassium-argon dating at Olduvai Gorge and Ngorongoro Crater. In: W. W. Bishop and J. A. Miller (Ed.), Calibration of Hominoid Evolution. Scottish Academic Press: Edinburgh.

Dana, E. S. 1892. Dana's systems of mineralogy, (6th edition) 403-404.

Davidson, A., and Rex, D., 1980. Age of volcanism and rifting in southern Ethiopia, Nature 283, 657-658.

Dasgupta, R. and Hirschmann, M. M., 2006. melting in the earth's deep upper mantle caused by carbon dioxide. Nature 440, 659-662.

Dasgupta, R., Hirschmann, M. M., and Smith, N. D., (in review). High pressure partial melting experiments of peridotite + CO_2 and genesis of alkalic oceanic island basalts. Journal of Petrology.

Dawson, J. B., 1962. The geology of Oldoinyo Lengai. Bulletin of Volcanology 24, 349-387.

Dawson, J. B., 1992. Neogene tectonics and volcanicity in the North Tanzania sector of the Gregory Rift Valley: contrasts with the Kenya sector. Tectonophysics 204, 81-92.

Dawson, J. B., 2002. Metasomatism and partial melting in upper-mantle peridotite xenoliths from the Lashaine volcano, northern Tanzania. Journal of Petrology 43, 1749-1777.

Dawson, J. B. and Smith, J. V., 1988. Metasomatised and veined upper-mantle xenoliths from Pello Hill, Tanzania: evidence for anomalously-light mantle beneath the Tanzanian sector of the East African Rift Valley. Contributions to Mineralogy and Petrology 100, 510-527.

Dawson, J. B., Smith, J. V. and Steele, I. M., 1995. Petrology and mineral chemistry of plutonic igneous xenoliths from the carbonatite volcano, Oldoinyo Lengai, Tanzania. Journal of Petrology 36, 797-826.

Day, M. H., Leakey, M. D. and Magori, C., 1980. A new hominid fossil skull (L. H. 18) from the Ngaloba Beds, Laetoli, northern Tanzania. Nature 284, 55-56.

Deer, W. A., Howie, R. A. and Zussman, J., 1992. An Introduction to Rock-forming Minerals: 2nd ed. Pearson Education Limited, Harlow, London.

Deino, A. L., McBrearty, S., 2002. $^{40}Ar/^{39}Ar$ dating of the Kapthurin Formation, Baringo, Kenya. Journal of Human Evolution 42, 185-210.

Delaney, J. S., Carswell, D. A., and Dawson, J. B., 1980. Chemistry of micas from kimberlites and xenoliths. Primary- and secondary-textured micas from peridotite xenoliths. Geochimica et Cosmochimica Acta 44, 857-872.

Deniel, C., Vidal, P., Coulon, C., Vellutini, P. –J. and Piguet, P., 1994. Temporal evolution of mantle sources during continental rifting: the volcanism of Djibouti (Afar). Journal of Geophysical Research 99, 2853-2869.

Deocampo, D., Blumenschine, R. and Ashley, G., 2002. Wetland diagenesis and trace of early hominids, Olduvai Gorge, Tanzania. Journal of Quaternary Research 57, 271-281.

Depaolo, D. J, 1981. Trace elements and isotopic effects of combined wall-rock assimilation and fractional crystallization. Earth and Planetary Science Letter 53, 189-202.

Devies, G. R. and Macdonald, R., 1987. Crustal influences in the petrogenesis of the Naivasha basalt-rhyolite complex: combined trace element and Sr-Nd-Pb isotope constraints. Journal of Petrology 28, 1009-1031.

Dickin, A. P., 1995. Radiogenic Isotope Geology. Cambridge University Press: Cambridge.

Donovan, J. D. and Rivers, M. L., 1990. PRSUPR: A PC-Based automation and analysis software for wavelength dispersive electron electron-beam microanalysis, In: J. R. Michael and P. Ingram (ed.) *Microbeam Analysis,* San Francisco Press.

Drake, R. and Curtis, G., (1987). K – Ar Geochronology of the Laetoli fossil localities. In: M.D. Leakey and J.M. Harris (Ed.) *Laetoli a Pliocene site in northern Tanzania*. Clarendon Press. Oxford.

Ebinger, C. J. and Sleep, N. H., 1998. Cenozoic magmatism throughout east Africa resulting from impact of a single plume. Nature 395, 788-791.

Ebinger, C. J., Bechtel, T. D., Forsyth, D. W. and Bowin, C. O., 1989. Effective elastic plastic thickness beneath the East African and Afar plates and dynamic compensation of the uplift. Journal Geophysical Research 94, 2883-2901.

Ebinger, C., Djomani, Y. P., Mbede, E., Foster, A. and Dawson, J. B., 1997. Rifting Archean lithosphere: the Eyasi-Manyara-Natron rifts, East Africa. Journal of Geological Society London 154, 947-960.

Ebinger, C. J., Jackson, J. A., Foster, A. N. and Hayward, N. J., 1999. Extensional basin geometry and the elastic lithosphere. Philosophical Transactions -Royal Society. Mathematical, Physical and Engineering Sciences 357, 741-765.

Ebinger, C. J., Yemane. T., Harding, D. J., Tesfaye, S., Kelley, S. and Rex, D. C., 2000. Rift deflection, migration, and propagation: Linkage of the Ethiopia and Eastern rifts, Africa. Geological Society of America Bulletin 112, 163-176.

Eggins, S. M, Woodhead, J. D, Kinsley, L. P. J, Sylvester, P., McCulloch, M. T., Hergt, J. M., and Handler, M. R., 1997. A simple method for the precise determination of 40 or more trace elements in geological samples by ICPMS using enriched isotope internal standardization. Geochemical Geology 134, 311-326.

Evernden, J. F. and Curtis, G. H., 1965. The potassium-argon dating of late Cenozoic rocks in East Africa and Italy. Current Anthropology 6, 343-364.

Fairhead, J. D., 1980. The structure of the cross-cutting volcanic chain of northern Tanzania and its relation to the East African rift system. Tectonophysics 65, 193-208.

Falloon, T. J. and Green, D. H., 1989. The solidus of carbonated, fertile peridotite. Earth and Planetary Science Letters 94, 364-370.

Foster, A., Ebinger, C., Mbede, E., Rex, D., 1997. Tectonic development of the northern Tanzanian sector of the East African Rift system. Journal of the Geological Society, London 154, 689-700.

Franz, G., Steiner, G., Volker, F., Pudlo, D. and Hammerschmidt, K., 1999. Plume related alkaline magmatism in Central Africa-the Meidob Hills (W. Sudan). Geochemical Geology 157, 27-47.

Foley, S., 1991. High-pressure stability of the fluoro-and hydroxyl- endmembers of pargasite and K-richterite. Geochimica et Cosmochimica Acta 55, 2689-2694.

Furman, T., 1995. Melting of metasomatized subcontinental lithosphere: undersaturated mafic lavas from Rungwe, Tanzania. Contributions to Mineralogy and Petrology 122, 97-115.

Furman, T., 2007. Geochemistry of East African Rift Basalts: An overview. Journal of African Earth Sciences. doi:10.1016/j.jafrearsci.2006.06.009.

Furman, T. and Grahams, D., 1999. Erosion of the lithospheric mantle beneath the east African rift system: evidence from the Kivu volcanic province. LITHOS 48, 237-262.

Furman, T., Bryce, J., Karson, J., and Iotti, A., 2004. East African Rift System (EARS) plume structure: Insights from Quaternary Mafic lavas from Turkana, Kenya. Journal of Petrology 45, 1069-1088.

Furman, T., Kaleta, K. M., Bryce, J. G., and Hanan, B. B., 2006. Tertiary mafic lavas of Turkana, Kenya: constraints on the East African plume structure and the occurrence of high-μ volcanism in Africa. Journal of Petrology 47, 1221-1244.

George, R., Rogers, N. and Kelley, S., 1998. Earliest magmatism in Ethiopia: Evidence for two mantle plumes in one flood basalt province. Geology 26, 923-926.

Girdler, R. W. and McConnell, D. A., 1994. The 1990 to 1991 Sudan earthquake sequence and the extent of the East African Rift. Science 264, 67-70.

Gladney, E. S., Jones, E. A., and Nickell, E. J., 1988. Compilation of elemental concentration data for USGS AGV-1, GSP-1 and G-2. Geostandards Newsletter 16, 111-300.

Grand, S. P., Van der Hilst, R. D. and Widiyantoro, S., 1997. Global seismic tomography: a snapshot of convection in Earth. GSA Today **7**, 1-7.

Grommé, C. S. and Hay, R. L. 1963. Magnetization of basalt in Bed I, Olduvai Gorge. Nature 200, 560-561.

Grommé, C. S. and Hay, R. L. 1967. Geomagnetic polarity epochs: New data from Olduvai Gorge. Earth and Planetary Science Letters 2, 111-115.

Grommé, C. S., Reilley, T. A., Mussett, A. E and Hay, R. L., 1970. Paleomagnetism and Potassium-Argon Ages of Volcanic Rocks of Ngorongoro Caldera, Tanzania. Geophysical Journal Royal Astronomical Society 22, 101-115.

Grommé, C. S. and Hay, R. L. 1971. Geomagnetic polarity epochs: Age and duration of the Olduvai normal polarity events. Earth and Planetary Science Letters 10, 179-185.

Guest, N. J., James, T. C., Pickering, R. and Dawson, J. B., 1961. Angata Salei. Geological Survey of Tanzania, Quarter Degree Sheet 39, scale 1:125,000.

Halliday, A. N., Dickin, A. P., Fallick, A. E. and Fitton, J. G., 1988. Mantle dynamics: a Nd, Sr, Pb and O isotopic study of the Cameroon line volcanic chain. Journal of Petrology 29, 181-211.

Hannah, R. S., Vogel, T. A., Patino, L. C., Alvarado, G. E., Pérez, W. and Smith, D. R., 2002. Origin of silicic volcanic rocks in Central Costa Rica: a study of a chemically variable ash-flow sheet in the Tiribí Tuff. Bulletin of Volcanology 64, 117-133.

Hart, S. R., 1984. A large-scale isotope anomaly in the southern hemisphere mantle. Nature 309, 753 -757.

Hart, S. R., Gerlach, D. C. and White W. M., 1986. A possible new Sr-Nd-Pb mantle array and consequences for mantle mixing. Geochimica et Cosmochimica Acta 50, 1551-1557.

Hart, S. R., Hauri, E. H., Oschmann, L. A., and Whitehead, J. A., 1992. Mantle plumes and entrainment: Isotopic evidence. Science 256, 517-520.

Hawkesworth, C. J., Roger, N. W., van Calsteren, P. W. C. and Menzies, M. A., 1984. Mantle enrichment processes. Nature 311, 331-335.

Hay, R. L, 1976. Geology of the Olduvai Gorge*: A study of sedimentation in a semi-arid basin*. University of California Press: Berkeley.

Hay, R. L., 1983. Natrocarbonatite tephra of Kerimasi volcano, Tanzania. Geology 11, 599-602.

Hay, R. L., 1987. Geology of Laetoli area, In: M. D. Leakey and J. M. Harris (Ed) *Laetoli a Pliocene Site in Northern Tanzania*. Oxford: Clarendon Press.

Hay, R. L., 1989. Holocene carbonatite-nephelinite tephra deposits of Oldoinyo Lengai, Tanzania. Journal of Volcanology and Geothermal Research 37, 77-91.

Hay, R. L., 1992. Potassium-Argon dating of bed I, Olduvai Gorge, 1961-1972. Quaternary International 13/14, 31-36.

Hay, R. L. and Kyser, T. K., 2001. Chemical sedimentology and paleoenvironmental history of Lake Olduvai, a Pliocene lake in northern Tanzania. Geological Society of America Bulletin, 113, 1505-1521.

Hay, D. E. and Wendlandt, R. F., 1995. Origin of Kenya Rift Plateau-type flood phonolites: Integrated petrologic and geophysical constraints on the evolution of the crust and upper mantle beneath the Kenya Rift. Journal of Geophysical Research 100, 10549-10557.

Herzberg, C. 2004. Geodynamic information in peridotite petrology. Journal of Petrology 45, 2507-2530.

Herzberg, C., 2006a. Distribution and size of pyroxenite bodies in mantle. *EOS* Transaction American Geophysical Union 87, Fall Meeting, Abstract.

Herzberg, C., 2006b. Petrology and thermal structure of the Hawaiian plume from Mauna Kea volcano. Nature 444, 605-609.

Herzberg, C. and O'Hara, M. J., 2002. Plume-associated ultramafic magmas of Phanerozoic age. Journal of Petrology 43, 1857-1883.

Herzberg, C., Asimow, P. D., Arndt, N., Niu, Y., Lesher, C. M., Fitton, J. G., Cheadle, M. J., Saunders, A. D., 2007. Temperatures in ambient mantle and plumes: constraints from basalts, picrites and komatiites. Geochemistry Geophysics Geosystems 8, 1- 34.

Hilton, D. R., Gronvold, K., Sveinbjornsdottir, A. E., and Hammerschmidt, K., 1998. Helium isotope evidence for off-axis degassing of the Icelandic hotspot. Chemical Geology 149, 173-187.

Hirose, K., 1997. Partial melt compositions of carbonated peridotite at 3 GPa and genesis of alkali basalt magmas. Geophysical Research Letters 24, 2837-2840.

Hirose, K. and Kushiro, I., 1993. Partial melting of dry peridotites at high pressures: determination of compositions of melts segregated from peridotite using aggregates of diamond. Earth and Planetary Science Letters 24, 2837-2840.

Hofmann, C., Courtillot, C., Féraud, G., Rochette, P., Yirgu, G., Ketefo, E. and Pik, R., 1997. Timing of the Ethiopian flood basalt event and implication for plume birth and global change. Nature 389, 838-841.

Huppert, H. E. and Sparks, R. S. J., 1985. Cooling and contamination of mafic and ultramafic magma during ascent through continental crust. Earth and Planetary Science Letters 74, 371-386.

Illies, J. H., 1981. Mechanism of graben formation. Tectonophysics 73, 249-266.

Isaac, G. L, Curtis, G. H., 1974. Age of early Acheulian industries from the Peninj Group, Tanzania. Nature 249, 624-627.

Johnson, D. C. and White, T. D., 1979. A systematic assessment of early African hominids. Science 203, 321-330.

Johnson, J. S., Gibson, S. A., Thompson, R. N., and Nowell, G. M., 2005. Volcanism in the Vitim volcanic field, Siberia: Geochemical evidence for a mantle plume beneath the Baikal rift zone. Journal of Petrology 46, 1309-1344.

Jones, A. P., Smith, J. V., Hansen, E. C., and Dawson, B. D., 1983. Metamorphism, partial melting and K-metasomatism of garnet-scapolite-kyanite granulite xenoliths from Lashaine, Tanzania. Journal of Geology 91, 143-165.

Julià, J., Ammon, C. J. and Nyblade, A. A., 2005. Evidence for mafic lower crust in Tanzania, East Africa, from joint inversion of receiver functions and Rayleigh wave dispersion velocities. Geophysical Journal International 162, 555-569.

Kalt, A., Hegner, E., and Satir, M., 1997. Nd, Sr, and Pb isotopic evidence for diverse lithospheric mantle sources of East African Rift carbonatites. Tectonics 278, 31-45.

Kampunzu, A. B. and Mohr, P., 1991. Magmatic evolution and petrogenesis in the East African Rift System. In: A.B. Kampunzu and R.T. Lubala (ed.), *Magmatism in Extensional Structural Settings, the Phanerozoic African Plate*. Springer-Verlag, Berlin.

Kawamoto, T. and Holloway, J. R., 1997. Melting temperature and partial melt chemistry of H_2O saturated mantle peridotite to 11 gigapascals. Science 276, 240-243.

Keen, C. E., 1985. The dynamics of rifting and deformation of lithosphere by active and passive driving forces. Geophysical Journal of the Royal Astronomical Society 80, 95 – 120.

Kelemen, P. B., Yogodzinski, G. M. and Scholl, D. W., (in review). Along-strike variation in lavas of the Aleutian island arc: Implications for the genesis of high Mg# andesite and the continental crust, In: J. Eiler (Ed.), AGU Monograph Series.

Keller, J., Zaitsev, A. N. and Wiedenmann, D., 2006. Primary magmas at Oldoinyo Lengai: The role of olivine melilitites. LITHOS 91, 150-172.

Key, R., Charsley, T., Hackman, B., Wilkinson, A., and Rundle, C., 1989. Superimposed Upper Proterozoic collision-controlled orogenies in the Mozambican Orogenic Belt of Kenya. Precambrian Research 44, 197-225.

King, B. C., 1978. Structure and volcanic evolution of the Gregory Rift Valley. In: Bishop, W. W. (Ed.) *Geological Background to Fossil Man*. Scottish Academic Press, Edinburgh, pp. 29-54.

King, S. D. and Ritsema, J., 2000. African hot spot volcanism: small-scale convection in the upper mantle beneath cratons. Science 290, 1137-1140.

Klaudius, J. and Keller, J., 2006. Peralkaline silicate lavas at Oldoinyo Lengai, Tanzania. LITHOS 91, 173-190.

Koenigswald, G. H., Von Genter, W. and Lippolt, H. J., 1961. Age of the basalt flow at Olduvai, East Africa. Nature 192, 720-721

Kushiro, I., 1996. Partial melting of a fertile mantle peridotite at high pressures: An experimental study using aggregates of diamond. In: Basu, A. and Hart, S. (Ed.) *Earth Process: Reading the Isotope Code*. Washington, DC: American Geophysical Union, 109-122.

Leakey, L. S. B., 1958. Recent discoveries at Olduvai Gorge, Tanganyika. Nature 181, 1099-1103.

Leakey, L. S. B., Curtis, G. H. and Evernden, J. F., 1962. Age of basalt underlying Bed I, Olduvai. Nature 194, 610-612.

Leakey, M., 1971. *Olduvai Gorge: excavations in Beds I and II; 1960-1963*. Cambridge University Press: Cambridge, UK.

Leakey, M. D., Hay, R. L., Curtis, G. H., Drake, R. E., Jackes, M. K., and White, T. D., 1976. Fossil hominids from the Laetolil Beds. Nature 262, 460-466.

LeBas, M. J., LeMaitre, R. W., Streckeisen, A. and Zanettin, B., 1986. A chemical classification of volcanic rocks based on the total alkali-silica diagram. Journal of Petrology 27, 745-750.

Lee, C.-T. and Rudnick, R.L., 1999. Compositionally stratified cratonic lithosphere: petrology and geochemistry of peridotite xenoliths from the Labait tuff cone, Tanzania, In: Gurney, J. J., Gurney, J. L., Pascoe, M. D. and Richardson, S. H., (Ed.) *The Nixon Volume, Proc. Seventh Int. Kimberlite Conf*. pp. 503-521.

Le Roex, A. P., Späth, A., Zartman, R. E., 2001. Lithospheric thickness beneath the southern Kenya rift: implication from basalt geochemistry. Contributions to Mineralogy and Petrology 142, 89-106.

Lippard, S. J., 1973. The petrology of phonolites from the Kenyan rift. LITHOS International Journal of Mineralogy, Petrology and Geochemistry 6, 217-234.

Lithgow-Bertelloni, C., and Silver, P. G., 1998. Dynamic topography, plate driving forces and the African superswell. Nature 395, 269-272.

Liutkus, C. M. and Ashley, G. M., 2003. Facies model of a semiarid freshwater wetland, Olduvai Gorge, Tanzania: Journal of Sedimentary Research 5.

Lloyd, F. E., Huntingdon, A. T., Davies, G. R., Nixon, P. H., 1991. Phanerozoic volcanism of southwestern Uganda: a case for regional K and LILE enrichment of the lithosphere beneath a domed and rifted continental plate. In: Kampunzu A. B. and Lubala, R. T (eds) Magmatism in externsional structural settings: the Pharenozoic African plate. Springer, Berlin, Heidelberg, New York, pp 23-72.

Maboko, M. A. H., 2000. Nd and Sr isotopic investigation of the Archean-Proterozoic boundary in north eastern Tanzania: constraints on the nature of Neoproterozoic tectonism in the Mozambique Belt. Precambrian Research 102, 87-98.

Maboko, M. A. H., Boelrijk, N. A. I. M., Prien, H. N. A., Verdurmen, E. A. T. H., 1985. Zircon U-Pb and biotite Rb-Sr dating of the Wami River granulites, Eastern granulites, Tanzania: evidence for approximately 715 Ma old granulite facies metamorphism and final Pan African cooling approximately 475 Ma ago. Precambrian Research 30, 361-378.

Manega, P. C., 1993. Geochronology, Geochemistry and Isotopic Study of the Plio-Pleistocene Hominid Sites and the Ngorongoro Volcanic Highlands in Northern Tanzania. Ph.D. Dissertation, University of Colorado, Boulder.

Macdonald, R., Davies, G., Bliss, C., Leat, P., Bailey, D., and Smith, R., 1987. Geochemistry of high-silica peralkaline rhyolite, Naivasha, Kenya Rift Valley. Journal of Petrology 28, 979-1008.

Macdonald, R., Rogers, N. W., Fitton, J. G., Black, S. and Smith, M., 2001. Plume-lithosphere interactions in the generation of the basalts of the Kenya Rift, East Africa. Journal of Petrology 42, 877-900.

Macintyre, R. M., Mitchell, J. G. and Dawson, J. B., 1974. Age of fault movements in Tanzanian sector of East African Rift. Nature 247, 354-356.

Marty, B., Pik, R., and Yirgu G., 1996. Helium isotopic variations in Ethiopian plume lavas: nature of magmatic sources and limit on lower mantle contribution. Earth and Planetary Science Letters 144, 223-237.

Masters, G., Johnson, S., Laske, G., and Bolton, H., 1996. A shear-velocity model of the mantle. Philosophical Transaction Research Association of London A 354, 1385-1411.

McConnell, R. B., 1972. Geological development of the rift system in eastern Africa. Geological Society of America Bulletin 83, 2549-2572

McDougall, I. and Harrison, M., 1999. Geochronology and Thermochronology by the $^{40}Ar/^{39}Ar$ Method. Second edition. Oxford University Press: New York.

McDougall, I. and Watkins, R. T., 2006. Geochronology of the Nabwal Hills: a record of earliest magmatism in the northern Kenyan Rift valley. Geological Magazine 143, 25-39.

McHenry, L. J, 2001. The geochemistry of feldspar, fresh glass, and melt inclusions within feldspar as potential tools for correlating fresh and altered tuff at Olduvai Gorge, Tanzania. American Geophysical Union supplement, Abstracts with programs, 82(47).

McHenry, L. J., 2003. Geochemistry of tephra from Bed I, Olduvai Gorge, Tanzania:

Stratigraphic correlations and implications for magmatic evolution. American Geophysical Union supplement, Abstract 176.

McHenry, L. J., 2004. Characterization and correlation of altered Plio-Pleistocene tephra using a “multiple technique” approach: Case study at Olduvai Gorge Tanzania. Ph.D. dissertation, Rutgers University: New Jersey.

McHenry, L. J., 2005. Phenocryst composition as a tool for correlating fresh and altered tephra, Bed I, Olduvai Gorge, Tanzania. Stratigraphy 2, 101-115

McHenry, L.J., Mollel, G.M., Swisher, C.C. III., (2007).Compositional and textural correlations between Olduvai Gorge Bed I tephra and volcanic sources in the Ngorongoro Volcanic Highlands, Tanzania, Quaternary International, doi:10.1016/j.quaint.2007.01.004.

Mengel, K and Green, D. H., 1989. Stability of amphibole and phlogopite in metasomatized peridotite under water-saturated and water-undersaturated conditions, In: Ross, J. (Ed.) *Proceedings of the 4th International Kimberlite Conference*. Perth: Geological Society of Australia, pp. 571 – 581.

Mertz, D. F., Weinrich, A. J., Sharp, W. D., and Renne, P. R., 2001. Alkaline intrusions in a near-trench setting, Franciscan complex, California: Constrains from geochemistry, petrology and $^{40}Ar/^{39}Ar$ chronology. American Journal of Science 301, 877-911.

Mitchell, J. G., 1968.The $^{40}Ar/^{39}Ar$ method for potassium-argon age determination. Geochimica Cosmochimica Acta 32, 781-790.

Mohr, P., 1982. Musings on continental rifts, In: Palmason, G. (Ed.) *Continental and Oceanic Rifts*. A. G. U., Washington DC., 293 – 309.

Mollel, G., 2002, Petrology and geochemistry of the southeastern Ngorongoro Volcanic Highland (NVH); and contribution to “sourcing” of stone tools at Olduvai Gorge, Tanzania. Masters Thesis, Rutgers University: New Jersey.

Mollel, G. F., Swisher, C. C., McHenry, L. J., and Feigenson, M.D., 2005. Geochronology and Geochemistry of lavas from Olmoti Crater, Tanzania: Implications for Olduvai Bed I Tephra and lava sources. Abstract: Geological Society of America annual meeting, October 2005

Mollel, G. F., Swisher III, C. C., Feigenson, M. D. and Carr, M. J., (in press). Petrology, geochemistry, and age of Satiman, Lemagurut and Oldeani: sources of the volcanic deposits of the Laetoli area. In: T. Harrison (Ed.) *Paleontology and Geology of Laetoli: Human Evolution in Context Volume 1*, Springer, Dordrecht

Möller, A, Mezger, K. and Schenk, V., 1998. Crustal age domains and the evolution of continental crust in Mozambique belt of Tanzania: combined Sm-Nd, Rb-Sr, and Pb-Pb isotopic evidence. Journal of Petrology 39, 749-783.

Montelli, R., Nolet, G., Dahlen, F., Masters, G., Engdahl, E. R., and Hung, S. 2004. Finite-frequence tomography reveals a variety of plumes in the mantle. Science 303, 338 - 348.

Ni, S. and Helmberger, D., 2003. Seismological constrains on the South African superplume; could be the oldest distinct structure on earth. Earth and Planetary Science Letters 206, 119-131.

Nyblade, A. A. and Robinson, S. W., 1994. The African superswell. Geophysical Research Letters 21, 765-768.

Nyblade, A. A. Birt, C., Langston, C. A., Owens, J. T., and Last, R. J., 1996. Seismic experiment reveals rifting of craton in Tanzania. EOS, Transaction American Geophysical Union 77, 517-521.

Nyblade, A. A., Owens, J. T., Gurrola, H., Retsema, J., and Langston, C. A., 2000. Seismic evidence for a deep upper mantle thermal anomaly beneath east Africa. Geology 28, 599-602.

Nyblade, A. A. and Langston, C. A., 2002. Broadband seismic experiments probe the East African Rift. EOS, Transactions, American Geophysical Union, 83, 405, 408-409.

Owens, J. T., Nyblade, A. A. and Langston, C. A., 1995.The Tanzania broadband experiment, IRIS News Letters, XIV, 1.

Owens, J. T., Nyblade, A. A., Gurrola, H. and Langston, C. A., 2000. Mantle transition zone structure beneath Tanzania, East Africa. Geophysical Research Letters 27**,** 827- 830.

Paslick, C., Halliday, A. N., James, D. and Dawson, J. B. 1995. Enrichment of Continental lithosphere by OIB melts: Isotopic evidence from the volcanic province of northern Tanzania. Earth and Planetary Science Letters 130, 109-126.

Paslick, C. and Halliday, A. N., 1996. Indirect crustal contamination: evidence from isotopic and chemical disequilibria in minerals from alkali basalts and nephelines from northern Tanzania. Contributions to Mineralogy and Petrology 125, 277-292.

Peters, C. R. and Blumenschine, R. J. 1996. Landscape perspectives on possible land use patterns for early Pleistocene hominids in the Olduvai basin, Tanzania: Part II, expanding the landscape models. Kaupia 6, 175-221.

Peters, C. and Blumenschine, R., 1995. Landscape perspectives on possible land use patterns for early hominids in the Olduvai Basin. Journal of Human Evolution 29, 321-362.

Pickering, R., 1964. Endulen. *Geological Survey of Tanzania,* Quarter Degree Sheet 52, scale 1:125,000.

Pickering, R., 1965. Ngorongoro. *Geological Survey of Tanzania,* Quarter Degree Sheet 53, scale 1:125,000.

Reene, P. R., Vogel, N., Deino A. L., Sharp, W. D., Becker, T. A., Jaouni, A. R. and Mundil, R., 2005. Alder Creek sanidine (ACs-2): A Quaternary $^{40}Ar/^{39}Ar$ dating standard tied to the Cobb Mountain geomagnetic event. Chemical Geology 218, 315-338.

Ritsema, J., Jan van Heijst, H. and Woodhouse, J. H., 1999. Complex shear wave velocity structure imaged beneath Africa and Iceland. Science 286, 1925-1928.

Renne, P., Swisher III, C., Deino, A., Kamer, D., Owens, T., DePaolo, D., 1998. Intercalibration of standards, absolute ages, and uncertainties in $^{40}Ar/^{39}Ar$ dating. Chemical Geology 145**,** 117 - 152.

Rogers, W. M., James, D., Kelley, S. P. and De Mulder, M, 1998. The generation of potassic lavas from eastern Virunga province, Rwanda. Journal of Petrology 39, 1223-1247.

Rogers, N., Macdonald, R., Fitton, J. G., George, R., Smith, M. and Barreiro, B., 2000. Two mantle plumes beneath the East African rift system: Sr, Nd and Pb isotope evidence from Kenya Rift basalts. Earth and Planetary Science Letters 176,

38-400.
Rudnick, R. L, McDonough, W. D., and Chappell, B. W., 1993. Carbonatite metesomatism in northern Tanzanian mantle: petrographic and geochemical characteristics. Earth and Planetary Science Letters 114, 463-475.
Saito, G., Stimac, J. A., Kawanabe, Y. and Goff, F., 2002. Mafic-felsic magma interaction at Satsuma-Iwojima Volcano, Japan; evidence from mafic inclusion in rhyolite. Earth, Planets and Space 54, 303-325.
Sandiford, M. and Powell, R., 1986. Deep crustal metamorphism during continental extension: modern and ancient examples. Earth and Planetary Science Letters 79, 151-158.
Scaillet, B., and Macdonald, R., 2003. Experimental constraints on the relationships between peralkaline rhyolites of the Kenya Rift Valley. Journal of Petrology 44, 1867-1894.
Scarsi, P. and Craig, H., 1996. Helium isotope ratios in Ethiopian Rift basalts. Earth and Planetary Science Letters 144, 505-516.
Schimitt, A. K., Lindsay, J. M., de Silva, S. and Trumbull, R. B., 2003. U-Pb zircon chronostratigraphy of early Pliocene ignimbrites from La Pacana, North Chile; implications for formation of stratified magma chambers. Journal of Volcanology and Geothermal Research 120, 43 – 53.
Shiraiwa, T., and Fujino, N. J., 1966. Theoretical calculation of fluorescent X-ray intensity in fluorescent x-ray petrochemical analysis Japan. Japanese Journal of Applied Physics 5, 886-892.
Skinner, A. R., Hay, R. L., Masao, F. T. and Blackwell, B. A. B., 2003. Dating the Naisiusiu Beds, Olduvai Gorge, by electron spin resonance. Quaternary Science Reviews 22, 1361-1366.
Slack, P., Davis, P. M. and the KRISP teleseismic working group, 1994. Attenuation and velocity of P-waves in the mantle beneath the East African Rift, Kenya. Tectonophysics 236, 331-358.
Smith, M. and Mosley, P., 1993. Crustal heterogeneity and basement influence on the development of the Kenya Rift, East Africa. Tectonics 12, 591-606.
Sommer, H., Kröner, A., Hauzenberger, C. A., Muhongo, S., Wingate, M. T. D., 2003. Metamorphic petrology and zircon geochronology of high-grade rocks from the central Mozambique Belt of Tanzania; crustal recycling of Archean and Paleoproterozoic materials during the Pan-African Orogeny. Journal of Metamorphic Geology 21, 915-934.
Späth, A., le Roex, A. P. and Duncan, A. R. 1996. The geochemistry of lavas from the Comores Archipelago, western Indian Ocean: petrogenesis and mantle source region characteristics. Journal of Petrology 37, 961-991.
Späth, A., le Roex, A., and Opiyo-Akech, N., 2001. Plume-Lithosphere interaction and the origin of continental rift-related alkaline volcanism-the Chyulu Hills Volcanic Province, southern Kenya. Journal of Petrology 42, 765-787.
Stern, R. J., 1994. Arc assembly and continental collision in the Neoproterozoic East African Orogen: Implication for consolidation of Gondwanaland Annual Reviews of Earth and Planetary Science Letters 22, 319-351.
Stewart, K. S. and Rogers, N. W., 1996. Mantle plume and lithosphere contributions to basalts from southern Ethiopia. Earth and Planetary Science Letters 139, 195-211.

Sun, S,-s. and McDonough, W. F., 1989. Chemical and isotopic systematics of oceanic basalts: Implications for mantle compositions and processes. In: A. D. Sauders and M. J. Norry (Ed.) Magmatism in the Oceanic Basins, Geological Society Special Publication 42, 313-345.

Takahashi, E., 1986. Melting of dry peridotite KLB-1 up to 14 GPa: Implications on the origin of peridotitic upper mantle. Journal of Geophysical Research 91, 9367-9382.

Takahashi, E. and Kushiro, I., 1983. Melting of dry peridotite at high pressures and basalt magma genesis. American Mineralogist 68, 859-879.

Tamrat, E., Thouveny, N., Taïeb, M., and Opdyke, N. D., 1995. Revised magnetostratigraphy of the Plio-Pleistocene sedimentary sequence of the Olduvai formation, Tanzania. Palaeogeography, Palaeoclimatology, Palaeoecology 114, 273-283.

Tatsumoto, M., Basu, A., Wangkang, H., Junwen, W. and Guanghong, X., 1992. Sr, Nd, and Pb isotopes of ultramafic xenoliths in volcanic rocks of Eastern China: enriched components EMI and EMII in subcontinental lithosphere. Earth and Planetary Science Letters 113, 107-128.

Thibault, Y., Edgar, A. D., and Llody, F. E., 1992. Experimental investigation of melts from a carbonated phlogopite lherzolites: implication for metasomatism in the continental lithosphere. American Mineralogy 77, 784-794.

Thirlwall, M. F. and Jones, N. W., 1983. Isotope geochemistry and contamination mechanisms of Tertiary lavas from Skye, northwest Scotland. In: C. J. Hawkesworth and M. J. Norry, (Ed.) Continental Basalts and Mantle Xenoliths. Shiva.

Trua, T., Deniel, C. and Mazzuoli, R., 1999. Crustal control in the genesis of Plio-Quaternary bimodal magmatism of the main Ethiopian Rift (MER): geochemical and isotopic (Sr, Nd, Pb) evidence. Chemical Geology 155, 201-231.

Turrin, B. D., Muffler, L. J. P., Clynne, M. A. and Champion, D. E., 2007. Robust 24 ± 6 ka $^{40}Ar/^{39}Ar$ age of a low-potassium tholeiitic basalt in the Lassen Region of NE California. Quaternary Research, doi:10.1016/j.yqres.2007.02.004

Valbracht, P. J., Staudacher, T., Malahoff, A., and Allègre, C. J., 1997. Noble gas systematics of deep rift zone glasses from Loihi Seamount, Hawaii. Earth and Planetary Science Letters 150, 399-411.

Van der Hilst, R., Widiyantoro, S. and Engdahl, R., 1997. Evidence for deep mantle circulation from global tomography. Nature 386, 578-584.

Van Westrenen, W., Blundy, J. D. and Wood, B. J., 2001. High field strength element/rare earth element fractionation during partial melting in the presence of garnet: Implication for identification of mantle heterogeneities. Geochemistry Geophysics and Geosystems 2, 1525-2027.

Velde, D., 1978. An aenigmatite-richterite-olivine trachyte from Puu Koae, West Maui, Hawaii. American Mineralogist 63, 771-778.

Walter, M. J., 1998. Melting of garnet peridotite and the origin of komatiite and depleted lithosphere. Journal of Petrology 131, 1-12.

Walter, R.C., Manega, P.C., Hay, R.L., Drake, R.E. and Curtis, G.H., 1991. $^{40}Ar/^{39}Ar$ dating of Bed I, Olduvai Gorge, Tanzania. Nature, 354, 145-149.

Walter, R.C., Manega, P.C. and Hay, R.L., 1992. Tephrochronology of Bed I, Olduvai Gorge: An application of laser fusion $^{40}Ar/^{39}Ar$ dating to calibrating biological and climatic change. Quaternary International 13, 37-46.

Weaver, S. D., Seal, J. S. and Gibson, I. L., 1972. Trace element data relevant to the origin of trachytes and pantelleritic lavas in the East African Rift System. Contributions to Mineralogy and Petrology 36, 181-194

Weeraratne, D. S., Forsyth, D. W., Fischer, K. M. and Nyblade, A. A., 2003. Evidence for an upper mantle plume beneath the Tanzania Craton from rayleigh wave tomography. Journal of Geophysical Research 108, 2427

White, T. D., 1981. Primitive hominid canine from Tanzania. Science 213, 348-349.

White, T. D., 1980. Additional fossil hominids from Laetoli, Tanzania: 1976-1979 specimens. American Journal of Physical Anthropologist 53, 487-504.

White, T. D., 1977. New fossil hominids from Laetoli, Tanzania. American Journal of Physical Anthropology 46, 197-229.

Wilkinson, P., Mitchell, J. G., Cattermole, P. J., and Downie, C., 1986. Volcanic chronology of the Meru-Kilimanjaro region, Northern Tanzania. Journal of Geological society, London 143, 601-605.

Williams, L.A.J., 1978. The volcanological development of the Kenya Rift, In: Neumann, E. R. & Ramberg, I. B. (Ed.) *Petrology and Geochemistry of Continental Rifts*. D. Reidel Publishing Co., Holland, pp. 101-121.

Williams, L.A.J., 1982. Physical aspects of magmatism in continental rifts, In: G. Palmson (Ed.) *Continental and Oceanic Rift, Geodynamic Series*. Washington, D.C: 193-222.

Wilson, M., 1989. *Igneous Petrogenesis*. Unwin Hyman: London.

Yogodzinski, G. M, Kay, R. W., Volynets, O. N., Koloskov, A. V. and Kay, S. M., 1995. Magnesian andesite in the western Aleutian Komandorsky region: Implications for slab melting and processes in the mantle wedge. GSA Bulletin 107, 505-519.

Zhang, J. and Herzberg, C., 1994. Melting experiment on anhydrous peridotite KLB-1 from 5.0 to 22.5 GPa. Journal of Geophysical Research 99, 17729-17742.

CARRICULUM VITAE

GODWIN F. MOLLEL

Education

Ph.D., 2007, Rutgers University. "Petrochemistry and geochronology of the Ngorongoro volcanic highland complex (NVHC) and its relationship to Laetoli and Olduvai Gorge, Tanzania." C.Swisher III, Advisor.

M.S., 2002, Rutgers University. "Petrology and geochemistry of southeastern Ngorongoro volcanic highland (NVH); and contribution to "sourcing" of stone tools at Olduvai Gorge, Tanzania." G.Ashley, Advisor.

B.S., 1995 Geology, University of Dar es salaam. "Identification of a new mining block at the Mbeya cement company." C.Kaaya, Advisor.

Profession Positions

2005-2007 *Baldwin Fellow*, Leakey Foundation

2000-2004 *Teaching Assistant*, Geological Sciences, Rutgers University

2000-2003 *Assistant Geologist,* Olduvai Landscape Paleoanthropology Project, Tanzania

1995-1999 *Geologist,* BHP Minerals Exploration Inc.

Publications

McHenry, L.J., Mollel, G.F., Swisher III, C C., 2007. Direct compositional correlations between Olduvai Gorge Bed I tephra and volcanic sources in the Ngorongoro Volcanic Highlands. Quaternary International, http://dx.doi.org/10.1016/j.quaint.2007.01.004.

Mollel, G.F., Swisher III, C.C., Feigenson, M.D., Carr, M.J., (in press). Petrology, geochemistry, and age of Satiman, Lemagurut, and Oldeani: sources of the volcanic deposits of the Laetoli area, northern Tanzania. In: T. Harrison (Eds.) *Paleontology and Geology of Laetoli: Human Evolution in Context Volume 1*, Springer, Dordrecht.